Chapter 8: Anthropogenic and Natural Radiative Forcing

Coordinating Lead Authors: Gunnar Myhre (Norway), Drew Shindell (USA)

Lead Authors: François-Marie Bréon (France), William Collins (UK), Jan Fuglestvedt (Norway), Jianping Huang (China), Dorothy Koch (USA), Jean-François Lamarque (USA), David Lee (UK), Blanca Mendoza (Mexico), Teruyuki Nakajima (Japan), Alan Robock (USA), Graeme Stephens (USA), Toshihiko Takemura (Japan), Hua Zhang (China)

Contributing Authors: Claire Granier (France), Joanna Haigh (UK), Brian O'Neill (USA), Leon Rotstayn (Australia), Paul Young (USA)

Review Editors: Daniel Jacob (USA), A.R. Ravishankara (USA), Keith Shine (UK)

Date of Draft: 16 December 2011

Notes: TSU Compiled Version

Table of Contents

Executive Summary

- The radiative forcing (RF) concept is valuable for comparing the global mean temperature response to most of the various components affecting Earth's radiation balance. The quantitative values provided in AR5 are consistent with those in previous IPCC reports. RF is estimated over the industrial era from 1750 to 2010 if other time periods are not explicitly stated.

- Adjusted forcing (AF) characterizes some of the more complex forcing agents that involve rapid feedbacks with some components of the atmosphere that are assumed constant in the RF concept. The AF and RF values are significantly different for the anthropogenic aerosols, due to their influence on clouds and on snow cover.

- Whereas in the RF concept all surface and tropospheric conditions are kept fixed, AF allows all variables to respond to perturbations except responses of the ocean and sea ice cover. The changes to clouds from aerosols are rapid responses and occur on a time scale much faster than responses of the ocean (even the upper layer) to forcings.

- Satellite observations of total solar irradiance (TSI) changes since 1980 spanning 3 solar cycle minimums show a RF of –0.04 ± 0.02 W m^{-2}. There is some diversity in the estimated trends of the composites of various satellite data, but a downward trend in TSI over this time period is very likely.

- Secular trends of TSI before the start of satellite observations (≈1980) are much less certain and rely on reconstructions. The best estimate of RF from TSI changes over the industrial era is 0.07 ± 0.05 W m^{-2}, which includes greater RF up to 1980 and then a small downward trend.

- The RF of stratospheric aerosols is well understood and has a large impact on the climate for a few years after major volcanic eruptions. There has not been any major volcanic eruption since Mt. Pinatubo in 1991, but several smaller eruptions, have caused an RF of about -0.1 ± XX W m^{-2} during the 2000 to 2010 period.

- The RF of long-lived greenhouse gases (LLGHG) in 2010 is 2.79 ± 0.28 W m^{-2}. This is an increase since AR4 of 0.15 ± 0.02 W m^{-2}, with most of the increase due to greater abundance of CO_2. The RF for CO_2 is 1.79 ± 0.18 W m^{-2}. Over the last 15 years, CO_2 has clearly been the dominant contributor to the increase in RF from the LLGHG, with RF of CO_2 having an average growth rate slightly less than 0.3 ± 0.03 W m^{-2}/decade.

- A small increase in the CH_4 concentration has increased its RF by 2% compared to AR4 to 0.49 ± 0.05 W m^{-2}. N_2O has increased by 6% since AR4 and has a RF of 0.17 ± 0.02 W m^{-2}. N_2O is expected to become the third largest LLGHG RF component within the next 1–2 years.

- The RF from halocarbons is very similar to the value in AR4, with a reduced RF from CFCs but increases in many of their replacements. Four of the halocarbons (CFC–11, CFC–12, CFC–113, and HCFC–22) account for 85% of the total halocarbon RF. The former three compounds have declining RF over the last five years but are more than compensated for by the increased RF from HCFC–22.

- The growth rate in RF from all LLGHG is weaker over the last decade than in the 1980s owing to a smaller increase in the non-CO_2 RF.

- The RF due to changes in tropospheric ozone is 0.34 ± 0.12 W m^{-2} and for stratospheric ozone is –0.05 ± 0.10 W m^{-2}. Newer studies show stronger links between the changes in tropospheric and stratospheric ozone. RF for stratospheric water vapour from CH_4 oxidation is 0.07 ± 0.05 W m^{-2}. Recent observations indicate a reduction in the stratospheric water vapour abundance, but this is not linked to CH_4 oxidation and is therefore not treated as a RF mechanism.

- For the various aerosol effects, the direct aerosol RF is given a best estimate of –0.30 ± 0.30 W m^{-2}, cloud albedo RF in the range between –1.0 to –0.1 W m^{-2}, and BC on snow and ice is 0.04 (with range from

0.01 to 0.10) W m^{-2}. A total aerosol indirect aerosol effect is also quantified in terms of the AF concept with an estimate of –1.5 to 0 W m^{-2}.

- The impact of land use change on the Earth albedo has an RF of –0.15 ± 0.1 W m^{-2}. However, land use change causes other modifications that are not radiative but impact the surface temperature. These are more uncertain and they are difficult to quantify, but tend to compensate the albedo change impact. There is no consensus on the sign of the change in global mean temperature as a result of land use change.

- The total anthropogenic RF has a best estimate of 2.15 ± 0.7 W m^{-2} and the AF 1.95 ± 0.9 W m^{-2}.

- The time evolution of the total anthropogenic RF shows an increase from 1750 to around 1950 with a decline or little change over the next decade. From 1970 until 2010 there has been a strong increase in the total anthropogenic RF. These results have substantial uncertainties due to the poorly constrained aerosol indirect effects.

- The net RF from natural sources has been near-zero over the past three decades (since 1980). During this time, net anthropogenic forcing has been ~0.7 W m^{-2} ± XX.

- [PLACEHOLDER FOR SECOND ORDER DRAFT: Future RF]

- Metrics are used to compare the potential climate effect of various forcing agents. The choice of metric depends strongly on the particular impact being investigated. Since AR4, the Global Temperature change Potential (GTP), which is based on the change in global surface temperature at chosen point in time, has become much more widely used.

- There are large uncertainties related to *net* effect of NOx, but most studies indicate that NOx emitted from surface sources gives a net cooling effect. In contrast, carbon monoxide (CO) has a clear warming impact.

- Changes in carbon dioxide are the largest single contributor to historical RF from either the perspective of changes in atmospheric concentration or changes in emissions. The relative importance of other forcing agents varies with the perspective chosen. In particular, methane emissions have a much larger forcing (~0.9 – 1.0 W m^{-2} over the industrial era) than methane concentration increases (~0.5 W m^{-2}) due to several indirect effects through atmospheric chemistry.

- Forcing can also be attributed to activities. From this perspective, a single year's worth of current global emissions from the power generation and industrial sectors have the largest contributions to warming over the next 25–100 years. Livestock, household cooking and heating, on-road transportation, and agriculture are also large contributors to warming, especially over shorter time horizons.

Notes: Uncertainties are given associated with best estimates of RF. The uncertainty values represent the 5 to 95% (90%) confidence range.

8.1 Radiative Forcing and Other Climate Change Metrics, including Greenhouse Gas Equivalent, Global Warming Potential (GWP) and Global Temperature Change Potential (GTP)

There are a variety of ways to facilitate understanding how various factors contribute to climate change. In principle, observations of the climate response to a single factor can be used to evaluate it's impact, and climate models can be used to study the impact of any given factor. In practice, however, it is usually very difficult to find measurements that are only influenced by a single change, and it is computationally prohibitive to simulate the response to every individual factor of interest. Hence multiple metrics are used to provide estimates of the climate impact of individual factors, with applications both in science and policy. Radiative forcing (RF) is one of the most widely used metrics, with many of the other metrics based upon RF. The utility and limitations of these metrics are the topic of this section.

8.1.1 The Radiative Forcing Concept

RF is a measure of the net change in the energy balance of the Earth system in response to some external perturbation. It is expressed in watts per square meter and quantifies the energy imbalance that occurs when the external change takes place. Though difficult to observe in most cases, RF provides a simple quantitative basis for comparing some aspects of the eventual climate responses to different external agents, and hence is widely used in the scientific community. Metrics that take into account the time-dependence of RF have been developed to compare the impact of different climate-altering pollutants (CAPs). Comparing radiative forcing over time, or the estimated temperature response over time, due to different forcing agents provides a fuller picture than the common analysis of the forcing at a single time.

8.1.1.1 Defining Radiative Forcing

Alternative definitions of RF have been developed, each with its own advantages and limitations. The instantaneous RF refers to an instantaneous change in net (down minus up) radiative flux (solar plus longwave; in W m^{-2}) into the climate system induced by a change to an external agent. This forcing is usually defined in terms of flux changes at the top of the atmosphere (TOA) or at the tropopause.

The instantaneous RF provides a simple, quantitative basis for judging the effectiveness of different external forcing agents in producing a given climate response. Climate change takes place when the system responds in order to counteract the flux changes, and all such responses to the changes in radiative fluxes are explicitly excluded from this definition of forcing. The assumed relation between the instantaneous RF forcing (F) and the equilibrium global mean surface temperature response (ΔT) is $\Delta T = \lambda F$ where λ is the climate sensitivity (cross ref to Chapter 7). The relationship between F and ΔT is a heuristic expression of the energy balance of the climate system and a simple reminder that the steady state global mean climate response to a given forcing is determined both by the forcing (F) and the feedbacks inherent in the quantification of λ.

The notional idea of RF is that the change in net irradiance at the tropopause or TOA that ultimately gives rise to the steady state global mean climate response can be separated from the changes in net irradiances that affect other parts of the system often associated with feedbacks. The effects of forcing and feedbacks on TOA fluxes are not always cleanly separable and thus some ambiguity exists in what may be considered a forcing versus what is responsible for feedbacks.

In both the TAR and AR4, the term radiative forcing (RF, as distinct from instantaneous RF) was defined as the change in net irradiance at the tropopause after allowing for stratospheric temperatures to readjust to radiative equilibrium, while holding surface and tropospheric temperatures and state variables such as water vapor and cloud cover fixed at the unperturbed values (except in the case of aerosol indirect effects, where the impact of aerosols on cloud albedo due to changes in droplet size with constant cloud liquid water is considered part of RF; see Section 8.4.4.3). RF is generally more indicative of that part of the forcing that is responsible for the surface and tropospheric temperature responses than instantaneous RF, especially for agents such as carbon dioxide or stratospheric ozone change.

To be consistent with TAR and AR4, RF is hereafter taken to mean the stratospherically-adjusted radiative forcing and will for many of the forcing agents be used throughout the chapter. For many forcing agents the RF concept gives a very useful and appropriate way to compare the relative importance of their potential climate effect. Although useful, instantaneous RF or RF are not necessarily accurate indicators of the eventual climate response for all forcing agents, especially for some of the aerosol cloud effects. The efficacy – a measure of the global mean equilibrium temperature response for a unit forcing relative to the response to a unit forcing from CO_2 – can in some special cases differ substantially from 1 (Forster et al., 2007) due to feedbacks that act over a variety of time scales and complicate the relationship between forcing and response. Most of these adjustments involve processes that occur rapidly compared to the slower equilibrium response of global mean surface temperature. For example: Aerosol forcing is considered 'direct' when dealing with the direct influence of aerosol on radiative fluxes but even in this case some part of the radiative perturbation, especially for absorbing aerosol, goes to change the internal thermodynamics or the temperature distribution of the system and not directly to affect global mean temperature. This has been called the semi-direct effect (Hansen et al., 2005) and Section 7.3.5.2. Similarly, part of the tropospheric CO_2 RF directly alters the thermodynamics of the atmosphere and does not directly apply to the equilibrium surface temperature response. These are termed fast feedbacks by Gregory et al. (2004) and occur over time scales similar to the semi-direct aerosol effect.

Aerosols also lead to other adjustments, especially by altering cloud properties leading to the indirect effect (Chapter 7.4). Although these adjustments are complex and not fully quantified, they are thought to occur both on the microphysical scale of the cloud particles as well as on a more macroscopic scale involving whole cloud systems (e.g., Penner et al., 2006; Quaas et al., 2009). A portion of these adjustments occurs over a short time period, on cloud-life cycle time scales, and is not part of a feedback from the surface temperature changes. Previously these adjustments have been termed 'fast feedbacks', where in AR5 they will be denoted 'rapid response' to make it distinctive from feedbacks from surface temperature changes. Traditional climate feedbacks mechanisms are also in some cases divided into fast and slow (see Chapters 9 and 12).

In recognition of this complication, a number of different measures of forcing have been introduced that attempt to include different types of responses. The stratospherically-adjusted forcing described above is one example of an applied adjustment to remove effects of stratospheric responses to the instantaneous RF. More rapid responses in the troposphere triggered by the RF have also been incorporated into forcing estimates. One example is the notion of rapid response that include effects on tropospheric temperature, water vapor and clouds induced by the RF of CO_2 (Gregory et al., 2004), and the separation of rapid and slow responses is discussed further by Andrews et al. (2010). A RF calculation allowing temperature throughout the atmosphere and on land to adjust has been shown to provide a better estimate of the eventual temperature change than either instantaneous RF or RF (Hansen et al., 2005). Lohmann et al. (2010) have also demonstrated the utility of including rapid response in comparison of forcing agents, especially for aerosol indirect effects.

In this chapter, we emphasize a forcing definition that accounts for the complicating effects of rapid responses on the radiation balance to allow quantification of additional forcing agents. This forcing is the adjusted forcing (AF), which is defined as the change in net irradiance at the TOA after allowing for atmospheric and land temperatures, water vapour, clouds and land albedo to adjust, but with sea surface temperatures (SSTs) and sea ice cover unchanged. This definition is chosen as one that (1) provides a good indication of the eventual climate response, (2) that allows evaluation of processes such as some aerosol indirect effects or so-called 'semi-direct' effects that influence climate but do not have an instantaneous forcing, and (3) that is readily calculated in model simulations with a comparatively small uncertainty range. Since the atmospheric temperature has been allowed to adjust, the AF would be identical if calculated at the tropopause instead of the TOA. Ideally, all known rapid responses would be included, but in practice calculations have to date largely been performed with models that have fixed composition and ecosystems (and hence neglect rapid responses of aerosols or ozone when calculating the response to CO_2 forcing, and neglect changes in vegetation cover when calculating aerosol indirect forcing, for example). The conceptual relation between instantaneous RF and AF is illustrated in Figure 8.1 and it implies the adjustments to the instantaneous RF involve effects of processes that occur more rapidly than the time scale of the response of the global mean surface temperature to the forcing. The AF thus represents that part of the instantaneous RF that more directly contributes to the steady-state climate response. Since the stratospheric adjustment

described above occurs on time scales of a few months, the RF is a more limited version of AF. Other main adjustments are the CO_2 rapid responses (Gregory and Webb, 2008) that occur on time scales of weeks, and aerosol indirect adjustments on clouds that occur on even shorter time scales typical of cloud lifecycles.

A combination of RF and AF will be used in this chapter to keep consistency with TAR and AR4 when practical, but also to allow quantification of more complex forcing agents through the AF concept.

8.1.1.2 Limitations of Radiative Forcing

Dedicated model simulations that are required to diagnose the AF are more computationally demanding than those for instantaneous RF or RF. However, in many cases the AF and RF are nearly equal. In particular, using fixed-SST simulations, Hansen et al. (2005) found that AF is virtually identical to RF for increased CO_2, tropospheric ozone and solar irradiance, and within 6% for methane, N_2O, stratospheric aerosols, and for the direct effect of reflective aerosols. A study of six GCMs found a substantial intermodel variation in the rapid tropospheric response to CO_2 using regression analysis in slab ocean models, with the ensemble mean result being an additional ~4% to the RF but with an uncertainty of ~21% (Andrews and Forster, 2008). Part of the large uncertainty range arises from the greater noise inherent in regression analyses of single runs in comparison with fixed-SST experiments. Lohmann et al. (2010) also report a small increase in the forcing from CO_2 using AF instead of RF, while finding no substantial difference for methane, direct aerosol forcing or aerosol indirect effects on cloud lifetime. In the fixed-SST simulations of Hansen et al. (2005), AF was substantially greater than RF for stratospheric ozone (~50%, though that forcing is small), ~20% less for the atmospheric effects of black carbon (BC) aerosols (not including aerosol-cloud microphysical interactions), and nearly 300% greater for the forcing due to BC snow albedo forcing (Hansen et al., 2007). Aerosol effects include the so-called semi-direct effect when using AF, and the impact of BC atmospheric heating on clouds varies strongly across models (see Chapter 7) so the above values are only an example. The various studies demonstrate that RF estimates can reasonably be used instead of the more demanding AF calculations in most cases, as the differences are very small, with the notable exceptions of BC direct and snow albedo forcings, stratospheric ozone, and, of course, aerosol indirect effects on clouds for which RF due to changes in cloud lifetime is not defined.

Whereas the global mean TOA or tropopause AF provides a useful indication of the eventual change in global-mean surface temperature, it does not necessarily reflect regional climate changes. In the case of agents that strongly absorb incoming solar radiation (such as BC, and to a lesser extent OC and ozone) the TOA forcing provides little indication of the change in radiation reaching the surface which can force local changes in evaporation and alter regional and general circulation patterns (e.g., Ramanathan and Carmichael, 2008; Wang et al., 2009). Hence the forcing at the surface, or the atmospheric heating, defined as the difference between surface and tropopause/TOA forcing, might also be a useful metric. Global mean precipitation changes can be related separately to atmospheric RF and to a slower response to global mean temperature changes (Andrews et al., 2010; Ming et al., 2010). Relationships between surface forcing and localized aspects of climate response have not yet been clearly quantified, however.

Evaluation of forcing from short-lived species also poses substantial challenges in both calculation and interpretation. While there is no strict definition of “short-lived”, here we define short-lived climate forcers (SLCFs) as species with atmospheric residence times of less than a year, which includes tropospheric ozone and aerosols. This timescale is short compared with atmospheric mixing times, so that the distribution of these species will be highly inhomogeneous. The response time of global mean surface temperature, however, is nearly a decade for the relatively rapidly responding component that involves the land and upper ocean (Boucher et al., 2009). Hence the global mean surface temperature response to tropospheric ozone and aerosol forcing takes place on this timescale, and thus SLCFs have often been defined to include methane, which has a similar timescale (i.e., methane is short-lived compared with surface temperature responses, but is long-lived compared with atmospheric transport and is thus relatively well-mixed).

In the case of a well-mixed gas, emissions from any location and at any time have comparable effects on atmospheric concentrations, so that the forcing can be related directly to the total change in emissions of that gas. In contrast, for SLCFs, the forcing can depend strongly on the location of the emissions (both geographical and vertical) and on timing of the emission of that species or its precursors. Hence calculating forcing requires detailed knowledge of the spatio-temporal patterns of concentrations, and the annual average

global mean RF does not necessarily provide a useful guide to the forcing (and hence temperature change) resulting from any particular individual emission of those compounds.

In general, most widely used definitions of RF and most forcing-based metrics are intended to yield the eventual temperature response, and most analyses to date have explored the global mean temperature response only. These metrics do not explicitly include impacts such as changes in precipitation, ocean acidity, air quality, surface sunlight available for photosynthesis, extreme events, etc, as well as regional temperatures, which can differ greatly from the global mean. Hence although they are quite useful for understanding the factors driving global mean temperature change, they provide only an imperfect and limited perspective on the factors driving broader climate change.

[INSERT FIGURE 8.1 HERE]

Figure 8.1: Cartoon comparing (a) instantaneous RF, (b) RF, which allows stratospheric temperature to adjust, (c) flux change when the surface temperature is fixed over the whole Earth, (d) AF, the adjusted forcing which allows atmospheric and land temperature to adjust while ocean conditions are fixed, and (e) the equilibrium response to the climate forcing agent. Updated from Hansen et al. (2005).

8.1.1.3 Historical and Forward-Looking Radiative Forcing

Analysis of the forcing change between preindustrial, defined here as 1750, and present provides an indication of the importance of different forcing agents to climate change during this period. Such analyses have been a mainstay of climate assessments. However, looking simply at two points in time does not take into account the varying time histories of the individual forcing components (detection and attribution studies often make use of the time-dependence of various forcings (Chapter 10)). Moreover, unless forcing has been constant for many decades, the full impact of forcings will not have been realized given the time lag in climate response. Hence the preindustrial to present-day forcing is more indicative of the contribution to the global mean surface temperature increase during this period plus the future temperature increase already 'in the system' due to past forcing than it is of the temperature change to date alone. One way to evaluate this is to examine how much each forcing is contributing to the Earth's current energy imbalance with space (see Section 8.5).

Multiple aspects of future RF are worth consideration. The impact of current conditions has been looked at in three main ways: (1) examining the forcing due to perpetual current atmospheric *concentrations* (equal to simply the present-day forcing), (2) examining the forcing due to current atmospheric *emissions*, again assuming that those stay constant in the future, or (3) examining the time-dependent forcing due to a single year's worth of current emissions (an emissions 'pulse'). AR4 referred to perpetual current concentrations as 'committed', though for carbon dioxide a substantial decrease in current emissions would be required to maintain current concentrations (as these are not in equilibrium). Constant current concentrations is equivalent to letting the temperature adjust to the current energy imbalance. Constant current emissions allow both current concentrations to adjust to emissions and temperature to adjust to the resulting energy imbalance. The influence of current emissions can be analyzed in terms of an emissions pulse or sustained emissions, but pulse-based approaches have usually been adopted in calculations of metrics because pulse emissions possess a greater generality (a choice of sustained emission metrics implies an assumption of constant future emissions). Scenarios of changing future emissions and land use are also developed based on various assumptions about socio-economic trends and choices. The RF resulting from such scenarios is also used to understand projected future climate changes. In any of these cases, forcing due to various components can easily be presented at a particular future time, but as with historical forcings the actual impact on temperature depends on both the time history of the forcings and the rate of response of various portions of the climate system. Metrics that attempt to account for these factors, and hence better indicate the eventual temperature response, by going beyond RF at a single time are widely used in forward-looking analyses (see Sections 8.1.2, 8.5.2 and 8.5.3).

8.1.1.4 Sensitivity of Forcing to Location

The strong interaction of aerosols with incoming solar radiation makes their forcing sensitive to the local surface albedo and cloud cover. Reflective aerosols will have a much larger impact over relatively dark, open ocean than over bright deserts or snow, and vice-versa for absorbing aerosols, for example. Similarly,

reflective aerosols will have less impact if located over bright clouds, whereas absorbing aerosols may have a greater impact. Ozone absorbs both incoming solar and outgoing terrestrial radiation, and hence its impact depends on location due to both the availability of sunlight and the difference between local layer temperature and the surface temperature. The result is that ozone changes in the tropical upper troposphere tend to have the greatest RF (Aghedo et al., 2011; Worden et al., 2011). Even well-mixed greenhouse gases do not have a uniform forcing, due to both geographic variations in vertical temperature gradients and cloud cover, though the inhomogeneity is small in comparison with most other forcing agents (Forster et al., 2007). Forcing tends to be greatest in the relatively cloud-free subtropics for both greenhouse gases and solar irradiance.

The inhomogeneously distributed forcings also have a different impact on climate from the quasi-homogeneous forcings due to well-mixed greenhouse gas or solar irradiance changes because they activate climate feedbacks based on their regional distribution. For example, forcings over Northern Hemisphere middle and high latitudes induce snow and ice albedo feedbacks more than forcings at lower latitudes or in the Southern Hemisphere (e.g., Shindell and Faluvegi, 2009). The influence of clouds on the interaction of aerosols with sunlight and the effect of aerosol heating on cloud formation can lead to very large differences in the impact of black carbon as a function of altitude (Hansen et al., 2005). The seasonal and diurnal cycles of insolation also affect the radiative forcing of agents that act on shortwave radiation. For example, volcanic aerosols in the polar night have no radiative forcing in the shortwave (although they still have a small longwave forcing).

8.1.2 Global Warming Potential (GWP), Global Temperature change Potential (GTP) and Other Emission Metrics

8.1.2.1 Introduction

To quantify and compare the climate impacts of various emissions – i.e., place their impacts on a common scale – one has to choose a climate impact parameter by which to measure the effects. Various types of models are needed for the steps down the cause-effect chain (See Figure 8. 2 and Box 8.1)

[INSERT FIGURE 8.2 HERE]

Figure 8.2: Cause-effect chain from emissions to climate change and impacts showing how metrics can be used to estimate responses to emissions (left side) and for development of multi-component mitigation (right side). (Adapted from Fuglestvedt et al. (2003) and Plattner et al. (2009)).

For assessments and evaluation one may apply simpler measures or *metrics* that are based on linearization of results from complex calculations – as an alternative to models that explicitly include physical processes resulting in forcing and responses.

Metrics can be used to quantify and communicate the relative contributions to climate change of emissions of different substances, and of emissions from regions/countries or sources/sectors. They can also serve in communicating the state of knowledge and uncertainties, as well as how effects depend on location of emissions. Furthermore, metrics can be used as exchange rates in multi-component mitigation policies.

It is common to use CO_2 as reference in metrics; i.e., the effect of an emission component is normalized to the effect of CO_2 for the same mass of emission. To transform the effects of different emission to a common scale – often called (somewhat misleadingly) "CO_2 equivalents" – the emissions can be multiplied with the adopted metric for a chosen time horizon: $M_i(H) \times E_i = CO_2\ eq(H)$, where M is the chosen metric, H is the chosen time horizon and *i* is component. Ideally, the climate effects should be the same regardless of composition of the equivalent CO_2 emissions, but in practice this is not possible. Metrics that are used for these purposes should be transparent and relatively easy to apply since the metrics are used by non-specialists (Shine, 2009; Skodvin and Fuglestvedt, 1997). Metrics that have been proposed in the literature include purely physical metrics as well as more comprehensive metrics that account for both physical and economic dimensions (see Section 8.1.2.6).

No single metric can accurately compare all consequences (i.e., responses in climate parameters over time) of different emissions, and therefore the most appropriate metric will depend on which aspects of climate

change are most important to a particular application, and different climate policy goals may lead to different conclusions about what is the most suitable metric with which to implement that policy (Plattner et al., 2009; Tol et al., 2009). It is important to note that the metrics do not define the goals and policy – they are tools that enable implementation of multi-gas policies (i.e., which emissions to abate).

More recently metrics have also attained wider applications. Cherubini et al. (2011) used GWP for comparing biogenic emission of CO_2 with fossil CO_2, while Bright et al. (2011) used GWP for assessment of albedo changes related to changes in boreal forests.

[START BOX 8.1 HERE]

Box 8.1: How Can Impacts of Emissions be Compared?

Several approaches are possible for quantification and comparison of different emissions. Such quantifications may be based on a set of model calculations, with complex or simplified models. As an alternative to models, metrics may be used for approximations of climate impact and the amount of a given species emitted can be multiplied by its metric value (left side of Figure 8.2). In any case, whether complex or simplified approaches are used, many choices related to impact parameter, time, space, or type of perturbation are needed (Fuglestvedt et al., 2003; Tanaka et al., 2010).

Typically the aim is to quantify and compare effects of emissions from different sources or sectors (e.g., Unger et al. (2010) and Fuglestvedt et al. (2008)), regions or nations (den Elzen et al., 2005; Hohne et al., 2011; Prather et al., 2009) or various components (e.g., Forster et al. (2007)). Results can be used in climate analyses and assessments and in climate agreements and implementation of climate policies.

As discussed in 8.1.1.3, there is a set of choices that are related to *time frames*: One can apply a *backward-looking* or a *forward-looking* perspective, and in the latter case one may use pulses, sustained emissions or scenarios. All choices of types of emission perturbations are somewhat artificial in construct and different choices serve different purposes.

The next set of choices is related to the parameter chosen for evaluating the effects of the emissions. Impacts of climate may be measured as RF, integrated RF, ΔT, or sea level change, for example; depending on what aspects of climate change one is most concerned about (Figure 8.2). For a chosen impact parameter one may use *level* of change or *rate* of change. Furthermore, the impacts may also be integrated over time, or discounting of future effects may be introduced. Impacts may also depend non-linearly on physical changes, e.g., environmental and societal responses might be formulated to vary with the square of temperature change or only occur when thresholds are exceeded.

There is also a spatial dimension involved, and this is related to both driver and response: It is important to distinguish between the fact that equal-mass emissions of SLCFs from different regions can induce varying global-mean climate responses and that the climate response to emissions of all CAPs also has a regional component irrespective of the regional variation in emissions.

Some of the choices that are needed in the assessment of impacts of emissions are scientific (e.g., type of model, and how processes are included or parameterized in the models). Choices of time frames and impact parameter are policy-related and cannot be based on science alone.

[END BOX 8.1 HERE]

8.1.2.2 The GWP Concept

The Global Warming Potential (GWP) was used in The First IPCC Report (Houghton et al., 1990) and it was stated that "*It must be stressed that there is no universally accepted methodology for combining all the relevant factors into a single [metric] . . . A simple approach [i.e., the GWP] has been adopted here to illustrate the difficulties inherent in the concept*." After this time the GWP was adopted as a metric to

implement the multi-gas approach embedded in the UNFCCC and made operational in the Kyoto Protocol. It has become the default metric for transferring emissions of different gases to a common scale; usually called "CO_2 equivalents".

The GWP is defined as the time-integrated radiative forcing due to a pulse emission of a given gas, relative to a pulse emission of an equal mass of CO_2 (Figure 8.3a), usually integrated over 20, 100 or 500 years. For gases with adjustment times shorter than the adjustment time for CO_2, the GWP values will decrease with increasing time horizon, since GWP is defined with the integrated RF of CO_2 in the denominator.

A time horizon of 100 years was adopted by the Kyoto Protocol and is the most frequently used time horizon for GWP in climate (policy) assessments. The choice of time horizon has a strong effect on the GWP values – and thus also on the calculated effects and contributions of emissions by component, sector or nation. As previously pointed out (e.g., Shine (2009); Fuglestvedt et al. (2003; 2009)) there is no conclusive scientific argument that can defend 100 years compared to other choices, and in the end the choice will be value-based.

The GWP is an indicator of magnitude of the RF of the climate system over time and does not translate directly into any specific climatic response parameter. Several studies have evaluated the concept and its application (Fuglestvedt et al., 2000; Fuglestvedt et al., 2003; Godal, 2003; Manne and Richels, 2001; Manning and Reisinger, 2011; O'Neill, 2000; Smith and Wigley, 2000a; Smith and Wigley, 2000b) and these studies have served to clarify the interpretation and limitations of the concept; e.g., that emissions that are equal in terms of CO_2 equivalents will *not* result in the same climate response over time. As shown by Fisher et al. (1990), O'Neill (2000) and Shine et al. (2005b) the ratio of integrated forcing from pulse emissions of two gases is similar to the ratio of the equilibrium temperature response of these gases for sustained emissions changes, which offers one interpretation of the GWP concept.

8.1.2.3 The GTP Concept

The Global Temperature change Potential (GTP) (Shine et al., 2005b) goes one step further down the cause-effect chain (Figure 8.2) and uses the *change in global mean temperature for a chosen point in time* as the impact parameter. While GWP is a metric integrative in time (Figure 8.3a), the GTP is based on the temperature change for a selected year, t, (Figure 8.3b). Like for the GWP, the impact from CO_2 is normally used as reference, hence, $GTP(t)_i = AGTP(t)_i / AGTP(t)_{CO2} = \Delta T(t)_i / \Delta T(t)_{CO2}$, where AGTP is the absolute GTP.

A modification of the GTP concept was introduced by Shine et al. (2007) in which the time horizon is determined by the proximity to a target year (see also Section 8.1.2.6).

The AGTP is also useful in its own right, as pulse-based AGTPs can be used to calculate the temperature change due any given emission scenario. This can be calculated as the integral over pulse emissions multiplied by the absolute temperature change potential (AGTP):

$$\Delta T(t_H) = \sum_i \int_{t_e=0}^{t_H} em_i(t_e) \cdot AGTP_i(t_H - t_e) dt_e$$

where *i* is component, and t_e is time of emission (Berntsen and Fuglestvedt, 2008; Borken-Kleefeld et al., 2011). The AGTP values need to be known for all times up to t_H.

By accounting for the climate sensitivity and the exchange of heat between the atmosphere and the ocean, the GTP includes more physical processes than does the GWP. The GTP accounts for the response and lag due to the ocean, thereby prolonging the response to emissions beyond what is controlled by the decay time of the atmospheric concentration (Fuglestvedt et al., 2010; Sausen and Schumann, 2000; Shine et al., 2005b; Solomon et al., 2010a). Shine et al. (2005b) presented the GTP for both pulse and sustained emissions, and used a simple model to account for the uptake of heat by the ocean. This has later been developed by accounting for the longer time scales of the ocean (Berntsen and Fuglestvedt, 2008; Boucher and Reddy, 2008; Collins et al., 2010; Fuglestvedt et al., 2010). Thus, there are two important categories of timescales included in the GTP; the atmospheric adjustment time of the component under consideration and the response time of the climate system. Since the climate sensitivity is built in to the GTP concept, it should in principle use efficacies when RF is used as input (rather than AF).

[INSERT FIGURE 8.3 HERE]

Figure 8.3: (a) The GWP is calculated by integrating the RF due to pulses over chosen time horizons; e.g., 20 and 100 years. The black field represent the integrated RF from a pulse of CO_2, while the green and red fields represent gases with 1.5 and 13 years lifetimes, respectively. (b) The GTP is based on the temperature response for selected years after emission; e.g., 20 or 100 years.

The GWP and GTP are fundamentally different by construction and different numerical values can be expected. In particular, the short-lived components get higher values with GWP due to the integrative nature of the metric. No climate response is explicitly included in the GWP concept and is based on the RF concept. A further key difference between the GTP and the GWP is that, because the GTP requires additional assumptions about the climate sensitivity and the uptake of heat by the ocean, its values can be significantly affected by these assumptions (Peters et al., 2011a); Shine et al. (2005b). Thus, the uncertainty ranges are wider for the GTP concept compared to GWP. But the additional uncertainty is not necessarily a weakness of the GTP concept itself and is a consequence of moving down the cause-effect chain and explicitly indicating impacts closer to responses of higher relevance (Figure 8.2). Since the formulation of the ocean response in the GTP has a significant impact on the values its characterization also represents a trade-off between simplicity and accuracy.

8.1.2.4 Uncertainties and Limitations

Uncertainties in the values of emission metrics in general can be classified as *structural* or *scientific* (Plattner et al., 2009; Shine et al., 2005a). Structural uncertainties refer to the consequences of using different types of metrics, or to choices about key aspects of a metric such as impact parameter, time horizon and whether discounting is applied. Scientific uncertainties refer to the range of values that can be calculated for a given metric due to incomplete knowledge of processes from emissions to climate change and impacts.

For the GWP, uncertainties in adjustment times and radiative efficiency determine the scientific uncertainty. Inclusion of indirect effects in metrics (e.g., through atmospheric chemistry, biogeochemistry or via interactions with clouds) will strongly increase the uncertainty in the metric values. For the reference gas CO_2, the scientific uncertainty includes the uncertainties in the *impulse response function* that describes the development in atmospheric concentration. Reisinger et al. (2010) have shown that the uncertainties in GWPs are larger than previously reported, primarily because of significant uncertainties in the global carbon cycle, , and because prior values were not consistent with the full range of carbon cycle and coupled ocean–atmosphere climate models used in AR4. Reisinger et al. (2010) also show that these uncertainties increase with time horizon because of fundamental questions involved in determining the details of long-term carbon cycle responses to both the additional atmospheric CO_2 and the resulting climate change (see Chapter 6). The impulse response function is sensitive to several factors; e.g., background levels of CO_2. Uncertainties in the impulse response function will impact on values of all metrics that use CO_2 as reference.

Usually a constant background atmosphere is assumed, but this is strictly not a part of the definition of GWP. The background concentrations influence both the turnover rates and the concentration-forcing relationships. Reisinger et al. (2011) studied the sensitivities of GWPs to changes in future atmospheric concentrations and found that GWP_{100} for CH_4 would increase up to 20% under the lowest RCP by 2100 but would decrease by up to 10% by mid-century under the highest RCP.

The same factors contribute to uncertainties in GTP, with a significant additional contribution from the parameters describing the ocean heat uptake and climate sensitivity. In the first presentation of the GTP, Shine et al. (2005b) used one time-constant for the climate response. A somewhat more sophisticated approach was used in Collins et al. (2010), Berntsen and Fuglestvedt (2008) and Fuglestvedt et al. (2010) that includes a representation of the deep ocean which increases the climate system's long-term memory to a pulse forcing. This was based on a temperature response function with two time-constants derived from GCM results. Use of a more realistic function that represents both the fast response of the land and upper ocean as well as the slower response of the deep ocean can change the GTP values of short-lived components by an order of magnitude (Shine et al. (2007) and Shine et al. (2005b)). Peters et al. (2011a) applied a set of different temperature impulse response functions from the literature, and found variations in GTP; especially

for the short-lived components (beyond a factor of 2). This indicates that further studies of impulse response functions for GTP are needed (Olivié et al., 2011).

The climate sensitivity parameter (λ) appears in both the numerator and denominator of the GTP expression and the GTP is less sensitive to variations in λ than the AGTP. However, over the range of uncertainty of λ , the GTP is still sensitive to the value of λ, in particular for short-lived species. Using a 2-box model (Berntsen and Fuglestvedt, 2008) across the range of likely climate sensitivities, the GTP_{50} for BC was found to vary by a factor of 2, the methane GTP_{50} varied by ~50%, while for the long-lived gas N_2O essentially no dependence was found (Fuglestvedt et al., 2010). Reisinger et al. (2010) indicate that the relative uncertainties for GTP are almost twice as high as for GWP for a time horizon of 100 years. These examples illustrate the association between increasing relevance of the end-point and increasing uncertainty (Figure 8.2).

Structural uncertainties such as the time horizon can greatly affect the numerical values obtained for CO_2 equivalents. For a change in time horizon from 20 to 100 years, the GWP for methane decreases by a factor of ~3 and its GTP by more than a factor of 10. Thus the calculated contributions of the emission to climate change will be very sensitive to choice of metric and time horizon and will strongly affect the calculated contributions from components, sources and sectors. For instance, aviation gets much higher values for calculated contributions to climate change with GWP than with GTP. The cooling from shipping also gets higher weight and appears to be more long-lived with a GWP-based view than with a GTP-based evaluation (Berntsen and Fuglestvedt, 2008; Eyring et al., 2010a; Fuglestvedt et al., 2010). In general, emission profiles with large contributions from components that are removed on timescales different from that of CO_2 will be most sensitive to these choices, e.g., sources/sectors with emissions of CH_4 and BC.

8.1.2.5 Short Lived Climate Forcers, Methane and Indirect Chemical Effects

Changing the emissions of SLCF (or their precursors) can have rapid impacts on atmospheric concentrations and RF (positive or negative), but these effects quickly equilibrate. Some halocarbons have short lifetimes, but at their current concentrations the short-lived halocarbons contribute little RF. Many of the SLCFs are not directly emitted into the atmosphere, but are formed through the reactions of emitted precursors. Therefore it is not possible to assign emission-based metrics to these secondary SLCFs. The climate effect of these secondary agents is included in that of their precursors (e.g., Collins et al., 2002; Derwent et al., 2001).

SLCFs tend to be distributed inhomogeneously, so the resulting forcing depends on where the species or their precursors are emitted (see Section 8.1.1.4). For secondary SLCFs there is an additional dependence on the local chemical regime. Species affecting the oxidation of methane have larger effects towards the tropics. NO_X has a larger impact on ozone when emitted into a clean environment, whereas VOCs and CO have large impacts on ozone in polluted environments (Berntsen et al., 2005; Derwent et al., 2001; Naik et al., 2005; Stevenson et al., 2004; West et al., 2007; Wild et al., 2001). This means that global-mean metrics such as GWP and GTP can depend on the location of the emissions, and that these global metrics may conceal large regional variations (Berntsen et al., 2005; Shine et al., 2005; Lund et al., 2011). There is no agreed way to generate regional metrics. Bond et al. (2011) suggest using a specific forcing pulse which gives the total energy input within a region, but this regional energy input does not relate easily to an observable impact. Shindell and Faluvegi (2010) propose a regional analogue of the GTP; the Regional Temperature change Potential (RTP). This is more relevant but relies on climate model response characteristics.

Emitting reactive chemicals into the atmosphere perturbs the chemical system affecting many secondary species and ideally all these indirect effects should be taken into account in the calculation of metrics. For instance, as well as its direct effect, methane has indirect effects through its chemical reactions. The indirect effects on its own lifetime, tropospheric ozone and stratospheric water have been traditionally included in its GWP (Houghton et al., 1990). Boucher et al. (2009) have quantified an indirect effect on CO_2 when fossil fuel methane is oxidised in the atmosphere. Shindell et al. (2009b) estimated the impact of reactive species emissions on both gaseous and aerosol forcing species and found that ozone precursors, including methane, had an additional substantial climate effect because they increased or decreased the rate of oxidation of SO_2 to sulphate aerosol. Studies with different formulations of sulphur cycle have found lower sensitivity (Collins et al., 2010).

Further indirect effects can be mediated via the biosphere when atmospheric constituents affect biospheric emissions or uptake of CO_2, methane and N_2O. Collins (2010) calculated that ozone precursors had an additional component to their GWP and GTP metrics due to the decreased productivity of plants under higher levels of surface ozone. The magnitude of this effect has only been calculated with one model.

8.1.2.6 New Metric Concepts and the Relationship to Economics

A number of new metric concepts have been introduced; often in an attempt to better account for economic aspects of metric applications. The use of purely physical metrics, in particular GWPs, in policy contexts has been criticized for many years by economists (Bradford, 2001; De Cara et al., 2008; Reilly, 1992). A prominent use of metrics is to set relative prices of greenhouse gases when implementing a multi-gas emissions reduction policy. In these applications, metrics play a fundamentally economic role, and theoretically appropriate metrics include economic dimensions such as mitigation costs, damage costs, and discount rates.

For example, if mitigation policy is set within a *cost-effectiveness* framework with the aim of making the least cost mix of emissions reductions across gases to meet a global average temperature target, the appropriate emissions metric is the "price ratio" (Manne and Richels, 2001). The price ratio, also called the Global Cost Potential (GCP; Tol et al., 2009), is defined as the ratio of the marginal abatement cost of a gas to the marginal abatement cost of CO_2 within a scenario that meets the target at least cost. Similarly, if policy is set within a *cost-benefit* framework, the appropriate index is the ratio of the marginal damages from the emission of a gas relative to the marginal damages of an emission of CO_2, known as the Global Damage Potential (Kandlikar, 1995). Both types of measures are typically determined within an integrated climate-economy model, since they are affected both by the response of the climate system to emissions as well as by economic factors.

Using strictly physical metrics such as the GWP, instead of economic metrics, within these settings will lead to higher mitigation costs, typically due to favouring reductions of short-lived gases more than would be economically optimal (van Vuuren et al., 2006). While the increase in costs at the global level may be relatively small (Aaheim et al., 2006; Johansson, 2011; Johansson et al., 2006; O'Neill, 2003) the implications at the project or country level could be significant (Shine, 2009).

Nonetheless, physical metrics remain attractive due to the added uncertainties in mitigation and damage costs introduced by economic metrics. Efforts have been made to view purely physical metrics such as GWPs and GTPs as approximations of more comprehensive economic indexes. GTPs, for example, can be interpreted as an approximation of a Global Cost Potential designed for use in a cost effectiveness setting (Shine et al., 2007; Tol et al., 2009). Quantitative values for GTPs, which indicate the contribution of an emission to warming in the target year, relative to CO_2, reproduce in broad terms several features of price ratios such as the initially low value of metrics for short-lived gases until a climate policy target is approached, see Figure 8.4, which show how the contributions from N_2O, CH_4 and BC to warming in the target year – relative to CO_2 – changes over time. Similarly, GWPs can be interpreted as approximations of the Global Damage Potential designed for use in a cost-benefit framework.

In both cases, a number of simplifying assumptions must be made for these approximations to hold. In the case of the GTP, one such assumption is that the influence of emissions on temperature change beyond the time at which a temperature target is reached does not affect the value of the metric. This highlights how even if one attempts to define a purely physical metric, there is an implicit economic valuation (in the case of GWP or GTP, no discounting through the time horizon H, with 100% discounting thereafter). A new metric, the Cost Effective Temperature Potential (CETP; Johansson, 2011) has been explicitly derived as an approximation to the GCP and is similar to the GTP but accounts for longer-term temperature effects. Like the GTP, it is based on the response of temperature to emissions and includes an assumption about the date at which a target is achieved. It also requires an assumption about one economic quantity, the discount rate, in order to account for longer-term temperature effects. Quantitative values for the CETP reproduce values of the GCP more closely than does the GTP (Johansson, 2011); more broadly, physical and economic indexes produce similar quantitative outcomes under some assumptions but not others (Johansson and Azar, 2011).

[INSERT FIGURE 8.4 HERE]

Figure 8.4: Global temperature change potential (GTP(t)) for methane, nitrous oxide and BC for each year from 2010 to the time at which the temperature change target is reached (2110). GTP(t) for CH_4 and N_2O on left axis; GTP(t) for BC on right axis. The (time-invariant) 100–year GWP is also shown for N_2O and CH_4 for comparison.

Other metrics have also been proposed that take into account temperature effects over a broader time horizon than does the GTP. For example, the Temperature Proxy (TEMP) index (Tanaka et al., 2009) is the index that, if used to convert an emission pathway of a non-CO_2 gas into an equivalent pathway of CO_2, would best reproduce the original pathway of temperature change over a specified time period. In this way it is similar to the Forcing Equivalent Index (FEI) (Manning and Reisinger, 2011; Wigley, 1998) which is designed to reproduce an original pathway of radiative forcing. TEMP values derived for the historical period have been shown to differ significantly from GWP_{100} values for CH_4 and N_2O, and to behave in a way that is qualitatively similar to GCP, GTP, and FEI (note that FEI values typically compare CO_2 forcing to non-CO_2 forcing, rather than the inverse as in other metrics, and so values fall over time rather than rise).

An integrated version of the GTP is another means of accounting for effects over a broader time horizon (Fuglestvedt et al., 2003; Shine, 2009). Such an approach was investigated quantitatively in the derivation of a GTP based on the time-averaged temperature response to a pulse emission (Mean Global Temperature Change Potential, MGTP (Gillett and Matthews, 2010)) and a GTP calculated in response to a sustained pulse emission (Sustained Global Temperature Change Potential, SGTP; Azar and Johansson, 2011). Both measures were shown to be quantitatively similar to GWPs if the time horizon is 100 years. O'Neill (2000) and Peters et al. (2011a; 2011b) present and discuss integrated Global Temperature change Potential (iGTP) and show that the values (except for the very short-lived species) are very close to the GWP values – which may give an interpretation of the GWP. One aspect of time dependent metrics like the GTP(t) that is lost in integrated measures is a reflection of the time path of the forcing, although it is possible that even integrated measures could also be given as function of time, which would recover this property.

8.1.2.7 Summary of Status

In addition to progress in understanding of GWP, new concepts have been introduced or further explored since AR4; both purely physical and some that combine perspectives from various disciplines. Among the alternatives, the GTP concept has reached the broadest application. The time variant version of GTP (Shine et al., 2007) introduces a more dynamical view of the contributions of the various species over time (in contrast to the static GWP).

As metrics use parameters further down the cause effect chain (Figure 8.2) the metrics become in general more relevant, but at the same time the uncertainties generally increase due to more degrees of freedom (though observations can sometimes constrain metrics further down the chain more than those above). The chosen type of metric and the adopted time horizon have strong effects on perceived impacts, costs and abatement strategies. While scientific choices of input data have to be made, there are value-based choices needed and this will strongly impact on the metric values and the calculated contributions of components, sources and sectors. In some economic metrics the value based choices are not always explicit and transparent, which may be desirable when metrics are used in a policy context.

All metrics discussed here (except the SFP (Bond et al., 2011) and RTP (Shindell and Faluvegi, 2010)) apply global mean values of RF or temperature as impact parameter. Consequently, they give no information about the spatial variability of the response. Many species, especially SLCF, produce a distinctly heterogeneous RF. Shine et al. (2005a) and Lund et al. (2011) discuss approaches to account for regional response patterns in global aggregated metrics.

In the application and evaluation of metrics, it is important to distinguish between two main types of uncertainty; structural and scientific. In order to improve the accuracy of metrics (and the calculated effects of emissions) the scientific uncertainty (such as lifetime, impulse response functions, RF, climate sensitivity, etc.) needs to be reduced. But one also needs to acknowledge the structural uncertainty which is linked to the application; e.g., using GWP as opposed to GTP will for many components have a much larger effect on calculated contributions than improved estimates of input parameters. Furthermore, metrics that account for regional variations in sensitivity to emissions or regional variation in response, could give a very different emphasis to various emissions.

As new metrics have continued to be developed and explored, a clear conclusion has been that there is no single best metric that is appropriate in all circumstances (Manning and Reisinger, 2011; Plattner et al., 2009; Shine, 2009; Tol et al., 2009). Rather, the most appropriate metric depends on the particular use to which it will be put and which aspect of climate change is considered relevant in a given context. As pointed out in several studies (Manne and Richels, 2001; Manning and Reisinger, 2011; Plattner et al., 2009; Reisinger et al., 2011; Shine et al., 2007; Tol et al., 2009), the time invariant GWP is not well suited for a policy context with a global concentration, forcing or temperature target. GTP(t) is generally more suitable, especially in that it captures temporal behavior. However, it only attempts to indicate global mean temperature change, and so a more complete evaluation of the consequences of a given policy choice would require additional metrics to evaluate the effects on other aspects of climate change such as regional temperature and precipitation changes, as well as on other environmental factors that will be influenced by these same emissions (such as air quality or ocean acidification).

8.2 Atmospheric Chemistry

8.2.1 Introduction

Besides carbon dioxide, most radiatively active compounds (greenhouse gases and aerosols) in the Earth's atmosphere are chemically active, meaning that atmospheric chemistry plays a large role in determining their burden and residence time. Chemical production and loss processes of a specific compound vary by time and location, depending on environmental conditions such as temperature, humidity and light. In addition, chemical reactions can take place on aerosols and in water (in cloud droplets or on aerosols or ice), which are referred to as heterogeneous reactions as they involve multiple phases. Finally, physical processes (wet removal and dry deposition) act on chemical compounds to further define their residence time in the atmosphere. Overall, the impact of atmospheric chemical composition on climate is through 1) radiative forcing, 2) aerosol-cloud interactions, 3) coupling with biogeochemical cycles and 4) deposition on the cryosphere.

Emissions of a multitude of chemically active and passive compounds come from a variety of natural and anthropogenic processes. Once released in the atmosphere, any chemically active compound will interact with other species in its immediate vicinity, the rate of reaction between these being a function of environmental conditions, the chemical nature of the species and their respective concentrations. Atmospheric chemistry is therefore a strongly interacting and highly variable system, leading to nonlinearities (Raes et al., 2010) and a wide range of timescales of importance (Isaksen et al., 2009).

8.2.2 Modelling

Global and regional modelling of atmospheric chemistry requires the numerical representation of emissions, chemical transformation, transport (by large-scale processes, e.g., wind and convection, and small-scale processes such as diffusion) and deposition.

As for the CMIP5 climate models (see discussion in Chapter 9), chemistry-climate models differ in their representation of physical processes and resolution, but also in the degree of complexity of chemistry (number of chemical species and reactions considered) and of coupling with the hydrologic cycle, representation of aerosols and the representation of natural emissions. While several CMIP5 models performed their simulations with interactive chemistry, there were still a significant number of models that used as input pre-computed distributions of radiatively active gases and/or aerosols. In order to assess the distributions of chemical species and their respective radiative forcing, many research groups participated in the Atmospheric Chemistry and Climate Model Intercomparison Project (ACCMIP, Table 8.1).

In all CMIP5/ACCMIP chemistry models, anthropogenic and biomass burning emissions are specified in all model simulations. More specifically, the simulations were performed with a single set of historical anthropogenic and biomass burning emissions (Lamarque et al., 2010) and one for each of the RCPs (van Vuuren et al., 2011) (Figure 8.5). This was designed to increase the comparability of simulations. However, because of the uncertainty in underlying fuel usage and emission factors (e.g., Bond et al., 2007; Lu et al., 2011), there is a considerable range (Granier et al., 2011) in the estimates and time evolution of recent

anthropogenic emissions (Figure 8.6). Historical reconstructions of biomass burning (wildfires and deforestation) also exhibit quite large uncertainties (Ito and Penner, 2005; van der Werf et al., 2010; Kasischke and Penner, 2004; Schultz et al., 2008). Finally, it is important to recognize that projections in the RCPs of biomass burning are only crudely represented, with no feedback between climate change and fires (Bowman et al., 2009; Thonicke et al., 2010; Pechony and Shindell, 2010). Evaluation of multiple models driven by these emissions thus provides a useful estimate of the uncertainty due to representation of physical processes in models, but does not incorporate uncertainty in historical emissions.

Table 8.1: List of models participating in ACCMIP with data presently available at the British Atmospheric Data Centre.

Research Centre	Model Name	CMIP5	Resolution	Chemistry	Vertical Extent	References
CICERO	OsloCTM2	N				
GISS	E2-R	Y				
GFDL	AM3	Y				
LSCE	LMDzORINCA	Y				
MeteoFrance	MOCAGE	N				
NCAR	CAM3.5	Y				
NCAR	CAM5.1	Y				
NCAR-LLNL	CESM1	Y				
NIWA	UM-CAM	N				
UKMO	HadGEM2	Y				

[INSERT FIGURE 8.5 HERE]

Figure 8.5: Time evolution of regional anthropogenic emissions 1850–2100 following RCP2.6 (blue), RCP4.5 (green), RCP6 (magenta) and RCP8.5 (red). Historical emissions (1850–2000) are from Lamarque et al. (2010). Regional estimates for United States of America, Western Europe, China, India and South America are shown, in addition to the global total.

[INSERT FIGURE 8.6 HERE]

Figure 8.6: Time evolution of regional anthropogenic emissions 1980–2010 for black carbon. Black dots indicate emissions from additional inventories (adapted from Granier et al., 2011).

The ACCMIP simulations (Table 8.2) were defined to provide information on the long-term changes in atmospheric composition with a few, well-constrained atmospheric simulations. These were used for extensive model evaluation. Research groups involved in global three-dimensional chemistry-climate modelling were openly invited to participate to this project; however, because of the nature of the simulations (pre-industrial, present-day and future climates), only a limited number of chemistry-transport models participated in the ACCMIP project, which instead drew primarily from the same GCMs as CMIP5.

Table 8.2: List of ACCMIP experiments.

Historical simulations									
Emissions/configuration	1850	1890	1910	1930	1950	1970	1980	1990	2000
Emissions and SSTs/GHGs for given year	C	1	1	C	1	1	C	1	C
Year 2000 emissions/1850 SSTs & GHGs				1			1		C

Future simulations				
Emissions/configuration	2010	2030	2050	2100
RCP2.6		C	1	C
RCP4.5	1	1	1	1
RCP6.0	C	C	1	C
RCP8.5		C	1	C
Year 2000 emissions/2100 RCP8.5 SSTs & GHGs		C		C

Notes:

C = core
1 = Tier 1
blank = not requested

8.2.3 Chemical Processes and Trace Gas Budgets

8.2.3.1 Tropospheric Ozone

The RF from tropospheric ozone is strongly height- and latitude-dependent (Lacis and Hansen, 1974; Worden et al., 2008). Consequently, to compute the forcing since pre-industrial times, it is necessary to know its full three-dimensional distribution, which can only be attained through simulations using global models.

Tropospheric ozone is a by-product of the oxidation of carbon monoxide, methane and non-methane hydrocarbons in the presence of nitrogen oxides. Ozone production is usually limited by the supply of HO_x ($OH + HO_2$) and NO_x ($NO + NO_2$) (Jacob and Winner, 2009). Because of the catalytic role of nitrogen oxides in ozone production (with ozone formation occurring as a result of photolysis of NO_2), tropospheric ozone chemistry is strongly nonlinear in its dependence on nitrogen oxides (Seinfeld and Pandis, 2006). As emissions of these precursors have increased (Figure 8.5), tropospheric ozone has increased since pre-industrial times (Volz and Kley, 1988; Marenco et al., 1994) and over the last decades (Parrish et al., 2009; Cooper et al., 2010). Its major loss pathway is through ozone photolysis (to O^1D, followed by reaction with water vapour), leading to couplings between stratospheric ozone (photolysis rate being a function of the overhead ozone column) and climate change (through water vapour). Observed surface ozone abundances typically range from less then 10 ppb over the remote tropical oceans to more than 100 ppb downwind of highly polluted regions. Its residence time in the troposphere varies strongly with season and location. It can be as little as one day in the boundary layer to several weeks in the remote atmosphere, leading to a global estimated lifetime of approximately 25 days.

For conditions relevant to the recent decade, the various components of the budget of tropospheric ozone (Figure 8.7) are estimated from the ACCMIP simulations and other model simulations since AR4 (Table 8.3). In particular, most recent models define a globally and annually averaged tropospheric ozone burden of ≈300 ± 50 Tg (or equivalently 32 Dobson Units (DU); 1 Dobson Unit corresponds to 2.69×10^{16} ozone molecules for every square centimetre of area at the base of an atmospheric column). A portion of inter-model variations arises from differences in the definition of the tropopause. The global annual tropospheric ozone burden estimate has not significantly changed since the ACCENT-AR4 estimates (Stevenson et al., 2006), and is in reasonable agreement with satellite-based OMI-MLS (Ziemke et al., 2011) and TES (Osterman et al., 2008) climatologies.

Table 8.3: Summary of model and observations of tropospheric ozone budget estimates for 2000 conditions. All studies since AR4 with explicit tropospheric ozone budget terms are listed here. Additional ACCMIP results will be included when fully available.

Burden	Prod	Loss	Dep	STE	Reference
Model					
323					(Archibald et al., 2011)
330	4876	4520	916	560	(Kawase et al., 2011)
334	3826	3373	1286	662	(Zeng et al., 2010)
324	4870	4570	801	502	(Wild and Palmer, 2008)
372	5042	4507	884	345	(Horowitz, 2006)
349	4384	3972	808	401	(Liao et al., 2006)
292	4758	4157	1278	677	(Hauglustaine et al., 2005)
307 ± 38	3948 ± 761	3745 ± 554	902 ± 255	636 ± 273	(Wild, 2007)(summary of 33 studies)
				515	(Hsu and Prather, 2009)
				655	(Hegglin and Shepherd, 2009)

Obs.	
333	(Fortuin and Kelder, 1998)
327	(Logan, 1999)
325	(Ziemke et al., 2011) value is from 60S–60N
310–351	(Osterman et al., 2008) value is from 60S–60N

[INSERT FIGURE 8.7 HERE]
Figure 8.7: Schematic representation of the tropospheric ozone budget. Numbers are approximative and will be finalized with ACCMIP results combined with Table 8.1. Adapted from The Royal Society (2008).

To establish credibility in simulating the recent atmospheric composition, model simulations for present-day conditions or the recent past are evaluated (Figures 8.8 and 8.9) against frequent ozonesonde measurements (Logan, 1999; Tilmes et al., 2011) and additional surface and aircraft measurements. The ACCMIP model simulations indicate a reasonable representation of tropospheric ozone, especially when the multi-model ensemble mean (or median) is considered. The overall range of model results is slightly smaller than the ACCENT-AR4 simulations, most likely coming from the use of common anthropogenic and biomass burning emission datasets. There are however additional aspects (natural emissions, speciation of non-methane hydrocarbons, degree of sophistication of simulated chemistry, depositional processes) that lead to inter-model differences.

[INSERT FIGURE 8.8 HERE]
Figure 8.8: Comparisons between observations and simulations for the monthly mean ozone concentration. (Stevenson et al., 2006)-type plot for ACCMIP results.

[INSERT FIGURE 8.9 HERE]
Figure 8.9: Comparison of ACCMIP ensemble mean (second column) with observations (left column). Bias (in %) and correlation are shown in columns 3 and 4.

Estimates of the ozone chemical sources and sinks are however more uncertain, with a net chemical production (production *minus* loss) of approximately 300 Tg yr^{-1} (Table 8.3). As noted in Stevenson et al., (2006) and Wu et al. (2007), since TAR and to some extent AR4, there has been a continuous increase in the overall production and loss contributions owing in part to the inclusion of additional hydrocarbon chemistry. In the ACCENT-AR4 model simulations, deposition of ozone to the surface was estimated to be in the range of 902 ± 255 Tg yr^{-1}. Finally, transport across the tropopause represents a net influx of ozone into the troposphere of 636 ± 273 Tg yr^{-1} based on the ACCENT-AR4 results. Additional model estimates (Hegglin and Shepherd, 2009; Hsu and Prather, 2009) fall within that range, as do estimates based on observations (Gettelman et al., 1997; Murphy and Fahey, 1994). In comparison, the estimated tropospheric ozone budget terms for 1850 indicates that the pre-industrial net chemical production was much smaller, due to the much smaller anthropogenic emissions of nitrogen oxides and other ozone precursors (Figure 8.5).

Similar to AR4, global chemistry-climate models used in ACCMIP (Table 8.1) provide an estimated tropospheric ozone increase (Figure 8.10 and Table 8.4) from 1850 to 2000 of approximately 8.9 ± 0.8 DU. It is important to note that, while the standard deviation among model estimates for the 1850 and 2000 estimate is more than 2 DU, the ozone field responds quite similarly to the changes in emissions and environmental conditions between 1850 and 2000.

Table 8.4: ACCMIP model results for tropospheric ozone column (in DU) in 1850 and 2000. The increase is shown as the last column. Multi-model mean and standard deviation are also included.

Model	1850	2000	Delta
A	19.8	29.2	9.6
B	23.0	32.2	9.2
C	24.1	33.4	9.3

D	21.0	29.8	8.8
E	27.6	34.9	7.3
F	23.4	32.5	9.1
Mean	23.2	32.0	8.9
Std.dev	2.7	2.2	0.8

[INSERT FIGURE 8.10 HERE]

Figure 8.10: Time evolution of tropospheric ozone column (in DU) from 1850 to 2005 from ACCMIP results and Kawase et al. (2011). The OMI-MLS (Ziemke et al., 2011) and TES (Osterman et al., 2008) satellite-based climatologies are also shown, along with the ACCENT-AR4 results.

8.2.3.2 Stratospheric Ozone and Water Vapour

Stratospheric ozone has experienced significant depletion since the 1970s due to bromine and chlorine-containing compounds (Solomon, 1999). Most of the ozone loss is associated with the long-lived bromine and chlorine containing compounds (chlorofluorocarbons and substitutes) released by human activities. This is in addition to a background level of natural emissions of short-lived halogens from oceanic and volcanic sources, which have been recently estimated to lead to an additional input of 4–8 ppt of inorganic bromine (Bry) (Salawitch et al., 2005; WMO, 2011). Increased methane and nitrous oxide also affect stratospheric composition, while increased CO_2 affects stratospheric temperature and hence ozone-related chemisty. In the absence of significant halogens in the stratosphere, nitrous oxide becomes the largest contributor to ozone loss (Ravishankara et al., 2009). Indeed, nitrous oxide is the main source of NO and NO_2 in the stratosphere, which are key to an ozone-destroying catalytic cycle.

Overall the major ozone losses over Antarctica since the 1970s and over the Arctic in recent years (especially the winter of 2010–2011, Manney et al. (2011)) provide a strong localized forcing with potential impacts into the troposphere (WMO, 2011; Polvani et al., 2011).

With the advent of the Montreal Protocol, emissions of CFCs and replacements have strongly declined (Montzka et al., 2011) and signs of ozone stabilization (i.e., slowing of ozone decline attributable to changes in ozone-depleting substances) have already occurred (WMO, 2011). In particular, the chemistry-climate models with resolved stratospheric chemistry and dynamics used in CCMVal provide an estimated global mean total ozone column recovery to 1980 levels to occur in 2032 (for the multi-model mean) under the A1B scenario (Eyring et al., 2010b; WMO, 2011). Increases in the stratospheric burden and in the stratospheric circulation will directly lead to an increase in the stratosphere-troposphere flux of ozone (Shindell et al., 2006b; Hegglin and Shepherd, 2009). This is clearly seen in RCP8.5 simulations, with the impact of increasing tropospheric burden (Kawase et al., 2011; Lamarque et al., 2011). [PLACEHOLDER FOR SECOND ORDER DRAFT: ACCMIP results will be added here when available].

Water vapour reaches the stratosphere through the very cold tropical tropopause (Brewer, 1949), leading to overall dry conditions (3–4 ppmv). In addition, in the stratosphere, the oxidation of methane results in the formation of water vapour. Consequently, between 1950 and 2000, stratospheric water vapour has experienced an estimated increase of 1% yr^{-1} (Rosenlof et al., 2001) from changes in the amount of water vapour penetrating the stratospheric through the tropical tropopause and in the amount of stratospheric methane. The specific role of increase in stratospheric methane is estimated to be about one third of the total (Rohs et al., 2006) . The water vapour increases have been most significant since 1980 (Scherer et al., 2008; Solomon et al., 2010b; WMO 2011).

8.2.3.3 Methane

Methane is the largest single contributor to anthropogenic RF after carbon dioxide (Montzka et al., 2011). Its concentration has increased by 2.5 times since pre-industrial times to reach a global average value of approximately 1.8 ppm (Dlugokencky et al., 2009; Dlugokencky et al., 2011); (Rigby et al., 2008) and some of the projections are indicating a further doubling by 2100 (Figure X in Chapter 2). In recent decades (from 1990 to 2005), the observed methane concentration has been rather steady, although there has been an

increase in the most recent years. Present-day methane emissions are of natural (1/3) and anthropogenic (2/3) origin, with an estimated total of 500 Tg yr^{-1} (Bergamaschi et al., 2009).

Natural emissions come primarily from wetlands with an amplitude of 150–180 Tg yr^{-1} (Bergamaschi et al., 2009; Bousquet et al., 2006), which respond to climate through variations in temperature and water table. While present-day emissions are dominated by the tropics, the potential melting of the permafrost (Lawrence and Slater, 2005) could provide extensive new areas for methane production at high latitudes (Walter et al., 2006; Schuur et al., 2009), although recent observations indicate a drying (Jung et al., 2010). Additional oceanic polar sources have also been recently observed (Shakhova et al., 2010). Anthropogenic emissions are a mix of agriculture (primarily from animal and rice activities) and fossil-fuel related activities (oil and gas extraction, distribution, mining) as well as municipal waste and wastewater. The main sink of methane is through its reaction with the hydroxyl radical OH in the troposphere, leading to an estimated tropospheric chemical lifetime of approximately 9 years (Montzka et al., 2011) although bacterial uptake provides an additional small, less well quantified loss process, with another small sink from chemical loss in the stratosphere. The chemical coupling between OH and CH_4 is so strong that it leads to a significant amplification of the emission impact; i.e., increasing methane emissions decreases tropospheric OH which in turn increases the methane lifetime and therefore its burden. The calculated OH feedback, $\delta\ln(OH)/\delta(\ln(CH4),))$, was estimated in Chapter 4 of TAR to be –0.32, leading to a 0.32% decrease in OH for a 1% increase in methane. A more recent study (Fiore et al., 2009) provides a slightly smaller value (-0.25 ± 0.03).

Strong interannual variability in both sources and sinks (Bousquet et al., 2006; Prinn et al., 2005) makes the understanding of recent variations incomplete, with contradicting interpretations (Aydin et al., 2011; Kai et al., 2011). Analysis of methane isotopes could lead to better constraints of the budget but is presently hampered by the scarcity and lack of long-term measurements.

The most recent model estimates of the present-day methane lifetime with respect to tropospheric OH vary quite widely (9.5 ± 2 years; Figure 8.11), similar to Bergamaschi et al. (2009); Fiore et al. (2009); Shindell et al. (2006d). This wide range reflects our lack of understanding or modelling capability for OH and/or the distribution and variability of natural sources of methane. The primary source of tropospheric OH is initiated by the photodissociation of O_3, followed by reaction with water vapour (Wennberg, 2006), with OH being involved in many of the fast reactions in the troposphere. Its main sinks are reactions with methane and carbon monoxide. As such, it is expected that OH will have changed since pre-industrial times. Clearly, the diverging model estimates also apply to the change in methane lifetime since 1850 (Figure 8.11). It is perhaps not surprising that OH trends vary greatly across models as they are sensitive to the balance between the influence of increasing NO_x emissions, which tend to increase OH, and increasing emissions of methane, non-methane hydrocarbons and carbon monoxide, which decrease OH. A partial explanation for these various responses to emission changes can be found in the degree of representation of chemistry in chemistry-climate models. Indeed, (Archibald et al., 2010a) showed that the response of OH to increasing nitrogen oxides strongly depends on the treatment of hydrocarbon chemistry in a model.

[INSERT FIGURE 8.11 HERE]

Figure 8.11: Time evolution of tropospheric methane lifetime (with respect to OH) from CMIP5 chemistry-climate models.

Recent theoretical studies and field experiments have shown that model simulated OH concentrations in regions of high isoprene emissions (a reactive hydrocarbon of biogenic origin) and low nitrogen oxides (NO_x) emissions are strongly underestimated (Lelieveld et al., 2008). All these point to a need to improve the understanding of OH recycling (or regeneration) under these conditions. At this point, there is no consensus as to which chemical processes are responsible for maintaining higher levels of OH (Crounse et al., 2011; Paulot et al., 2009; Peeters et al., 2009; Taraborrelli et al., 2009). While some preliminary studies (Archibald et al., 2010b; Stavrakou et al., 2010) are exploring the impact of some of these new chemistry pathways, no impact on methane lifetime can be assessed at this point.

8.2.3.4 Nitrous Oxide (N_2O)

Present-day nitrous oxide concentration is approximately 322 ppb (Montzka et al., 2011), almost 20% above its pre-industrial level. Anthropogenic emissions represent around 40% of the present-day global estimates, mostly from agricultural (fertilizer) and fossil-fuel activities. Natural emissions come mostly from terrestrial microbial activity in the soil (itself subject to increasing fertilizer use and nitrogen deposition). The main sink for nitrous oxide is through photolysis and oxidation reactions in the stratosphere, leading to a lifetime of 120 years (Prather and Hsu, 2010).

8.2.3.5 Montreal Protocol Gases and Substitutes and Other Long-Lived Gases

Primary ozone depleting substances (ODSs, as the stratospheric ozone hole is their most significant environmental impact, WMO, 2011) are also greenhouse gases. Most of those compounds (chlorofluorocarbons, carbon tetrachloride, methyl chloroform, methyl bromide and halons) do not have natural emissions and, because of the application of the Montreal Protocol, total emissions of ODSs have sharply decreased since the 1990s to an aggregate emission of approximately 1 $GtCO_2$–eq yr^{-1} based on the GWP(100) metric (Montzka et al., 2011). The main loss is through photolysis in the stratosphere (WMO, 2011). Substitutes for the primary ODSs (hydrochlorofluorocarbons, HCFCs, and hydrofluorocarbons, HFCs) are also potent greenhouse gases (WMO, 2011) and their global concentration has steadily risen over the recent past (Montzka et al., 2010; WMO, 2011; see Chapter 2).

8.2.3.6 Aerosols

Aerosol particles are present in the atmosphere with size ranges from a few nanometres to tens of micrometres. They are the results of direct emission (primary aerosols: black carbon, primary organic, sea-salt, dust) into the atmosphere or as products of chemical reactions (secondary aerosols: sulphate, nitrate, ammonium and secondary organic aerosols (SOA)) occurring in the atmosphere. The formation of sulphate is a result of the reaction of sulphur dioxide in both gas and aqueous-phase processes. Ammonia (NH_3) and nitric acid (HNO_3) can react to form ammonium nitrate (NH_4NO_3); it is formed in areas with high ammonia and nitric acid concentrations and low sulphate concentrations. In the presence of large amounts of sulphate, $(NH_4)_2SO_4$ is the preferred form of sulphate and only the portion of NH_4 not used is available for the formation of ammonium nitrate (Seinfeld and Pandis, 2006). SOA are the result of chemical reactions of non-methane hydrocarbons (and their products) with the hydroxyl radical (OH), ozone, nitrate (NO_3) or photolysis (Hallquist et al., 2009); there is tremendous complexity and still much uncertainty in the processes involved in the formation of secondary-organic aerosols (Carslaw et al., 2010; Hallquist et al., 2009) Additional information can be found in Chapter 7.

Once generated, the size and composition of aerosol particles can be modified by additional chemical reactions, condensation or evaporation of gaseous species and coagulation (Seinfeld and Pandis, 2006) . It is this set of processes that defines their physical, chemical and optical properties, and hence their impact on radiation and clouds, with large regional and global differences (Jimenez et al., 2009; Chapter 7). Furthermore, their distribution is affected by transport and deposition, defining a residence time in the atmosphere of usually a few days (Textor et al., 2006).

The direct effect of aerosols on solar and terrestrial radiation depends on their chemical composition, and aerosols are characterized by their refractive index, of which the real (imaginary) part defines the nonabsorbing (absorbing) component. The net effect of their interaction with radiation therefore ranges from mostly reflective (sulfate particles) to mostly absorbing (black carbon) (UNEP, 2011; Goto et al., 2011) The indirect effect of aerosols (through clouds, Chapter 7) is also affected by their chemical composition and more specifically their hygroscopicity.

Long-term records from ice cores indicate that, in the high-latitude Northern Hemisphere (at least in and downwind of Greenland), black carbon was actually higher in the early part of the 20th century than later on (McConnell et al., 2007). In contrast, at similar sites, sulphate was found to peak around 1980 (Lamarque et al., 2010). On the other hand, as a result of recent regional increases in emissions, sulphate aerosols (Zhao et al., 2011) and black carbon (Xu et al., 2009) have been found to still be increasing in Asian ice cores.

Since AR4, most of the development in the chemistry of aerosols has focused on the formation and impact of SOA (Hallquist et al., 2009). It has been recently discussed that the rate of production of biogenic secondary

organic aerosols is not independent from anthropogenic emissions (Hoyle et al., 2011), with nitrogen oxides possibly playing an important role (Carlton et al., 2010; Pye et al., 2010).

8.2.4 Open Questions and Future Directions for Atmospheric Chemistry

8.2.4.1 Ranges in Emissions and Associated Uncertainties

In the case of anthropogenic and biomass burning emissions, the CMIP5 simulations have used a single set of emissions (Lamarque et al., 2010). While there is still inter-model variation in natural emissions, it is clear that a single set of emissions (as opposed to using the full range of estimates, see Figure 8.6) limits the range of simulated conditions. Furthermore, the historical estimates were constructed independently from the land use-land cover change (Hurtt et al., 2011) used for the carbon cycle simulations. All these point to the need of additional studies that would expand the range of simulated tropospheric chemistry changes during the historical and future periods.

8.2.4.2 Importance of Missing Tropospheric Chemistry

Conventional ozone photochemistry cannot account for the observed ozone variability in the tropical marine boundary layer (Read et al., 2008). Indeed, measurements of low ozone levels (<10 ppbv) and large diurnal variability of surface ozone have been reported over the tropical regions (Saiz-Lopez et al., 2011). It has been suggested that reactive halogen species released into the atmosphere by the photodecomposition of organohalogens (including iodine-containing species) and via autocatalytic recycling on sea-salt aerosols contributes to ozone destruction in this environment (Read et al., 2008). The limited number of studies available indicates that it is likely that tropospheric halogen chemistry is of importance to the marine boundary layer, but further studies are needed to fully explore the range of impacts on tropospheric chemistry and climate. Biases in near-surface ozone in marine areas would have only very minor impacts on RF, however, as the forcing sensitivity per unit ozone change is very small near the surface (Lacis and Hansen, 1974).

8.2.4.3 Coupling with Biogeochemical Cycles

Coupling of atmospheric chemistry with biogeochemical cycles can occur through the impact of atmospheric composition on biological activity, with potential feedbacks through biogenic emissions (Arneth et al., 2010b; Carslaw et al., 2010). Biogenic emissions of VOCs are of great importance for the tropospheric ozone budget and secondary-organic aerosols (Goldstein and Galbally, 2007; Hallquist et al., 2009). It is well established that their emissions are strongly regulated by temperature, moisture availability and light (Guenther et al., 2006; Schurgers et al., 2009). There is now some field evidence that isoprene emissions are also inversely dependent on the atmospheric CO_2 concentration; i.e., emissions decrease moving to a high-CO_2 environment (Arneth et al., 2007; Young et al., 2009). It is also well established that ozone detrimentally affects plant productivity (Ashmore, 2005), albeit estimating its impact on chemistry and climate, while possible significant, is still limited to a few studies (Sitch et al., 2007b; UNEP, 2011). Finally, a field study (Kiendler-Scharr et al., 2009) has indicated that isoprene emissions could actually inhibit aerosol formation; more experimental work is needed to assess the representativity of this observation.

The biogenic emissions of primary biological aerosol particles (bacteria, viruses, fungal spores, plant debris and algae) are also being considered (Carslaw et al., 2010) but their overall role in the climate system is still a matter of research. Also, the knowledge of oceanic biological response to composition and climate change is very limited, outside limited studies on dimethyl sulfide (CH_3SCH_3, DMS) (Cameron-Smith et al., 2011; Carslaw et al., 2010) and dust/iron fertilization experiments.

The land biosphere responds strongly to nitrogen deposition. Up to a level of approximately 2000 mg(N)/m^2, nitrogen deposition is believed to provide additional fertilizing to enable additional CO_2 uptake (Reay et al., 2008). Since AR4, the coupling of soil nitrogen cycle with the carbon cycle has demonstrated the importance of nitrogen deposition (Chapter 4; Thornton et al., 2009; Zaehle et al., 2010). However, this coupling likely leads to release of N_2O (Zaehle et al., 2011), offsetting the potential gains from higher CO_2 uptake.

Methane emission from wetlands is a potentially very important feedback between chemistry and climate (Gedney et al., 2004; Shindell et al., 2004) as this source represents approximately 30–40% of the present-day total methane emissions. However, owing to the difficulties in representing the small-scale processes associated with wetland formation, water table and methane production (Walter and Heimann, 2000), projections of future wetland emissions are quite uncertain (Arneth et al., 2010a). In addition, there is evidence that increasing sulphur deposition, through its perturbation of redox cycles, reduces wetland methane emissions. Another major concern is the possible degradation or thaw of terrestrial permafrost due to climate change, where the amount of carbon stored in permafrost, the rate at which it will thaw, and the ratio of methane to carbon dioxide emissions upon decomposition form the main uncertainties (O'Connor et al., 2010). Finally, while additional emissions from methane clathrates (land or ocean) are potentially very large, they are not expected to be a significant threat within the next century (Krey et al., 2009).

8.3 Natural Radiative Forcing Changes: Solar and Volcanic

There are several natural drivers of climate change operating on multiple timescales. Solar variability takes place at many timescales as the radiant energy output of the Sun changes. The astronomical alignment between the Sun and Earth caused RF, but this is substantial only at millennial and longer timescales. Volcanic forcing is highly episodic, but can have dramatic, rapid impacts on climate. Asteroid impacts are rare, but are thought to have played a large role in several climate change events in Earth's history. This section discusses solar and volcanic forcings, the two dominant natural contributors of climate change since the preindustrial.

8.3.1 Radiative Forcing of Solar Irradiance on Climate

The instantaneous RF at TOA is the solar irradiance change divided by 4 and multiplied by ~0.7: The Earth absorbs solar radiation as $(1-A)I/4$, where A is the albedo (~0.3) and I is the Total Solar Irradiance (TSI). The factor of 4 arises since the Earth intercepts $\pi R^2 I$ energy per unit time (R is the mean Earth radius), but this is averaged over the surface area of the Earth $4\pi R^2$. In AR4 a best solar forcing estimate of 0.12 W m^{-2} was given between 1750 and the present. Similar to previous IPCC estimates this forcing was estimated as the instantaneous RF at TOA. However, due to wavelength-albedo dependence, solar activity-wavelength dependence and absorption within the stratosphere and the resulting stratospheric adjustment, the RF is reduced to 78% of the TOA instantaneous RF, this last factor has an uncertainty of ~5% (Gray et al., 2009). For a consistent treatment of all forcing agents, hereafter we use RF while numbers quoted from AR4 will be provided both as RF and instantaneous RF at TOA.

8.3.1.1 Observed Variations of TSI

8.3.1.1.1 Satellite measurements

Since 1978, several independent space-based instruments have directly measured the TSI. Three main composite series were constructed (see Figure 8.12) referred to as the Active Cavity Radiometer Irradiance Monitor (ACRIM) (Wilson and Mordvinov, 2003), the Institut Royal Meteorologique Belgique (IRMB) (Dewitte et al., 2004) and the Physikalisch-Meteorologisches Observatorium Davos (PMOD) (Frohlich, 2006). The differences among them have the most important implications for the long-term trends: ACRIM gives a rise up until 1996 and a subsequent decline, IRMB presents an upward trend and PMOD shows a decline since 1985 which unlike the other two composites, follows the solar-cycle-averaged sunspot number (Lockwood, 2010). Analysis of instrument degradation and pointing issues (Frohlich, 2006), independent modeling based on solar magnetograms (Wenzler et al., 2006) and long-term trend calculations (Lockwood, 2010) suggest that PMOD is more accurate than the other composites.

Variations of ~0.1% were observed between the sunspot maximum and sunspot minimum of the 11-year solar activity cycle (SC) in PMOD (Frohlich, 2006), and were also obtained in a recent average of the three composites mentioned above (Frohlich, 2006). This modulation is mainly due to a compensation between relatively dark sunspots, bright faculae and bright network elements (Foukal et al., 2006). The PMOD declining trend since 1985 is evidenced in the lower peak seen during SC 23 (1996–2009) minimum compared to the previous two minima: the mean for September 2008 is 1365.26 ± 0.16 W m^{-2}, while in the minimum of 1996 it was 1365.45 ± 0.10 W m^{-2} and in the minimum of 1986 it was 1365.57 ± 0.01 W m^{-2}

(Frohlich, 2009), then between the minima of 1986 and 2008 there is a negative RF of −0.04 ± 0.02 W m^{-2}. Using the PMOD annual data, a negative RF between 1986 and 2010 of –0.02 ± 0.01 W m^{-2} is calculated.

The more recent Solar Radiation and Climate Experiment (SORCE) measurements indicates a TSI of 1360.8 ± 0.5 W m^{-2} during 2008 (Kopp and Lean, 2011), which is 4.46 W m^{-2} lower than the PMOD results. Following extensive comparisons between ground-based versions of the instruments and laboratory references, validation of aperture area calibrations using flight spares from each instrument, and corrections for diffraction from view-limiting aperture (a correction not applied by all instrument teams), it was concluded that uncorrected scattering and diffraction in the earlier instruments produces erroneously high TSI values. Then Kopp and Lean (2011) conclude that the SORCE TSI value is the most probable value because it is validated by both a NISR-calibrated cryogenic radiometer and a new state-of-the-art TSI radiometer facility. If this lower measurements probe to be correct, then the general circulation models are calibrated to incorrectly higher values. However, given the shortness of the series (measurements started in 2004), a maximum-to-minimum RF is not yet published from SORCE. As the maximum to minimum percentage change is well-constrained from observations, and historical variations are calculated as percentage changes relative to modern values, a revision of the TSI affects RF by the same percentage as it affects TSI. The downward revision of TSI, being 0.3%, thus has a negligible impact on RF.

[INSERT FIGURE 8.12 HERE]

Figure 8.12: Annual average **c**omposites of measured Total Solar Irradiance: The Active Cavity Radiometer Irradiance Monitor (ACRIM) (Willson and Mordvinov, 2003) , the Institut Royal Meteorologique Belgique (IRMB) (Dewitte et al., 2004) and the Physikalisch-Meteorologisches Observatorium Davos (PMOD) (Frohlich, 2006).

8.3.1.2 TSI Variations Since Preindustrial Time

The year of 1750 is used as the nominal representation of the preindustrial atmosphere. Considering reconstructions of TSI, from 1750 to 2005, the AR4 indicates that the RF was 0.09 W m^{-2} (0.12 W m^{-2} for instantaneous forcing at TOA) with a range of estimates of 0.05–0.23W m^{-2}. Using two recent reconstructions, the Krivova et al. (2010), based on the evolution of the total solar photospheric magnetic flux from the sunspot record, and the Steinhilber et al. (2009) based on linear extrapolations of an empirical relation between open flux and TSI (the open flux is obtained from ice core ^{10}Be), these reconstructions show an average positive RF of 0.07 W m^{-2} with a range of 0.02–0.12 W m^{-2} between 1750 and 2010. This average value is found from adjusting a linear trend to the 11-years running mean of each series (as the correlation between both series is higher than 0.5, we can average the trends), the range is given by the RF of each reconstruction. An analysis of TSI reconstructions using various proxy data (see Figure 8.13**)** shows a similar range (Schmidt et al., 2011). Hence we adopt this mean and range for the AR5. Although this RF is close to the AR4 estimate, the upper and lower limits of its range are each reduced to nearly half their AR4 values. Given the low agreement (a factor of ~5 difference across the range) and medium evidence, this RF value has a low confidence level.

Gray et al. (2010) point out that choosing the years of 1700 or 1800 would substantially increase solar RF while leaving the anthropogenic forcings essentially unchanged. These years are within the Maunder and Dalton solar activity minima, respectively. For the Maunder minimum the AR4 RF (Table 2.10) shows a range of ~0.08–0.22 W m^{-2}; the estimates based on irradiance changes at cycle minima derived from brightness fluctuations in Sun-like stars are not included in this range because they are no longer considered valid (e.g., Krivova et al., 2007). The reconstructions in Schmidt et al. (2011) indicate a Maunder minimum-to-present RF range of 0.08–0.18 W m^{-2}, which is within the AR4 range although narrower. Choosing the year 1850 we find solar activity conditions similar to those in 1750.

The recent analysis of Shapiro et al. (2011) falls outside this range. They find a very large decrease in solar output during the Maunder Minimum, assuming that in addition to the cyclic variation in active regions, there is a background change in the Sun so that during the Maunder Minimum every part of the Sun was only as bright as the dimmest part of the modern ‘quiet’ area observations. Though possible, this is certainly not the case for the modern solar minima that we have observed, during which there is a still a large amount of magnetic activity in ‘quiet’ areas. Shapiro et al. (2011) then assume that the background ‘quiet’ areas changed through time with the long-term average solar magnetic field, and therefore follow ice core isotope records (an ‘active’ region indicator). There are no observations to support this link, and there are no proxies

for the 'quiet' areas themselves, so this remains quite speculative. Studies of magnetic field indicators suggest that changes over the 19th and 20th centuries were in fact more modest than those assumed in the Shapiro et al. (2011) reconstruction (Lockwood and Owens, 2011; Svalgaard and Cliver, 2010). Analysis by Feulner (2011) finds that simulations driven by such a large solar forcing are inconsistent with reconstructed and observed historical temperatures, while use of a forcing in line with the range presented here is consistent with instrumental and proxy records. Hence we do not include the larger forcing within our assessed range.

Schrijver et al.(2011) instead argue that the recent 2008–2009 solar minimum, which was unusually long by modern standards and contained many days with a nearly sunspot free Sun, demonstrates that even during an extended quiet period, a minimum level of activity is maintained that is greater than many have assumed. Though the modern aspect of their study is based on observations, it is a leap to infer that the recent minimum was analogous to the Maunder Minimum (which the authors acknowledge). Hence the Maunder to modern forcing based on their work is only ~0.1 W/m^2. Foukal et al. (2011) argue that the relationship between solar activity and solar output becomes non-linear at low sunspot numbers, leading to an intermediate level of Maunder to modern forcing which is of the order of the RF range given above. The large variation between these recent estimates is consistent with our low confidence level for solar forcing over the preindustrial to present-day (though confidence is higher for the last three decades).

[INSERT FIGURE 8.13 HERE]

Figure 8.13: Annual mean reconstructions of Total Solar Irradiance since 1750: Wang et al. (2005), with and without an independent change in the background level of irradiance, Steinhilber et al. (2009) (here we show an interpolation of their 5-year time resolution series), The Krivova et al. (2010) time series , and the PMOD composite time series (Frohlich, 2006).

8.3.1.3 Attempts to Estimate Future Centennial Trends of TSI

Proxy records of solar activity such as the ^{10}Be and ^{14}C cosmogenic radioisotopes of the last 10,000 years (Horiuchi et al., 2008; Stuiver et al., 1998; Vonmoos et al., 2006) show several secular minima and maxima. Frequency analysis of these series (Tobias et al., 2004) present several significant long-term periodicities such as the ~80–100 years (Gleissberg cycle), ~200 years (de Vries or Suess cycle) or the ~2300 years (Hallstatt cycle), motivating attempts to estimate future trends in solar activity.

Cosmogenic isotope and sunspot data (Rigozo et al., 2001; Usoskin et al., 2003) reveal that we are within a grand activity maximum that began ~1920. However, SC 23 showed a previously unseen activity decline (McComas et al., 2008; Russell et al., 2010; Smith and Balogh, 2008). Most current estimations suggest that the forthcoming solar cycles will have lower TSI than the previous ones (Abreu et al., 2008; Lockwood et al., 2009; Rigozo et al., 2010; Russell et al., 2010; Velasco-Herrera, 2011). Mean estimates of the TSI between the modern maximum and the 21st century minimum indicate a RF of no more than ~0.2 W m^{-2} (Jones et al., 2011; Velasco-Herrera et al., 2011). However, much more evidence is needed and at present we have a very low confidence concerning future solar forcing estimates. Nevertheless, if there is such a diminishing solar activity, the Earth´s temperature will continue to be dominated by the much larger projected increased forcing due to greenhouse gases.

8.3.1.4 Variations in Spectral Irradiance

8.3.1.4.1 Satellite measurements

Solar spectral irradiance (SSI) variations in the far (120–200 nm) and middle (200–300 nm) UV are the primary driver for heating, composition, and dynamic changes of the middle atmosphere. Measurements of the UV spectrum made by UARS go back to 1991 (Brueckner et al., 1993; Rottman et al., 1993). These indicate SC variations of ~50% at wavelengths ~120 nm, ~10% near 200 nm and ~3% near 300 nm. The UV variations account for ~30% of the SC TSI variations, while ~70% are produced by visible and infrared wavelengths (Rottman, 2006). The SORCE measurements (Harder et al., 2009) suggest that over the SC 23 declining phase, the 200–400 nm UV flux decreased far more than in prior observations and in phase with the TSI trend however, the visible presents surprisingly an opposite trend. These trends are apparent in the first few years of SORCE data but latter years show similar behaviour to prior observations.

8.3.1.4.2 Reconstructions of preindustrial UV variations

Krivova et al. (2010) reconstructed spectra from what is known about spectral properties of sunspots, and the relationship between TSI and magnetic fields, then they interpolated backwards based on sunspots and magnetic information. Their results show smoothed 11-years UV SSI changes between 1750 and the present of ~25% at ~120 nm, ~8% at 130 to 175 nm, ~4% at 175–200 nm, and ~0.5% at 200 to 350 nm. Thus, the UV SSI appears to have generally increased over the past four centuries with larger trends at shorter wavelengths. As few reconstructions are available, these values have a very low confidence.

8.3.1.4.3 Impacts of UV variations on the stratosphere

Ozone is the main gas involved in stratospheric radiative heating. Variations in ozone production rate are largely due to solar UV irradiance changes (HAIGH, 1994), with observations showing statistically significant variations in the upper stratosphere of 2–4% along the SC (Soukharev and Hood, 2006). UV variations may also produce transport-induced ozone changes due to indirect effects on circulation (Shindell et al., 2006a). Additionally, statistically significant evidence for an 11-year variation in stratospheric temperature and zonal winds is attributed to UV radiation (Frame and Gray, 2010).

The RF due to solar-induced ozone changes is a small fraction of the solar RF discussed above (Gray et al., 2009). Incorporating the ozone response to UV variations and taking the SORCE results (Harder et al., 2009), Haigh et al. (2010) found a solar radiative forcing of the surface climate which is out of phase with solar activity because the in-phase UV component does not reach the tropopause while the out-of-phase visible component does. Additional analyses are needed to determine if the difference between the few years of SORCE measurements and previous observations results from instrument biases or represents a real difference in the Sun´s behaviour, and if the latter, how representative such behaviour is for longer-term changes in the Sun's output.

8.3.1.5 The Effects of Galactic Cosmic Rays (GCR) on Clouds

Changing cloud amount or properties modify the Earth's albedo and therefore affect climate. It has been hypothesized that GCR create atmospheric ions which facilitates aerosol nucleation and new particle formation with a further impact on the cloud formation. Further, the GCR flux would modify cloudiness in a way that would amplify the warming effect expected from high solar activity. Studies that seek to establish a causal relationship between cosmic rays and aerosols/clouds by looking at correlations between the two quantities on timescales of days to decades indicate statistically significant correlations to support the hypothesis in some locations but in other cases contradictory results are found. There is no evidence that their effect is large enough to influence global concentrations of cloud condensation nuclei or their change over the last century or during a solar cycle. A more detailed exposition is found in Section 7.4.7.

8.3.1.6 Limitations of the Solar Forcing Metric

The overall global solar mean RF from 1750 to 2010 is very small. During the last three decades with direct satellite observations, there is a negative trend of the solar RF. As the efficacy of solar forcing is near 1 (although the SORCE results may challenge this value if they are confirmed), these RFs provide a good indication of the impact of solar forcing on global mean annual average temperature change. Though the ozone responses to solar irradiance variations have a minimal impact on the efficacy of solar forcing, studies have shown that they can play a significant role in driving circulation anomalies that lead to regional temperature and precipitation changes (Frame and Gray, 2010; Gray et al., 2010; Haigh, 1999; Shindell et al., 2006a). These effects are primarily due to differential heating driven by both the SSI changes and the resulting ozone changes. Solar forcing can also influence the state of natural modes of circulation such as the Northern Annular Mode (e.g., Ineson et al., 2011; Shindell et al., 2001). Additionally, changes in solar irradiance will lead to a surface forcing in clear sky areas such as the subtropics that is substantially larger than the surface forcing in cloudy regions such as the tropics, and this differential may also induce ocean-atmosphere response (e.g., Meehl et al., 2008). The RF metric is unable to capture these aspects of the climate response to solar forcing.

8.3.2 Volcanic Radiative Forcing

8.3.2.1 Introduction

Explosive volcanic eruptions that inject substantial amounts of SO_2 into the stratosphere are the dominant natural cause of climate change on the annual and multi-decadal time scales, and can explain much of the preindustrial climate change of the last millennium (Brovkin et al., 2010; Legras et al., 2010; Schneider et al., 2009). While volcanic eruptions inject both mineral particles (called ash or tephra) and sulphate aerosol precursors into the atmosphere, it is the sulphate aerosols, because of their small size and long lifetimes, that are responsible for radiative forcing important for climate. The emissions of CO_2 from volcanic eruptions are at least 100 times smaller than anthropogenic emissions, and inconsequential for climate on century time scales (Gerlach, 2011). Only eruptions that are powerful enough to inject sulphur into the stratosphere are important for climate change, as the e-folding lifetime of aerosols in the troposphere is only about one week, while sulphate aerosols in the stratosphere from tropical eruptions have a lifetime of about one year, and those from high-latitude eruptions last several months. Robock (2000) and AR4 (Forster et al., 2007) provide summaries of this relatively well understood forcing agent. The efficacy of the RF for volcanic aerosols with the standard definition in Section 8.1.1., the efficacy of volcanic forcing has been determined to be 0.91 (Hansen et al., 2005).

There have been no large volcanic eruptions with a detectable climatic response since the 1991 Mt. Pinatubo eruption, but several moderate high latitude eruptions have led to a better understanding of their effects. For example, Mercado et al. (2009) showed that enhanced diffuse radiation from stratospheric volcanic layers increase the terrestrial carbon sink. New work has also produced a better understanding of the hydrological response to volcanic eruptions (Anchukaitis et al., 2010; Trenberth and Dai, 2007), better long-term records of past volcanism, and better understanding of the effects of very large eruptions.

There are several ways to measure both the SO_2 precursor and sulphate aerosols in the stratosphere, using balloons, airplanes, and both ground- and satellite-based remote sensing. While both the infrared and ultraviolet signals sensed by satellite instruments can measure SO_2, the resulting aerosols are harder to observe. There is no organized system to be ready for the next big eruption, but several existing systems were used to observe eruptions of the past decade (Kravitz et al., 2011; Solomon et al., 2011) There are two limb-scanning satellites now in orbit that can provide measurements of stratospheric aerosol (Bourassa et al., 2008; Bourassa et al., 2010; Llewellyn et al., 2004; Kyrola et al., 2004). In addition, the satellite-borne Cloud-Aerosol Lidar with Orthogonal Polarization (CALIOP) can measure the vertical profile of aerosol layers and several ground-based lidars are ready to look up at stratospheric clouds, but there are few in the tropics.

As clearly described by Forster et al. (2007), there are four mechanisms by which volcanic forcing influences climate: direct RF; differential (vertical or horizontal) heating, producing gradients and circulation; interactions with other modes of circulation, such as El Niño/Southern Oscillation (ENSO); and ozone depletion with its effects on stratospheric heating, which depends on anthropogenic chlorine. Stratospheric ozone will increase with a volcanic eruption under low-chlorine conditions.

8.3.2.2 Recent Eruptions

The background stratospheric aerosol concentration has had an upward trend for the past decade (Hofmann et al., 2009). The decadal trend, while small, was produced by a number of small eruptions (Vernier et al., 2011), and had a small, but important impact on RF (Solomon et al., 2011). Two recent high-latitude eruptions, of Kasatochi Volcano (52.1°N, 175.3°W) on August 8, 2008 and of Sarychev Volcano (48.1°N, 153.2°E) on June 12–16, 2009, each injected ~1.5 Tg SO_2 into the stratosphere, but did not produce detectable climate response. Their eruptions, however, led to better understanding of the dependence of the amount of material and time of year of high-latitude injections to produce climate impacts (Haywood et al., 2010; Kravitz and Robock, 2011; Kravitz et al., 2010; Kravitz et al., 2011). The RF from high-latitude eruptions is a function of seasonal distribution of insolation and the 3–4 month e-folding lifetime of high-latitude volcanic aerosols. Kravitz and Robock (2011) showed that eruptions must inject at least 5 Tg SO_2 into the lower stratosphere in the spring or summer, and much more in fall or winter, to have a detectible climatic response.

On April 14, 2010 the Eyjafjallajökull volcano in Iceland (63.6°N, 19.6°W) began an explosive eruption phase that shut down air traffic in Europe for 6 days and continued to disrupt it for another month. While the 1991 Mt. Pinatubo eruption injected about 20 Tg SO_2 into the lower stratosphere, Eyjafjallajökull emitted much less than 0.01 Tg of SO_2 per day into the troposphere for several weeks. Thus, because of the difference in total emissions by a factor of 1,000 and difference in lifetime by a factor of 50, the climatic impact of Eyjafjallajökull was 50,000 times less than that of Pinatubo and was therefore undetectable amidst the chaotic weather noise in the atmosphere (Robock, 2010). 2011 saw the continuation of a number of small eruptions with significant tropospheric SO_2 and ash injections, including Puyehue-Cordón Caulle in Chile, Nabro in Eritria, and Grimsvötn in Iceland. None have been shown to have produced an important RF.

Figure 8.14 shows a reconstruction of volcanic aerosol optical depth since 1750 and Figure 8.15 shows observations since 1985.

[INSERT FIGURE 8.14 HERE]

Figure 8.14: Two volcanic reconstructions of aerosol optical depth (at 550 μm) as developed for the Paleoclimate Model Intercomparison Project (top), with a comparison to the updated estimates of Sato et al. (1993) (bottom, note the different vertical scales in the two panels). Figure from Schmidt et al. (2011). [PLACEHOLDER FOR SECOND ORDER DRAFT: this will be re-drafted later for only 1750 to present; pre-1750 will be in Chapter 5.]

[INSERT FIGURE 8.15 HERE]

Figure 8.15: (a) Mean stratospheric Aerosol Optical Depth in the tropics [20°N–20°S] between 20–30 km since 1985 from the Stratospheric Aerosol and Gas Experiment (SAGE) II (black diamonds), the Global Ozone Monitoring by Occultation of Stars (GOMOS) (red stars), CALIOP (blue triangles) and combined satellites (black line) (Figure 5 from Vernier et al., 2011). (b) Monthly mean extinction ratio (525 nm) profile evolution in the tropics [20°N–20°S] from January 1985 to June 2010 derived from (left) SAGE II extinction in 1985–2005 and (right) CALIOP scattering ratio in 2006–2010, after removing clouds below 18 km based on their wavelength dependence (SAGE II) and depolarization properties (CALIOP) compared to aerosols. Black contours represent the extinction ratio in log-scale from 0.1 to 100. The position of each volcanic eruption occurring during the period is displayed with its first two letters on the horizontal axis, where tropical eruptions are noted in red. The eruptions were Nevado del Ruiz (Ne), Augustine (Au), Chikurachki (Ch), Kliuchevskoi (Kl), Kelut (Ke), Pinatubo (Pi), Cerro Hudson (Ce), Spur (Sp), Lascar (La), Rabaul (Ra), Ulawun (Ul), Shiveluch (Sh), Ruang (Ru), Reventador (Ra), Manam (Ma), Soufrière Hills (So), Tavurvur (Ta), Chaiten (Ch), Okmok (Ok), Kasatochi (Ka), Fire/Victoria (Vi*), Sarychev (Sa). Superimposed is the Singapore zonal wind speed component at 10 hPa (white line) (Figure 1 from Vernier et al., 2011).

8.3.2.3 Long-Term Effects

While lunar brightness and colour during eclipses (Stothers, 2007) and tree ring records (Salzer and Hughes, 2007) are useful for producing records of past volcanism, because ice cores actually preserve the very material that was in the stratosphere they are the most useful way of producing such records. New work using ice core records of sulphur deposition has produced better records of volcanic forcing for use in climate models and analyses of past climate change. Gao et al. (2006) showed that the 1452 or 1453 Kuwae eruption was even larger in terms of RF than the 1815 Tambora eruption. Accounting for the dependence of the spatial distribution of sulphate on precipitation (Gao et al., 2007) and using more than 40 ice core records from Greenland and Antarctica, Gao et al. (2008, 2009) produced a record of volcanic forcing of climate for the past 1500 years that is a function of latitude, month, and altitude that is being used for new climate model simulations for this period (see Section [x]).

New work on the mechanisms by which a supereruption (Self and Blake, 2008) could force climate has focused on the 74,000 B.P. eruption of the Toba volcano (2.5°N, 99.0°E). (Robock et al., 2009) used simulations of up to 900 times the 1991 Pinatubo sulphate injection to show that the forcing is not linear as a function of the injection after a substantial part of the solar radiation is blocked. They also showed that chemical interactions with ozone had small impacts on the forcing and that the idea of (Bekki et al., 1996) that water vapour would limit and prolong the growth of aerosols was not supported. (Timmreck et al., 2010) however, incorporating the idea of (Pinto et al., 1989) that aerosols would grow and therefore both have less RF per unit mass and fall out of the atmosphere more quickly, found much less of a radiative impact from such a large stratospheric input.

8.3.2.4 Future Effects

How well can we predict the next climatically-important eruption? Ammann and Naveau (2003) and Stothers (2007) suggested an 80-year periodicity in past eruptions, but the data record is quite short and imperfect. While the period 1912–1963 C.E. was unusual for the past 500 years in having no large volcanic eruptions, and the period 1250–1300 C.E. had the most climatically-significant eruptions in the past 1500 years (Gao et al., 2008), current knowledge only allows us to predict such periods on a statistical basis, assuming that the recent past distributions are stationary. Ammann and Naveau (2003), Gusev (2008), and Deligne et al. (2010) studied these statistical properties and Ammann and Naveau (2010) showed how they could be used to produce a statistical distribution for future simulations.

While the future forcing from volcanic eruptions will only depend on the stratospheric aerosol loading for most forcing mechanisms, the future effects on ozone will diminish as ozone depleting substances diminish in the future (Eyring et al., 2010c).

8.3.2.5 Volcanic Eruptions as Analogues

Volcanic eruptions provide a natural experiment of a stratospheric aerosol cloud that can serve to inform us of the impacts of the proposed production of such a cloud as a means to control the climate, which is called geoengineering (Rasch et al., 2008) (see Chapters 1 and 7). For example, Trenberth and Dai (2007) showed that the Asian and African summer monsoon, as well as the global hydrological cycle, was weaker for the year following the 1991 Pinatubo eruption, as has been found with climate models (Robock et al., 2008), and MacMynowski et al. (2011) showed that because the climate system response of the hydrological cycle is rapid, forcing from volcanic eruptions, which typically last about a year, can serve as good analogues for longer-lived forcing. The formation of sulphate aerosols, their transport and removal, their impacts on ozone chemistry, their RF, and the climate response all also serve as good analogues for geoengineering proposals.

Volcanic eruptions also serve as an analogue that support climate model simulations of the transport and removal of stratospheric soot aerosols, their impacts on ozone chemistry, their RF, and the climate response. Nuclear war poses a great threat to the planet from humans, as smoke from burning cities and industrial targets could be lofted into the stratosphere, blown around the world, remaining there for more than a decade, and making it dark, cold and dry at the Earth's surface as well as destroying ozone and increasing the surface UV flux. Recent work (Robock et al., 2007a; Toon et al., 2008) showed that a nuclear war between Russia and the United States, using the reduced arsenals of 4,000 total nuclear weapons that will result by 2017 in response to the New START treaty, could still produce nuclear winter, with continental temperatures plunging below freezing in summer and catastrophic impacts on the food and water supply. A much smaller nuclear war, which would be possible between any of the nine current nuclear nations except North Korea, with each country using 50 Hiroshima-sized atom bombs (much less than 1% of the current global nuclear arsenal) as airbursts on urban areas, could produce climate change unprecedented in recorded human history and global-scale ozone depletion (Mills et al., 2008; Robock et al., 2007b; Toon et al., 2007).

8.4 Present-Day Anthropogenic Radiative Forcing

Human activity has caused a variety of changes in different forcing agents in the atmosphere or land surface. A large number of greenhouse gases have had a substantial increase over the industrial era and some of these gases are entirely of anthropogenic origin. Some of the gases are directly emitted to the atmosphere whereas other greenhouse gases are secondary products from human emitted species and the lifetime of these different gases vary substantially. Atmospheric aerosols have diverse and complex influences on the climate. Human activity has modified the land cover and changed the surface albedo. This section discusses all known anthropogenic forcing agents of non-negligible importance and their quantification in terms of RF or AF based on changes in abundance over the 1750–2010 period.

8.4.1 Changes in Our Understanding of the Spectral Properties of Radiative Transfer and Representation in Radiative Transfer Codes

RF estimates are performed with a combination of radiative transfer codes typical for GCMs as well as more detailed radiative transfer codes. Physical properties are needed in the radiative transfer codes such as

absorption data for gases. HITRAN (High Resolution Transmission) (Rothman, 2010) is widely used in radiative transfer models and satellite retrievals and the current edition is HITRAN 2008 (Rothman et al., 2009). Some researchers studied the difference among different editions of HITRAN databases for diverse uses (Feng et al., 2007; Kratz, 2008; Feng and Zhao, 2009; Fomin and Falaleeva, 2009). Model calculations have shown that modifications of the spectroscopic characteristics tend to have a modest effect on the determination of spectrally integrated radiances, fluxes and RF estimates, with the largest differences being of order 1 W/m^2 (0.5%) for the total thermal infrared fluxes, and of order 2–3% of the calculated RF at the tropopause attributed to the combined doubling of CO_2, N_2O and CH_4. These results showed that even the largest overall RF induced by differences among the HITRAN databases is considerably smaller than the range reported for the modelled RF estimates, thus, the line parameter updates to the HITRAN database are not a significant source for discrepancies in the RF calculations appearing in the IPCC reports (Kratz, 2008). There has been substantial progress on the water vapour continuum with regards to theory, measurements and modelling. There are many water continuum codes (Clough et al., 1992; Clough et al., 2005; Roberts et al., 1976). It is found that the differences among the continuum formulations tend to be comparable to the differences among the various HITRAN databases; but use of the older continuum formula produces significantly larger flux differences, thus, replacement of the older continuum is warranted (Kratz, 2008).

Line-by-line (LBL) models using the HITRAN dataset as an input are the benchmark of radiative transfer models. The accuracy given by LBL is important to evaluate the calculated RF by diverse models. Some researchers compared different LBL models (Zhang et al., 2005; Collins et al., 2006) and line-wing cutoff, line-shape function and gas continuum absorption treatment effect on LBL calculations (Zhang et al., 2008; Fomin and Falaleeva, 2009). Prior experience indicated that LBL codes generally agree with each other very well (Collins et al., 2006). Myhre et al. (2009) found that the differences of radiative forcing due to contrails among two LBL codes agree within about 15% for longwave and shortwave, whereas for stratospheric water vapour the differences were 30% for the shortwave RF. Forster et al. (2011) evaluated global mean radiatively important properties of chemistry climate models (CCMs) and found that the combined long-lived greenhouse gas global annual mean instantaneous net RF at the tropopause is within 30% of LBL models for all CCM radiation codes tested, problems remained in simulating RF for stratospheric water vapour and ozone changes with errors between 3% and 200% compared to LBL models. Between the LBL codes the differences were less than 10%, except for stratospheric water vapour were differences up to 100% for shortwave and 50% for longwave RF occurred. Correlated-K method for gas absorption is widely used in GCM RT codes because of its high accuracy and fast speed. Many researchers improved their expressions in GCMs with using the updated spectral dataset (Fomin, 2004; Fomin and Correa, 2005; Zhang et al., 2006; Zhang et al., 2006; Moncet et al., 2008; Hasekamp and Butz, 2008; Shi et al., 2009; Hogan, 2010; Li et al., 2010). Zhang et al. (2003) has shown the accuracy of the radiative forcing for the double CO_2 concentration is 2.5% with correlated-K method compared with LBL. Fomin (2004) has shown the error in simulation the RF at the tropopause is below 3%. Li et al. (2010) showed that the CH_4 shortwave effect can be included in a correlated k-distribution model, with the additional flux being accurately simulated in comparison with LBL models. Collins et al. (2006) found that the average longwave forcings calculated from the AOGCMs (Atmosphere-Ocean General Circulation Models) and LBL codes due to the increase in LLGHG from 1860 to 2000 differ by less than 0.12 W m^{-2} at the top of model, surface, and pseudo tropopause at 200 hPa. The errors in the corresponding mean shortwave forcings are larger, increasing from 0.06 W m^{-2} at top of model to 0.37 W m^{-2} at the surface (a 43% relative error). The biases in the shortwave forcings are caused primarily by the omission of CH_4 and N_2O from the shortwave parameterizations in all of the participation AOGCMs. The mean shortwave shortwave forcings by CO_2 are consistent with the LBL estimates.

It is shown that cloud can greatly reduce the magnitude of radiative forcing due to greenhouse gases. For example , the maximum decrease of HFCs, PFCs and SF_6 forcing due to clouds is about –25% (Zhang et al., 2011a;Zhang et al., 2011b). So, the accurate expression of clouds is also very important in radiative transfer models.

8.4.2 Long-Lived Greenhouse Gases

A contribution to the uncertainty in the anthropogenic forcing of the long-lived greenhouse gases (LLGHGs) comes from the choice of the baseline date (1750) representing the division between natural and anthropogenic driven changes. The trends in the major LLGHGs (CO_2, CH_4, N_2O) were not flat in 1750 but

were varying, partly due to climate and partly due to anthropogenic emissions (agriculture, residential waste, wood fuel and biomass burning) (Meure et al., 2006).

8.4.2.1 CO_2

As shown in Chapter 2 the atmospheric mixing ration of CO_2 has increased globally by about 111 ppm from 278 ± 1.2 ppm (MacFarling Meure et al., 2006) in 1750 (before large scale industrialisation) to 388.5 ppm in 2010. More than half of the CO_2 growth has occurred since 1970 (64 ppm at Mauna Loa NOAA/ESRL (www.esrl.noaa.gov/gmd/ccgg/trends/)).

The increases in global atmospheric CO_2 since 1750 are mainly due to emissions from fossil fuel combustion, cement production, land use change and biomass burning. As described in Section 6.3.2.6 only a fraction (known as the "airborne fraction") of the historical CO_2 emissions have remained in the atmosphere. Approximately half have been taken up by the land and ocean

Using the simple formula from Ramaswamy et al. (2001), the CO_2 radiative forcing (as defined in Section 8.1) from 1750 to 2010 is 1.79 W m^{-2}. The uncertainties in the total forcing from Ramaswamy et al. (2001) are approximately 10%. There has been no new information to update this uncertainty. The impact of land use change on CO_2 from 1850 to 2000 was assessed in AR4 to be 12–35 ppm (0.17–0.51 W m^{-2}, this is included in the RF for CO_2 rather than land-use).

Table 8.5 shows the concentrations and RF in AR4 (2005) and 2010 for the most important LLGHGs. Figure 8.16 shows the time evolution of RF and its rate of change. Since AR4 the RF of CO_2 for the industrial era has increased by 0.13 W m^{-2} and follows the increase noted in AR4 of almost 0.3 W m^{-2}/decade. As shown in Figure 8.16 CO_2 is responsible for almost all the increase in the RF from the LLGHGs over the last 15 years.

[INSERT FIGURE 8.16 HERE]

Figure 8.16: (a) Radiative forcing from the major long-lived greenhouse gases and groups of halocarbons from 1850 to 2010 (data currently from NASA GISS http://data.giss.nasa.gov/modelforce/ghgases/). (b) Radiative forcing from the minor long-lived greenhouse gases from 1950 to 2010. (c) Rate of change in forcing from the major long-lived greenhouse gases and groups of halocarbons from 1950 to 2010.

CO_2 can directly affect plant physiology, reducing the conductance of the plant stomata and hence the transpiration of water. Doutriaux-Boucher et al. (2009) indicate that this reduces low level cloud, enhancing the radiative forcing of CO_2 by 10%.

8.4.2.2 CH_4

Global averaged (surface) methane concentrations have risen from 715 ± 4 ppb in 1750 to 1799 ppb by 2010. Over that timescale the rise has been predominantly due to changes in anthropogenic-related methane emissions including fossil fuel extraction and transport, agriculture, and waste management. Anthropogenic emissions of other compounds have also affected methane concentrations. As described in Section 8.2, emissions of oxidised nitrogen (NO_X) increase the removal of methane from the atmosphere, whereas emissions of carbon monoxide and non-methane hydrocarbons tend to decrease the rate of methane removal. Recent trends in methane are discussed in Chapter 6.

Using the formula from Ramaswamy et al. (2001) the RF for methane from 1750 to 2010 is 0.49 W m^{-2}, with an uncertainty of ±10% from the radiative transfer codes. This increase of 0.01 W m^{-2} since AR4 is due to the 25 ppb increase in the methane mixing ratio driven by a combination of increase in net natural and anthropogenic emissions and change in oxidising capacity, but the various contributions are not well quantified. We note that the RF for a particular change in methane depends on the base amount in a different way than CO_2 (which is logarithmic with concentration, while methane's RF is proportional to the square root).

In this section only the direct forcing from changing methane concentrations is addressed. Methane emissions can also have indirect effects on climate through impacts on CO_2, stratospheric water vapour,

ozone, sulphate aerosol, and vegetation (Boucher et al., 2009; Collins et al., 2010; Shindell et al., 2009a). These are covered in Section 8.1.2.5 and 8.5.2.

8.4.2.3 N_2O

Concentrations of nitrous oxide have risen from 270 ppb in 1750 to 323 ppb in 2010, leading to a forcing of 0.17 W m^{-2} (0.16 W m^{-2} in AR4). This is an increase of 4 ppb since 2005. Again, only the direct RF from changing nitrous oxide concentrations is included, and indirect effects of N_2O emissions on stratospheric ozone are not taken into account here.

8.4.2.4 Others

Radiative forcing of the other long-lived greenhouse gases are shown in Figure 8.16 (b). The contribution of groups of halocarbons to the rate of change of forcing is shown in Figure 8.16 (c). Between 1970 and 1990 halocarbons made a significant contribution to the rate of change of forcing. Since the Montreal Protocol, the rate of change of forcing from halocarbons has been much less, but still positive as the growth of HCFCs and HFCs more than compensates for the decline in CFC emissions.

8.4.2.4.1 Halocarbons

The Montreal Protocol gases contribute approximately 11% of the LLGHG forcing. Although emissions have been drastically reduced for CFCs, their long lifetimes mean this takes time to affect their concentrations. The forcing from CFCs has declined since 2005 (mainly due to a reduction in the concentration of CFC-12), whereas the forcing from HCFCs is still rising (mainly due an increase in the concentrations of HCFC-22).

8.4.2.4.2 PFCs and SF6

These gases have lifetimes of thousands to tens of thousands of years (Table 8.5), therefore emissions essentially accumulate permanently in the atmosphere. They currently contribute 0.25% of the total forcing.

8.4.2.4.3 New species

Nitrogen Trifluoride is used in the electronics industry, sulfuryl fluoride is used as a fumigant. Both have rapdily increasing emissions and high GWPs, but currently contribute only 0.0001 W m^{-2} and 0.0003 W m^{-2} to anthropogenic radiative forcing, respectively (Andersen et al., 2009; Muhle et al., 2009; Weiss et al., 2008).

Table 8.5: Present-day concentrations (in ppt except where specified) and RF (in W m^{-2}) for the measured LLGHGs. The data for 2005 (the time of the AR4 estimates) are also shown.

	Concentrations (ppt)		Radiative forcing[a]	
Species	*2010*	*2005*	*2010*	*2005*
CO_2 (ppm)	388.5	378.7	1.79	1.66
CH_4 (ppb)	1799.1	1774.5	0.49	0.48
N_2O (ppb)	323.1	319.2	0.17	0.16
CFC-11	239.8	249.6	0.060	0.062
CFC-12	532.8	543.2	0.17	0.174
CFC-13			0.00068	
CFC-113	75.2	78.5	0.023	0.024
CFC-115	8.372	8.356	0.0015	0.0015
HCFC-22	206.6	169.7	0.041	0.034
HCFC-141b	20.5	17.8	0.0029	0.0025
HCFC-142b	20.7	15.8	0.0041	0.0032
HFC-23	23.2	18.8	0.0044	0.0036
HFC-32	4.1	1.2	0.00045	0.00013
HFC-125	8.2	3.8	0.0019	0.00087
HFC-134a	57.8	34.9	0.0092	0.0056

HFC-143a	10.9	5.7	0.0014	0.00074
HFC-152a	6.3	3.7	0.00057	0.00033
SF_6	6.99	5.63	0.0036	0.0029
CF_4	78.3	75.0	0.0038	0.0035
C_2F_6	4.1	3.7	0.0011	0.00096
CH_3CCl_3	7.5	18.2	0.00045	0.0011
CCl_4	86.3	91.8	0.011	0.012
CFCs			0.26[b]	0.27[c]
HCFCs			0.048	0.040
Montreal Gases			0.32	0.32
Halocarbons			0.35	0.34
Total			**2.79**	**2.64**

Notes:
(a) Pre-industrial values are zero except for CO_2 (278 ppm), CH_4 (715 ppb), N_2O (270 ppb), and CF_4 (40 ppt).
(b) Totals includes 0.007 W m^{-2} to account for CFC-114, Halon-1211 and Halon-1301.
(c) Totals includes 0.009 W m^{-2} forcing (as in AR4) to account for CFC-13, CHF-114, CFC-115, Halon-1211 and Halon-1301.

8.4.3 Short-Lived Gases

8.4.3.1 Tropospheric Ozone (including by Precursor)

Ozone is not emitted directly into the atmosphere; instead it is formed by photochemical reactions. In the troposphere these reactions involve precursor species such as oxides of nitrogen and organic compounds that are emitted into the atmosphere from a variety of natural and anthropogenic sources (Section 8.2.3). Transport across the tropopause means that changes in the troposphere can affect the stratosphere and vice-versa. Changes to tropospheric ozone precursors can influence ozone in the lower stratosphere either by advection of tropospheric ozone, or by direct photochemistry. Similarly changes in stratospheric ozone depleting substances (ODSs) can affect tropospheric ozone.

The tropospheric ozone RF is often calculated by scaling the tropospheric column by the normalised radiative forcing (NRF) in W $m^{-2}DU^{-1}$. The NRF is sensitive to the vertical profile of the ozone change and to the latitudinal profile to a smaller extent. Calculations from ACCMIP, Sovde et al. (2011) and Fry et al. (2011) give a NRF of 0.037 ± 0.007 W $m^{-2}DU^{-1}$ and lower than the value of 0.042 W $m^{-2}DU^{-1}$ in TAR (Ramaswamy et al., 2001), which was based on a large number of studies. It is not clear whether the NRF depends on which species generated the ozone. The Fry et al. (2011) results suggest a lower NRF for ozone generated from methane oxidation, but little dependence on other ozone precursor species emitted from the northern hemisphere. In contrast Shindell et al. (2005) found a higher NRF for methane, CO and VOCs. Estimates of the long-wave component of the NRF can be made from satellite measurements such as TES (Worden et al., 2011). Due to the limited spatial and temporal coverage of observations, models of tropospheric photochemistry are needed to estimate both the pre-industrial and present day ozone distributions.

Anthropogenic emissions of precursor species have increased the concentration of tropospheric ozone since 1750. The tropospheric ozone forcing is sensitive to the assumed pre-industrial emissions (Mickley et al., 2001). The most recent estimates of changes in anthropogenic and biomass burning emissions over the historical period come from Lamarque et al. (2010). Emissions of ozone precursors from biomass burning decreased until around 1970 before increasing to levels above the pre-industrial values (Mieville et al., 2010)., Although models using the latest emissions are still unable to reproduce all recent trends in surface ozone or pre-industrial levels (Lamarque et al., 2010), the low emissions used in Mickley et al. (2001) are inconsistent with recent estimates. Hence their high forcing estimates are not included in the assessed range here. Changes in climate have also affected tropospheric ozone concentrations through changes in chemistry, natural emissions and transport from the stratosphere (Isaksen et al., 2009). The time evolution of the tropospheric ozone forcing is shown in Figure 8.17, along with the other short-lived gases. There is a noticeable acceleration in the forcing after 1950.

The most recent estimate of the tropospheric ozone forcing comes from a multi-model study of (currently 5) models contributing to the ACCMIP project. The average tropospheric ozone radiative forcing from 1850 to present day is 0.33 ± 0.12 W m^{-2} due to both an increase in ozone precursors and a changing stratospheric concentration. Søvde et al. (2011) report a forcing of 0.38 W m^{-2}, 0.44W m^{-2} from ozone precursors and –0.06W m^{-2} from the impact of stratospheric ozone depletion on the troposphere. The ozone precursor forcing can be attributed to between the different precursor species. Shindell et al. (2006c) calculate a tropospheric ozone forcing of 0.37 W m^{-2} of which 0.28 W m^{-2} is due to methane emissions since 1750, 0.04 W m^{-2} from NO_X emissions, and 0.05 W m^{-2} from CO and VOCs. These results were calculated by holding emissions of all precursors at present day levels and reducing one at a time to pre-industrial levels. Due to the non-linearity of the chemistry, starting from pre-industrial conditions and increasing precursor emissions singly may give a different result. Note that as well as inducing an ozone forcing, these ozone precursor species can also strongly effect the concentrations of methane and aerosols, adding extra terms (both positive and negative) to their total indirect forcings.

[PLACEHOLDER FOR SECOND ORDER DRAFT: The best estimate of tropospheric ozone forcing is taken as the average of the 6 ACCMIP models and the Søvde et al. result, giving 0.34 ± 0.12 W m^{-2}, where the uncertainty is given for the 5–95% confidence range. Note that this is given for the period 1850–2010 and will be extended back to 1750 condition.]

Tropospheric ozone can also affect the radiation balance indirectly by reducing the natural uptake of carbon dioxide by terrestrial vegetation. Sitch et al. (2007a) found that this indirect affect could have contributed to about 0.2–0.4 W m^{-2} of the total CO_2 forcing (Section 8.4.2.1). This would thus roughly double the overall climate impact of tropospheric ozone. Collins et al. (2010) included this in calculations of the GTP of ozone precursors (see Section 8.5.2). To date only one study has attempted to quantify this effect, so the numbers should be considered very uncertain.

[INSERT FIGURE 8.17 HERE]

Figure 8.17: Time evolution of the forcing of short-lived components from 1850 to 2010. Tropospheric ozone data are from Skeie et al. (2011b) scaled to give 0.34 W m^{-2} at 2010, stratospheric water vapour forcing is calculated by scaling the methane forcing by 15%, stratospheric ozone forcing is from WMO (2010) scaled to give 0.05 W m^{-2} at 2010.

Table 8.6: Contributions of tropospheric and stratospheric ozone changes to radiative forcing.

Troposphere	Forster et al. (2007)	0.35 (–0.1,+0.3)
	Shindell et al. (2006b)	0.37
	Søvde et al.(2011)	0.38
	ACCMIP	0.33 ± 0.12
	AR5	0.34 ± 0.12
Stratosphere	Forster et al. (2007)	–0.05 ± 0.1
	WMO (2010) model	–0.03 ± 0.2
	WMO (2010) obs	+0.03
	AR5	–0.05 ± 0.1

8.4.3.2 Stratospheric Ozone

Stratospheric ozone concentrations have been reduced due to emissions of ozone-depleting substance (ODSs), whereas emissions of tropospheric precursors increase ozone concentrations in the troposphere and lower stratosphere (see Section 8.2.3). Changes in stratospheric climate (temperature and circulation) caused by both increases in CO_2 and deceases in ozone also affect the ozone concentrations. Stratospheric ozone has a forcing both in the short wave (reducing the flux into the troposphere) and a greenhouse effect in the long-wave as well as affecting the adjusted stratospheric temperature profile. The short wave and long-wave effects act in opposite directions leaving a residual forcing that is the sum of two larger terms. In the lower stratosphere the long wave effect tends to be larger, whereas in the upper stratosphere the short wave dominates. Thus whether stratospheric ozone depletion has contributed an overall net positive or negative

forcing depends on the vertical profile of the change (Forster and Shine, 1997).WMO (2010) assessed the RF from 1960 to 2005 from observed ozone changes (Randel and Wu, 2007) and results from 17 models. The observed and model mean ozone changes gave RF of different signs (see Table 8.6). The model spread encompasses the observed value and reflects the different magnitudes and profiles of the ozone depletion between the model chemistry schemes. These more recent data fall within the Forster et al. (2007) range and hence the assessed forcing and the range for AR5 remains unchanged since AR4 then at –0.05 ± 0.1 W m^{-2}. The stratospheric ozone forcing roughly follows the trajectory of the changes in the stratospheric equivalent chlorine loading. It starts in the late 1970s, reaches a minimum in the late 1990s and has started to recover since then (Figure 8.17).

As described in Section 8.4.3.1, transport of tropospheric ozone and ozone precursors can also affect ozone in the lower stratosphere (Shindell et al., 2006b; Sovde et al., 2011). Other than the direct radiative forcing, stratospheric ozone depletion can indirectly affect surface temperature and sea ice by altering circulation patterns such as the Southern Annular Mode (WMO, 2010). These are discussed in more detail in Chapters 11 and 12.

It should be noted that the direct radiative forcing from ODSs far outweighs their contribution to the ozone forcing (see Section 8.4.2).

8.4.3.3 Stratospheric Water

Stratospheric water vapour is dependent upon the amount entering from the tropical troposphere (which is in turn largely governed by temperature) and chemical production from the oxidation of methane. The latter can be considered as an anthropogenic forcing. This contrasts with tropospheric water vapour which is almost entirely controlled by the balance between evaporation and precipitation (see FAQ 8.1). Stratospheric water vapour can also vary through changes in dynamics (Solomon et al., 2010b) and through volcanic emission (Joshi and Jones, 2009), neither of which can be considered an anthropogenic forcing.

Myhre et al. (2007) used observations of the vertical profile of methane to deduce a contribution from oxidation of anthropogenic methane of 0.083 W m^{-2} which compares with the value of 0.07 W m^{-2} from calculations in a 2D model in Hansen et al. (2005). Both these values are consistent with the AR4 which obtained the stratospheric water vapour forcing by scaling the methane direct forcing by 15%. Thus the time evolution of this forcing is also obtained by scaling the methane forcing by 15%. The best estimate and uncertainty range from AR4 of 0.07 ± 0.05 W m^{-2} remain unchanged and the large uncertainty range is partly remaining due to large differences found in the intercomparison studies of change in stratospheric water vapour (see Section 8.4.1).

Water vapour is directly emitted into the stratosphere by aircraft. Contributions from the current subsonic aircraft fleet are very small. Lee et al. (2009) estimate an anthropogenic contribution in 2005 of 0.0028 W m^{-2}, based on scaling up calculations of Sausen et al. (2005) to 2005 emissions.

8.4.4 Aerosols and Cloud Effects

8.4.4.1 Introduction and Summary of AR4

In AR4, RF estimates were provided for three aerosol effects. These were the direct aerosol effect, the cloud albedo effect (an indirect aerosol effect), and the impact of black carbon on snow and ice surface albedo. The direct aerosol effect is scattering and absorption of shortwave and longwave radiation by atmospheric aerosols. Several different aerosol types from various sources are present in the atmosphere. Most of the aerosols primarily scatter solar radiation, but some components absorb solar radiation to various extents with black carbon as the most absorbing component. Scattering aerosols exert a negative RF, whereas strongly absorbing components give a positive RF, which also depends on the underlying surface albedo. A best estimate RF of –0.5 ± 0.4 W m^{-2} was given in AR4 for the net direct aerosol effect and a medium to low level of scientific understanding (LOSU).

An increase in the hygroscopic aerosol abundance may enhance the concentration of cloud condensation nuclei (CCN). This may increase the cloud albedo and under the assumption of fixed cloud water content it

is referred to as the 'cloud albedo effect'. For the cloud albedo effect a best estimate RF of –0.7 W m^{-2} (range from –1.8 to –0.3) was given in AR4 and a low LOSU.

Black carbon in the snow or ice can lead to a decrease of the surface albedo. This leads to a positive RF. In AR4 this mechanism was given a best estimate of 0.1 ± 0.1 W m^{-2} and a low LOSU.

Impacts on clouds from the cloud lifetime effect and the semi-direct effect were not in accordance with the radiative forcing concept, because they involve tropospheric changes in variables other than the forcing agent, so no best RF estimates were provided in AR4 (see Section 8.1). However, the cloud lifetime effect and the semi-direct effect were included in the discussion of total aerosol effect in Chapter 7 in AR4 (Denman et al., 2007). The mechanisms influenced by anthropogenic aerosol including the aerosol cloud interactions are discussed in detail in this assessment in Chapter 7 and summarized in the subsections below.

8.4.4.2 Direct Aerosol Effect by Component

Several aerosol components contribute to the direct aerosol effect, most of them mainly scatter solar radiation whereas a few also absorb solar radiation to various extents. The local RF is dependent of the mixture of aerosols and their optical properties, aerosol vertical profile in relation to the cloud distribution, and the underlying surface albedo (Forster et al., 2007). Based on a combination of global aerosol models and observation-based methods, the best estimate of the total direct aerosol effect is –0.30 ± 0.30 W m^{-2}. The best estimate of the total direct aerosol effect is thus weaker than in AR4 and with a somewhat reduced uncertainty range (see further description in Chapter 7). The main source of this estimate is based on updated simulations in AeroCom, which is an intercomparison exercise of many global aerosol models that includes extensive evaluation against measurements.

The direct aerosol effect is separated into 7 components in this report; namely sulphate, BC from fossil fuel and biofuel, OC from fossil fuel and biofuel, BC and OC combined from biomass burning, nitrate, SOA, and mineral dust. BC and OC from biomass burning are combined due to the joint sources, whereas treated separately for fossil fuel and biofuel since there is larger variability in the ratio of BC to OC in the fossil fuel and biofuel emissions. This approach is consistent with TAR and AR4. Figure 8.18 shows the global and annual mean RF of the 7 aerosol components. In magnitude the sulphate and BC from use of fossil fuel and biofuel dominate. It is important to note that the BB RF is small in magnitude but consists of larger, offsetting terms in magnitude from OC and BC. Therefore the total BC RF is larger than that from fossil fuel and bio fuel only, and the total OC RF is also stronger than that from fossil fuel and biofuel only due to additional contributions from SOA and biomass burning. A total RF from BC from a combination of fossil fuel, biofuel, and biomass burning is provided in Chapter 7. Table 8.7 compares the best estimates of the direct aerosol effect on various components in this report with values in SAR, TAR and AR4. The changes in the estimates of the direct aerosol effect of the various components have been rather modest compared to AR4. The RF from sulphate has the same uncertainty range as in AR4, but the best estimate is re-evaluated to be weaker. SOA is a new component compared to AR4. Anthropogenic SOA precursors contribute only modestly to the anthropogenic change in SOA. The increase in SOA is mostly from biogenic precursors and enhanced partitioning of SOA into existing particles from anthropogenic sources and changes in the atmospheric oxidation. This change in SOA is therefore of anthropogenic origin, but natural emission of SOA precursors are important (Hoyle et al., 2011).

[INSERT FIGURE 8.18 HERE]

Figure 8.18: Best estimate of the RF for 7 aerosol components and the total direct aerosol effect shown as bars with lines indicating the uncertainty (90% confidence interval).

Table 8.7: Global and annual mean RF of 7 aerosol components. Values and uncertainties from SAR, TAR, AR4 and AR5 are provided when available.

Global Mean Radiative Forcing (W m^{-2})					
	SAR	TAR	AR4	AR5	Comment
Sulphate aerosol	–0.40 [2x]	–0.40 [2x]	–0.40 [±0.20]	–0.30 [–0.2, –0.6]	Re-evaluated to be weaker
BC aerosol from fossil	+0.10 [3x]	+0.20 [2x]	+0.20 [±0.15]	+0.20 [±0.20]	Best estimate

fuel and biofuel					unchanged, but slightly larger uncertainty
OC aerosol from fossil fuel and biofuel	Not estimated	–0.10 [3x]	–0.05 [±0.05]	–0.05 [±0.05]	Estimate unchanged
Biomass burning	–0.20 [3x]	–0.20 [3x]	+0.03 [±0.12]	–0.01 [–0.15, 0.10]	Re-evaluated
Secondary organic aerosols	Not estimated	Not estimated	Not estimated	–0.04 [–0.07, –0.03]	Newly estimated
Nitrate	Not estimated	Not estimated	–0.10 [±0.10]	–0.10 [±0.08]	Best estimate unchanged
Dust	Not estimated	–0.60 to +0.40	–0.10 [±0.20]	–0.10 [±0.20]	Estimate unchanged

Notes: For the AR4 and AR5 columns the 90% uncertainty values are provided in brackets. The [2x] and [3x] provided for the uncertainties in SAR and TAR represent a factor of 2 and 3 relative uncertainty, respectively.

The time evolution of the RF of the direct aerosol effect is more uncertain than the current RF. Improvements in the observations of aerosols have been substantial with availability of remote sensing from the ground-based optical observational network AERONET and the launch of the MODIS and MISR instruments (starting in 2000) as well as other satellite data. This has contributed to constrain the current RF by aerosol observations. The aerosol observations are very limited backward in time and uncertainties in the emission of aerosols and their precursors used in the global aerosol modeling are larger previously than for current condition. Emissions of carbonaceous aerosols are particularly uncertain in the 1800s due to a significant biofuel source in this period, and somewhat unlike the SO_2 emissions that were very small until the end of the 1800s. The uncertainty in the biomass burning emissions increases backward in time. Figure 8.19 shows an example [PLACEHOLDER FOR THE SECOND ORDER DRAFT: this will be improved by using several models.] of the time evolution of the direct aerosol effect as a total and separated into six aerosol components. The total direct aerosol effect is shown to be weak until 1920 due to a compensation of the negative sulphate RF by the positive BC RF. From 1950 to 1990 there was a strengthening of the RF of the direct aerosol effect, mainly due to a strong enhancement of the sulphate RF. After 1990 the change has been small with even a weakening of the direct aerosol RF, mainly due to a stronger BC RF as a result of increased emissions in East Asia.

[INSERT FIGURE 8.19 HERE]

Figure 8.19: Time evolution of RF of the direct aerosol effect (total as well as by components). Solid lines show the mean of individual model results and dotted lines ± one standard deviation. [PLACEHOLDER FOR THE SECOND ORDER DRAFT: So far results from two models are used, but the figure will be updated by more models and be made consistent with the best estimates.]

8.4.4.3 Aggregated Indirect Effect

The indirect effect of aerosol on radiative forcing is the net result of an aggregate of a number of different processes that alter the albedo of clouds. The indirect forcing can be considered as an instantaneous RF that is then adjusted by a series of rapidly forming processes producing a net AF. The instantaneous forcing is a change in the RF arising from a change in the size distribution of cloud water or ice that instantaneously occurs in response to a change in the aerosol environment. For the case of warm clouds, this is the familiar Twomey effect (Twomey, 1974) but this assumes that no other changes to the clouds occur when aerosol are changed. This is generally a poor assumption as typically a variety of other processes are triggered by the aerosol change that produces an adjustment to the initial instantaneous forcing.

The adjustment processes themselves are not well understood, and generally not well quantified especially in clouds that contain ice or are mixed phase. For warm clouds, processes of adjustment are generally lumped together and referred to as the lifetime effect and include macroscopic changes to clouds such as changes in depth, changes to liquid water content, and changes in precipitation as well as changes to cloud cover. These responses are also rapid and it is the AF of the aerosol indirect effect that is the net forcing felt by the climate system. The RF is the most widely diagnosed forcing in models and the estimate of this forcing from models is typically around –1.3 W m^{-2} (see Figure [7.x]). Different amounts of warm cloud adjustments operate in

models. These adjustments either enhance the RF (from –1.3 to –1.5 W m^{-2}, Figure [7.x]) in all models or compensate one another.

Since it is not possible to observe one process alone separate from others, observational estimates provide only a measure of the AF. The picture emerging from observations, however, is very different from that emerging from models. Lebsock et al. (2008) estimate the aerosol indirect RF to be –0.4 W m^{-2} which is considerably weaker than model estimates. Recent analysis of satellite observations of ship tracks by Christensen and Stephens (2011; 2011) has revealed how the response of low warm clouds to aerosol increases depends strongly on the mesoscale nature of convection into which the aerosol are injected (whether closed or open cellular convection). This finding also supports recent results from high resolution large-eddy simulation model studies (Wang and Feingold, 2009). In the more prevalent case of closed cellular convection, observed changes to cloud albedo induced by aerosol increases are weaker than that of RF due to compensating adjustments. This reduced AF occurs from reductions to the liquid water path that compensate almost entirely the effects of decreased particle size on the observed albedo (Christensen and Stephens, 2011). For the less prevalent open cellular convection which, contrary to the closed cellular example, the aerosol indirect effects are actually enhanced over the purely Twomey effect dues to elevated water paths that result in the presence of higher concentrations of aerosol. A great deal of uncertainty remains as to the source of the apparent discrepancies between the estimates from observations and models (e.g., Penner et al., 2011; Chapter 7).

Figure 8.20 shows RF and AF estimates for various components of the aerosol indirect effect (AIE), direct aerosol effect of sulphate and all aerosols, and CO_2. The direct aerosol effect of sulphate will not initiate any of the rapid responses and AF will therefore be very similar to RF. As discussed in Section 8.1.1 there is a semi-direct for CO_2 and the mean AF from several models is rather similar to the RF, but the uncertainty is larger (Andrews and Forster, 2008). The AF for the AIE is stronger than the RF since cloud cover and other rapid responses are included in the AF concept. As discussed above the AF and RF estimates based on satellite data are weaker than the model estimates as illustrated by the large differences in magnitude of forcing in Figure 8.20. Observations suggest that liquid water path adjusts tend to compensate particle size effects leading to an overall adjusted forcing that is less that the initial radiative forcing that can be assigned to particle size changes alone.

[INSERT FIGURE 8.20 HERE]

Figure 8.20: The RF and AF estimates of various forcing agents of the climate systems. The direct aerosol radiative forcing and its AF (that includes the semi-direct effects) include the effects of the components (sulphates and black carbon) also shown. The aerosol indirect effect (AIE) RF is meant to represent the Twomey effect where all cloud property remain fixed expect for changes in the drop size distribution. The aerosol indirect effect (AIE) AF includes the rapid cloud-scale adjustments, including cloud cover, and cloud water path changes. Rapid response processes differ from model to model. The observed AIE RF is taken from global satellite observations binned by fixed cloud liquid water thus representing a close analogue to the Twomey effect. [PLACEHOLDER FOR SECOND ORDER DRAFT: All the values will be made consistent with estimates from Chapter 7; BC RF and AF will be added.]

8.4.4.4 Semi-Direct Effects

The non-cloud radiative effects of aerosol enter the climate system along two pathways. The first is a direct radiative effect that represents the change in radiative flux that occurs as a result of some change in aerosol. It is straightforward to deduce this radiative effect if the aerosol concentrations are properties are known. The direct effect is an unadjusted aerosol radiative effect and the forcing inferred from this effect is the change in flux attributed to the anthropogenic component of the aerosol direct effect. The second effect, often referred to as the semi-direct effect, is a form of rapid response that results in response to the radiative heating that is induced by absorbing aerosol in the atmosphere. This heating indirectly changes the atmospheric stability with potential downstream effects on surface convective fluxes, cloudiness and precipitation.

The responses of the climate system to these AF are not well understood and not well quantified. A number of process-scale studies (refer to Chapter 7 Section 7.3.5.2) hint at causal relationships between local changes of various cloud properties including cloud cover and the AF. These studies indicate the responses to the adjusted semi-direct forcing is complicated and differ regionally. The more global importance of the

AF, however, is far less obvious. GCM estimated forcings range not only in magnitude but also in sign and is weak in many GCMs.

The semi-direct is assessed in Chapter 7 to have a near zero AF but a substantial uncertainty range. As described above the direct aerosol effect has a RF best estimate of –0.30 ± 0.30 W m^{-2} and the estimate for AF for the direct aerosol effect including the semi-direct effect is –0.30 ± 0.40 W m^{-2}.

8.4.4.5 Black Carbon Deposition in Snow and Ice

Because absorption by ice is very week at visible and UV spectra, black carbon in snow make the snow darker. For example, 40 parts per billion of black carbon can reduce the albedo by 1–3% (depending on snow grain size). This is not enough darkening to see by eye, but it is enough to be important for climate (Clarke and Noone, 1985; Warren and Wiscombe, 1980). The RF estimation due to reduced surface albedo caused by BC in snow and ice was begun by Hansen and Nazarenko (2004) and Jacobson (2004). In AR4 this mechanism was given a best estimate of 0.1 W m^{-2} and a low LOSU. Since AR4, however, several studies have re-examined this issue and find that the RF may be weaker than the estimates of Hansen and Nazarenko (2004) and AR4 (Flanner et al., 2007; Koch et al., 2009; Rypdal et al., 2009). Estimates by Flanner et al. (2007) of present-day global-mean radiative forcing from black carbon (BC) in snow are 0.05 W m^{-2}. The global and annual mean RF estimate is 0.01 W m^{-2} (change from 1890 to 1995) from Koch et al. (2009) and 0.03 W m^{-2} from Rypdal et al. (2009), which is significantly lower than AR4. As noted in Section 8.1.1 the BC on snow and ice are among the forcing agents with important rapid responses and the efficacy is very different from 1 (Flanner et al., 2009; Koch et al., 2009). The mean efficacy in one model from five experiment/control pairs was 3.17, with a range of 2.1–4.5 (Flanner et al., 2007). Hansen et al. (2005) reported a similarly large efficacy of 2.7 for BC in snow. Efficacy in Koch et al. (2009) is much higher, however (~18, though the forcing was small making the efficacy sensitive to small variations in that diagnostic). The anthropogenic BC on snow/ice is assessed to have a positive RF of +0.04 W m^{-2}, with a 0.01–0.10 W m^{-2} 5–95% uncertainty range (see further description in Chapter 7 Section 7.3.5.5).

Regional BC albedo forcing can be quite large. The change in albedo from BC in snow is simulated to –0.12% for the global mean, and –1.1% for the Arctic from 1890 to 1995 (Koch et al., 2009). The mean surface forcing caused by black carbon over springtime Eurasian and North American snow are estimated to be 3.9 W m^{-2} and 1.2 W m^{-2}, averaged for 1979–2000, and contributions from mineral dust to albedo forcing in these regions are 1.2 and 0.2 W m^{-2}, respectively (Flanner et al., 2009).Deposition of BC onto Greenland is most sensitive to North American emissions. North America and Europe each contribute ~40% of the total BC deposition to Greenland, with ~20% from East Asia (Shindell et al., 2008b). However, the Greenland Ice Sheet has the lowest BC concentrations of the Arctic (Doherty et al., 2010). The BC concentration in the Arctic atmosphere is observed to be declining since 1990, at least in the Western Hemisphere portion (Sharma et al., 2004), which should lead to less deposition of BC on the snow surface, and surface BC in the Arctic is also found to have little influence from Asia (Gong et al., 2010). A large-area field campaign (Huang et al., 2011) found that the BC content of snow in northeast China is comparable to values found in Europe (20-800 ppb). The steep drop off in BC content of snow with latitude in northeast China may indicate that a small fraction of the BC emitted in China in the winter is exported northward to the Arctic (Huang et al., 2011). Doherty et al. (2010) showed that 20–50% of the light absorption by particles in the Arctic snowpack is by non-black-carbon constituents, such as brown carbon and mineral dust. The chemical fingerprint associated with the light-absorbing aerosol (Hegg et al., 2010; Hegg et al., 2009) indicates that brown carbon is the source of most of the non-BC light absorption, and that the source of most Arctic BC is biomass or biofuel burning in Canada and Western Russia throughout the winter and spring and for Greenland in winter and spring.

Figure 8.21 shows the time evolution of RF due to BC on snow and ice. The two studies included in the figure differ in the representation of BC emission taken into account. Koch et al. (2011) included BC from fossil fuel, biofuel and biomass burning, whereas Skeie et al. (2011a) included fossil fuel and biofuel emissions. The two studies differ in the strength of the increase in RF around 1900, but both studies show small change in RF since 1920. Further, they have both a decline in the RF between 1990 and 2000 where reduction in the Artic region in accordance to measurements is a probably a major cause.

[INSERT FIGURE 8.21 HERE]

Figure 8.21: Time evolution of RF due to BC on snow and ice. The two studies included show results for somewhat different time period with Koch et al. (2011) for the period 1890–2000 and Skeie et al. (2011a) for the period 1750–2000. The figure will be updated for SOD with further studies.

8.4.5 Land Surface Changes

8.4.5.1 Introduction

Anthropogenic land cover change has a direct impact on the Earth radiation budget through a change in the surface albedo. It also impacts the climate through modifications in the surface roughness, latent heat flux, and river runoff. In addition, human activity may change the water cycle through irrigation and power plant cooling, and also generate direct input of heat to the atmosphere by consuming energy. Land use change, and in particular deforestation, also has significant impacts on LLGHG concentration, which are discussed in Chapter 6.

AR4 referenced a large number of RF estimates resulting from a change in land cover Albedo. It discussed the uncertainties due to the reconstruction of historical vegetation, the characterization of present day vegetation and the surface radiation processes. On this basis, AR4 gave a best estimate of RF relative to 1750 due to land-use related surface albedo at -0.2 ± 0.2 W m^{-2} with a level of scientific understanding at medium-low.

8.4.5.2 Land Cover Changes

Hurtt et al. (2006) estimate that 42–68% of the land surface was impacted by land-use activities (crop, pasture, wood harvest) during the 1700–2000 period. Until the mid-20th century most land use change took place over the temperate regions of the Northern hemisphere. Since then, reforestation is observed in Western Europe and North America as a result of land abandonment, while deforestation is concentrated in the tropics. After a rapid increase of the rate of deforestation during the 1980s and 1990s, satellite data indicate a slowdown in the past decade (FAO, 2010).

Since AR4, Pongratz et al. (2008) and Kaplan et al. (2011) extended existing reconstructions on land use back in time to the past millennium, accounting for the progress of agriculture technique, historical events such as the black death or war invasions. As agriculture was already widespread over Europe and South-Asia by 1750, the radiative forcing, that is defined with respect to this date, is weaker than the radiative flux change form the state of natural vegetation cover (see Figure 8.22). Deforestation in Europe and Asia during the last millennium led to a significant negative forcing. Betts et al. (2007) and Goosse et al. (2006) argue that it probably contributed to the "Little Ice Age", together with natural solar and volcanic activity components, before the increase in greenhouse gas concentration led to temperature similar to those experienced in the early part of the second millennium. There is still significant uncertainty in the anthropogenic land cover change, and in particular its time evolution (Gaillard et al., 2010).

8.4.5.3 Surface Albedo and Radiative Forcing

Surface albedo is the ratio between reflected and incident solar radiation at the surface. It varies with the surface cover. Most forests are darker (i.e., lower albedo) than grasses and croplands, which are darker than barren land and desert. As a consequence, deforestation tends to increase the Earth albedo (negative RF) while cultivation of some bright surfaces may have the opposite effect. Deforestation also leads to a large increase in surface albedo in case of snow cover as low vegetation is more easily covered by snow that reflects sunlight much more than vegetation does.

The pre-industrial impact of the Earth albedo increase due to land use change, including the reduced snow masking by tall vegetation, is estimated to be on the order of -0.05 W m^{-2} (Pongratz et al., 2009). Since then, the increase in world population and agriculture development led to additional forcing. Based on reconstruction of land use since the beginning of the industrial era, Betts et al. (2007) and Pongratz et al. (2009) computed spatially and temporally distributed estimates of the land use radiative forcing. They estimate that the present day flux change due to albedo change from vegetation is on the order of -0.2 W m^{-2}

(range –0.21 to –0.24). The RF, defined with respect to 1750, is in the range –0.17 to –0.18. A slightly stronger value (–0.22 W m^{-2}) was found by Davin et al. (2007) for the period 1860–1992.

In recent years, the availability of global scale MODIS data (Schaaf et al., 2002) has improved surface albedo estimates (Rechid et al., 2009). These data have been used by Myhre et al. (2005a) and Kvalevag et al. (2010). They argue that the observed albedo difference between natural vegetation and croplands is less than usually assumed in climate simulations, so that the RF due to land use change is weaker than in estimates that do not use the satellite data. On the other hand, Nair et al. (2007) show observational evidence of an underestimate of the surface albedo change in land use analysis. Overall, there is still a significant range of RF estimates for the albedo component of land use forcing.

Deforestation has a direct impact on the atmospheric CO_2 concentration, and therefore contributes to the LLGHG RF as quantified in Section 8.4.2.1. Several authors have compared the radiative impact of deforestation/afforestation that results from the albedo change with the greenhouse effect of CO_2 released/sequestered. Pongratz et al. (2010) shows that the historic land use change has had a warming impact (i.e., greenhouse effect dominates) at the global scale and over most regions with the exception of Europe and India. Bala et al. (2007) results show latitudinal contrast where the greenhouse effect dominates for low latitude deforestation while the combined effect of albedo and evapotranspiration impact does at high-latitude. These results are confirmed by Bathiany et al. (2010). Similarly, Lohila et al. (2010) shows that the afforestation of boreal peatlands results in a balanced RF between the albedo and greenhouse effect. Rotenberg and Yakir (2010) show that for a semi-Arid forest in southern Israel, the greenhouse impact of deforestation is only partly counterbalanced by the albedo impact.

8.4.5.4 Other Impacts of Land Cover Change on the Earth's Albedo

Over semi-arid areas, the development of agriculture favours the generation of dust. Mulitza et al. (2010) demonstrates a very large increase of dust emission and deposition in the Sahel concomitant with the development of agriculture in this area. This suggests that a significant fraction of the dust that is transported over the Atlantic, which impacts the Earth albedo, has an anthropogenic origin. There is no full estimate of the resulting RF, however (dust forcing estimate in Section 8.4.4.2 include both land-use contributions and change in wind-driven emissions).

Burn scars resulting from agriculture practices, uncontrolled fires or deforestation (Bowman et al., 2009) have a lower albedo than unperturbed vegetation (Jin and Roy, 2005). On the other hand, at high latitude, burnt areas are more easily covered by snow, which may result in an overall increase of the surface albedo. Myhre et al. (2005b) estimates a global radiative effect due to African fires of 0.015 W m^{-2}.

Both dust and biomass burning aerosol may impact the Earth surface albedo as these particles can be deposed on snow, which has a large impact on its absorption, in particular for soot. This is discussed in Section 8.4.4.5. Campra et al. (2008) report very large (+0.09) change in albedo and –20 W m^{-2} radiative forcing over the province of Almeria in southeastern Spain, a consequence of greenhouse horticulture development, which led to significant cooling, in contrast with the temperature trend in nearby regions.

Concerning the oceans, Gatebe et al. (2011) argues that ship wakes increase the ocean albedo with a cooling effect on climate. However, a first order estimate of the impact on the Earth albedo is three orders of magnitude smaller than that of land use change.

8.4.5.5 Other Impacts of Surface Change on Climate

Davin et al. (2007) argue that the climate sensitivity to land use forcing (i.e., the climate efficacy as defined in AR4) is lower than that for other forcings, due to its spatial distribution but also the role of non-radiative processes. Indeed, in addition to the impact on the surface albedo, land use change also modifies the evaporation and surface roughness, with counterbalancing consequences on the lower atmosphere temperature. There is increasing evidence that the impact of land use on evapotranspiration – a non radiative forcing on climate – is comparable to, but of opposite sign than, the albedo effect, so that RF is not as useful a metric as it is for gases and aerosols. For instance, Findell et al. (2007) climate simulations show a negligible impact of land use change on the global mean temperature, although there are some significant

regional changes. The Adjusted Forcing concept may be more appropriate for land use change, although no quantitative estimates are available yet.

Numerical climate experiments demonstrate that the impact of land use on climate is much more complex than just the RF. This is due in part to the very heterogeneous nature of land use change (Barnes and Roy, 2008), but mostly due to the impact on the hydrological cycle through evapotranspiration and root depth. As a consequence, the forcing on climate is not purely radiative and the net impact on the surface temperature may be either positive or negative depending on the latitude (Bala et al., 2007). Davin and de Noblet-Ducoudre (2010) analyze the impact on climate of large scale deforestation; the albedo cooling effect dominates for high latitude whereas reduced evapotranspiration dominates in the tropics.

Irrigated areas have continuously increased during the 20st century although a slowdown has been observed in recent decades (Bonfils and Lobell, 2007). There is clear evidence that irrigation leads to local cooling of several degrees (Kueppers et al., 2007). Irrigation also affects cloudiness and precipitation (Puma and Cook, 2010). In the United States, DeAngelis et al. (2010) found that irrigation in the Great Plains in the summer produced enhanced precipitation in the Midwest 1,000 km to the northeast.

Urbanization also leads to significant local climate change referred to as the Urban Heat Island. This is due partly to reduced evaporation, and also to the impact of waste heat from anthropogenic activity. Although the global-average energy input is small (0.03 W m^{-2}) it may reach several hundred W m^{-2} in some cities and the local warming can be as large as that estimated for a doubling of CO_2 (McCarthy et al., 2010).

8.4.5.6 Conclusions

There is still a rather wide range of estimates of the albedo change due to anthropogenic land use change, and its impact on radiative forcing. Although most published studies provide an estimate close to –0.2 W m^{-2}, there is convincing evidence that it may be somewhat weaker as the albedo difference between natural and anthropogenic land cover may have been overestimated. In addition, non-radiative impact of land use have a similar magnitude, and may be of opposite sign, as the albedo effect (though these are not part of RF). A comparison of the impact of land use change according to seven climate models showed a wide range of results (Pitman et al., 2009), partly due to difference in the implementation of land cover change, but mostly due to different assumptions. There is no agreement on the sign of the temperature change induced by anthropogenic land use change. It is very likely that land use change led to an increase of the Earth albedo with a RF of –0.15 ± 0.10 W m^{-2}, but a net cooling of the surface – accounting for processes that are not limited to the albedo – is about as likely as not.

[INSERT FIGURE 8.22 HERE]

Figure 8.22: Change in TOA SW flux [W m^{-2}] following the change in albedo as a result of anthropogenic Land Use Change for three periods (1750, 1900 and 1992 from top to bottom). By definition, the RF is with respect to 1750. The lower right inset shows the globally averaged impact of the surface albedo change to the TOA SW flux (left scale) as well as the corresponding RF (right scale). Based on simulations by Pongratz et al. (2009).

8.5 Synthesis (Global Mean Temporal Evolution)

Comparing the relative and absolute impacts of the different forcing agents can be done in many ways. The RF can be used to assess the various contributions to climate change over the industrial era or the various contributions to future climate change. There are multiple ways in which RF can be attributed to underlying causes, each providing a valuable perspective on the importance of the different factors driving climate change. In this section, evaluations are made by abundance of the RF agents, by the emitted components, and by the activity that alters RF. This section illustrates different ways to summarize RF with these perspectives on different time scales.

8.5.1 Summary of Radiative Forcing by Species and Uncertainties

This section gives a summary of the current understanding of the various RF agents discussed in the chapter. Table 8.8 has an overview of the RF agents considered and each of them is given a confidence level for the change in RF over the industrial era at the present day. The confidence level is based on the evidence

(robust, medium, and limited) and the agreement (high, medium, and low). Some of the RF agents have robust evidence such as LLGHG with well documented increase based on high precision measurements and contrails which can be seen over industrialized regions by direct observations. However, for some RF agents the evidence is more limited regarding their existence such as aerosol influence on cloud cover. The consistency in the findings for a particular forcing agent decides the evaluation of the evidence. A combination of different methods, e.g., observations and modeling, is important for this evaluation. The agreement is a qualitative judgment of the difference between the various RF estimates for a particular RF agent. Figure 8.23 shows how the combined evidence and agreement results in five levels for the confidence level. The colour codes used in Figure 8.23 for the confidence level are adopted in Table 8.8.

[INSERT FIGURE 8.23 HERE]

Figure 8.23: The basis for the confidence level is given as a combination of evidence (limited, medium, robust) and agreement (low, medium, and high). The confidence level is given for five levels (very high, high, medium, low, and very low) and given in colours.

Table 8.8: Confidence level for the RF agents for the 1750–2010 period. The confidence level is based on the evidence and the agreement and given in the table. The basis for the confidence level and change since AR4 is provided. An asterisk is added to the RF agents with substantially greater confidence level over the period 1980–2010, compared to over the whole industrial era.

	Evidence	Agreement	Confidence level	Basis for uncertainty estimates	Change in Understanding Since AR4
LLGHG	Robust	High	Very high	Uncertainty assessment of measured trends from different observed data sets and differences between radiative transfer models	No major change
Tropospheric ozone	Robust	Medium	High	Observed trends of ozone in the troposphere and differences between model estimates of RF	No major change
Stratospheric ozone	Robust	Medium	High	Observed trends in stratospheric and total ozone and differences between estimates of RF	No major change
Stratospheric water vapour from CH_4	Robust	Low	Medium	Similarities in independent methods to estimate the RF	Elevated due to more studies
Direct aerosol effect	Robust	Medium?	High	A large set of observations and similarities in independent estimates of RF	Elevated due to improved understanding
Cloud albedo effect	Medium	Low	Low	Observational data and the spread in the model and observational based estimates of RF	No major change
Total aerosol indirect effect	Limited	Low	Very low	Observational evidence and spread in model estimates of RF	Not available
Semi-direct effect	Limited	Low	Very low	Observational evidence and spread in model estimates of RF	Not available
Surface albedo (land use)	Robust	Medium	High	Estimates of deforestation for agricultural purposes and spread in model estimates of RF	Elevated due to the availability of high quality satellite data
Surface albedo (BC aerosol on snow and ice)	Medium	Low	Low	Observations of snow samples and spread in model estimates of RF	No major change
Contrails	Robust	Medium	High	Observed contrails and spread in model estimates of RF	Elevated due to improved understanding
Contrail induced cirrus	Medium	Low	Low	Observations of a few events of contrail induced cirrus	Elevated due to additional studies

Solar irradiance*	Medium	Low	Low	Satellite information over last decades and spread in reconstructions based on proxy data	No major change
Volcanic aerosol*	Robust	Medium	High	Observations of recent volcanic eruptions and reconstructions of past eruptions	Elevated due to improved understanding

Evidence is robust for several of the RF agents because of long term observations of trends over the indutrial era and well defined links between atmospheric or land surfaced changes and radiative effect. Evidence is medium for a few agents where the changes or the link between the forcing agent and radiative effect are less certain. Medium evidence can be assigned in cases where observations or modelling provide a diversity of information and thus not a consistent picture for a given forcing agents. Limited evidence is given for two RF agents related to clouds where model studies in some cases indicate changes but direct observations of clouds changes are scarce. High agreement is only given for the LLGHG where the relative uncertainties in the RF estimates are much smaller than for the other RF agents. Low agreement can either be due to large diversity in estimates of the magnitude of the forcing or from the fact that the method to estimate the forcing has a large uncertainty. Stratospheric water vapour is an example of the latter with modest difference in the few available estimates but a known large uncertainty in the radiative transfer calculations (see further description in Section 8.4.1).

Figure 8.24 shows the development in the level of scientific understanding (LOSU) over the last 4 IPCC assessments of the various RF mechanisms. The LOSU terminiology is not regularly used in AR5, but for comparison with previous IPCC assessments the confindence level is converted approximately to LOSU. The figure shows a general increased LOSU but also that more RF mechanisms have been included over time. The LOSU for direct aerosol effect, surface albedo, contrails and volcanic aerosols has been raised and are now at the same ranking as change in stratospheric and tropospheric ozone. This is due to an increased understanding of key parameteres and its uncertainty for the elevated RF agents, e.g., for contrails the optical depth is better constrained. For tropospheric and stratospheric ozone changes research has shown further complexities with changes primarily influencing the troposphere or the stratosphere being linked to some extent (see Section 8.4.3). The cloud lifetime effect and the semi-direct effect are included for the first time and given a very low confindence level.

[INSERT FIGURE 8.24 HERE]

Figure 8.24: Level of scientific understanding (LOSU) of the RF mechanisms in the 4 last IPCC assessments. The LOSU terminology is not regularly used in AR5, but for comparison with previous IPCC assessments the confindence level is converted approximately to LOSU. The thickness of the bars represents the relative magnitude of the RF (with a minimum value for clarity of presentation).

The RF bar chart with time evolution is shown in Figure 8.25a for the whole industrial era, whereas over the period 1980–2010 shown in Figure 8.25b. The latter period is chosen due to more observational data are available over this period for quantification of the RF agents. The time evolution shows a strong enhancement in the magnitude of anthropogenic RF. This is the case both for CO_2 and other LLGHG as well as several individual aerosol components. The RF from CO_2 and other LLGHG has increased continuously with a somewhat larger growth for CO_2 over the last decades. The global mean aerosol RF was rather weak until 1950 and has strengthened in the later half of last century and in particular in the period between 1950 and 1980. The total anthropogenic RF follows to a large extend the CO_2 RF due to compensation of negative aerosol RF and positive RF from other GHG.

The volcanic RF has a very irregular temporal pattern and for certain years has a strongly negative RF. There has not been a major volcanic eruption in the past decade, but some weaker eruptions give a current RF that is slightly negative (see Section 8.3.2) [PLACEHOLDER FOR THE SECOND ORDER DRAFT: the figure needs to be updated for some of the RF agents.]

Over the three decades from 1980 to 2010 the total anthropogenic RF has steadily increased (with a RF of around 0.7 W m^{-2}) rather similar to the RF of CO_2. The natural RF agents of solar and volcanic show year to

year variation and this is particularly large for volcanic aerosols. Their net effect has been a near zero RF over the past three decades.

[INSERT FIGURE 8.25 HERE]

Figure 8.25: RF bar chart with time evolution of RF from major components. Panel (a) shows time evolution over the whole industrial era (1750–2010) whereas panel (b) shows the period 1980–2010 [PLACEHOLDER FOR SECOND ORDER DRAFT: The figure will be updated with ACCMIP results and current RF will be made consistent with best estimate RF.]. (c) Bar chart for RF (solid) and AF (hatched) for the period 1750–2010 (aerosol indirect forcing RF and AF are given as ranges), where the total anthropogenic RF and AF are derived from panel d. (d) Probability density function (PDF) of total GHG RF, aerosol forcing, and total anthropogenic forcing. The PDFs are generated based on uncertainties provided in Table 8.9. The combination of the individual RF agents to derive total anthropogenic forcing are done by Monte Carlo simulations and based on the method in Boucher and Haywood (2001). PDF of the RF from surface albedo changes is included in the total anthropogenic forcing, but not shown as a separate PDF. [PLACEHOLDER FOR THE SECOND ORDER DRAFT: Note that for the total anthropogenic AF, the AF for GHG and surface albedo change is assumed to be equal to RF. This assumption will be investigated before the SOD.]

Table 8.9 shows the best estimate of the RF for the various RF agents. Since TAR the RF due to LLGHG has increased by 15%. The increase in the LLGHG RF is due to increased concentration, whereas the other changes for the anthropogenic RF agents compared to AR4 are due to re-evaluations and in some cases from improved understanding. Increased number of studies, additional observational data, and better agreement between models and observations can be the causes for such re-evaluations. The best estimates for the direct aerosol effect, BC on snow, and solar irradiance are all weaker than in AR4, otherwise the modifications to the best estimates are rather small. For the direct aerosol effect and BC on snow the changes in the estimates are based on additional new studies since AR4 (see Section 8.4.4 and Chapter 7). On the other hand the change in the estimate of the solar irradiance is caused mainly how the RF is calculated and a downward trend in the solar activity (see Section 8.3.1). The cloud lifetime effect as part of the total aerosol indirect effect and the semi-direct effect are included for the first time with an AF. [PLACEHOLDER FOR SECOND ORDER DRAFT: Some text on the differences between RF and AF values will be added for those RF agents where this is available.]

Figure 8.25c shows bar chart of the RF agents listed in Table 8.9 over the 1750–2010 period. Solid bars are given for RF, whereas AF values for total direct aerosol effect (including semi-direct effect), total aerosol indirect effect and total anthropogenic forcing are given as additional hatched bars. As evident from the figure important process for the forcing are taken into for the aerosol indirect effect when rapid responses are allowed. The strengthening in the forcing from the strict cloud albedo effect definition to a total aerosol indirect effect broaden the shape and of the PDF and shift the PDF to slightly stronger values (see further description in 8.4.4.3 and Chapter 7). The semi-direct effect increase the uncertainty but not the best estimate of the direct aerosol effect (see further discussion in 8.4.4.4 and Chapter 7). Total anthropogenic RF and AF are calculated from Monte Carlo simulations shown in Figure 8.25d, with a best estimate of 2.10 W m^{-2} and 1.95 W m^{-2}, respectively for RF and AF. For each of the forcing agents a probability density function (PDF) is generated based on uncertainties provided in Table 8.9. The combination of the individual RF agents to derive total anthropogenic forcing follows the same approach as in AR4 (Forster et al., 2007) which is based on the method in Boucher and Haywood (2001). The PDF of the GHGs (sum of LLGHG, ozone, and stratospheric water vapour) has a much more narrow shape than the PDF for the aerosols due to the much lower uncertainty. Therefore, the large uncertainty in the aerosol forcing is the cause for the large uncertainty in the total anthropogenic RF and AF. The probability for a negative total anthropogenic forcing is very small even if rapid responses (and thus quantified by AF) are taken into account for the aerosol effects.

Table 8.9: Summary table of RF estimates for AR5 and comparison with the 3 previous IPCC assessment reports. AF values for AR5 are included [PLACEHOLDER FOR SECOND ORDER DRAFT: AR5 values will be included later.].

	Global Mean Radiative Forcing (W m^{-2})					AF (W m^{-2})
	SAR (1750–1993)	*TAR (1750–1998)*	*AR4 (1750–2005)*	*AR5 (1750–2010)*	*Comment*	*AR5*
Long-lived Greenhouse Gases (CO_2, CH_4, N_2O, and halocarbons)	2.45 [15%]	2.43 [10%]	2.63 [±0.26]	2.79 [±0.28]	Change due to increase in concentration	Will be included later

Tropospheric ozone	+0.40 [50%]	+0.35 [43%]	+0.35 [–0.1, +0.3]	+0.34 [±0.12]	Slightly modified estimate	
Stratospheric ozone	–0.1 [2x]	–0.15 [67%]	–0.05 [±0.10]	–0.05 [±0.10]	Estimate unchanged	
Stratospheric water vapour from CH_4	Not estimated	+0.01 to +0.03	+0.07 [±0.05]	+0.07 [±0.05]	No major change	
Total direct aerosol effect	Not estimated	Not estimated	–0.50 [±0.40]	–0.30 [±0.30]	Re-evaluated to be weaker and smaller uncertainty range	
Total direct aerosol effect including the semi-direct effect	Not estimated	Not estimated	Not estimated	Not estimated	Newly estimated	–0.30 [±0.40]
Cloud albedo effect	0 to –1.5 (sulphate only)	0 to –2.0 (all aerosols)	–0.70 [–1.1, +0.4] (all aerosols)	–1.1 to –0.1	Re-evaluated with no best estimate	
Total aerosol indirect effect including the cloud lifetime effect	Not estimated	Not estimated	Not estimated	Not estimated		–1.5 to 0.0
Surface albedo (land use)	Not estimated	–0.20 [100%]	–0.20 [±0.20]	–0.15 [±0.10]	Re-evaluated to be slightly weaker	
Surface albedo (BC aerosol on snow and ice)	Not estimated	Not estimated	+0.10 [±0.10]	+0.04 [0.01, 0.10]	Re-evaluated to be weaker	Will be included later
Contrails	Not estimated	0.02 [3.5x]	0.01 [–0.007, +0.02]	0.02 [±0.01]	Re-evaluated to be stronger	
Contrail induced cirrus	Not estimated	Not estimated	0.03 [–0.02, +0.05]	Not estimated	Best estimate unchanged	0.03 [0.01, 0.06]
Solar irradiance	+0.30 [67%]	+0.30 [67%]	+0.12 [–0.06, +0.18]	0.07 [0.02, 0.12]	Re-evaluated to be weaker	

Notes: For the AR5 column the 90% uncertainty values are given in brackets, whereas in the AR4 column the numbers in brackets must be added to the best estimate to obtain the 5 to 95% confidence range. The [2x] and [3x] provided for the uncertainties in SAR and TAR represent a factor of 2 and 3 relative uncertainty, respectively.

8.5.2 Impacts by Emissions

The RF due to changes in the concentration of a single forcing agent can have contributions from emissions of several compounds. Thus, while Figure 8.25 shows the RF relative to pre-industrial times by atmospheric constituent, the RF may also be given related to the various emissions – or "drivers" – of the changes in atmospheric composition. Such a perspective can be useful both for evaluation of historical changes, a *backward-looking* view, and for gaining insight into the impact of current emissions on the future, a *forward-looking* view. To facilitate a forward-looking assessment, we first present an evaluation of the requisite impact metrics (see Section 8.1.2) by emission.

8.5.2.1 Emission Metrics

We present updated GWP and GTP values for the long-lived GHGs based on updated radiative efficiencies and lifetimes (or adjustment times) for both CO_2 and non-CO_2 LLGHG; see Table 8.10 and appendix [PLACHOLDER FOR THE SECOND ORDER DRAFT: Appendix will be added later]. We [will] also use values from the WMO/UNEP Ozone Assessment 2010 (WMO, 2010), which gives an update of GWPs for various CFCs, HCFCs, HFCs, chlorocarbons, bromocarbons and halons, fully fluorinated species and halogenated alcohols and ethers based on new numbers for radiative efficiency and lifetimes. Indirect effects of ODS via changes in stratospheric O_3 have been included in the given GWPs.

In previous IPCC assessments the GWP for CH_4 included the effect on its own adjustment time (OH feedback; Section 8.2) as well as the effects on tropospheric O_3 and stratospheric H_2O. Various new studies provide updated values and inclusion of more effects. By accounting for aerosol responses, Shindell et al. (2009b) found that GWP for CH_4 increased by ~40%. Collins et al. (2010) found that the GTP values of methane increased by 5–30% when the effect of O_3 on CO_2 was included. Boucher et al. (2009) include the effect on CO_2 for methane from fossil sources and calculate a GWP_{100} value higher than given in AR4; i.e., 27–28 vs 25. Inclusion of this effect has a higher impact on GTP values, and for GTP_{100} this contribution was found to be larger than the direct CH_4 effect. In applications of metrics, inclusion of the CO_2 effect of fossil methane must be done with caution to avoid any double-counting since CO_2 emissions numbers are often based on total carbon content.

Prather and Hsu (2010) analyzed the effect of increased N_2O abundance on CH_4 changes via stratospheric O_3, UV fluxes and OH levels. The reduction in methane (–36% per unit change in mixing ratio of N_2O) offsets some of the climate impact from N_2O emissions (i.e., would reduce the GWP or GTP of N_2O).

Table 8.10: Specific radiative forcings, lifetimes/adjustment times, GWPs for 20 and 100 years and GTP values for 20, 50 and 100 years, for selected GHGs [PLACEHOLDER FOR SECOND ORDER DRAFT: Preliminary numbers].

	Radiative efficiency	**Lifetime or Adjustment Time**	**GWP**		**GTP**		
	W m^{-2} ppb^{-1}	Years	**H=20**	**H=100**	**H=20**	**H=50**	**H=100**
CO_2*	1.38E–05		1	1	1	1	1
CH_4** fossil §	3.7E–04	13.7 ± 1.5	80.7–81.5	30.2–31.5	67–67.9		6.4–7.8
CH_4** non-fossil	3.7E–04	13.7 ± 1.5	80	29	66	16	5
N_2O **	3.03E–03	121 ± 9.6	297	311	311	335	282
HFC-23 #	0.19	222	12,170	14,555	12,920	15,403	15,259
HFC-134a #	0.16	13.4	3,810	1,396	3,127	763	220
SF_6 +	0.52	3,200	16,584	23,266	17,869	23,843	28,561
PFC-14 +	0.10	50,000	5,314	7,543	5,732	7,709	9,359
PFC-116 +	0.26	10,000	8,808	12,462	9,498	12,746	15,418

Notes: The GTP values are calculated with a temperature impulse response function taken from Boucher and Reddy, 2007, which has a climate sensitivity of 1.06 K(W m^{-2})$^{-1}$, equivalent to a 3.9 K equilibrium response to 2xCO_2 [PLACHOLDER FOR SECOND ORDER DRAFT: The impulse response function for temperature will be updated later].
* For emissions of fossil CO_2 we have used the impulse response function from Joos et al. (1996) that was updated for AR4, see footnote to table 2.14 in Forster et al., 2007 [PLACEHOLDER FOR SECOND ORDER DRAFT: The impulse response function for CO_2 will be updated later]. For calculation of radiative efficiency for CO_2, an atmospheric level of 386.3 ppm is assumed.
** Adjustment times for N_2O and CH_4 from Prather/ACCMIP; radiative efficiencies from AR4. A factor 1.4 is applied for methane to account for effects on tropospheric ozone (1.25) and stratospheric water vapour (1.15) (Forster et al., 2007). The factor for tropospheric ozone has been used in AR4 and TAR and is based in the IPCC report Climate Change 1994 [PLACEHOLDER FOR SECOND ORDER DRAFT: This factor will be updated based on a set of new model studies.].
§ Preliminary corrections for fossil fuel methane added based on Boucher et al. (2009) [PLACEHOLDER FOR SECOND ORDER DRAFT: Will be updated later and range made consistent with discussion above.]
# Specific forcing and lifetimes from WMO 2010.
+ Specific forcing and lifetimes from AR4.

For fossil fuel emissions of CO_2 it is common to use the impulse response function from Joos et al. (1996) which was updated in Forster et al. (2007). However, for *biogenic* CO_2 a modified impulse response function that accounts for uptake and regrowth of forests may be used, and Cherubini et al. (2011) showed that CO_2 from biofuels has a GWP between 0 and 1. The GWP decreases with increasing time horizon and with reduced rotation time for forests. The modified impulse response function becomes negative in periods, which indicates a net removal of CO_2 in the case of burning of biofuel.

In previous IPCC assessments, GWP values were given for 20, 100 and 500 year time horizons, while we here only use 20 and 100 years. Instead of using GWP values for 500 years we show the response to emissions of some extremely long-lived gases such as PFCs; see Figure 8.26. Once these gases are emitted they stay in the atmosphere and contribute to warming on very long time scales (99% of an emission of PFC-14 is still in the atmosphere after 500 years). For comparison we also include gases with lifetimes of the order of centuries down to a decade. One kilo emitted SF_6 has a temperature effect after 500 years that is almost 40,000 times larger than that of CO_2. The corresponding numbers for CF_4 and C_2F_6 are 14,000 and 23,000, respectively. There are obviously large uncertainties related to global temperature responses (as well as the CO_2 response) on scales of centuries, but this nevertheless indicate the persistence and long-lived warming effects of these gases.

One reason for not using a time horizon of 500 years here is ambiguity regarding the meaning of the GWP_{500} values, especially for gases with short adjustment times relative to that of CO_2. As explained in Section 8.1.2, the GWP gives the ratio of two integrals – one of a pulse of a non-CO_2 gas approaching zero and that of the CO_2 response that has a persistent fraction around 0.2 for centuries. Figure 8.26 also shows that the temperature response to a pulse of HFC-134a is close to zero for centuries up to 500 years, while the GWP_{500} is 416 (as reported by WMO 2010). Thus, the GWP_{500} value may give misleading information about the climate impacts on this time scale. A similar argument can be made for methane.

[INSERT FIGURE 8.26 HERE]

Figure 8.26: Temperature response due to 1-kg pulse emissions of greenhouse gases with a range of lifetimes (given in parentheses). Calculated with a temperature impulse response function taken from Boucher and Reddy (2007) which has a climate sensitivity of 1.06 K $(W\ m^{-2})^{-1}$, equivalent to a 3.9 K equilibrium response to 2 x CO_2.

When the GWP concept was introduced it was mainly used for the long-lived and well-mixed GHGs, but later the concept has been used for SLCFs as well. There are, however, substantial challenges related to calculations of GWP (and GTP) values for these components, which is reflected in the ranges of values in the literature. Below we present and assess the current status of knowledge and quantification of metrics for various short-lived components. In general, there are large variations across the components in magnitudes and robustness of the estimated metric values (see Section 8.5.3. for sector specific metrics).

8.5.2.1.1 Nitrogen oxides (NOx)

The metric values for NOx available in the literature usually include the short-lived O_3 effect, CH_4 changes and the CH_4-controlled O_3 response. In addition, NOx causes RF through nitrate formation, and via methane it affects stratospheric H_2O. Due to high reactivity and the many non-linear chemical interactions operating on different timescales, as well as short lifetime and heterogeneous emission patterns, calculation of *net* climate effects of NOx is difficult. The net effect is a balance of large opposing effects with very different temporal behaviours. There is also a large spread in values between regions due to variations in chemical and physical characteristics of the atmosphere.

Table 8.11 shows published GWP and GTP values for global and regional emissions. The general pattern for NOx is that the short-lived ozone forcing is always positive, while the methane-induced ozone forcing and methane forcing are always negative. For a time horizon of 100 years, all GWP estimates for surface NOx emissions in Table 8.11 are negative. For 20 years, however, the sign varies between regions, reflecting the variations in chemical and physical conditions and different balances of the effects initiated by NOx. However, these calculations did not include the impact of NOx on nitrate aerosols. Its inclusion would decrease all GWPs, and as the nitrate response is rapid it would especially affect the values for GWP_{20}. For the GTP, all estimates for NOx from surface sources give a negative net effect. The GWP values for global emissions of NOx also show large variations across studies.

As shown in Table 8.11 the GTP and GWP values are very different. This is due the fundamentally different nature of these two metrics and the way they capture the time-dependent effects of NOx. As shown in Figure 8.3, the GWP integrates forcing along the path and hence retains information on the effect of the pulse at early times, whereas the GTP is an end-point metric, where the impact of the early effect of the pulse decreases over time. Time variation of GTP for NOx is complex, which is not directly seen by the somewhat arbitrary choices of time horizon and the net GTP is a fine balance between the contributing terms.

Collins et al. (2010) included the effect of O_3 on CO_2 levels via vegetation impacts, and found that that this effect, which vary strongly across regions, adds a large warming contribution to the net effect of NOx. For GTP_{20} this leads to a change from net cooling to net warming, while on a 50 year timescale it was only for emissions in Europe that a net warming was calculated. There are significant uncertainties related to the numbers, and so far there is only one study that has included this effect in the metric values.

Shindell et al. (2009b) estimated the impact of reactive species emissions on both gaseous and aerosol forcing species and found that a substantial climate impact of ozone precursors was manifested through perturbations to the sulphur cycle in addition to ozone itself. For NOx this reduced the GWP_{100} down to between -100 and -250. However, studies with different formulations of the sulfur cycle have found lower sensitivity (Collins et al., 2010; Fry et al., 2011).

The metric estimates for NOx reflect the level of knowledge, but they also depend on experimental design, treatment of transport processes, modelling of background levels. The multi-model study by Fry et al. (2011) gives useful information about robustness and uncertainties and the estimates show that the uncertainty is so large that it is not possible to conclude whether NOx causes cooling or warming in some regions. The effect on nitrate was omitted in that study. Based on Bauer et al. (2007), Fry et al. (2011) point out that this effect could contribute to NO_X GWP on the order of -80 for GWP_{20} and -20 for GWP_{100}, which is quite substantial.

Table 8.11: GWP and GTP for NOx for time horizons of 20 and 100 years from the literature. All values are on a per kg N basis. Uncertainty for Fry et al. numbers refer to 1SD.

	GWP		GTP	
	H = 20	**H =100**	**H = 20**	**H =100**
NOx East Asia [a]	3.4 (±41.5)	–6.3 (±13.7)	–56.0 (±24.9)	–1.4 (±1.7)
NOx EU+N-Africa [a]	–41.3 (±17.8)	–16.2 (±6.7)	–48.9 (±13.1)	–1.9 (±1.1)
NOx North America [a]	–5.6 (±30.7)	–9.3 (±11.7)	–62.5 (±25.2)	–1.9 (±1.9)
NOx South Asia [a]	–46.6 (±79.7)	–27.4 (±27.8)	–126.2 (±55.7)	–3.7 (±3.9)
NOx 4 above regions [a]	–18.9 (±33.2)	–12.6 (±12.0)	–62.8 (±24)	–2.0 (±1.8)
Mid-Latitude NOx [c]	–43 to +23	–18 to +1.6	–55 to –37	–29 to –0.02
Tropical NOx [c]	43 to 130	–28 to –10	–260 to –220	–6.6 to –5.4
NOx global [b]	19	–11	–87	–2.9
NOx global [d]	–108 ± 35 –335 ± 110 –560 ± 279	–31 ± 10 –95 ± 31 –159 ± 79		

Notes:
(a) Fry et al.
(b) Fuglestvedt et al. (2010); based on Wild et al.
(c) Fuglestvedt et al., 2010
(d) Shindell et al., 2009. Three values are given: First, without aerosols, second, direct aerosol effect included (sulfate and nitrate), third, direct and indirect aerosol effects included. Uncertainty ranges from Shindell et al., 2009 are given for 95% confidence levels.

8.5.2.1.2 Carbon monoxide (CO) and Volatile organic carbons (VOC)

Emissions of carbon monoxide (CO) and volatile organic carbons (VOC) lead to production of ozone on short timescales and by affecting OH and thereby the levels of methane it also initiates a long-term O_3 effect.

With its lifetime of 2–3 months, the effect of CO emissions is less dependent on location than what is the case of NOx; see Table 8.12. There is also less variation across models; i.e., 25–30%. However, Collins et al. (2010) found that inclusion of vegetation effects of O_3 increased the GTP values for CO by 20–50%. By including aerosol responses Shindell et al. (2009b) found an increase in GWP_{100} by a factor of ~2.5.

VOC is not a well-defined group of hydrocarbons. This group of gases with different lifetimes is treated differently across model experiments, since various numbers of gases are lumped together in different ways or some representative key species are modeled explicitly. However, the spread in metric values in Table

8.13 is moderate across regions, with highest values for emissions in S-Asia (of the four regions studied). For each region the uncertainties across models is in the range 20–50%.

The effects via O_3 and CH_4 cause warming, and the additional effects via interactions with aerosols and via the O_3-CO_2 link increase the warming effect further. Thus, the net effects of CO and VOC are less uncertain than for NOx.

Table 8.12: GWP and GTP for CO for time horizons of 20 and 100 years from the literature. Uncertainty for Fry et al. numbers refer to 1SD.

	GWP		GTP	
	H = 20	**H = 100**	**H = 20**	**H = 100**
CO East Asia [1]	5.5 (±1.8)	1.8 (±0.6)	3.6(±1.3)	0.3(±0.1)
CO EU+N-Africa [1]	5.0 (±1.3)	1.6 (±0.4)	3.3(±0.9)	0.2(±0.1)
CO North America [1]	5.7 (±1.8)	1.9 (±0.6)	3.8(±1.4)	0.3(±0.1)
CO South Asia [1]	5.8 (±1.1)	1.8 (±0.4)	3.5(±0.8)	0.3(±0.1)
CO 4 regions above [1]	5.5 (±1.5)	1.8 (±0.5)	3.6(±1.1)	0.3(±0.1)
CO global [2]	6 to 9.3	2 to 3.3	3.7 to 6.1	0.29 to 0.55
CO global[3]	7.8 ± 2.0	2.2 ± 0.6		
	11.4 ± 2.9	3.3 ± 0.8		
	18.6 ± 8.3	5.3 ± 2.3		

Notes:
[1] Fry et al.
[2] Fuglestvedt et al. 2010
[3] Shindell et al., 2009. Three values are given: First, without aerosols, second, direct aerosol effect included, third, direct and indirect aerosol effects included. Uncertainty ranges from Shindell et al., 2009 are given for 95% confidence levels.

Table 8.13: GWP and GTP for VOC for time horizons of 20 and 100 years from the literature.

	GWP		GTP	
	H = 20	**H = 100**	**H = 20**	**H = 100**
VOC East Asia [1]	16.5 (±6.8)	5.1 (±2.3)	8.6 (±4.9)	0.9 (±0.4)
VOC EU+N-Africa [1]	18.2 (±8.0)	5.7 (±2.7)	9.8 (±6.1)	0.8 (±0.5)
VOC North America [1]	16.4 (±8.1)	5.1 (±2.6)	8.9 (±5.4)	0.8 (±0.4)
VOC South Asia [1]	28.2 (±9.3)	8.9 (±3.3)	16.1 (±7.6)	1.3 (±0.6)
VOC 4 regions above	18.9 (±7.7)	5.9 (±2.6)	10.3 (±5.8)	0.9 (±0.5)
VOC global [2]	14	4.5	7.5	0.66

Notes:
[1] Fry et al.
[2] Fuglestvedt et al. (2010), based on Collins et al. (2002)

8.5.2.1.3 Black carbon (BC) and organic carbon (OC)

Several studies have focused on the effects of emissions of BC and OC from different regions, thus making it possible to derive regional metric values (Bauer et al., 2007; Koch et al., 2007; Naik et al., 2007; Reddy and Boucher, 2007; Rypdal et al., 2009; Shindell et al., 2011). However, an examination of the output from these models (Fuglestvedt et al.; 2010) reveals that there is not a robust relationship between the region of emission and the metric value – hence, regions that yield the highest metric value in one study, do not, in general, do so in the other studies. This could be because of differences in the representations of atmospheric processes in the models, or differences in the experimental design.

Most of the metric values for BC in the literature include the direct effect and the albedo effect of BC, though whether external or internal mixing is used varies between the studies. Bond et al. (2011) calculate GWPs and find that when albedo effect is included the values increase by 5–15%. The RF from the albedo effect of BC is much lower than the AF, and hence using albedo RF in GWPs can lead to underestimates of the climate response.

Rypdal et al. (2009) calculate GWPs (for direct and albedo effect) for emissions in various regions and find GWP_{100} values in the range 700–1,320 and GWP_{20} in the range 2,500–4,600. In general, they find that the contribution to the direct effect is stronger for emissions at lower latitudes, while the albedo contribution increases for higher latitudes. The former variation dominates giving higher metric values for lower latitudes. Reddy and Boucher (2007) calculated a BC GWP_{100} of 480 (for the direct effect) with a range from 374 to 677 for BC emissions in various regions. Assuming a global RF of 0.1 W m^{-2} for the snow albedo effect (which is larger than recent estimates) they also calculated regional GWPs for this effect apportioned according to their contribution to BC deposition at high latitudes.

Jacobson (2010) included indirect effects of BC and calculated the 20- and 100-year Surface Temperature Response per unit emissions, STRE, (which is similar to GTP for sustained emissions) and found values in the range 4,500–7,200 and 2,900–4,600 for 20 and 100 years, respectively, for BC from fossil fuels. For BC from solid biofuels the ranges were 2,100–4,000 and 1,060–2,020. Since these metric values assume sustained emissions – in contrast to pulses – they cannot be compared directly to the other estimates discussed here.

The metric values for OC are quite consistent across studies, but fewer studies are available. Based on Koch et al. (2007) and Berntsen et al. (2006), Rypdal et al. (2009) derive GWPs for OC emissions in various regions and find GWP_{100} values in the range –28 to –82 and GWP_{20} in the range –100 to –290.

Table 8.14: GWP and GTP from the literature for BC and OC for time horizons of 20 and 100 years.

	GWP		GTP	
	H = 20	**H = 100**	**H = 20**	**H = 100**
BC global [a]	1,600	460	470	64
BC dir+albedo Global [b]	2,900 ± 1,500	830 ± 440		
OC global [a]	–240	–69	–71	–10
OC global [b]	–160 (–60, –320)	–46 (–18, –92)		

Notes:
(a) Fuglestvedt et al. (2010)
(b) Bond et al. (2011). Uncertainties for OC are asymmetric and are presented as ranges.

8.5.2.1.4 Other components

Derwent et al. (2001) report values of GWP_{100} of 3.4 for the effect of H_2 on CH_4 and 2.4 from the effect on O_3, giving a total of 5.8. For global emissions of SO_2 Fuglestvedt et al. (2010) calculated GWPs of –140 and –40 for 20 and 100 years, respectively. The GTPs are –41 and –6 for the same horizons (for both metrics the values are given on an SO_2-basis and account only for the direct effect of sulphate.). For SO_2 Shindell et al. (2009b) calculated –22 ± 20 (direct only) and –76 ± 69 (direct and indirect effects) for GWP_{100}, and –78 ± 70 and –268 ± 241 for GWP_{20}.

For NH_3 Shindell et al. (2009b) calculated –19 ± 22 (direct only) and –15 ± 18 (direct and indirect effects) for GWP_{100}, and –65 ± 76 and –53 ± 62 for GWP_{20}. Due to competition for ammonium between nitrate and sulphate, the net aerosol forcing from either SO_2 or NH_3 emissions is the residual of larger responses of opposite signs, which leads to the high uncertainty in their numbers.

8.5.2.1.5 Summary of status of metrics for SLCF

While significant progress has been made since AR4 in our understanding of impacts of SLCF, there are still large uncertainties related to the quantifications of climate effects. The metrics provide a format for comparing the magnitudes of the various effects from different studies as well as for comparing effects of emissions from different regions. Much of the spread in results is due to differences in experimental design and how the models treat physical and chemical processes. Unlike most of the LLGHGs, many of the SLCFs are tightly coupled to the hydrologic cycle and to atmospheric chemistry, leading to a much larger spread in results as these are highly complex processes that are difficult to validate on the requisite small spatial and short temporal scales. The scientific confidence is low for NOx, BC and OC. While the direct effect of SO_2

is quite well understood there are large uncertainties and limitations in our understanding of indirect effects; and the metrics for this gas should be seen in light of this. There are particular difficulties for NOx, because the net impact is a small residual of opposing effects which have quite different spatial distributions and temporal behaviour. The sign of the *net* effect of NOx emissions is also uncertain.

8.5.2.2 Contribution by Emitted Component

Figure 8.27 shows RF associated with each principal emission including indirect RFs related to perturbations of other forcing agents. Both Figures 8.25 and 8.27 are *backward-looking* and show RF due to changes since pre-industrial times. They thus present complementary views of the same changes in atmospheric composition.

[INSERT FIGURE 8.27 HERE]
Figure 8.27: Components of RF for emissions of principal gases, aerosols and aerosol precursors and other changes. Values represent RF in 20XX due to emissions and changes since 1750. [PLACEHOLDER FOR SECOND ORDER DRAFT: Figure 2.21 from AR4 will be updated based on ACCMIP and published studies.]

We now use the metrics evaluated in the previous section to estimate climate impacts of various components (in a forward looking perspective). In these examples we have used metrics given in the previous section and present-day (2000) emissions data are taken from Unger et al. (2010) as well as Fuglestvedt et al. (2010).

Figure 8.28 shows global anthropogenic emissions weighted by GWP and GTP. The time horizons are chosen merely as examples and illustrate how the perceived impacts of components – relative to the impact of the reference gas CO_2 – vary strongly as function of impact parameter (integrated RF as in GWP or temperature as in GTP) and with time horizon. Indirect aerosol effects are not included.

[INSERT FIGURE 8.28 HERE]
Figure 8.28: Global anthropogenic emissions weighted by GWP and GTP for chosen time horizons. [PLACEHOLDER FOR SECOND ORDER DRAFT: This figure may be merged with Figures 8.27 and 8.29 to one panel showing 4 figures together. To be updated to AR5 emissions inventory.]

While Figure 8.28 used *integrated RF* and end-point temperature as indicators of climate impact for chosen time horizons, we may also calculate the temporal development of the temperature responses to pulse or sustained emissions. Figure 8.29a shows that for one-year pulses the impacts of SLCF decay quickly due to their atmospheric adjustment times even if effects are prolonged due to climate response time. In the case of constant emissions (Figure 8.29b), the effects of SLCF reach approximately constant levels since emissions are replenished every year, while long-lived components accumulate causing increasing warming effect over time. Figure 8.29 also shows how some components have strong short-lived effects – of both signs – while CO_2 has a weaker initial effect but one that persists to create a long-lived warming effect.

[INSERT FIGURE 8.29 HERE]
Figure 8.29: Temperature response by component for total man-made emissions for (a) a one-year pulse (year 2000) (upper) and (b) for emissions kept constant at 2000 level (lower). The effects of aerosols on clouds (and in the case of black carbon, on surface albedo) as well as aviation-induced cirrus are not included. [PLACEHOLDER FOR SECOND ORDER DRAFT: To be updated to AR5 emissions inventory.]

The examples given here show that the outcome of comparisons of effects of emissions depends strongly on i) the time perspective adopted – both for emissions and the response; ii) the chosen impact parameter (RF, integrated RF, temperature, etc) and iii) type of emission perturbation (pulses or sustained emissions; or scenarios). Such choices will have a strong influence on the calculated contributions from SLCF vs LLGHG or non-CO_2 vs CO_2 emissions. Thus, each specific analysis should use a design chosen in light of the context and questions being asked.

8.5.3 Impacts by Sector

While Section 8.5.2 showed the impacts by emissions and used a *component-by-component* view a *sectoral* view may be used as an alternative.

Among the various sectors, the transport sectors have received most attention in terms of studies quantifying climate impacts of a broad set of emissions (Balkanski et al., 2010; Berntsen and Fuglestvedt, 2008; Corbett et al., 2010; Eyring et al., 2010a; Fuglestvedt et al., 2008; IPCC, 1999; Lee et al., 2009; Lee et al., 2010; Skeie et al., 2009; Stevenson and Derwent, 2009; Uherek et al., 2010). There are also some broader studies including other sectors such as power production, households, etc. (Henze et al., 2011; Shindell and Faluvegi, 2010; Unger et al., 2009; Unger et al., 2008; Unger et al., 2010). In addition, there are several studies on impacts of a subset of emission from specific activities or sectors; e.g., BC and OC from biomass burning and cloud effects of aviation (e.g., Naik et al. (2007); Burkhardt and Kärcher (2011)). The study by Unger et al. (2010) is the only published analysis covering all sectors and including a broad set of components.

While the emissions of LLGHGs vary strongly between sectors, the climate impacts of these emissions are independent of sector. This is not the case for SLCF, due to the dependence of their impact on the emission location. Since most sectors have multiple co-emissions, and for SLCFs some of these are warming while others are cooling, the net impact of a given sector is also not obvious without explicit calculations. Since AR4 there has been significant progress in the understanding and quantification of climate impacts of SLCF from sectors such as the transport sectors, power production, biomass burning etc. Many of the studies provide metrics for the components that are important for the assessment of the various sectors. Table 8.15 gives an overview of recent published metric values for various components by sector [PLACEHOLDER FOR SECOND ORDER DRAFT: Results from Henze et al. (2011); will be added to the table].

Focusing on BC, OC, NH_3 and SO_2, Henze et al. (2011) show how RF efficiencies of many individual emission perturbations differ considerably from region or sectoral averages. Figure 8.30 shows the sensitivity of global mean direct RF to location of emissions. One important implication of their results is that RF estimates aggregated over regions or sectors may not represent the impacts of emissions changes on finer scales.

[INSERT FIGURE 8.30 HERE]

Figure 8.30: Yearly average radiative forcing efficiencies for (a) BC, (b) SO_2, (c) OC and (d) NH_3. Values in a particular grid cell show the response of global aerosol DRF to perturbations of emissions in that grid cell (Henze et al., 2011).

Metrics for individual land-based sectors can sometimes be similar to the global mean metric values (e.g., in Shindell et al. (2008a), the BC and OC metrics for the individual land-based sectors in Asia are similar to global means.) In contrast, metrics for emissions from aviation and shipping usually show large differences from global mean metric values (Table 8.14 vs Table 8.15); especially for NOx from shipping. Though there can sometimes be substantial variation in the impact of land-based sectors from one region to another, and for a particular region even from one sector to another, the general pattern is that variability between different land-based sources is generally smaller than between land, sea and air emissions.

For NOx from *aviation* the GWP_{20} values are positive due to the strong effect of the short-lived O_3. For GWP_{100} and GTP_{100} the values are of either sign due to the differences in balance between the individual effects modelled. Thus, there are large uncertainties related to the net effect of NOx from aviation. Even if the models agree on net effect of NOx, the individual contributions can differ significantly. In the multi-model study by Myhre et al. (2011) it is shown that differences in the methane response relative to the O_3 response drive much of the spread. Holmes et al. (2011) found that processes controlling the background tropospheric concentrations of NOx are likely to be the main reason for the modelling uncertainty in climate impacts of NOx from aviation.

Based on detailed studies in the literature, Fuglestvedt et al. (2010) also produced GWP and GTP for contrails, water vapor, and aviation-induced cirrus (AIC). Due to limitations in our knowledge about these components and mechanisms, there are large uncertainties connected to these metric values.

The GWP and GTPs for NOx from *shipping* are strongly negative for all time horizons. The stronger positive effect via O_3 due to the low NOx environment into which ships generally emit NOx is outweighed by the stronger effect on methane destruction at lower latitudes.

Table 8.15 also shows metric values for emissions of SO_2 from the sectors shipping and petroleum production in the Arctic. The direct GWP_{100} for shipping ranges from –11 to –43. The indirect GWPs and GTPs are in some cases 10 times larger than the direct values, but the uncertainty in the metrics for indirect effects is likely to be much larger than for the direct. Only one study (Lauer et al., 2007) has so far reported detailed calculations of the indirect forcing specifically for this sector (and they include the albedo and lifetime indirect effects.) Lauer et al. (2007) also find a wide spread of values depending on the emission inventory. The values from Shindell and Faluvegi (2010) for SO_2 from power production are similar to those for shipping.

Unger et al. (2010) calculated RF for a set of components emitted from each sector. They account for interactions and non-linearities among the emitted species. Such studies are relevant for policymaking that focuses on regulating the *total activity* of that sector or for understanding the contributions from the sector to climate change. On the other hand, the fixed mix of emissions makes it less general and relevant for different emission cases and variations in mix of emission. Alternatively, one may adopt a component-by-component view which is relevant for policy making directed towards specific components (though controlling an individual pollutant in isolation is often not practical). But this view will not capture interactions and non-linearities within the suite of components emitted by most sectors. The effects of specific emission control technologies or policies on the mix of emissions is probably the most relevant type of analysis, but there are an enormous number of possible actions and regional details that could be investigated.

RF at chosen points in time (20 and 100 years) for *sustained* emissions was used by Unger et al. (2010) as the metric for comparison. This is approximately equal to using integrated RF up to the chosen times for *pulse* emissions (and is thus consistent with the GWP perspective). Such a "package view" can be obtained by studying the effect of the suite of emissions per sector in a model. Alternatively, one may adopt a component-by-component view and use emission data directly with metrics, i.e., $E_i \times M(H)_i$, where *i* is component, *H* is time horizon and *M* is the chosen metric.

In the assessment of climate impacts of *current* emissions by sectors we here apply a forward looking perspective on effects in terms *temperature change.* Then the GTP concept can be used to study how the various components develop over time. Figure 8.31a shows the *net* temperature effect over time for 13 sectors (the effects of aerosols on clouds – and in the case of black carbon, on surface albedo – as well as aviation induced cloudiness are not included.). One year of global emissions (i.e., one year pulses) are taken from Unger et al. (2010) [PLACEHOLDER FOR SECOND ORDER DRAFT: to be updated to AR5 emissions inventory] while the metric values are taken from tables in Sections 8.5.2 and Table 8.15. The effects of the sectors are summed over all the individual contributions from the various components and the figure shows that the temperature responses are of different sign and operate on very different timescales. The sectors Industry and Power production cause cooling effects during the first years after emissions (mainly due to SO_2 emissions) but change sign with a peak warming after a few decades and thereafter a long term warming, mainly from CO_2. In order to see the contributions from the various components we can look at the contributions after 20 years; see Figure 8.31b.

[INSERT FIGURE 8.31 HERE]

Figure 8.31: (a) Net dT(t) by sector from total man-made emissions (one year pulse); (b) Net dT(t) by sector after 20 years (for one year pulse emissions). Numbers in parentheses after the sectors give the *net* temperature effect in mK. CT: Contrails. The effects of aerosols on clouds (and in the case of black carbon, on surface albedo) and aviation-induced cirrus are not included. [PLACEHOLDER FOR SECOND ORDER DRAFT: To be updated to AR5 emissions inventory.]

In addition, we also show effect of keeping year 2000 emissions constant (sustained emissions cases). Figure 8.32 illustrates the effects of mix of components in the emissions profiles of the various sectors; the role of cooling vs warming agents and their differing lifetimes. [PLACEHOLDER FOR SECOND ORDER DRAFT: The aerosol portion of the results of the forward looking calculations (shown in 8.28) will be compared with results from Henze et al. (2011), as will the forcing results from the forward modelling of Unger et al. (2010). The latter will be used to put these estimates into context with potential impacts of AIE as well (as those were included in the Unger et al analysis).]

[INSERT FIGURE 8.32 HERE]

Figure 8.32: Net dT(t) by sector from total man-made emissions kept constant; CT: Contrails. The effects of aerosols on clouds (and in the case of black carbon, on surface albedo) and aviation-induced cirrus are not included. [PLACEHOLDER FOR SECOND ORDER DRAFT: To be updated to AR5 emissions inventory.]

Analysing climate change impacts by using the net effect of particular activities or sectors may – compared to other perspectives – provide clearer insight into how societal actions influence climate. Due to large variations in mix of short- and long-lived components, as well as cooling and warming effects, the results will also in these cases depend strongly on choices related to time perspective, impact parameter and type of emission perturbation; as emphasized in the previous section. Improved understanding of aerosol indirect effects and how those are attributed to individual components is clearly necessary to refine estimates of sectoral or emitted component impacts.

Table 8.15: GWPs and GTPs for NOx, BC, OC and SO_2 from various sectors (metrics for SO_2 are given on SO_2 basis, while for NOx they are given on N basis).

	GWP		GTP	
	H = 20	**H = 100**	**H = 20**	**H = 100**
Aviation				
NO_X [a]	92 to 338	–21 to 67	–396 to –121	–5.8 to 7.9
NOx [b]	120 to 470	–2.1 to 71	–590 to –200	–9.5 to 7.6
Shipping				
NO_X [b]	–76 to –31	–36 to –25	–190 to –130	–6.1 to –42
NOx shipping [c]	–107	–73	–135	–30
Shipping SO_2 (direct) [b]	–150 to –37	–43 to –11	–44 to –11	–6.1 to –1.5
Shipping SO_2 (indirect) [b]	–1,600 to –760	–440 to –220	–450 to –220	–63 to –31
SO_2, Arctic shipping [e]	–65	–18		
Arctic shipping SO_2 (indirect) [e]	–283	–80		
OC (Shipping, Arctic) [e]	–209	–59		
BC direct (shipping, Arctic) [e]	2,816	801		
BC snow (shipping, Arctic) [e]	1,056	300		
Energy related				
BC direct + albedo [y]	2,800 ± 1,800	790 ± 530		
OC Energy related [y]	–100 (–40,–210)	–30 (–12, –60)		
Industrial/Power BC, Asia [f]	3,260	910		
Household BC, Asia [f]	2,680	750		
Transport BC, Asia [f]	2,640	740		
Transport BC, North America [f]	3,900	1,090		
Household OC, Asia [f]	–260	–72		
Transport OC, Asia [f]	–180	–50		
Industrial/Power SO_2, Asia [f]	–106 (direct)	–30 (direct)		
Industrial/Power SO_2, N-America[f]	–215 (direct) 20	–60 (direct)		
Global coal-fired power, NOx [d]	–189 (direct)	–53 (direct)		
Global coal-fired power, SO_2 [d]	–377 (dir+ind)	–106 (dir + ind)		
Petroleum production				
BC direct (Arctic emissions) [e]	2,369	673		
BC snow (Arctic emissions) [e]	4,104	1,166		
SO_2, Arctic petroleum [e]	–64	–18		
Arctic petroleum SO_2 [e] (indir)	–48	–14		
OC (Arctic emissions) [e]	–152	–13		
Open biomass				
BC dir + albedo [y]	3,100 ± 1,300	880 ± 370		

OC Open biomass [y]	–180 (–70, –360)	–53 (–20, –100)

Notes:
(a) Myhre et al. (2011)
(b) Fuglestvedt et al. (201[x])
(c) Collins et al. (2011)
(d) Shindell & Faluvegi (2010) and Bond et al. (2010)
(e) Ødemark et al. (2011)
(f) Shindell et al. (2008) (ACP)

8.5.4 Future Radiative Forcing

[PLACEHOLDER FOR SECOND ORDER DRAFT:

-This section will rely on results from the ACCMIP initiative (see Section 8.2). Results from this initiative are not yet fully analysed, but a lot of simulations are underway or already completed.

-Table 8.2 shows the planned simulations and the models that so far have submitted results are shown in Table 8.1. Additional models are expected. Note, that the future simulations will be performed for 3 time-slices and for 4 scenarios (for most models, some are run as transients). Preliminary analysis of the spatial pattern of forcing at two of the time slices is shown in Figure 8.36.

-Forcing results for LLGHG and SLCF will be included, and aerosol AF will be diagnosed as well as traditional RFs.

-Results will be shown as time evolutions for different LLGHG and SLCFs for various scenarios. This will be complemented by bar charts with uncertainties (such as in Figure 8.25 for several scenarios for selected time-slices).

-Several aspects will be given particularly attention, such as the reduction of several of the aerosol components. In this respect nitrate will be especially investigated since it is expected to increase due to reduction of sulphate and increased ammonia emissions (maybe included Bellouin et al. (2011)).

-The detailed forcing simulations with the multi-models within ACCMIP will be compared to simple estimates of relationships between emissions and forcing.]

8.6 Geographic Distribution of Radiative Forcing

The spatial pattern of forcing influences multiple aspects of the climate response. Here we discuss how the pattern has evolved for various forcing agents over the Industrial Era and current understanding of how the forcing distribution affects temperature, precipitation, and other aspects of climate change. Patterns of forcing under future scenarios are also presented, complementing the subsequent discussion of the projected climate response (Chapters 11 and 12).

8.6.1 Spatial Distribution of Current Radiative Forcing

The spatial pattern of the RF of the various RF mechanisms varies substantially (Ramaswamy et al., 2001) particularly for the SLCFs. The LLGHGs such as CO_2 have a rather homogenous spatial RF pattern, with largest forcing in the tropics, decreasing modestly toward the poles. CO_2 forcing is also largest in warm and dry regions and smaller in moist regions and in high-altitude regions (Taylor et al., 2011).

For the short-lived components like tropospheric ozone and aerosols the spatial pattern in their concentrations and therefore their RF pattern are highly inhomogeneous, and again meteorological factors such as temperature (for ozone), humidity, clouds, and surface albedo influence how concentration translates to RF.

For components that primarily scatter radiation such as sulphate or the aerosol cloud albedo effect, the radiative forcing felt at the surface is similar to the RF (according to the definition in Section 8.1.1). However for components that absorb radiation in the atmosphere the radiation reaching the surface is reduced (Andrews et al., 2010; Forster et al., 2007; Ramanathan and Carmichael, 2008). For absorbing aerosols, the sign of the surface forcing is negative while the RF may be positive.

Figure 8.33 shows the RF spatial distribution of the major SLCF together with standard deviation among the models. Note that the models used unified emissions of aerosol and ozone precursors, so that the model diversity in RF is due only to differences in model chemical and climate features, and would be larger if uncertainty in the emissions were also included.

The aerosol direct effect RF (first row) is the sum of the scattering and absorbing (mostly BC) components and is dominated by the former. The RF is greatest in the NH and near populated and biomass burning regions. The standard deviation for the net aerosol forcing is largest over regions where vegetation changes are largest, resulting both in changes to open biomass burning and secondary organics sources (e.g., South Asia, central Africa and Southeast United States); some of the spread among models is due to SOA treatment differences. Carbonaceous aerosol forcing, including absorbing BC (second row), is greatest in South and East Asia. Absorbing aerosols also have enhanced forcing when they overlie regions of high albedo, including cryosphere, desert or clouds and estimated that as much as 50% of black carbon RF occurs from black carbon above clouds. Atmospheric absorption by aerosols makes a strong contribution to the surface forcing (fifth row), and is again generally largest over pollution and biomass burning regions, and their outflow regions.

The net adjusted aerosol forcing (Figure 8.33; third row), includes both direct and indirect effects. The spatial pattern correlates strongly with the aerosol direct effect alone (panel a), except with stronger effect in the outflow regions over oceans (e.g., the Pacific Ocean downwind of Asia, the Atlantic downwind of the Eastern U.S.). The standard deviation also resembles that of the direct effect, but with larger model spread in the Arctic, the Amazon and in some oceanic regions. The large standard deviation in oceanic regions results in part from ongoing uncertainty regarding the importance of indirect effects over land versus ocean. Quaas et al. (2009) showed in satellite retrievals that the correlation between AOD changes and droplet number changes is stronger over oceans than over land and that models tend to overestimate the strength of the relation over land. However, Penner et al. (2011) show that satellite retrievals, due to their dependence on present-day conditions only, tend to underestimate the indirect effect, especially over land. Furthermore, Wang and Penner (2009) showed that if models include boundary layer nucleation and increase the fraction of sulphur emitted as a primary particle, both poorly represented processes in models, the effect over land is increased relative to over ocean. The flux change is clearly larger in the NH compared to the SH (e.g., by nearly a factor of 3 according to Ming et al. (2007)), and has been shown in the modelling study of Ming et al. (2007) to reduce precipitation in the NH as well as to cause a southward shift in the ITCZ.

The tropospheric ozone RF (Figure 8.33; fourth row) is largest at low latitudes, particularly over South Asia and Northern Africa but also with substantial forcing over mid-latitudes of the Northern Hemisphere.

The net aerosol adjusted surface forcing (Figure 8.33, fifth row) has spatial pattern appropriately similar to the combination of the direct (first row) and the adjusted forcing (third row), with strong effects over both land and ocean in polluted and biomass burning regions. The largest standard deviation among models overlies land masses in the NH which however does not correlate with the standard deviations of the direct or adjusted forcings.

[INSERT FIGURE 8.33 HERE]

Figure 8.33: Total aerosol direct RF (first row), total carbonaceous aerosol direct RF (second row), net atmospheric aerosol AF due to aerosols (direct and indirect effects; third row), tropospheric ozone RF (fourth row), and adjusted surface forcing due to aerosols (fifth row). Average of models in left column, standard deviation in right column, with global area-weighted means given in the upper right (all in W m^{-2}). RF values from ACCMIP simulations, AF from ACCMIP and CMIP5 simulations. Note that RF and AF means are shown with different color scales, and standard deviation color scales vary between rows.

8.6.2 Spatial Evolution of Radiative Forcing and Response over the Industrial Era

8.6.2.1 Regional Forcing Changes During Industrial Era

The magnitude of the LLGHG RF has changed over the industrial era, but the spatial distribution has not changed. However the RF spatial distributions for the short-lived components has changed with emissions, due to the timing of regional developments and implementation of pollution standards. Figure 8.34 shows how the distributions of the net direct aerosol effect, carbonaceous aerosols, ozone, and surface radiation have changed from 1850 to 1930, 1980 and 2000.

Substantial industrial activity, especially coal-burning in the early part of the 20th century occurred in the eastern United States and western Europe, leading to large sulphate and BC forcing near those regions (Figure 8.34, first row). Between 1950 and 1970, coal burning was replaced by oil and gasoline, leading to more sulphate but reduced BC. Peak aerosol forcing in North America and Europe occurred around 1970–1980 (Figure 8.34, second row). Between 1970 and 2000 population growth and development of South and East Asia resulted in increased biofuel and fossil fuel pollution there, generating carbonaceous and sulphate aerosols (Figure 8.34, third row). Meanwhile desulphurization controls reduced sulphur emissions especially from North America and Europe. Biomass burning generated significant NH high-latitude ozone and carbonaceous aerosols early in the century, which decreased thereafter while tropical burning increased especially from mid to late century.

[INSERT FIGURE 8.34 HERE]

Figure 8.34: Multi-model mean direct RF (W m^{-2}) for the indicated times from all aerosols based on the ACCMIP simulations. Global area-weighted means given in the upper right. [PLACEHOLDER FOR SECOND ORDER DFAFT: Eventually to be: direct effect of all aerosols, carbonaceous aerosols, ozone, aerosol AF, and surface radiation (from aerosols) for 1930, 1980, and 2000 vs 1850.]

Figure 8.35 shows the zonal mean RF as a time evolution from 1900 to 2000 with 1850 as a reference. The zonal mean RF pattern of tropospheric ozone has been rather similar, with largest forcing around 30N and with a secondary peak around 20S and with the largest change over the time period has been from 1960 to 1980. For sulphate the peak forcing was at mid-latitudes of the NH, with a maximum around 1980, and a shift southward thereafter. BC evolves similarly except that the forcing continued to increase from 1980 to 2000 as it also shifted southward, due mainly to the substantial biofuel combustion in the developing South and East Asia.

Soil dust has changed since the pre-industrial due to changes in climate and land disturbance. To the extent that the dust source has changed in response to climate conditions, the effects would be considered a feedback rather than a forcing. Mahowald et al. (2010) presented observations showing significant increases in dust loading, approximately doubling, over the 20th century, with largest increase from the 1950s to the 1980s and with the responsible source regions being primarily the Saharan and Middle Eastern deserts. Over the century, their model estimated the corresponding effect to by about –0.1 W m^{-2}, but the mid-century value was about –0.3 W m^{-2}. The increased dustiness reduced model precipitation within the Saharan source region, improving model agreement with observed precipitation.

A likely consequence of aerosol loading changes during the past century is the observed reduction of surface radiation, which peaked in many regions such as North America and Europe in the 1980s and has reversed to brighter conditions since (Wild, 2009) while surface radiation over South and East Asia have had particularly strong reductions with little or no reversal in trend. It has been argued that aerosol direct and indirect effects are largely responsible for these surface radiation changes. Many of the AR4 models simulated the observed trends but greatly underestimated the magnitudes of the surface radiation reductions (Wild, 2009).

[INSERT FIGURE 8.35 HERE]

Figure 8.35: Zonal mean radiative forcing as a time evolution from 1900 to 2000 with a reference to 1850 conditions, (a) tropospheric ozone, (b) total direct aerosol effect, (c) direct aerosol effect of sulphate, (d) direct aerosol effect of BC. [PLACEHOLDER FOR SECOND ORDER DRAFT: These are preliminary results that will be updated with more modeling results.]

8.6.2.2 Relationship Between Regional Forcing Patterns and Climate Response During the Industrial Era

In general it is not possible to attribute detailed spatial patterns of temperature or other climate changes to specific patterns of radiative forcing. It has been argued, using climate models, that surface temperature correlates best to net change in TOA flux, and the TOA flux is largely determined by the climate feedback spatial pattern rather than the forcing pattern (Boer and Yu, 2003; Taylor et al., 2011), with the lapse rate, surface albedo and cloud feedbacks explaining most of the temperature response.

Nevertheless, some broad links between forcing and climate response have been identified. Shindell et al. (2010) used multiple models to show that surface temperature changes are not very sensitive to longitudinal variations in forcing, but are sensitive to latitudinal forcings. Shindell et al. (2009b) showed that increased aerosol loading during the last half of the century in the Northern Hemisphere contributed to mid-century dampening of climate warming; and Northern Hemisphere aerosol reduction was associated with over 70% of Arctic warming from the 1970s to the 2000s. This study also showed that the Arctic climate is influenced by forcing changes at lower latitudes more than locally and that the Arctic and much of the Southern Hemisphere surface temperature changes are not sensitive to local forcing changes. Voulgarakis and Shindell (2010) defined a regional transient temperature sensitivity parameter, or temperature response per unit forcing for each four-degree latitude band. They applied this to observed surface air temperature changes and showed that the parameter is best constrained from 50S to 25N, where the value is smaller than at northern higher latitudes, and is found to be 0.35C $(W\ m^{-2})^{-1}$. This value is lower by 35% than in AR4 models, suggesting that models were too sensitive at low latitudes. Crook and Forster (2011) showed that both the spatial distribution of climate feedbacks and of heterogeneous forcing played important roles in the patterns of 20th century temperature changes.

Aerosols influence the distribution of clouds and other hydrologic features such as precipitation, both by changing the cloud microphysical properties and by changing the thermal and energy structures of the atmosphere (see Chapter 7). An increase in aerosol loading in the Northern Hemisphere has been implicated in the observed southward shift of the intertropical convergence zone (ITCZ) up to the 1980s followed by reversal or northward shift since. These shifts have been simulated in models and attributed to aerosols, especially for simulations including indirect effect (e.g., Rotstayn et al., 2000; Zhang et al., 2007). Chang et al. (2011) analyzed observations and climate models coupled to dynamic oceans, and isolated the influences of various forcings. They confirmed that sulphate (direct and indirect) effects are most likely responsible for the ITCZ shift and that the shift is unlikely to have resulted from natural variations. They showed that the sulphate forcing peak in the 1980s correlates with the observed timing of the ITCZ shift. This study did not include the effects of non-sulphate anthropogenic aerosols. Many regional climate patterns may be associated with the ITCZ shift, including drying of the Sahel and northwestern Brazil (e.g., Biasutti and Giannini, 2006; Cox et al., 2008), which also peaked in the 1980s (e.g., Rotstayn and Lohmann, 2002).

Absorbing aerosols have been shown to shift cloud distributions, but again not necessarily in the vicinity of the aerosols. For example, Perlwitz and Miller (2010) showed in a climate model study that for sufficiently absorbing (Saharan) dust, co-located with the convergence zone, low-level convergence and the region of rising air is broadened, moisture is increased, altering the Hadley circulation, and resulting in increased cloud cover in distant oceanic regions as well as near the ITCZ band. Absorbing aerosols may also influence precipitation in monsoon regions, such as over Africa or south Asia. For example, modeling studies by Stephens et al. (2004) and Miller et al. (2004) showed that dust absorption over Africa can enhance low-level convergence and increase vertical velocities so that monsoon circulation and precipitation are enhanced by dust loading over Africa.

On the other hand, Kawase et al. (2011) showed that black carbon from biomass burning may be responsible for the decreasing trend in precipitation in tropical Africa during austral summer, due to reduction in evaporation and enhanced subsidence. The aerosol effects on the Indian monsoon are similarly complex, and have been the subject of numerous studies (e.g., Lau et al., 2006; Wang et al., 2009; Wang et al., 2009; Ramanathan et al., 2005; Chung and Ramanathan, 2006), but a clear picture of how the pattern of regional aerosol forcing correlates with responses has not yet fully emerged.

The temperature response to the aerosol-cloud effects are typically shifted poleward from the cloud changes according to model studies (Chen et al., 2010; Koch et al., 2009) most likely due to cryospheric feedbacks and atmospheric dynamical responses (e.g.Kristjansson et al., 2005).

Forcing resulting from land surface changes may impact local climate more directly than atmospheric forcers do. The spatial distribution of the land use, land cover change effect on AF as it evolved from 1750 to the late 20th century, assuming constant global mean snow cover, is shown in Figure 8.22 above. As discussed in Section 8.4.5, land surface changes over the last century resulted mainly from the change of forests to crops and grasslands, impacting both the surface albedo and the surface energy fluxes. The surface albedo change was primarily a brightening due both to a shift to brighter vegetation and to reduced masking of snow by the canopy, with largest albedo reductions in South and Southeast Asia, Eastern United States, biomass burning regions of South America and Africa, and parts of Australia. These albedo effects cause local cooling according to climate models (e.g., Eliseev and Mokhov, 2011). The indirect vegetation forcing changes due to the reduction in evapotranspiration from plants as stomata open less as CO_2 rises, resulting in drying, warming, and is modeled to be largest over the Amazon, the central African forest, and to a smaller extent over boreal and temporal forests (Andrews et al., 2011). In the coupled climate modeling study of Lawrence and Chase (2010), the vegetation changes caused significant reduction in evapotranspiration, drying and warming in tropical and subtropical regions, with insignificant cooling at higher latitudes. In general, land use changes may have caused cooling at high latitudes and warming at low latitudes, but the uncertainties are significant.

In the Arctic, loss of snow and ice lead to darker surfaces, which enhances Arctic climate warming. For example, strong snow-cover reduction of North America leads to warmer North American summertime temperature in models having a strong snow albedo feedback. These forcings can have non-local impacts that result from enhanced land-ocean temperature contrast, increasing surface convergence over land and divergence over oceans. A poleward intensification of the high pressure patterns and subtropical jet may also result (Fletcher et al., 2009).

BC contributions to darkening of snow has been modeled to cause 20%–50%, of the reduced Arctic snow/ice cover and to have around 20% of Arctic warming over the previous century (Koch et al., 2011; Shindell et al., 2010). However, reductions in Arctic soot during the past two decades (e.g., Hegg et al., 2009) have likely reversed that trend (e.g., Koch et al., 2011; Skeie et al., 2011a). The magnitude of this effect remains very uncertain.

Solar forcing has increased during much of the past century. The pattern of temperature response can be less uniform than the forcing. For example, in one model study there is warming in the NH but little response in the SH, with the SH temperatures apparently moderated by windspeed enhancement effects on ocean circulation (Swingedouw et al., 2011). Ensemble experiments performed with a global coupled climate model, using an older TSI reconstruction from Hoyt and Schatten (1993) that is much larger than current estimates, found the net solar radiation absorbed at the surface. The TSI forcing reconstruction is positive for the period between the 1936–1954 with respect to the 1900–1909, with a value of ~0.4 W m^{-2} at the top of the atmosphere. The results indicate that the net solar absorbed radiation at the surface has a global change near zero, with small increases over oceans (0.16 W m^{-2} in winter and 0.07 W m^{-2} in summer) offset by small decreases over land (–0.20 W m^{-2} in winter and –0.10 W m^{-2} in summer), mostly comparable to the standard deviations (Meehl et al., 2003). The same results roughly apply to present modern maximum times (year 2000). Note, however, that while surface forcing may influence regional response patterns, it's also clear that regional responses to solar forcing are mediated by the stratosphere, so that reproducing such change requires spectrally varying solar forcing rather than the TSI forcing used in this study (see Section 8.3.1.6).

Concerning the 11-year solar cycle, the same type of experiments were performed, but now using older two TSI reconstructions from Hoyt and Schatten (1993) and from Lean et al. (1995). The results indicate that at solar maximum during winter the net solar absorbed radiation at the surface is larger than 1 W m^{-2} in some relatively cloud-free areas in the subtropics, and greater than 2 W m^{-2} in parts of the equatorial Pacific (Meehl et al., 2008). This is a 10 to 20 times larger forcing compared to the PMOD-TSI forcing (Frohlich, 2006) between maximum and minimum of ~0.1 W m^{-2} at the top of the atmosphere.

Large volcanic eruptions produce stratospheric sulphate aerosol clouds that can persist for several years. Aerosol clouds produced by tropical eruptions spread poleward and can cover an entire hemisphere or the entire globe, depending on the initial latitudinal spread. The 1963 Agung eruption aerosol cloud was confined mainly to the Southern Hemisphere; the 1982 El Chichón eruption aerosol cloud was confined mainly to the Northern Hemisphere; and the 1991 Pinatubo eruption aerosol cloud covered the globe. All of them had an *e*-folding lifetime of about 1 year (e.g., Antuña et al., 2003). High-latitude eruptions produce aerosol clouds that stay confined to the mid- high-latitudes of hemisphere of the eruption, and have *e*-folding lifetimes of 2–4 months (Kravitz and Robock, 2011).

RF from volcanic aerosol clouds is mainly by scattering of solar radiation back to space, as well as by absorbing longwave radiation. The vertical distribution of insolation reduction is rather uniform, with the same forcing felt at the top of the atmosphere, at the tropopause, and at the surface. Of course, like all other forcings that interact with solar radiation, this forcing only appears when the Sun is up, with no forcing at night or in the winter polar regions. But stratospheric aerosols also absorb both near-IR solar radiation as well as terrestrial radiation, heating the layer where they reside. This produces a distinct vertical distribution of the heating rate, and also produces a horizontal distribution in the stratosphere. The heating and chemical effects of the aerosols also destroy ozone, which somewhat counteracts the radiative heating, but the net effect is still heating (Stenchikov et al., 2002). For tropical eruptions, this produces a response in atmospheric dynamics, with a stronger polar vortex, a positive mode of the Arctic Oscillation (Northern Annular Mode), and winter warming over Northern Hemisphere continents (Robock, 2000).

8.6.3 Spatial Evolution of Radiative Forcing and Response for the Future

In general it is expected that air quality standards will result in decreased emissions of aerosols and ozone precursors over the next century. The RCP emissions for aerosol and ozone precursors used by the AR5 models all predict reduction in pollution in the coming century (refer to emission plot in Section 8.2). The emission scenarios for AR4 and TAR had less optimistic future projections for pollutants, at least for some scenarios, and particularly for carbonaceous aerosols. However it is not expected that carbonaceous aerosols will significantly increase in the future (e.g., Streets et al., 2004). The AR5 RCPs, like previous ones, indicate that the maximum latitude of pollution, and therefore of RF, is projected to shift somewhat southward (e.g., Lamarque et al., 2011).

Figure 8.36 shows the change in aerosol forcing for RCP 2.6 and 8.5. Both scenarios indicate reduced aerosol loading and positive forcing over Europe, North America and biomass burning regions. Reduced black carbon also contributes substantial negative forcing (~ –0.2 W m^{-2} for RCP 2.6 in 2100). Early in the century, both scenarios indicate increased aerosol forcing over Southeast Asia, with reversal between 2030 and 2100. The net direct aerosol forcing is rather small due to offsetting effects, with reductions in carbonaceous aerosols and in most scattering aerosols causing substantially more forcing in the RCP2.6 case, for example, than the net. Nitrate aerosols continue to increase in all the RCP scenarios, however, as ammonia emissions rise steadily due to agricultural usage (Figure 8.5), contributing additional negative forcing.

Although sulphate precursor emissions are projected to decrease, nitrate is expected to increase in response to that decline as well, as nitrate and sulphate compete for ammonia (e.g., Bauer et al., 2007). This partial compensation in scattering and CCN will mitigate some of the warming expected from pollution reduction.

The shift of aerosol distributions southward is expected to cause the ITCZ to continue to shift northward (e.g., for RCP 2.6 in Figure 8.36). This, in combination with warming and drying over tropical land, has been modelled to lead to greatly enhanced drought conditions in the Amazon (Cox et al., 2008). On the other hand, if the low-latitude aerosol is sufficiently absorbing, broadening of the ITCZ convergence region and enhanced cloud cover could result, as modelled for dust by Perlwitz and Miller (2010).

The reduction in high-latitude black carbon is expected to continue to contribute to Arctic cooling (e.g., Koch et al., 2011), due to reduction in black carbon deposition on snow. On the other hand, reduction in mid-high-latitude scattering aerosols is expected to lead to warming, particularly at high latitudes (Koch et al., 2011; Shindell et al., 2010).

[PLACEHOLDER FOR SECOND ORDER DRAFT: Section will be updated with ACCMIP/CMIP5 results as more become available.]

[INSERT FIGURE 8.36 HERE]

Figure 8.36: Multi-model mean direct RF (W m^{-2}) for the indicated times and RCPs from all aerosols based on the ACCMIP simulations. Global area-weighted means given in the upper right of each panel. [PLACEHOLDER FOR SECOND ORDER DRAFT: Eventually to be: direct effect of all aerosols, carbonaceous aerosols, ozone, aerosol AF, and surface radiation (from aerosols) for these times.]

[START FAQ 8.1 HERE]

FAQ 8.1: How Important is Water Vapour for Climate Change?

Water vapour is the primary greenhouse gas (GHG) in the Earth's atmosphere. The contribution of water vapour to the greenhouse effect relative to that of carbon dioxide depends on the accounting method, but can be considered to be approximately two to three times greater. Additional water vapour is injected into the atmosphere as a result of anthropogenic activities, mostly through enhanced evaporation from irrigated crops, but also through power plant cooling, and marginally through the combustion of fossil fuel. One may therefore question why there is so much focus on carbon dioxide, and not on water vapour, as a forcing to climate change.

Water vapour behaves differently to carbon dioxide in one fundamental way: it can condense and precipitate. The capacity of air to contain water vapour increases with its temperature. When air with high humidity cools, some of the vapour condenses into water droplets and precipitates. The typical residence time of water vapour in the atmosphere is one week. As a consequence, any additional water vapour injected into the atmosphere is rapidly eliminated, so that it has a negligible impact on its concentration, and does not contribute significantly to the long-term greenhouse effect. This is the fundamental reason why tropospheric water vapour (i.e., typically below 10 km altitude) is not considered to be an anthropogenic gas contributing significantly to radiative forcing.

On the other hand, the amount of water vapour in the stratosphere (i.e., above 10 km altitude) has shown variations in the past decades, with significant impacts on the greenhouse effect. An increase in concentration was observed up to year 2000, which could be explained in part by the increase in atmospheric methane as a result of anthropogenic emissions. In this case it is considered a RF agent. However, the full extent of the variations of stratospheric water vapour concentration, and in particular the decrease that is observed since 2000, is not well understood.

The amount of water vapour that can be in the atmosphere increases rapidly with its temperature. A typical polar air atmospheric column may contain a few kilogram of water vapour per square metre while the equivalent for a tropical air mass is up to 100 kilograms. If an initial forcing warms the air temperature, the atmosphere will increase its potential to contain water vapour. The water vapour concentration will then increase (less precipitation than evaporation during the transition period) which leads to a further increase in the greenhouse effect and therefore to an additional temperature increase. This process, referred to as the water vapour feedback, is well understood and quantified. Although an increase in the atmosphere water vapour content has been observed, this change is understood as a climate feedback and cannot be interpreted as a RF. The water vapour feedback is included in all climate models used to estimate climate change.

In the present-day Earth atmosphere, water vapour has the largest greenhouse effect. However, other greenhouse gases, and primarily carbon dioxide, are necessary to sustain the presence of water vapour in the atmosphere. Indeed, if these other GHGs were removed from the atmosphere, its temperature would drop sufficiently to induce a decrease of water vapour, leading to a runaway drop of the greenhouse effect that would plunge the Earth into a frozen state. So GHGs other than water vapour have provided the temperature structure that sustains current levels of atmospheric water vapour. Therefore, although carbon dioxide is the main control knob on climate, water vapour is a strong and fast feedback that amplifies any initial forcing by a factor of typically three. Water vapour is not a significant initial forcing, but is nevertheless a fundamental agent of climate change.

[END FAQ 8.1 HERE]

[START FAQ 8.2 HERE]

FAQ 8.2: Do Improvements in Air Quality have an Effect on Climate Change?

Yes they do, but their impact on climate can be cooling or warming. Depending on the specific pollution control(s) and associated targeted emissions, the response becomes a combination of positive and negative forcings, leading to an uncertain overall climate impact.

Air quality usually refers to surface conditions associated with ozone, carbon monoxide, nitrogen oxides and aerosols or equivalently particulate matter (PM; it is frequently defined in terms of a maximum considered size such as 1 micrometer, PM1, or 2.5 micrometers, PM2.5) or airborne particles. Exposure to such particles and ozone raises mortality from respiratory and cardiovascular diseases. Therefore, policies are being implemented in many regions of the world to reduce such dangerous exposures.

The critical aspect in how air pollutants influence surface temperature relates to their composition. Specific pollution controls target specific emissions. As a result of those changes in emissions, generated greenhouse gases will primarily impact climate through radiation, while aerosols will impact climate through radiation and cloud-aerosol interactions. Impacts on aspects of climate other than surface temperature may also be large, especially on precipitation, but are less well quantified.

Measures to lower surface ozone (controls on precursor emissions such as nitrogen oxides, carbon monoxide, methane or volatile organic compounds, VOCs) will have a cooling impact, depending on how much these measures affect tropospheric ozone in the mid-troposphere and above. However, the impact of a specific set of emission changes (e.g., transportation) can become quite complicated owing to atmospheric chemistry couplings between all targeted emissions. For example, while reducing tropospheric ozone, nitrogen oxide emission controls lead to an overall warming through their impact on methane lifetime and aerosol formation.

Because of their varying shape and composition, the net effect of the interaction of aerosols with radiation ranges from mostly reflective (sulfate particles) to mostly absorbing (black carbon). Consequently, from a purely radiative standpoint, air pollution measures that reduce production of sulfate particles have a detrimental effect on climate. The most important counterpart is black carbon, for which the combined effect of heat absorption in the atmosphere and impact on snow albedo makes it a strong candidate for combining air quality and climate improvements. Beyond radiation, the interaction between hydrophilic aerosols and clouds leads to several additional effects, with an estimated significant net cooling between pre-industrial conditions and present-day, especially during the second-half of the 20th century.

Unlike carbon dioxide and other long-lived greenhouse gases, tropospheric ozone and aerosols have a quite short residence time in the atmosphere (a few days to a few months). While there can be some indirect couplings within the Earth system to prolong their impact, these pollutants tend to mostly affect regions near their source of origin or close downstream. This might lead to a global estimate of radiative forcing that is globally rather small, but could be regionally quite significant.

Specific sectors of anthropogenic activity are primarily responsible for specific emissions. For example, black carbon emissions are dominated by the domestic and transportation sectors. The power and shipping sectors dominate sulfate production. Satellites observations have clearly shown the increase in sulfur dioxide (the primary precursor to sulfate aerosols) over Eastern Asia. While there are signs that many of the new power plants are using scrubbers to reduce such emissions, it is unclear whether developing countries will follow the same overall curb of sulfur emissions with growing population and gross domestic product that the United States of America and Western Europe has enforced since the 1970s. Regardless, it is important to remember that, even with the short-term climate cooling of sulfate aerosols, carbon dioxide is still being emitted from the combustion of coal, and will be present in the atmosphere for many times longer than aerosols.

One major additional uncertainty resides on understanding the effect of climate change on air quality. It is clear that air quality is strongly affected by weather patterns, from the clean conditions occurring after the passage of a front to the highly polluted conditions associated with hot and stagnant conditions prevailing under a high-pressure system. While not fully understood, the observed positive correlation between surface ozone and temperature in polluted regions indicate the potential danger looming with some future scenarios and associated climate change. Based on model studies this impact of climate change (sometimes referred to as "climate penalty") could in some regions outweigh many measures taken to improve air quality. This "climate penalty" is difficult to assess and will be regionally-dependent, with additional impacts from precipitation and humidity changes on wet deposition processes.

Many direct and indirect couplings between short-lived pollutants and climate are still poorly understood and even not represented in models, limiting our ability to fully quantify the impact of pollution controls. But it is becoming clear that controls of surface air quality impact climate.

[INSERT FAQ 8.2, FIGURE 1 HERE]

FAQ 8.2, Figure 1: Schematic diagram of the impact of pollution controls on specific emissions and climate impact. Solid black line indicates known impact, dashed line indicates uncertain impact.

[END FAQ 8.2 HERE]

References

Aaheim, A., J. Fuglestvedt, and O. Godal, 2006: Costs savings of a flexible multi-gas climate policy. *Energy Journal*, 485-501.

Abreu, J., J. Beer, F. Steinhilber, S. Tobias, and N. Weiss, 2008: For how long will the current grand maximum of solar activity persist? *Geophysical Research Letters*, **35,** -.

Aghedo, A., et al., 2011: The vertical distribution of ozone instantaneous radiative forcing from satellite and chemistry climate models. *Journal of Geophysical Research-Atmospheres*, ARTN D01305, DOI 10.1029/2010JD014243, -.

Ammann, C. M., and P. Naveau, 2003: Statistical analysis of tropical explosive volcanism occurrences over the last 6 centuries. *Geophysical Research Letters*, **30,** 4.

——, 2010: A statistical volcanic forcing scenario generator for climate simulations. *Journal of Geophysical Research-Atmospheres*, **115**.

Anchukaitis, K. J., B. M. Buckley, E. R. Cook, B. I. Cook, R. D. D'Arrigo, and C. M. Ammann, 2010: Influence of volcanic eruptions on the climate of the Asian monsoon region. *Geophysical Research Letters*, **37**.

Andersen, M., D. Blake, F. Rowland, M. Hurley, and T. Wallington, 2009: Atmospheric Chemistry of Sulfuryl Fluoride: Reaction with OH Radicals, CI Atoms and O-3, Atmospheric Lifetime, IR Spectrum, and Global Warming Potential. *Environmental Science & Technology*, DOI 10.1021/es802439f, 1067-1070.

Andrews, T., and P. M. Forster, 2008: CO2 forcing induces semi-direct effects with consequences for climate feedback interpretations. *Geophysical Research Letters*, **35**.

Andrews, T., M. Doutriaux-Boucher, O. Boucher, and P. M. Forster, 2011: A regional and global analysis of carbon dioxide physiological forcing and its impact on climate. *Climate Dynamics*, **36,** 783-792.

Andrews, T., P. Forster, O. Boucher, N. Bellouin, and A. Jones, 2010: Precipitation, radiative forcing and global temperature change. *Geophysical Research Letters*, ARTN L14701, DOI 10.1029/2010GL043991, -.

Antuna, J. C., A. Robock, G. Stenchikov, J. Zhou, C. David, J. Barnes, and L. Thomason, 2003: Spatial and temporal variability of the stratospheric aerosol cloud produced by the 1991 Mount Pinatubo eruption. *Journal of Geophysical Research-Atmospheres*, **108**.

Archibald, A. T., M. E. Jenkin, and D. E. Shallcross, 2010a: An isoprene mechanism intercomparison. *Atmospheric Environment*, **44,** 5356-5364.

Archibald, A. T., M. C. Cooke, S. R. Utembe, D. E. Shallcross, R. G. Derwent, and M. E. Jenkin, 2010b: Impacts of mechanistic changes on HO(x) formation and recycling in the oxidation of isoprene. *Atmospheric Chemistry and Physics*, **10,** 8097-8118.

Archibald, A. T., et al., 2011: Impacts of HO(x) regeneration and recycling in the oxidation of isoprene: Consequences for the composition of past, present and future atmospheres. *Geophysical Research Letters*, **38**.

Arneth, A., P. A. Miller, M. Scholze, T. Hickler, G. Schurgers, B. Smith, and I. C. Prentice, 2007: CO2 inhibition of global terrestrial isoprene emissions: Potential implications for atmospheric chemistry. *Geophysical Research Letters*, **34**.

Arneth, A., et al., 2010a: From biota to chemistry and climate: towards a comprehensive description of trace gas exchange between the biosphere and atmosphere. *Biogeosciences*, **7,** 121-149.

Arneth, A., et al., 2010b: Terrestrial biogeochemical feedbacks in the climate system. *Nature Geoscience*, **3,** 525-532.

Ashmore, M. R., 2005: Assessing the future global impacts of ozone on vegetation. *Plant Cell and Environment*, **28,** 949-964.

Aydin, M., et al., 2011: Recent decreases in fossil-fuel emissions of ethane and methane derived from firn air. *Nature*, **476,** 198-201.

Bala, G., K. Caldeira, M. Wickett, T. J. Phillips, D. B. Lobell, C. Delire, and A. Mirin, 2007: Combined climate and carbon-cycle effects of large-scale deforestation. *Proceedings of the National Academy of Sciences of the United States of America*, **104,** 6550-6555.

Balkanski, Y., G. Myhre, M. Gauss, G. Radel, E. Highwood, and K. Shine, 2010: Direct radiative effect of aerosols emitted by transport: from road, shipping and aviation. *Atmospheric Chemistry and Physics*, DOI 10.5194/acp-10-4477-2010, 4477-4489.

Barnes, C. A., and D. P. Roy, 2008: Radiative forcing over the conterminous United States due to contemporary land cover land use albedo change. *Geophysical Research Letters*, **35,** -.

Bathiany, S., M. Claussen, V. Brovkin, T. Raddatz, and V. Gayler, 2010: Combined biogeophysical and biogeochemical effects of large-scale forest cover changes in the MPI earth system model. *Biogeosciences*, **7,** 1383-1399.

Bauer, S., D. Koch, N. Unger, S. Metzger, D. Shindell, and D. Streets, 2007: Nitrate aerosols today and in 2030: a global simulation including aerosols and tropospheric ozone. *Atmospheric Chemistry and Physics*, **7,** 5043-5059.

Bekki, S., J. A. Pyle, W. Zhong, R. Toumi, J. D. Haigh, and D. M. Pyle, 1996: The role of microphysical and chemical processes in prolonging the climate forcing of the Toba eruption. *Geophysical Research Letters*, **23,** 2669-2672.

Bergamaschi, P., et al., 2009: Inverse modeling of global and regional CH(4) emissions using SCIAMACHY satellite retrievals. *Journal of Geophysical Research-Atmospheres*, **114**.

Berntsen, T., and J. Fuglestvedt, 2008: Global temperature responses to current emissions from the transport sectors. *Proceedings of the National Academy of Sciences of the United States of America*, DOI 10.1073/pnas.0804844105**,** 19154-19159.
Berntsen, T., J. Fuglestvedt, G. Myhre, F. Stordal, and T. F. Berglen, 2006: Abatement of greenhouse gases: Does location matter? *Climatic Change*, **74,** 377-411.
Berntsen, T. K., et al., 2005: Response of climate to regional emissions of ozone precursors: sensitivities and warming potentials. *Tellus Series B-Chemical and Physical Meteorology*, **57,** 283-304.
Betts, R. A., P. D. Falloon, K. K. Goldewijk, and N. Ramankutty, 2007: Biogeophysical effects of land use on climate: Model simulations of radiative forcing and large-scale temperature change. *Agricultural and Forest Meteorology*, **142,** 216-233.
Biasutti, M., and A. Giannini, 2006: Robust Sahel drying in response to late 20th century forcings. *Geophysical Research Letters*, **33**.
Boer, G. J., and B. Yu, 2003: Climate sensitivity and response. *Climate Dynamics*, **20,** 415-429.
Bond, T., C. Zarzycki, M. Flanner, and D. Koch, 2011: Quantifying immediate radiative forcing by black carbon and organic matter with the Specific Forcing Pulse. *Atmospheric Chemistry and Physics*, **11,** 1505-1525.
Bond, T. C., et al., 2007: Historical emissions of black and organic carbon aerosol from energy-related combustion, 1850-2000. *Global Biogeochemical Cycles*, **21,** 16.
Bonfils, C., and D. Lobell, 2007: Empirical evidence for a recent slowdown in irrigation-induced cooling. *Proceedings of the National Academy of Sciences of the United States of America*, **104,** 13582-13587.
Borken-Kleefeld, J., T. Berntsen, and J. Fuglestvedt, 2011: Times Matted!-Response to Wallington et al. *Environmental Science & Technology*, **45,** 3167-3168.
Boucher, O., and J. Haywood, 2001: On summing the components of radiative forcing of climate change. *Climate Dynamics*, **18,** 297-302.
Boucher, O., and M. Reddy, 2008: Climate trade-off between black carbon and carbon dioxide emissions. *Energy Policy*, DOI 10.1016/j.enpol.2007.08.039**,** 193-200.
Boucher, O., P. Friedlingstein, B. Collins, and K. P. Shine, 2009: The indirect global warming potential and global temperature change potential due to methane oxidation. *Environmental Research Letters*, **4**.
Bourassa, A. E., D. A. Degenstein, and E. J. Llewellyn, 2008: Retrieval of stratospheric aerosol size information from OSIRIS limb scattered sunlight spectra. *Atmospheric Chemistry and Physics*, **8,** 6375-6380.
Bourassa, A. E., D. A. Degenstein, B. J. Elash, and E. J. Llewellyn, 2010: Evolution of the stratospheric aerosol enhancement following the eruptions of Okmok and Kasatochi: Odin-OSIRIS measurements. *Journal of Geophysical Research-Atmospheres*, **115**.
Bousquet, P., et al., 2006: Contribution of anthropogenic and natural sources to atmospheric methane variability. *Nature*, **443,** 439-443.
Bowman, D., et al., 2009: Fire in the Earth System. *Science*, **324,** 481-484.
Bradford, D., 2001: Global change - Time, money and tradeoffs. *Nature***,** 649-650.
BREWER, A., 1949: EVIDENCE FOR A WORLD CIRCULATION PROVIDED BY THE MEASUREMENTS OF HELIUM AND WATER VAPOUR DISTRIBUTION IN THE STRATOSPHERE. *Quarterly Journal of the Royal Meteorological Society*, **75,** 351-363.
Bright, R., A. Stromman, and G. Peters, 2011: Radiative Forcing Impacts of Boreal Forest Biofuels: A Scenario Study for Norway in Light of Albedo. *Environmental Science & Technology*, **45,** 7570-7580.
Brovkin, V., et al., 2010: Sensitivity of a coupled climate-carbon cycle model to large volcanic eruptions during the last millennium. *Tellus Series B-Chemical and Physical Meteorology*, **62,** 674-681.
BRUECKNER, G., K. EDLOW, L. FLOYD, J. LEAN, and M. VANHOOSIER, 1993: THE SOLAR ULTRAVIOLET SPECTRAL IRRADIANCE MONITOR (SUSIM) EXPERIMENT ON BOARD THE UPPER-ATMOSPHERE RESEARCH SATELLITE (UARS). *Journal of Geophysical Research-Atmospheres*, **98,** 10695-10711.
Burkhardt, U., and B. Karcher, 2011: Global radiative forcing from contrail cirrus. *Nature Climate Change*, **1,** 54-58.
Cameron-Smith, P. C.-S. P., S. Elliott, M. Maltrud, D. Erickson, and O. Wingenter, 2011: Changes in dimethyl sulfide oceanic distribution due to climate change. *Geophysical Research Letters*, **38**.
Campra, P., M. Garcia, Y. Canton, and A. Palacios-Orueta, 2008: Surface temperature cooling trends and negative radiative forcing due to land use change toward greenhouse farming in southeastern Spain. *Journal of Geophysical Research-Atmospheres*, **113,** -.
Carlton, A. G., R. W. Pinder, P. V. Bhave, and G. A. Pouliot, 2010: To What Extent Can Biogenic SOA be Controlled? *Environmental Science & Technology*, **44,** 3376-3380.
Carslaw, K. S., O. Boucher, D. V. Spracklen, G. W. Mann, J. G. L. Rae, S. Woodward, and M. Kulmala, 2010: A review of natural aerosol interactions and feedbacks within the Earth system. *Atmospheric Chemistry and Physics*, **10,** 1701-1737.
Chang, C. Y., J. C. H. Chiang, M. F. Wehner, A. R. Friedman, and R. Ruedy, 2011: Sulfate Aerosol Control of Tropical Atlantic Climate over the Twentieth Century. *Journal of Climate*, **24,** 2540-2555.
Chen, W. T., A. Nenes, H. Liao, P. J. Adams, J. L. F. Li, and J. H. Seinfeld, 2010: Global climate response to anthropogenic aerosol indirect effects: Present day and year 2100. *Journal of Geophysical Research-Atmospheres*, **115**.

Cherubini, F., G. Peters, T. Berntsen, A. Stromman, and E. Hertwich, 2011: CO2 emissions from biomass combustion for bioenergy: atmospheric decay and contribution to global warming. *Global Change Biology Bioenergy*, **3,** 413-426.
Christensen, M., and G. Stephens 2011: Microphysical and macrophysical responses of marine stratocumulus polluted by underlying ships Part II: Impacts of drizzle. *J. Geophys. Res.***,** in press.
Christensen, M., and G. Stephens, 2011: Microphysical and macrophysical responses of marine stratocumulus polluted by underlying ships: Evidence of cloud deepening. *Journal of Geophysical Research-Atmospheres*, **116,** D03201.
CLARKE, A., and K. NOONE, 1985: SOOT IN THE ARCTIC SNOWPACK - A CAUSE FOR PERTURBATIONS IN RADIATIVE-TRANSFER. *Atmospheric Environment*, **19,** 2045-2053.
CLOUGH, S., M. IACONO, and J. MONCET, 1992: LINE-BY-LINE CALCULATIONS OF ATMOSPHERIC FLUXES AND COOLING RATES - APPLICATION TO WATER-VAPOR. *Journal of Geophysical Research-Atmospheres*, **97,** 15761-15785.
Clough, S., et al., 2005: Atmospheric radiative transfer modeling: a summary of the AER codes. *Journal of Quantitative Spectroscopy & Radiative Transfer*, **91,** 233-244.
COLLINS, W., R. DERWENT, C. JOHNSON, and D. STEVENSON, 2002: The oxidation of organic compounds in the troposphere and their global warming potentials. *CLIMATIC CHANGE*, **52,** 453-479.
Collins, W. D., et al., 2006: Radiative forcing by well-mixed greenhouse gases: Estimates from climate models in the Intergovernmental Panel on Climate Change (IPCC) Fourth Assessment Report (AR4). *Journal of Geophysical Research-Atmospheres*, **111**.
Collins, W. J., S. Sitch, and O. Boucher, 2010: How vegetation impacts affect climate metrics for ozone precursors. *Journal of Geophysical Research-Atmospheres*, **115**.
Cooper, O. R., et al., 2010: Increasing springtime ozone mixing ratios in the free troposphere over western North America. *Nature*, **463,** 344-348.
Corbett, J., D. Lack, J. Winebrake, S. Harder, J. Silberman, and M. Gold, 2010: Arctic shipping emissions inventories and future scenarios. *Atmospheric Chemistry and Physics*, DOI 10.5194/acp-10-9689-2010**,** 9689-9704.
Cox, P. M., et al., 2008: Increasing risk of Amazonian drought due to decreasing aerosol pollution. *Nature*, **453,** 212-U217.
Crook, J., and P. Forster, 2011: A balance between radiative forcing and climate feedback in the modeled 20th century temperature response. *Journal of Geophysical Research-Atmospheres*, **116,** -.
Crounse, J. D., F. Paulot, H. G. Kjaergaard, and P. O. Wennberg, 2011: Peroxy radical isomerization in the oxidation of isoprene. *Physical Chemistry Chemical Physics*, **13,** 13607-13613.
Davin, E. L., and N. de Noblet-Ducoudre, 2010: Climatic Impact of Global-Scale Deforestation: Radiative versus Nonradiative Processes. *Journal of Climate*, **23,** 97-112.
Davin, E. L., N. de Noblet-Ducoudre, and P. Friedlingstein, 2007: Impact of land cover change on surface climate: Relevance of the radiative forcing concept. *Geophysical Research Letters*, **34,** -.
De Cara, S., E. Galko, and P. Jayet, 2008: The Global Warming Potential Paradox: Implications for the Design of Climate Policy. *Design of Climate Policy***,** 359-384.
DeAngelis, A., F. Dominguez, Y. Fan, A. Robock, M. D. Kustu, and D. Robinson, 2010: Evidence of enhanced precipitation due to irrigation over the Great Plains of the United States. *Journal of Geophysical Research-Atmospheres*, **115**.
Deligne, N. I., S. G. Coles, and R. S. J. Sparks, 2010: Recurrence rates of large explosive volcanic eruptions. *Journal of Geophysical Research-Solid Earth*, **115**.
den Elzen, M., et al., 2005: Analysing countries' contribution to climate change: scientific and policy-related choices. *Environmental Science & Policy*, DOI 10.1016/j.envsci.2005.06.007**,** 614-636.
Denman, K. L., et al., 2007: Couplings Between Changes in the Climate System and Biogeochemistry. *Climate Change 2007: The Physical Science Basis. Contribution of Working Group I to the Fourth Assessment Report of the Intergovernmental Panel on Climate Change*, Cambridge University Press.
DERWENT, R., W. COLLINS, C. JOHNSON, and D. STEVENSON, 2001: Transient behaviour of tropospheric ozone precursors in a global 3-D CTM and their indirect greenhouse effects. *CLIMATIC CHANGE*, **49,** 463-487.
Dewitte, S., D. Crommelynck, S. Mekaoui, and A. Joukoff, 2004: Measurement and uncertainty of the long-term total solar irradiance trend. *Solar Physics*, **224,** 209-216.
Dlugokencky, E. J., et al., 2009: Observational constraints on recent increases in the atmospheric CH(4) burden. *Geophysical Research Letters*, **36**.
Dlugokencky, E. J. D. E. J., E. G. Nisbet, R. Fisher, and D. Lowry, 2011: Global atmospheric methane: budget, changes and dangers. *Philosophical Transactions of the Royal Society a-Mathematical Physical and Engineering Sciences*, **369,** 2058-2072.
Doherty, S. J., S. G. Warren, T. C. Grenfell, A. D. Clarke, and R. E. Brandt, 2010: Light-absorbing impurities in Arctic snow. *Atmospheric Chemistry and Physics*, **10,** 11647-11680.
Doutriaux-Boucher, M., M. Webb, J. Gregory, and O. Boucher, 2009: Carbon dioxide induced stomatal closure increases radiative forcing via a rapid reduction in low cloud. *Geophysical Research Letters*, ARTN L02703, DOI 10.1029/2008GL036273**,** -.

Eliseev, A. V., and Mokhov, II, 2011: Effect of including land-use driven radiative forcing of the surface albedo of land on climate response in the 16th-21st centuries. *Izvestiya Atmospheric and Oceanic Physics*, **47,** 15-30.
Eyring, V., et al., 2010a: Transport impacts on atmosphere and climate: Shipping. *Atmospheric Environment*, **44,** 4735-4771.
Eyring, V., et al., 2010b: Sensitivity of 21st century stratospheric ozone to greenhouse gas scenarios. *Geophysical Research Letters*, **37**.
Eyring, V., et al., 2010c: Multi-model assessment of stratospheric ozone return dates and ozone recovery in CCMVal-2 models. *Atmospheric Chemistry and Physics*, **10,** 9451-9472.
FAO, 2010: *Global Forest Resources Assessment 2010.*
Feng, X., and F. Zhao, 2009: Effect of changes of the HITRAN database on transmittance calculations in the near-infrared region. *Journal of Quantitative Spectroscopy & Radiative Transfer*, **110,** 247-255.
Feng, X., F. Zhao, and W. Gao, 2007: Effect of the improvement of the HITIRAN database on the radiative transfer calculation. *Journal of Quantitative Spectroscopy & Radiative Transfer*, **108,** 308-318.
Feulner, G., 2011: Are the most recent estimates for the Maunder Minimum solar irradiance in agreement with temperature reconstructions? *Geophysical Research Letters*, **38,** L16706.
Findell, K. L., E. Shevliakova, P. C. D. Milly, and R. J. Stouffer, 2007: Modeled impact of anthropogenic land cover change on climate. *Journal of Climate*, **20,** 3621-3634.
Fiore, A. M., et al., 2009: Multimodel estimates of intercontinental source-receptor relationships for ozone pollution. *Journal of Geophysical Research-Atmospheres*, **114**.
FISHER, D., et al., 1990: MODEL-CALCULATIONS OF THE RELATIVE EFFECTS OF CFCS AND THEIR REPLACEMENTS ON STRATOSPHERIC OZONE. *Nature***,** 508-512.
Flanner, M. G., C. S. Zender, J. T. Randerson, and P. J. Rasch, 2007: Present-day climate forcing and response from black carbon in snow. *Journal of Geophysical Research-Atmospheres*, **112**.
Flanner, M. G., C. S. Zender, P. G. Hess, N. M. Mahowald, T. H. Painter, V. Ramanathan, and P. J. Rasch, 2009: Springtime warming and reduced snow cover from carbonaceous particles. *Atmospheric Chemistry and Physics*, **9,** 2481-2497.
Fletcher, C. G., P. J. Kushner, A. Hall, and X. Qu, 2009: Circulation responses to snow albedo feedback in climate change. *Geophysical Research Letters*, **36**.
Fomin, B., 2004: A k-distribution technique for radiative transfer simulation in inhomogeneous atmosphere: 1. FKDM, fast k-distribution model for the longwave. *Journal of Geophysical Research-Atmospheres*, **109,** -.
Fomin, B., and M. Correa, 2005: A k-distribution technique for radiative transfer simulation in inhomogeneous atmosphere: 2. FKDM, fast k-distribution model for the shortwave. *Journal of Geophysical Research-Atmospheres*, **110,** -.
Fomin, B. A., and V. A. Falaleeva, 2009: Recent progress in spectroscopy and its effect on line-by-line calculations for the validation of radiation codes for climate models. *Atmos. Oceanic Opt.*, **22,** 626-629.
Forster, P., and K. Shine, 1997: Radiative forcing and temperature trends from stratospheric ozone changes. *Journal of Geophysical Research-Atmospheres*, **102,** 10841-10855.
Forster, P., et al., 2007: Changes in Atmospheric Constituents and in Radiative Forcing. *Climate Change 2007: The Physical Science Basis. Contribution of Working Group I to the Fourth Assessment Report of the Intergovernmental Panel on Climate Change*, Cambridge University Press.
Forster, P., et al., 2011: Evaluation of radiation scheme performance within chemistry climate models. *Journal of Geophysical Research-Atmospheres*, **116,** -.
Fortuin, J. P. F., and H. Kelder, 1998: An ozone climatology based on ozonesonde and satellite measurements. *Journal of Geophysical Research-Atmospheres*, **103,** 31709-31734.
Foukal, P., A. Ortiz, and R. Schnerr, 2011: Dimming of the 17th century Sun. *Astrophysical Journal Letters*, **733,** L38.
Foukal, P., C. Frohlich, H. Spruit, and T. Wigley, 2006: Variations in solar luminosity and their effect on the Earth's climate. *Nature*, **443,** 161-166.
Frame, T., and L. Gray, 2010: The 11-Yr Solar Cycle in ERA-40 Data: An Update to 2008. *Journal of Climate*, **23,** 2213-2222.
Frohlich, C., 2006: Solar irradiance variability since 1978 - Revision of the PMOD composite during solar cycle 21. *Space Science Reviews*, **125,** 53-65.
——, 2009: Evidence of a long-term trend in total solar irradiance. *Astronomy & Astrophysics*, **501,** L27-U508.
Fry, M., V. Naik, and e. al., 2011: The influence of ozone precursor emissions from four world regions on tropospheric composition and radiative climate forcing.
Fuglestvedt, J., T. Berntsen, O. Godal, and T. Skodvin, 2000: Climate implications of GWP-based reductions in greenhouse gas emissions. *Geophysical Research Letters***,** 409-412.
Fuglestvedt, J., T. Berntsen, G. Myhre, K. Rypdal, and R. Skeie, 2008: Climate forcing from the transport sectors. *Proceedings of the National Academy of Sciences of the United States of America*, DOI 10.1073/pnas.0702958104**,** 454-458.
Fuglestvedt, J., T. Berntsen, O. Godal, R. Sausen, K. Shine, and T. Skodvin, 2003: Metrics of climate change: Assessing radiative forcing and emission indices. *Climatic Change***,** 267-331.
Fuglestvedt, J. S., et al., 2010: Transport impacts on atmosphere and climate: Metrics. *Atmospheric Environment*, **44,** 4648-4677.

Gaillard, M. J., et al., 2010: Holocene land-cover reconstructions for studies on land cover-climate feedbacks. *Climate of the Past*, **6,** 483-499.
Gao, C., A. Robock, and C. Ammann, 2008: Volcanic forcing of climate over the past 1500 years: An improved ice core-based index for climate models. *Journal of Geophysical Research-Atmospheres*, **113**.
——, 2009: Correction to "Volcanic forcing of climate over the past 1500 years: An improved ice core-based index for climate models (vol 113, D23111, 2008)". *Journal of Geophysical Research-Atmospheres*, **114**.
Gao, C., L. Oman, A. Robock, and G. L. Stenchikov, 2007: Atmospheric volcanic loading derived from bipolar ice cores: Accounting for the spatial distribution of volcanic deposition. *Journal of Geophysical Research-Atmospheres*, **112**.
Gao, C., et al., 2006: The 1452 or 1453 AD Kuwae eruption signal derived from multiple ice core records: Greatest volcanic sulfate event of the past 700 years. *Journal of Geophysical Research-Atmospheres*, **111**.
Gatebe, C. K., E. Wilcox, R. Poudyal, and J. Wang, 2011: Effects of ship wakes on ocean brightness and radiative forcing over ocean. *Geophysical Research Letters*, **38**.
Gedney, N., P. M. Cox, and C. Huntingford, 2004: Climate feedback from wetland methane emissions. *Geophysical Research Letters*, **31**.
Gerlach, T., 2011: Volcanic versus anthropogenic carbon dioxide. *Eos*, **92**.
Gettelman, A., J. Holton, and K. Rosenlof, 1997: Mass fluxes of O-3, CH4, N2O and CF2Cl2 in the lower stratosphere calculated from observational data. *Journal of Geophysical Research-Atmospheres*, **102,** 19149-19159.
Gillett, N., and H. Matthews, 2010: Accounting for carbon cycle feedbacks in a comparison of the global warming effects of greenhouse gases. *Environmental Research Letters*, **5,** -.
Godal, O., 2003: The IPCC's assessment of multidisciplinary issues: The case of greenhouse gas indices - An editorial essay. *Climatic Change***,** 243-249.
Goldstein, A. H., and I. E. Galbally, 2007: Known and unexplored organic constituents in the earth's atmosphere. *Environmental Science & Technology*, **41,** 1514-1521.
Gong, S. L., et al., 2010: Identification of trends and interannual variability of sulfate and black carbon in the Canadian High Arctic: 1981-2007. *Journal of Geophysical Research-Atmospheres*, **115**.
Goosse, H., et al., 2006: The origin of the European "Medieval Warm Period". *Climate of the Past*, **2,** 99-113.
Goto, D., T. Takemura, T. Nakajima, and K. V. S. Badarinath, 2011: Global aerosol model-derived black carbon concentration and single scattering albedo over Indian region and its comparison with ground observations. *Atmospheric Environment*, **45,** 3277-3285.
Granier, C., et al., 2011: Evolution of anthropogenic and biomass burning emissions of air pollutants at global and regional scales during the 1980–2010 period. *Climatic Change*, **109,** 163-190.
Gray, L., S. Rumbold, and K. Shine, 2009: Stratospheric Temperature and Radiative Forcing Response to 11-Year Solar Cycle Changes in Irradiance and Ozone. *Journal of the Atmospheric Sciences*, **66,** 2402-2417.
Gray, L., et al., 2010: SOLAR INFLUENCES ON CLIMATE. *Reviews of Geophysics*, **48,** -.
Gregory, J., and M. Webb, 2008: Tropospheric adjustment induces a cloud component in CO2 forcing. *Journal of Climate*, **21,** 58-71.
Gregory, J., et al., 2004: A new method for diagnosing radiative forcing and climate sensitivity. *Geophysical Research Letters*, **31,** -.
Guenther, A., T. Karl, P. Harley, C. Wiedinmyer, P. I. Palmer, and C. Geron, 2006: Estimates of global terrestrial isoprene emissions using MEGAN (Model of Emissions of Gases and Aerosols from Nature). *Atmospheric Chemistry and Physics*, **6,** 3181-3210.
Gusev, A. A., 2008: Temporal structure of the global sequence of volcanic eruptions: Order clustering and intermittent discharge rate. *Physics of the Earth and Planetary Interiors*, **166,** 203-218.
HAIGH, J., 1994: THE ROLE OF STRATOSPHERIC OZONE IN MODULATING THE SOLAR RADIATIVE FORCING OF CLIMATE. *Nature*, **370,** 544-546.
——, 1999: A GCM study of climate change in response to the 11-year solar cycle. *Quarterly Journal of the Royal Meteorological Society*, **125,** 871-892.
Haigh, J., A. Winning, R. Toumi, and J. Harder, 2010: An influence of solar spectral variations on radiative forcing of climate. *Nature*, **467,** 696-699.
Hallquist, M., et al., 2009: The formation, properties and impact of secondary organic aerosol: current and emerging issues. *Atmospheric Chemistry and Physics*, **9,** 5155-5236.
Hansen, J., and L. Nazarenko, 2004: Soot climate forcing via snow and ice albedos. *Proceedings of the National Academy of Sciences of the United States of America*, **101,** 423-428.
Hansen, J., et al., 2005: Efficacy of climate forcings. *Journal of Geophysical Research-Atmospheres*, **110**.
Hansen, J., et al., 2007: Climate simulations for 1880-2003 with GISS modelE. *Climate Dynamics*, **29,** 661-696.
Harder, J., J. Fontenla, P. Pilewskie, E. Richard, and T. Woods, 2009: Trends in solar spectral irradiance variability in the visible and infrared. *Geophysical Research Letters*, **36,** -.
Hasekamp, O., and A. Butz, 2008: Efficient calculation of intensity and polarization spectra in vertically inhomogeneous scattering and absorbing atmospheres. *Journal of Geophysical Research-Atmospheres*, **113,** -.
Hauglustaine, D. A., J. Lathiere, S. Szopa, and G. A. Folberth, 2005: Future tropospheric ozone simulated with a climate-chemistry-biosphere model. *Geophysical Research Letters*, **32**.

Haywood, J. M., et al., 2010: Observations of the eruption of the Sarychev volcano and simulations using the HadGEM2 climate model. *Journal of Geophysical Research-Atmospheres*, **115**.
Hegg, D. A., S. G. Warren, T. C. Grenfell, S. J. Doherty, and A. D. Clarke, 2010: Sources of light-absorbing aerosol in arctic snow and their seasonal variation. *Atmospheric Chemistry and Physics*, **10,** 10923-10938.
Hegg, D. A., S. G. Warren, T. C. Grenfell, S. J. Doherty, T. V. Larson, and A. D. Clarke, 2009: Source Attribution of Black Carbon in Arctic Snow. *Environmental Science & Technology*, **43,** 4016-4021.
Hegglin, M. I., and T. G. Shepherd, 2009: Large climate-induced changes in ultraviolet index and stratosphere-to-troposphere ozone flux. *Nature Geoscience*, **2,** 687-691.
Henze, D. K., et al., 2011: Spatially refined aersol direct radiative forcing efficiencies.
Hofmann, D., J. Barnes, M. O'Neill, M. Trudeau, and R. Neely, 2009: Increase in background stratospheric aerosol observed with lidar at Mauna Loa Observatory and Boulder, Colorado. *Geophysical Research Letters*, **36**.
Hogan, R., 2010: The Full-Spectrum Correlated-k Method for Longwave Atmospheric Radiative Transfer Using an Effective Planck Function. *Journal of the Atmospheric Sciences*, **67,** 2086-2100.
Hohne, N., et al., 2011: Contributions of individual countries' emissions to climate change and their uncertainty. *Climatic Change*, **106,** 359-391.
Holmes, C., Q. Tang, and M. Prather, 2011: Uncertainties in climate assessment for the case of aviation NO. *Proceedings of the National Academy of Sciences of the United States of America*, **108,** 10997-11002.
Horiuchi, K., T. Uchida, Y. Sakamoto, A. Ohta, H. Matsuzaki, Y. Shibata, and H. Motoyama, 2008: Ice core record of Be-10 over the past millennium from Dome Fuji, Antarctica: A new proxy record of past solar activity and a powerful tool for stratigraphic dating. *Quaternary Geochronology*, **3,** 253-261.
Horowitz, L. W., 2006: Past, present, and future concentrations of tropospheric ozone and aerosols: Methodology, ozone evaluation, and sensitivity to aerosol wet removal. *Journal of Geophysical Research-Atmospheres*, **111**.
Houghton, J. T., G. J. Jenkins, and J. J. Ephraums, 1990: *Climate Change. The IPCC Scientific Assessment*, 364 pp pp.
Hoyle, C., et al., 2011: A review of the anthropogenic influence on biogenic secondary organic aerosol. *Atmospheric Chemistry and Physics*, **11,** 321-343.
Hoyt, D. V., and K. H. Schatten, 1993: A DISCUSSION OF PLAUSIBLE SOLAR IRRADIANCE VARIATIONS, 1700-1992. *Journal of Geophysical Research-Space Physics*, **98,** 18895-18906.
Hsu, J., and M. J. Prather, 2009: Stratospheric variability and tropospheric ozone. *Journal of Geophysical Research-Atmospheres*, **114**.
Huang, J., Q. Fu, W. Zhang, X. Wang, R. Zhang, H. Ye, and S. Warren, 2011: DUST AND BLACK CARBON IN SEASONAL SNOW ACROSS NORTHERN CHINA. *Bulletin of the American Meteorological Society*, **92,** 175-+.
Hurtt, G., et al., 2011: Harmonization of land-use scenarios for the period 1500–2100: 600 years of global gridded annual land-use transitions, wood harvest, and resulting secondary lands. *Climatic Change*, **109,** 117-161.
Hurtt, G. C., et al., 2006: The underpinnings of land-use history: three centuries of global gridded land-use transitions, wood-harvest activity, and resulting secondary lands. *Global Change Biology*, **12,** 1208-1229.
Ineson, S., A. A. Scaife, J. R. Knight, J. C. Manners, N. J. Dunstone, L. J. Gray, and J. D. Haigh, 2011: Solar forcing of winter climate variability in the Northern Hemisphere. *Nature Geoscience*, **4,** 753-757.
IPCC, 1999: IPCC Special Report on Aviation and the Global Atmosphere. Prepared by Working Group I and III of the Intergovernmental Panel on Climate Change in collaboration with the Scientific Assessment Panel to the Montreal Protocol on Substances that deplete the Ozone Layer.
Isaksen, I., et al., 2009: Atmospheric composition change: Climate-Chemistry interactions. *Atmospheric Environment*, DOI 10.1016/j.atmosenv.2009.08.003**,** 5138-5192.
Ito, A., and J. E. Penner, 2005: Historical emissions of carbonaceous aerosols from biomass and fossil fuel burning for the period 1870-2000. *Global Biogeochemical Cycles*, **19**.
Jacob, D. J., and D. A. Winner, 2009: Effect of climate change on air quality. *Atmospheric Environment*, **43,** 51-63.
Jacobson, M., 2010: Short-term effects of controlling fossil-fuel soot, biofuel soot and gases, and methane on climate, Arctic ice, and air pollution health. *Journal of Geophysical Research-Atmospheres*, **115,** -.
Jacobson, M. Z., 2004: Climate response of fossil fuel and biofuel soot, accounting for soot's feedback to snow and sea ice albedo and emissivity. *Journal of Geophysical Research-Atmospheres*, **109**.
Jimenez, J. L., et al., 2009: Evolution of Organic Aerosols in the Atmosphere. *Science*, **326,** 1525-1529.
Jin, Y., and D. P. Roy, 2005: Fire-induced albedo change and its radiative forcing at the surface in northern Australia. *Geophysical Research Letters*, **32,** -.
Johansson, D., 2011: Economics- and physical-based metrics for comparing grenhouse gases.
Johansson, D., and C. Azar, 2011: Valuing the non-CO_2 climate impacts of aviation.
Johansson, D., U. Persson, and C. Azar, 2006: The cost of using global warming potentials: Analysing the trade off between CO2, CH4 and N2O. *Climatic Change*, DOI 10.1007/s10584-006-9054-1**,** 291-309.
Jones, G. S., M. Lockwood, and P. A. Stott, 2011: What influence will future solar activity changes over the 21st century have on projected global near surface temperature changes? *Journal of Geophysical Research*.
Joos, F., M. Bruno, R. Fink, U. Siegenthaler, T. Stocker, and C. LeQuere, 1996: An efficient and accurate representation of complex oceanic and biospheric models of anthropogenic carbon uptake. *Tellus Series B-Chemical and Physical Meteorology*, **48,** 397-417.

Joshi, M. M., and G. S. Jones, 2009: The climatic effects of the direct injection of water vapour into the stratosphere by large volcanic eruptions. *Atmospheric Chemistry and Physics*, **9,** 6109-6118.
Jung, M., et al., 2010: Recent decline in the global land evapotranspiration trend due to limited moisture supply. *Nature*, **467,** 951-954.
Kai, F. M., S. C. Tyler, J. T. Randerson, and D. R. Blake, 2011: Reduced methane growth rate explained by decreased Northern Hemisphere microbial sources. *Nature*, **476,** 194-197.
KANDLIKAR, M., 1995: THE RELATIVE ROLE OF TRACE GAS EMISSIONS IN GREENHOUSE ABATEMENT POLICIES. *Energy Policy***,** 879-883.
Kaplan, J. O., K. M. Krumhardt, E. C. Ellis, W. F. Ruddiman, C. Lemmen, and K. K. Goldewijk, 2011: Holocene carbon emissions as a result of anthropogenic land cover change. *Holocene*, **21,** 775-791.
Kasischke, E. S., and J. E. Penner, 2004: Improving global estimates of atmospheric emissions from biomass burning. *Journal of Geophysical Research-Atmospheres*, **109**.
Kawase, H., T. Nagashima, K. Sudo, and T. Nozawa, 2011: Future changes in tropospheric ozone under Representative Concentration Pathways (RCPs). *Geophysical Research Letters*, **38**.
Kiendler-Scharr, A., et al., 2009: New particle formation in forests inhibited by isoprene emissions. *Nature*, **461,** 381-384.
Koch, D., T. Bond, D. Streets, N. Unger, and G. van der Werf, 2007: Global impacts of aerosols from particular source regions and sectors. *Journal of Geophysical Research-Atmospheres*, **112,** -.
Koch, D., S. Menon, A. Del Genio, R. Ruedy, I. Alienov, and G. A. Schmidt, 2009: Distinguishing Aerosol Impacts on Climate over the Past Century. *Journal of Climate*, **22,** 2659-2677.
Koch, D., et al., 2011: Coupled Aerosol-Chemistry-Climate Twentieth-Century Transient Model Investigation: Trends in Short-Lived Species and Climate Responses. *Journal of Climate*, **24,** 2693-2714.
Kopp, G., and J. Lean, 2011: A new, lower value of total solar irradiance: Evidence and climate significance. *Geophysical Research Letters*, **38,** -.
Kratz, D., 2008: The sensitivity of radiative transfer calculations to the changes in the HITRAN database from 1982 to 2004. *Journal of Quantitative Spectroscopy & Radiative Transfer*, **109,** 1060-1080.
Kravitz, B., and A. Robock, 2011: Climate effects of high-latitude volcanic eruptions: Role of the time of year. *Journal of Geophysical Research-Atmospheres*, **116,** -.
Kravitz, B., A. Robock, and A. Bourassa, 2010: Negligible climatic effects from the 2008 Okmok and Kasatochi volcanic eruptions. *Journal of Geophysical Research-Atmospheres*, **115**.
Kravitz, B., et al., 2011: Simulation and observations of stratospheric aerosols from the 2009 Sarychev volcanic eruption. *Journal of Geophysical Research-Atmospheres*, **116,** -.
Krey, V., et al., 2009: Gas hydrates: entrance to a methane age or climate threat? *Environmental Research Letters*, **4**.
Kristjansson, J. E., T. Iversen, A. Kirkevag, O. Seland, and J. Debernard, 2005: Response of the climate system to aerosol direct and indirect forcing: Role of cloud feedbacks. *Journal of Geophysical Research-Atmospheres*, **110**.
Krivova, N., L. Balmaceda, and S. Solanki, 2007: Reconstruction of solar total irradiance since 1700 from the surface magnetic flux. *Astronomy & Astrophysics*, **467,** 335-346.
Krivova, N., L. Vieira, and S. Solanki, 2010: Reconstruction of solar spectral irradiance since the Maunder minimum. *Journal of Geophysical Research-Space Physics*, **115,** -.
Kueppers, L. M., M. A. Snyder, and L. C. Sloan, 2007: Irrigation cooling effect: Regional climate forcing by land-use change. *Geophysical Research Letters*, **34,** -.
Kvalevag, M. M., G. Myhre, G. Bonan, and S. Levis, 2010: Anthropogenic land cover changes in a GCM with surface albedo changes based on MODIS data. *International Journal of Climatology*, **30,** 2105-2117.
Kyrola, E., et al., 2004: GOMOS on Envisat: an overview. *Climate Change Processes in the Stratosphere, Earth-Atmosphere-Ocean Systems, and Oceanographic Processes from Satellite Data*, **33,** 1020-1028.
Lacis, A. A., and J. E. Hansen, 1974: PARAMETERIZATION FOR ABSORPTION OF SOLAR-RADIATION IN EARTHS ATMOSPHERE. *Journal of the Atmospheric Sciences*, **31,** 118-133.
Lamarque, J.-F., et al., 2011: Global and regional evolution of short-lived radiatively-active gases and aerosols in the Representative Concentration Pathways. *Climatic Change*, **109,** 191-212.
Lamarque, J., et al., 2010: Historical (1850-2000) gridded anthropogenic and biomass burning emissions of reactive gases and aerosols: methodology and application. *Atmospheric Chemistry and Physics*, DOI 10.5194/acp-10-7017-2010**,** 7017-7039.
Lau, K. M., M. K. Kim, and K. M. Kim, 2006: Asian summer monsoon anomalies induced by aerosol direct forcing: the role of the Tibetan Plateau. *Climate Dynamics*, **26,** 855-864.
Lauer, A., V. Eyring, J. Hendricks, P. Jockel, and U. Lohmann, 2007: Global model simulations of the impact of ocean-going ships on aerosols, clouds, and the radiation budget. *Atmospheric Chemistry and Physics*, **7,** 5061-5079.
Lawrence, D. M., and A. G. Slater, 2005: A projection of severe near-surface permafrost degradation during the 21st century. *Geophysical Research Letters*, **32**.
Lawrence, P. J., and T. N. Chase, 2010: Investigating the climate impacts of global land cover change in the community climate system model. *International Journal of Climatology*, **30,** 2066-2087.
Lean, J., J. Beer, and R. Bradley, 1995: RECONSTRUCTION OF SOLAR IRRADIANCE SINCE 1610 - IMPLICATIONS FOR CLIMATE-CHANGE. *Geophysical Research Letters*, **22,** 3195-3198.

Lebsock, M., G. Stephens, and C. Kummerow, 2008: Multisensor satellite observations of aerosol effects on warm clouds. *Journal of Geophysical Research-Atmospheres*, **113,** -.
Lee, D., et al., 2009: Aviation and global climate change in the 21st century. *Atmospheric Environment*, DOI 10.1016/j.atmosenv.2009.04.024**,** 3520-3537.
Lee, D. S., et al., 2010: Transport impacts on atmosphere and climate: Aviation. *Atmospheric Environment*, **44,** 4678-4734.
Legras, B., O. Mestre, E. Bard, and P. Yiou, 2010: A critical look at solar-climate relationships from long temperature series. *Climate of the Past*, **6,** 745-758.
Lelieveld, J., et al., 2008: Atmospheric oxidation capacity sustained by a tropical forest. *Nature*, **452,** 737-740.
Li, J., C. Curry, Z. Sun, and F. Zhang, 2010: Overlap of Solar and Infrared Spectra and the Shortwave Radiative Effect of Methane. *Journal of the Atmospheric Sciences*, **67,** 2372-2389.
Liao, H., W. T. Chen, and J. H. Seinfeld, 2006: Role of climate change in global predictions of future tropospheric ozone and aerosols. *Journal of Geophysical Research-Atmospheres*, **111**.
Llewellyn, E., et al., 2004: The OSIRIS instrument on the Odin spacecraft. *Canadian Journal of Physics*, **82,** 411-422.
Lockwood, M., 2010: Solar change and climate: an update in the light of the current exceptional solar minimum. *Proceedings of the Royal Society a-Mathematical Physical and Engineering Sciences*, **466,** 303-329.
Lockwood, M., and M. Owens, 2011: Centennial changes in the heliospheric magnetic field and open solar flux: The consensus view from geomagnetic data and cosmogenic isotopes and its implications. *Journal of Geophysical Research-Space Physics*, **116,** -.
Lockwood, M., A. Rouillard, and I. Finch, 2009: THE RISE AND FALL OF OPEN SOLAR FLUX DURING THE CURRENT GRAND SOLAR MAXIMUM. *Astrophysical Journal*, **700,** 937-944.
Logan, J. A., 1999: An analysis of ozonesonde data for the troposphere: Recommendations for testing 3-D models and development of a gridded climatology for tropospheric ozone. *Journal of Geophysical Research-Atmospheres*, **104,** 16115-16149.
Lohila, A., et al., 2010: Forestation of boreal peatlands: Impacts of changing albedo and greenhouse gas fluxes on radiative forcing. *Journal of Geophysical Research-Biogeosciences*, **115,** -.
Lohmann, U., et al., 2010: Total aerosol effect: radiative forcing or radiative flux perturbation? *Atmospheric Chemistry and Physics*, **10,** 3235-3246.
Lu, Z., Q. Zhang, and D. G. Streets, 2011: Sulfur dioxide and primary carbonaceous aerosol emissions in China and India, 1996-2010. *Atmospheric Chemistry and Physics*, **11,** 9839-9864.
Lund, M., T. Berntsen, J. Fuglestvedt, M. Ponater, and K. Shine, 2011: How much information is lost by using global-mean climate metrics? An example using the transport sector.
MacMynowski, D., H. Shin, and K. Caldeira, 2011: The frequency response of temperature and precipitation in a climate model. *Geophysical Research Letters*, **38,** -.
Mahowald, N. M., et al., 2010: Observed 20th century desert dust variability: impact on climate and biogeochemistry. *Atmospheric Chemistry and Physics*, **10,** 10875-10893.
Manne, A., and R. Richels, 2001: An alternative approach to establishing trade-offs among greenhouse gases. *Nature***,** 675-677.
Manney, G. L., M. L. Santee, M. Rex, and N. J. Livesey, 2011: Unprecedented Arctic ozone loss in 2011. *Nature***,** doi:10.1038/nature10556.
Manning, M., and A. Reisinger, 2011: Broader perspectives for comparing different greenhouse gases. *Philosophical Transactions of the Royal Society a-Mathematical Physical and Engineering Sciences*, **369,** 1891-1905.
Marenco, A., H. Gouget, P. Nedelec, J. P. Pages, and F. Karcher, 1994: EVIDENCE OF A LONG-TERM INCREASE IN TROPOSPHERIC OZONE FROM PIC DU MIDI DATA SERIES - CONSEQUENCES - POSITIVE RADIATIVE FORCING. *Journal of Geophysical Research-Atmospheres*, **99,** 16617-16632.
McCarthy, M. P., M. J. Best, and R. A. Betts, 2010: Climate change in cities due to global warming and urban effects. *Geophysical Research Letters*, **37,** -.
McComas, D., R. Ebert, H. Elliott, B. Goldstein, J. Gosling, N. Schwadron, and R. Skoug, 2008: Weaker solar wind from the polar coronal holes and the whole Sun. *Geophysical Research Letters*, **35,** -.
McConnell, J. R., et al., 2007: 20th-century industrial black carbon emissions altered arctic climate forcing. *Science*, **317,** 1381-1384.
Meehl, G., J. Arblaster, G. Branstator, and H. van Loon, 2008: A coupled air-sea response mechanism to solar forcing in the Pacific region. *Journal of Climate*, **21,** 2883-2897.
Meehl, G. A., W. M. Washington, T. M. L. Wigley, J. M. Arblaster, and A. Dai, 2003: Solar and greenhouse gas forcing and climate response in the twentieth century. *Journal of Climate*, **16,** 426-444.
Mercado, L. M., N. Bellouin, S. Sitch, O. Boucher, C. Huntingford, M. Wild, and P. M. Cox, 2009: Impact of changes in diffuse radiation on the global land carbon sink. *Nature*, **458,** 1014-U1087.
Meure, C., et al., 2006: Law Dome CO2, CH4 and N2O ice core records extended to 2000 years BP. *Geophysical Research Letters*, ARTN L14810, DOI 10.1029/2006GL026152**,** -.
Mickley, L., D. Jacob, and D. Rind, 2001: Uncertainty in preindustrial abundance of tropospheric ozone: Implications for radiative forcing calculations. *Journal of Geophysical Research-Atmospheres***,** 3389-3399.
Mieville, A., et al., 2010: Emissions of gases and particles from biomass burning during the 20th century using satellite data and an historical reconstruction. *Atmospheric Environment*, **44,** 1469-1477.

Miller, R. L., I. Tegen, and J. Perlwitz, 2004: Surface radiative forcing by soil dust aerosols and the hydrologic cycle. *Journal of Geophysical Research-Atmospheres*, **109**.
Mills, M. J., O. B. Toon, R. P. Turco, D. E. Kinnison, and R. R. Garcia, 2008: Massive global ozone loss predicted following regional nuclear conflict. *Proceedings of the National Academy of Sciences of the United States of America*, **105,** 5307-5312.
Ming, Y., V. Ramaswamy, and G. Persad, 2010: Two opposing effects of absorbing aerosols on global-mean precipitation. *Geophysical Research Letters*, **37,** -.
Ming, Y., V. Ramaswamy, L. J. Donner, V. T. J. Phillips, S. A. Klein, P. A. Ginoux, and L. W. Horowitz, 2007: Modeling the interactions between aerosols and liquid water clouds with a self-consistent cloud scheme in a general circulation model. *Journal of the Atmospheric Sciences*, **64,** 1189-1209.
Moncet, J., G. Uymin, A. Lipton, and H. Snell, 2008: Infrared Radiance Modeling by Optimal Spectral Sampling. *Journal of the Atmospheric Sciences*, **65,** 3917-3934.
Montzka, S. A., E. J. Dlugokencky, and J. H. Butler, 2011: Non-CO(2) greenhouse gases and climate change. *Nature*, **476,** 43-50.
Montzka, S. A., L. Kuijpers, M. O. Battle, M. Aydin, K. R. Verhulst, E. S. Saltzman, and D. W. Fahey, 2010: Recent increases in global HFC-23 emissions. *Geophysical Research Letters*, **37**.
Muhle, J., et al., 2009: Sulfuryl fluoride in the global atmosphere (vol 114, D05306, 2009). *Journal of Geophysical Research-Atmospheres*, ARTN D10303, DOI 10.1029/2009JD012306**,** -.
Mulitza, S., et al., 2010: Increase in African dust flux at the onset of commercial agriculture in the Sahel region. *Nature*, **466,** 226-228.
Murphy, D., and D. Fahey, 1994: An estimate of the flux of stratospheric reactive nitrogen and ozone into the troposphere. *Journal of Geophysical Research-Atmospheres*, **99,** 5325-5332.
Myhre, G., M. M. Kvalevag, and C. B. Schaaf, 2005a: Radiative forcing due to anthropogenic vegetation change based on MODIS surface albedo data. *Geophysical Research Letters*, **32,** -.
Myhre, G., Y. Govaerts, J. M. Haywood, T. K. Berntsen, and A. Lattanzio, 2005b: Radiative effect of surface albedo change from biomass burning. *Geophysical Research Letters*, **32,** -.
Myhre, G., J. Nilsen, L. Gulstad, K. Shine, B. Rognerud, and I. Isaksen, 2007: Radiative forcing due to stratospheric water vapour from CH4 oxidation. *Geophysical Research Letters*, ARTN L01807, DOI 10.1029/2006GL027472**,** -.
Myhre, G., et al., 2009: Intercomparison of radiative forcing calculations of stratospheric water vapour and contrails. *Meteorologische Zeitschrift*, **18,** 585-596.
Myhre, G., et al., 2011: Radiative forcing due to changes in ozone and methane caused by the transport sector. *Atmospheric Environment*, **45,** 387-394.
Naik, V., D. Mauzerall, L. Horowitz, M. D. Schwarzkopf, V. Ramaswamy, and M. Oppenheimer, 2005: Net radiative forcing due to changes in regional emissions of tropospheric ozone precursors. *Journal of Geophysical Research-Atmospheres*, **110**.
Naik, V., D. L. Mauzerall, L. W. Horowitz, M. D. Schwarzkopf, V. Ramaswamy, and M. Oppenheimer, 2007: On the sensitivity of radiative forcing from biomass burning aerosols and ozone to emission location. *Geophysical Research Letters*, **34**.
Nair, U. S., D. K. Ray, J. Wang, S. A. Christopher, T. J. Lyons, R. M. Welch, and R. A. Pielke, 2007: Observational estimates of radiative forcing due to land use change in southwest Australia. *Journal of Geophysical Research-Atmospheres*, **112,** -.
O'Connor, F. M., et al., 2010: POSSIBLE ROLE OF WETLANDS, PERMAFROST, AND METHANE HYDRATES IN THE METHANE CYCLE UNDER FUTURE CLIMATE CHANGE: A REVIEW. *Reviews of Geophysics*, **48**.
O'Neill, B., 2000: The jury is still out on global warming potentials. *Climatic Change***,** 427-443.
——, 2003: Economics, natural science, and the costs of global warming potentials - An editorial comment. *Climatic Change***,** 251-260.
Olivié, D. J. L., G. Peters, and D. Saint-Martin, 2011: Calibration of a linear response Simple Climate Model.
Osterman, G. B., et al., 2008: Validation of Tropospheric Emission Spectrometer (TES) measurements of the total, stratospheric, and tropospheric column abundance of ozone. *Journal of Geophysical Research-Atmospheres*, **113**.
Parrish, D. D., D. B. Millet, and A. H. Goldstein, 2009: Increasing ozone in marine boundary layer inflow at the west coasts of North America and Europe. *Atmospheric Chemistry and Physics*, **9,** 1303-1323.
Paulot, F., J. D. Crounse, H. G. Kjaergaard, A. Kurten, J. M. St Clair, J. H. Seinfeld, and P. O. Wennberg, 2009: Unexpected Epoxide Formation in the Gas-Phase Photooxidation of Isoprene. *Science*, **325,** 730-733.
Pechony, O., and D. Shindell, 2010: Driving forces of global wildfires over the past millennium and the forthcoming century. *Proceedings of the National Academy of Sciences of the United States of America*, **107,** 19167-19170.
Peeters, J., T. L. Nguyen, and L. Vereecken, 2009: HO(x) radical regeneration in the oxidation of isoprene. *Physical Chemistry Chemical Physics*, **11,** 5935-5939.
Penner, J., L. Xu, and M. Wang, 2011: Satellite methods underestimate indirect climate forcing by aerosols. *Proceedings of the National Academy of Sciences of the United States of America*, **108,** 13404-13408.

Penner, J., et al., 2006: Model intercomparison of indirect aerosol effects. *Atmospheric Chemistry and Physics*, **6,** 3391-3405.
Perlwitz, J., and R. L. Miller, 2010: Cloud cover increase with increasing aerosol absorptivity: A counterexample to the conventional semidirect aerosol effect. *Journal of Geophysical Research-Atmospheres*, **115**.
Peters, G., B. Aamaas, T. Berntsen, and J. Fuglestvedt, 2011a: The integrated Global Temperature change Potential (iGTP) and relationships between emission metrics.
Peters, G. P., B. Aamaas, M. Lund, C. Solli, and J. Fuglestvedt, 2011b: Alternative 'Global Warming' Metrics in Life Cycle Assessment: A case study with existing transportation data. *Environmental Science and Technology (published online)*.
Pinto, J. P., R. P. Turco, and O. B. Toon, 1989: Self-limiting physical and chemical effects in volcanic-eruption clouds. *Journal of Geophysical Research-Atmospheres*, **94,** 11165-11174.
Pitman, A. J., et al., 2009: Uncertainties in climate responses to past land cover change: First results from the LUCID intercomparison study. *Geophysical Research Letters*, **36,** -.
Plattner, G.-K., T. Stocker, P. Midgley, and M. Tignor, 2009: IPCC Expert Meeting on the Science of Alternative Metrics: Meeting Report.
Polvani, L. M., D. W. Waugh, G. J. P. Correa, and S. W. Son, 2011: Stratospheric Ozone Depletion: The Main Driver of Twentieth-Century Atmospheric Circulation Changes in the Southern Hemisphere. *Journal of Climate*, **24,** 795-812.
Pongratz, J., C. Reick, T. Raddatz, and M. Claussen, 2008: A reconstruction of global agricultural areas and land cover for the last millennium. *Global Biogeochemical Cycles*, **22,** -.
Pongratz, J., C. H. Reick, T. Raddatz, and M. Claussen, 2010: Biogeophysical versus biogeochemical climate response to historical anthropogenic land cover change. *Geophysical Research Letters*, **37,** -.
Pongratz, J., T. Raddatz, C. H. Reick, M. Esch, and M. Claussen, 2009: Radiative forcing from anthropogenic land cover change since AD 800. *Geophysical Research Letters*, **36,** -.
Prather, M., and J. Hsu, 2010: Coupling of Nitrous Oxide and Methane by Global Atmospheric Chemistry. *Science*, **330,** 952-954.
Prather, M., et al., 2009: Tracking uncertainties in the causal chain from human activities to climate. *Geophysical Research Letters*, ARTN L05707, DOI 10.1029/2008GL036474**,** -.
Prinn, R. G., et al., 2005: Evidence for variability of atmospheric hydroxyl radicals over the past quarter century. *Geophysical Research Letters*, **32**.
Puma, M. J., and B. I. Cook, 2010: Effects of irrigation on global climate during the 20th century. *Journal of Geophysical Research-Atmospheres*, **115,** -.
Pye, H. O. T., A. W. H. Chan, M. P. Barkley, and J. H. Seinfeld, 2010: Global modeling of organic aerosol: the importance of reactive nitrogen (NO(x) and NO(3)). *Atmospheric Chemistry and Physics*, **10,** 11261-11276.
Quaas, J., et al., 2009: Aerosol indirect effects - general circulation model intercomparison and evaluation with satellite data. *Atmospheric Chemistry and Physics*, **9,** 8697-8717.
Raes, F., H. Liao, W. T. Chen, and J. H. Seinfeld, 2010: Atmospheric chemistry-climate feedbacks. *Journal of Geophysical Research-Atmospheres*, **115,** 14.
Ramanathan, V., and G. Carmichael, 2008: Global and regional climate changes due to black carbon. *Nature Geoscience*, **1,** 221-227.
Ramaswamy, V., et al., 2001: Radiative Forcing of Climate Change. *Climate Change 2001: The Scientific Basis. Contribution of Working Group I to the Third Assessment Report of the Intergovernmental Panel on Climate Change*, Cambridge University Press.
Randel, W., and F. Wu, 2007: A stratospheric ozone profile data set for 1979-2005: Variability, trends, and comparisons with column ozone data. *Journal of Geophysical Research-Atmospheres*, ARTN D06313, DOI 10.1029/2006JD007339**,** -.
Rasch, P. J., et al., 2008: An overview of geoengineering of climate using stratospheric sulphate aerosols. *Philosophical Transactions of the Royal Society a-Mathematical Physical and Engineering Sciences*, **366,** 4007-4037.
Ravishankara, A. R., J. S. Daniel, and R. W. Portmann, 2009: Nitrous Oxide (N(2)O): The Dominant Ozone-Depleting Substance Emitted in the 21st Century. *Science*, **326,** 123-125.
Read, K. A., et al., 2008: Extensive halogen-mediated ozone destruction over the tropical Atlantic Ocean. *Nature*, **453,** 1232-1235.
Reay, D. S., F. Dentener, P. Smith, J. Grace, and R. A. Feely, 2008: Global nitrogen deposition and carbon sinks. *Nature Geoscience*, **1,** 430-437.
Rechid, D., T. Raddatz, and D. Jacob, 2009: Parameterization of snow-free land surface albedo as a function of vegetation phenology based on MODIS data and applied in climate modelling. *Theoretical and Applied Climatology*, **95,** 245-255.
Reddy, M., and O. Boucher, 2007: Climate impact of black carbon emitted from energy consumption in the world's regions. *Geophysical Research Letters*, ARTN L11802, DOI 10.1029/2006GL028904**,** -.
REILLY, J., 1992: CLIMATE-CHANGE DAMAGE AND THE TRACE-GAS-INDEX ISSUE. *Economic Issues in Global Climate Change***,** 72-88.
Reisinger, A., M. Meinshausen, and M. Manning, 2011: Future changes in global warming potentials under representative concentration pathways. *Environmental Research Letters*, **6,** -.

Reisinger, A., M. Meinshausen, M. Manning, and G. Bodeker, 2010: Uncertainties of global warming metrics: CO2 and CH4. *Geophysical Research Letters*, **37,** -.
Rigby, M., et al., 2008: Renewed growth of atmospheric methane. *Geophysical Research Letters*, **35**.
Rigozo, N., E. Echer, L. Vieira, and D. Nordemann, 2001: Reconstruction of Wolf sunspot numbers on the basis of spectral characteristics and estimates of associated radio flux and solar wind parameters for the last millennium. *Solar Physics*, **203,** 179-191.
Rigozo, N., D. Nordemann, E. Echer, M. Echer, and H. Silva, 2010: Prediction of solar minimum and maximum epochs on the basis of spectral characteristics for the next millennium. *Planetary and Space Science*, **58,** 1971-1976.
ROBERTS, R., J. SELBY, and L. BIBERMAN, 1976: INFRARED CONTINUUM ABSORPTION BY ATMOSPHERIC WATER-VAPOR IN 8-12-MUM WINDOW. *Applied Optics*, **15,** 2085-2090.
Robock, A., 2000: Volcanic eruptions and climate. *Reviews of Geophysics*, **38,** 191-219.
Robock, A., 2010: New START, Eyjafjallajökull, and Nuclear Winter. *Eos*, **91,** 444-445.
Robock, A., L. Oman, and G. L. Stenchikov, 2007a: Nuclear winter revisited with a modern climate model and current nuclear arsenals: Still catastrophic consequences. *Journal of Geophysical Research-Atmospheres*, **112**.
Robock, A., L. Oman, and G. L. Stenchikov, 2008: Regional climate responses to geoengineering with tropical and Arctic SO_2 injections. *Journal of Geophysical Research-Atmospheres*, **113**.
Robock, A., L. Oman, G. L. Stenchikov, O. B. Toon, C. Bardeen, and R. P. Turco, 2007b: Climatic consequences of regional nuclear conflicts. *Atmospheric Chemistry and Physics*, **7,** 2003-2012.
Robock, A., C. M. Ammann, L. Oman, D. Shindell, S. Levis, and G. Stenchikov, 2009: Did the Toba volcanic eruption of similar to 74 ka BP produce widespread glaciation? *Journal of Geophysical Research-Atmospheres*, **114**.
Rohs, S., et al., 2006: Long-term changes of methane and hydrogen in the stratosphere in the period 1978-2003 and their impact on the abundance of stratospheric water vapor. *Journal of Geophysical Research-Atmospheres*, **111**.
Rosenlof, K. H., et al., 2001: Stratospheric water vapor increases over the past half-century. *Geophysical Research Letters*, **28,** 1195-1198.
Rotenberg, E., and D. Yakir, 2010: Contribution of Semi-Arid Forests to the Climate System. *Science*, **327,** 451-454.
Rothman, L., 2010: The evolution and impact of the HITRAN molecular spectroscopic database. *Journal of Quantitative Spectroscopy & Radiative Transfer*, **111,** 1565-1567.
Rothman, L., et al., 2009: The HITRAN 2008 molecular spectroscopic database. *Journal of Quantitative Spectroscopy & Radiative Transfer*, **110,** 533-572.
Rotstayn, L. D., and U. Lohmann, 2002: Tropical rainfall trends and the indirect aerosol effect. *Journal of Climate*, **15,** 2103-2116.
Rotstayn, L. D., B. F. Ryan, and J. E. Penner, 2000: Precipitation changes in a GCM resulting from the indirect effects of anthropogenic aerosols. *Geophysical Research Letters*, **27,** 3045-3048.
Rottman, G., 2006: Measurement of total and spectral solar irradiance. *Space Science Reviews*, **125,** 39-51.
ROTTMAN, G., T. WOODS, and T. SPARN, 1993: SOLAR-STELLAR IRRADIANCE COMPARISON EXPERIMENT-1 .1. INSTRUMENT DESIGN AND OPERATION. *Journal of Geophysical Research-Atmospheres*, **98,** 10667-10677.
Russell, C., J. Luhmann, and L. Jian, 2010: HOW UNPRECEDENTED A SOLAR MINIMUM? *Reviews of Geophysics*, **48,** -.
Rypdal, K., N. Rive, T. Berntsen, Z. Klimont, T. Mideksa, G. Myhre, and R. Skeie, 2009: Costs and global impacts of black carbon abatement strategies. *Tellus Series B-Chemical and Physical Meteorology*, DOI 10.1111/j.1600-0889.2009.00430.x**,** 625-641.
Saiz-Lopez, A., and e. al., 2011: Estimating the climate significance of halogen-driven ozone loss in the tropical marine troposphere.
Salawitch, R. J., et al., 2005: Sensitivity of ozone to bromine in the lower stratosphere. *Geophysical Research Letters*, **32**.
Salzer, M. W., and M. K. Hughes, 2007: Bristlecone pine tree rings and volcanic eruptions over the last 5000 yr. *Quaternary Research*, **67,** 57-68.
Sato, M., J. E. Hansen, M. P. McCormick, and J. B. Pollack, 1993: STRATOSPHERIC AEROSOL OPTICAL DEPTHS, 1850-1990. *Journal of Geophysical Research-Atmospheres*, **98,** 22987-22994.
Sausen, R., and U. Schumann, 2000: Estimates of the climate response to aircraft CO2 and NOx emissions scenarios. *Climatic Change***,** 27-58.
Sausen, R., et al., 2005: Aviation radiative forcing in 2000: An update on IPCC (1999). *Meteorologische Zeitschrift*, DOI 10.1127/0941-2948/2005/0049**,** 555-561.
Schaaf, C., et al., 2002: First operational BRDF, albedo nadir reflectance products from MODIS. *Remote Sensing of Environment*, **83,** 135-148.
Scherer, M., H. Vomel, S. Fueglistaler, S. J. Oltmans, and J. Staehelin, 2008: Trends and variability of midlatitude stratospheric water vapour deduced from the re-evaluated Boulder balloon series and HALOE. *Atmospheric Chemistry and Physics*, **8,** 1391-1402.
Schmidt, G., et al., 2011: Climate forcing reconstructions for use in PMIP simulations of the last millennium (v1.0). *Geoscientific Model Development*, **4,** 33-45.

Schneider, D. P., C. M. Ammann, B. L. Otto-Bliesner, and D. S. Kaufman, 2009: Climate response to large, high-latitude and low-latitude volcanic eruptions in the Community Climate System Model. *Journal of Geophysical Research-Atmospheres*, **114**.
Schrijver, C. J., W. C. Livingston, T. N. Woods, and R. A. Mewaldt, 2011: The minimal solar activity in 2008-2009 and its implications for long-term climate modeling. *Geophysical Research Letters*, **38,** L06701.
Schultz, M. G., et al., 2008: Global wildland fire emissions from 1960 to 2000. *Global Biogeochemical Cycles*, **22**.
Schurgers, G., A. Arneth, R. Holzinger, and A. H. Goldstein, 2009: Process-based modelling of biogenic monoterpene emissions combining production and release from storage. *Atmospheric Chemistry and Physics*, **9,** 3409-3423.
Schuur, E. A. G., J. G. Vogel, K. G. Crummer, H. Lee, J. O. Sickman, and T. E. Osterkamp, 2009: The effect of permafrost thaw on old carbon release and net carbon exchange from tundra. *Nature*, **459,** 556-559.
Seinfeld, J. H., and S. N. Pandis, 2006: *Atmospheric chemistry and physics: from air pollution to climate change.* Wiley.
Self, S., and S. Blake, 2008: Consequences of explosive supereruptions. *Elements*, **4,** 41-46.
Shakhova, N., I. Semiletov, A. Salyuk, V. Yusupov, D. Kosmach, and O. Gustafsson, 2010: Extensive Methane Venting to the Atmosphere from Sediments of the East Siberian Arctic Shelf. *Science*, **327,** 1246-1250.
Shapiro, A. I., W. Schmutz, E. Rozanov, M. Schoell, M. Haberreiter, A. V. Shapiro, and S. Nyeki, 2011: A new approach to the long-term reconstruction of the solar irradiance leads to large historical solar forcing. *Astronomy and Astrophysics*, **529,** A67.
Sharma, S., D. Lavoue, H. Cachier, L. Barrie, and S. Gong, 2004: Long-term trends of the black carbon concentrations in the Canadian Arctic. *Journal of Geophysical Research-Atmospheres*, **109,** -.
Shi, G., N. Xu, B. Wang, T. Dai, and J. Zhao, 2009: An improved treatment of overlapping absorption bands based on the correlated k distribution model for thermal infrared radiative transfer calculations. *Journal of Quantitative Spectroscopy & Radiative Transfer*, **110,** 435-451.
Shindell, D., and G. Faluvegi, 2009: Climate response to regional radiative forcing during the twentieth century. *Nature Geoscience*, **2,** 294-300.
——, 2010: The net climate impact of coal-fired power plant emissions. *Atmospheric Chemistry and Physics*, **10,** 3247-3260.
Shindell, D., G. Schmidt, M. Mann, D. Rind, and A. Waple, 2001: Solar forcing of regional climate change during the maunder minimum. *Science*, **294,** 2149-2152.
Shindell, D., G. Faluvegi, R. Miller, G. Schmidt, J. Hansen, and S. Sun, 2006a: Solar and anthropogenic forcing of tropical hydrology. *Geophysical Research Letters*, **33,** -.
Shindell, D., G. Faluvegi, D. Koch, G. Schmidt, N. Unger, and S. Bauer, 2009a: Improved Attribution of Climate Forcing to Emissions. *Science*, DOI 10.1126/science.1174760**,** 716-718.
Shindell, D., M. Schulz, Y. Ming, T. Takemura, G. Faluvegi, and V. Ramaswamy, 2010: Spatial scales of climate response to inhomogeneous radiative forcing. *Journal of Geophysical Research-Atmospheres*, **115**.
Shindell, D., et al., 2006b: Simulations of preindustrial, present-day, and 2100 conditions in the NASA GISS composition and climate model G-PUCCINI. *Atmospheric Chemistry and Physics***,** 4427-4459.
Shindell, D., et al., 2008a: Climate forcing and air quality change due to regional emissions reductions by economic sector. *Atmospheric Chemistry and Physics*, **8,** 7101-7113.
Shindell, D., et al., 2011: Climate, health, agricultural and economic impacts of tighter vehicle-emission standards. *Nature Climate Change*, **1,** 59-66.
Shindell, D. T., B. P. Walter, and G. Faluvegi, 2004: Impacts of climate change on methane emissions from wetlands. *Geophysical Research Letters*, **31**.
Shindell, D. T., G. Faluvegi, D. M. Koch, G. A. Schmidt, N. Unger, and S. E. Bauer, 2009b: Improved Attribution of Climate Forcing to Emissions. *Science*, **326,** 716-718.
Shindell, D. T., et al., 2006c: Simulations of preindustrial, present-day, and 2100 conditions in the NASA GISS composition and climate model G-PUCCINI. *Atmospheric Chemistry and Physics*, **6,** 4427-4459.
Shindell, D. T., et al., 2008b: A multi-model assessment of pollution transport to the Arctic. *Atmospheric Chemistry and Physics*, **8,** 5353-5372.
Shindell, D. T., et al., 2006d: Multimodel simulations of carbon monoxide: Comparison with observations and projected near-future changes. *Journal of Geophysical Research-Atmospheres*, **111**.
Shine, K., 2009: The global warming potential-the need for an interdisciplinary retrial. *Climatic Change*, DOI 10.1007/s10584-009-9647-6**,** 467-472.
Shine, K., T. Berntsen, J. Fuglestvedt, and R. Sausen, 2005a: Scientific issues in the design of metrics for inclusion of oxides of nitrogen in global climate agreements. *Proceedings of the National Academy of Sciences of the United States of America*, DOI 10.1073/pnas.0506865102**,** 15768-15773.
Shine, K., J. Fuglestvedt, K. Hailemariam, and N. Stuber, 2005b: Alternatives to the global warming potential for comparing climate impacts of emissions of greenhouse gases. *Climatic Change***,** 281-302.
Shine, K., T. Berntsen, J. Fuglestvedt, R. Skeie, and N. Stuber, 2007: Comparing the climate effect of emissions of short- and long-lived climate agents. *Philosophical Transactions of the Royal Society a-Mathematical Physical and Engineering Sciences*, DOI 10.1098/rsta.2007.2050**,** 1903-1914.
Sitch, S., P. M. Cox, W. J. Collins, and C. Huntingford, 2007a: Indirect radiative forcing of climate change through ozone effects on the land-carbon sink. *Nature*, **448,** 791-U794.

Sitch, S., P. Cox, W. Collins, and C. Huntingford, 2007b: Indirect radiative forcing of climate change through ozone effects on the land-carbon sink. *Nature*, DOI 10.1038/nature06059**,** 791-U794.
Skeie, R., T. Berntsen, G. Myhre, C. Pedersen, J. Strom, S. Gerland, and J. Ogren, 2011a: Black carbon in the atmosphere and snow, from pre-industrial times until present. *Atmospheric Chemistry and Physics*, **11,** 6809-6836.
Skeie, R. B., T. K. Berntsen, G. Myhre, K. Tanaka, and M. M. H. Kvalevåg, C.R., 2011b: Anthropogenic radiative forcing time series from pre-industrial times until 2010. *Atmos. Phys. Chem. Disc.*, **11,** 22545–22617.
Skeie, R. B., J. Fuglestvedt, T. Berntsen, M. T. Lund, G. Myhre, and K. Rypdal, 2009: Global temperature change from the transport sectors: Historical development and future scenarios. *Atmospheric Environment*, **43,** 6260-6270.
Skodvin, T., and J. Fuglestvedt, 1997: A comprehensive approach to climate change: Political and scientific considerations. *Ambio***,** 351-358.
Smith, E., and A. Balogh, 2008: Decrease in heliospheric magnetic flux in this solar minimum: Recent Ulysses magnetic field observations. *Geophysical Research Letters*, **35,** -.
Smith, S., and T. Wigley, 2000a: Global warming potentials: 2. Accuracy. *Climatic Change***,** 459-469.
Smith, S., and M. Wigley, 2000b: Global warming potentials: 1. Climatic implications of emissions reductions. *Climatic Change***,** 445-457.
Society, R., 2008: Ground-level ozone in the 21st century: future trends, impacts and policy implications. **148**.
Solomon, S., 1999: Stratospheric ozone depletion: A review of concepts and history. *Reviews of Geophysics*, **37,** 275-316.
Solomon, S., J. S. Daniel, R. R. Neely, J. P. Vernier, E. G. Dutton, and L. W. Thomason, 2011: The Persistently Variable "Background" Stratospheric Aerosol Layer and Global Climate Change. *Science*, **333,** 866-870.
Solomon, S., J. Daniel, T. Sanford, D. Murphy, G. Plattner, R. Knutti, and P. Friedlingstein, 2010a: Persistence of climate changes due to a range of greenhouse gases. *Proceedings of the National Academy of Sciences of the United States of America*, DOI 10.1073/pnas.1006282107**,** 18354-18359.
Solomon, S., K. Rosenlof, R. Portmann, J. Daniel, S. Davis, T. Sanford, and G. Plattner, 2010b: Contributions of Stratospheric Water Vapor to Decadal Changes in the Rate of Global Warming. *Science*, DOI 10.1126/science.1182488**,** 1219-1223.
Soukharev, B., and L. Hood, 2006: Solar cycle variation of stratospheric ozone: Multiple regression analysis of long-term satellite data sets and comparisons with models. *Journal of Geophysical Research-Atmospheres*, **111,** -.
Sovde, O., C. Hoyle, G. Myhre, and I. Isaksen, 2011: The HNO3 forming branch of the HO2 + NO reaction: pre-industrial-to-present trends in atmospheric species and radiative forcings. *Atmospheric Chemistry and Physics*, **11,** 8929-8943.
Stavrakou, T., J. Peeters, and J. F. Muller, 2010: Improved global modelling of HO(x) recycling in isoprene oxidation: evaluation against the GABRIEL and INTEX-A aircraft campaign measurements. *Atmospheric Chemistry and Physics*, **10,** 9863-9878.
Steinhilber, F., J. Beer, and C. Frohlich, 2009: Total solar irradiance during the Holocene. *Geophysical Research Letters*, **36,** -.
Stenchikov, G., A. Robock, V. Ramaswamy, M. D. Schwarzkopf, K. Hamilton, and S. Ramachandran, 2002: Arctic Oscillation response to the 1991 Mount Pinatubo eruption: Effects of volcanic aerosols and ozone depletion. *Journal of Geophysical Research-Atmospheres*, **107**.
Stephens, G. L., N. B. Wood, and L. A. Pakula, 2004: On the radiative effects of dust on tropical convection. *Geophysical Research Letters*, **31**.
Stevenson, D., and R. Derwent, 2009: Does the location of aircraft nitrogen oxide emissions affect their climate impact? *Geophysical Research Letters*, ARTN L17810, DOI 10.1029/2009GL039422**,** -.
STEVENSON, D., R. DOHERTY, M. SANDERSON, W. COLLINS, C. JOHNSON, and R. DERWENT, 2004: Radiative forcing from aircraft NOx emissions: Mechanisms and seasonal dependence. *JOURNAL OF GEOPHYSICAL RESEARCH-ATMOSPHERES*, **109**.
Stevenson, D. S., et al., 2006: Multimodel ensemble simulations of present-day and near-future tropospheric ozone. *Journal of Geophysical Research-Atmospheres*, **111**.
Stothers, R. B., 2007: Three centuries of observation of stratospheric transparency. *Climatic Change*, **83,** 515-521.
Streets, D. G., T. C. Bond, T. Lee, and C. Jang, 2004: On the future of carbonaceous aerosol emissions. *Journal of Geophysical Research-Atmospheres*, **109**.
Stuiver, M., et al., 1998: INTCAL 98 radiocarbon age calibration, 24, 000-0 BP. *Radiocarbon*, **40,** 1041-1083.
Svalgaard, L., and E. Cliver, 2010: Heliospheric magnetic field 1835-2009. *Journal of Geophysical Research-Space Physics*, **115,** -.
Tanaka, K., G. Peters, and J. S. Fuglestvedt, 2010: Multicomponent climate policy: why do emission metrics matter? *Carbon Management*, **1,** *191-197*.
Tanaka, K., B. O'Neill, D. Rokityanskiy, M. Obersteiner, and R. Tol, 2009: Evaluating Global Warming Potentials with historical temperature. *Climatic Change*, DOI 10.1007/s10584-009-9566-6**,** 443-466.
Taraborrelli, D., M. G. Lawrence, T. M. Butler, R. Sander, and J. Lelieveld, 2009: Mainz Isoprene Mechanism 2 (MIM2): an isoprene oxidation mechanism for regional and global atmospheric modelling. *Atmospheric Chemistry and Physics*, **9,** 2751-2777.

Taylor, P. C., R. G. Ellingson, and M. Cai, 2011: Seasonal Variations of Climate Feedbacks in the NCAR CCSM3. *Journal of Climate*, **24,** 3433-3444.
Textor, C., et al., 2006: Analysis and quantification of the diversities of aerosol life cycles within AeroCom. *Atmospheric Chemistry and Physics*, **6,** 1777-1813.
Thonicke, K., A. Spessa, I. C. Prentice, S. P. Harrison, L. Dong, and C. Carmona-Moreno, 2010: The influence of vegetation, fire spread and fire behaviour on biomass burning and trace gas emissions: results from a process-based model. *Biogeosciences*, **7,** 1991-2011.
Thornton, P. E., et al., 2009: Carbon-nitrogen interactions regulate climate-carbon cycle feedbacks: results from an atmosphere-ocean general circulation model. *Biogeosciences*, **6,** 2099-2120.
Tilmes, S., et al., 2011: Ozonesonde climatology between 1995 and 2009: description, evaluation and applications. 28747-28796.
Timmreck, C., et al., 2010: Aerosol size confines climate response to volcanic super-eruptions. *Geophysical Research Letters*, **37,** -.
Tobias, S., N. Weiss, and J. Beer, 2004: Long-sterm prediction of solar activity - a discussion ... *Astronomy & Geophysics*, **45,** 6-6.
Tol, R. S. J., T. K. Berntsen, B. C. O'Neill, J. S. Fuglestvedt, and K. P. Shine, 2009: A UNIFYING FRAMEWORK FOR METRICS FOR AGGREGATING THE CLIMATE EFFECT OF DIFFERENT EMISSIONS. *submitted*.
Toon, O. B., A. Robock, and R. P. Turco, 2008: Environmental consequences of nuclear war. *Physics Today*, **61,** 37-42.
Toon, O. B., R. P. Turco, A. Robock, C. Bardeen, L. Oman, and G. L. Stenchikov, 2007: Atmospheric effects and societal consequences of regional scale nuclear conflicts and acts of individual nuclear terrorism. *Atmospheric Chemistry and Physics*, **7,** 1973-2002.
Trenberth, K. E., and A. Dai, 2007: Effects of Mount Pinatubo volcanic eruption on the hydrological cycle as an analog of geoengineering. *Geophysical Research Letters*, **34**.
TWOMEY, S., 1974: POLLUTION AND PLANETARY ALBEDO. *Atmospheric Environment*, **8,** 1251-1256.
Uherek, E., et al., 2010: Transport impacts on atmosphere and climate: Land transport. *Atmospheric Environment*, DOI 10.1016/j.atmosenv.2010.01.002**,** 4772-4816.
Unger, N., D. T. Shindell, and J. S. Wang, 2009: Climate forcing by the on-road transportation and power generation sectors. *Atmospheric Environment*, **43,** 3077-3085.
Unger, N., D. T. Shindell, D. M. Koch, and D. G. Streets, 2008: Air pollution radiative forcing from specific emissions sectors at 2030. *Journal of Geophysical Research-Atmospheres*, **113**.
Unger, N., T. C. Bond, J. S. Wang, D. M. Koch, S. Menon, D. T. Shindell, and S. Bauer, 2010: Attribution of climate forcing to economic sectors. *Proceedings of the National Academy of Sciences of the United States of America*, **107,** 3382-3387.
Usoskin, I., S. Solanki, M. Schussler, K. Mursula, and K. Alanko, 2003: Millennium-scale sunspot number reconstruction: Evidence for an unusually active Sun since the 1940s. *Physical Review Letters*, **91,** -.
van der Werf, G. R., et al., 2010: Global fire emissions and the contribution of deforestation, savanna, forest, agricultural, and peat fires (1997-2009). *Atmospheric Chemistry and Physics*, **10,** 11707-11735.
van Vuuren, D., J. Weyant, and F. de la Chesnaye, 2006: Multi-gas scenarios to stabilize radiative forcing. *Energy Economics*, DOI 10.1016/j.eneco.2005.10.003**,** 102-120.
van Vuuren, D., J. Edmonds, M. Kainuma, K. Riahi, and J. Weyant, 2011: A special issue on the RCPs. *Climatic Change*, **109,** 1-4.
Velasco-Herrera, V. M., 2011: Prediction for the Next Solar Secular Minimum. *Solar. Phys.*
Velasco-Herrera, V. M., B. Mendoza, and G. Velasco, 2011: Estimations of the Total Solar Irradiance during the 21st century. *Phys. Rev. Lett.***,** accepted.
Vernier, J. P., et al., 2011: Major influence of tropical volcanic eruptions on the stratospheric aerosol layer during the last decade. *Geophysical Research Letters*, **38,** 8.
Volz, A., and D. Kley, 1988: EVALUATION OF THE MONTSOURIS SERIES OF OZONE MEASUREMENTS MADE IN THE 19TH-CENTURY. *Nature*, **332,** 240-242.
Vonmoos, M., J. Beer, and R. Muscheler, 2006: Large variations in Holocene solar activity: Constraints from Be-10 in the Greenland Ice Core Project ice core. *Journal of Geophysical Research-Space Physics*, **111,** -.
Voulgarakis, A., and D. T. Shindell, 2010: Constraining the Sensitivity of Regional Climate with the Use of Historical Observations. *Journal of Climate*, **23,** 6068-6073.
Walter, B. P., and M. Heimann, 2000: A process-based, climate-sensitive model to derive methane emissions from natural wetlands: Application to five wetland sites, sensitivity to model parameters, and climate. *Global Biogeochemical Cycles*, **14,** 745-765.
Walter, K. M., S. A. Zimov, J. P. Chanton, D. Verbyla, and F. S. Chapin, 2006: Methane bubbling from Siberian thaw lakes as a positive feedback to climate warming. *Nature*, **443,** 71-75.
Wang, C., D. Kim, A. Ekman, M. Barth, and P. Rasch, 2009: Impact of anthropogenic aerosols on Indian summer monsoon. *Geophysical Research Letters*, **36,** -.
Wang, H., and G. Feingold, 2009: Modeling Mesoscale Cellular Structures and Drizzle in Marine Stratocumulus. Part II: The Microphysics and Dynamics of the Boundary Region between Open and Closed Cells. *Journal of the Atmospheric Sciences*, **66,** 3257-3275.

Wang, M., and J. E. Penner, 2009: Aerosol indirect forcing in a global model with particle nucleation. *Atmospheric Chemistry and Physics*, **9,** 239-260.
Wang, Y., J. Lean, and N. Sheeley, 2005: Modeling the sun's magnetic field and irradiance since 1713. *Astrophysical Journal*, **625,** 522-538.
WARREN, S., and W. WISCOMBE, 1980: A MODEL FOR THE SPECTRAL ALBEDO OF SNOW .2. SNOW CONTAINING ATMOSPHERIC AEROSOLS. *Journal of the Atmospheric Sciences*, **37,** 2734-2745.
Weiss, R., J. Muhle, P. Salameh, and C. Harth, 2008: Nitrogen trifluoride in the global atmosphere. *Geophysical Research Letters*, ARTN L20821, DOI 10.1029/2008GL035913**,** -.
Wennberg, P. O., 2006: Atmospheric chemistry - Radicals follow the sun. *Nature*, **442,** 145-146.
Wenzler, T., S. Solanki, N. Krivova, and C. Frohlich, 2006: Reconstruction of solar irradiance variations in cycles 21-23 based on surface magnetic fields. *Astronomy & Astrophysics*, **460,** 583-595.
West, J. J., A. M. Fiore, V. Naik, L. W. Horowitz, M. D. Schwarzkopf, and D. L. Mauzerall, 2007: Ozone air quality and radiative forcing consequences of changes in ozone precursor emissions. *Geophysical Research Letters*, **34**.
Wigley, T., 1998: The Kyoto Protocol: CO2, CH4 and climate implications. *Geophysical Research Letters*, **25,** 2285-2288.
Wild, M., 2009: How well do IPCC-AR4/CMIP3 climate models simulate global dimming/brightening and twentieth-century daytime and nighttime warming? *Journal of Geophysical Research-Atmospheres*, **114**.
Wild, O., 2007: Modelling the global tropospheric ozone budget: exploring the variability in current models. *Atmospheric Chemistry and Physics*, **7,** 2643-2660.
Wild, O., and P. I. Palmer, 2008: How sensitive is tropospheric oxidation to anthropogenic emissions? *Geophysical Research Letters*, **35**.
Wild, O., M. Prather, and H. Akimoto, 2001: Indirect long-term global radiative cooling from NOx emissions. *Geophysical Research Letters*, **28,** 1719-1722.
Willson, R., and A. Mordvinov, 2003: Secular total solar irradiance trend during solar cycles 21-23. *Geophysical Research Letters*, **30,** -.
Wilson, R. C., and A. Mordvinov, 2003: Secular total solar irradiance trend during solar cycles 21–23. *Geopphysical Research Letters*, **30**.
WMO, 2010: *Scientific Assessment of Ozone Depletion 2010.* Vol. 52, World Meteorological Organisation.
Worden, H., K. Bowman, S. Kulawik, and A. Aghedo, 2011: Sensitivity of outgoing longwave radiative flux to the global vertical distribution of ozone characterized by instantaneous radiative kernels from Aura-TES. *Journal of Geophysical Research-Atmospheres*, **116,** -.
Worden, H., K. Bowman, J. Worden, A. Eldering, and R. Beer, 2008: Satellite measurements of the clear-sky greenhouse effect from tropospheric ozone. *Nature Geoscience*, DOI 10.1038/ngeo182**,** 305-308.
Wu, S. L., L. J. Mickley, D. J. Jacob, J. A. Logan, R. M. Yantosca, and D. Rind, 2007: Why are there large differences between models in global budgets of tropospheric ozone? *Journal of Geophysical Research-Atmospheres*, **112**.
Xu, B. Q., et al., 2009: Black soot and the survival of Tibetan glaciers. *Proceedings of the National Academy of Sciences of the United States of America*, **106,** 22114-22118.
Young, P. J., A. Arneth, G. Schurgers, G. Zeng, and J. A. Pyle, 2009: The CO2 inhibition of terrestrial isoprene emission significantly affects future ozone projections. *Atmospheric Chemistry and Physics*, **9,** 2793-2803.
Zaehle, S., P. Ciais, A. D. Friend, and V. Prieur, 2011: Carbon benefits of anthropogenic reactive nitrogen offset by nitrous oxide emissions. *Nature Geoscience*, **4,** 601-605.
Zaehle, S., A. D. Friend, P. Friedlingstein, F. Dentener, P. Peylin, and M. Schulz, 2010: Carbon and nitrogen cycle dynamics in the O-CN land surface model: 2. Role of the nitrogen cycle in the historical terrestrial carbon balance. *Global Biogeochemical Cycles*, **24**.
Zeng, G., O. Morgenstern, P. Braesicke, and J. A. Pyle, 2010: Impact of stratospheric ozone recovery on tropospheric ozone and its budget. *Geophysical Research Letters*, **37**.
Zhang, H., G. Y. Shi, and Y. Liu, 2005: A Comparison Between the Two Line-by-Line Integration Algorithms. *Chinese Journal of Atmospheric Sciences*, **29,** 581-593.
Zhang, H., G. Shi, and Y. Liu, 2008: The effects of line-wing cutoff in LBL integration on radiation calculations. *Acta Meteorologica Sinica*, **22,** 248-255.
Zhang, H., J. Wu, and P. Luc, 2011a: A study of the radiative forcing and global warming potentials of hydrofluorocarbons. *Journal of Quantitative Spectroscopy & Radiative Transfer*, **112,** 220-229.
Zhang, H., J. Wu, and Z. Shen, 2011b: Radiative forcing and global warming potential of perfluorocarbons and sulfur hexafluoride. *Science China-Earth Sciences*, **54,** 764-772.
Zhang, H., G. Shi, T. Nakajima, and T. Suzuki, 2006: The effects of the choice of the k-interval number on radiative calculations. *Journal of Quantitative Spectroscopy & Radiative Transfer*, **98,** 31-43.
Zhang, H., T. Nakajima, G. Shi, T. Suzuki, and R. Imasu, 2003: An optimal approach to overlapping bands with correlated k distribution method and its application to radiative calculations. *Journal of Geophysical Research-Atmospheres*, **108,** -.
Zhang, X. B., et al., 2007: Detection of human influence on twentieth-century precipitation trends. *Nature*, **448,** 461-U464.
Zhao, H. B., B. Q. Xu, T. D. Yao, L. D. Tian, and Z. Li, 2011: Records of sulfate and nitrate in an ice core from Mount Muztagata, central Asia. *Journal of Geophysical Research-Atmospheres*, **116**.

Ziemke, J. R., S. Chandra, G. J. Labow, P. K. Bhartia, L. Froidevaux, and J. C. Witte, 2011: A global climatology of tropospheric and stratospheric ozone derived from Aura OMI and MLS measurements. *Atmospheric Chemistry and Physics*, **11,** 9237-9251.

Chapter 8: Anthropogenic and Natural Radiative Forcing

Coordinating Lead Authors: Gunnar Myhre (Norway), Drew Shindell (USA)

Lead Authors: François-Marie Bréon (France), William Collins (UK), Jan Fuglestvedt (Norway), Jianping Huang (China), Dorothy Koch (USA), Jean-François Lamarque (USA), David Lee (UK), Blanca Mendoza (Mexico), Teruyuki Nakajima (Japan), Alan Robock (USA), Graeme Stephens (USA), Toshihiko Takemura (Japan), Hua Zhang (China)

Contributing Authors: Claire Granier (France), Joanna Haigh (UK), Brian O'Neill (USA), Leon Rotstayn (Australia), Paul Young (USA)

Review Editors: Daniel Jacob (USA), A.R. Ravishankara (USA), Keith Shine (UK)

Date of Draft: 16 December 2011

Notes: TSU Compiled Version

Figures

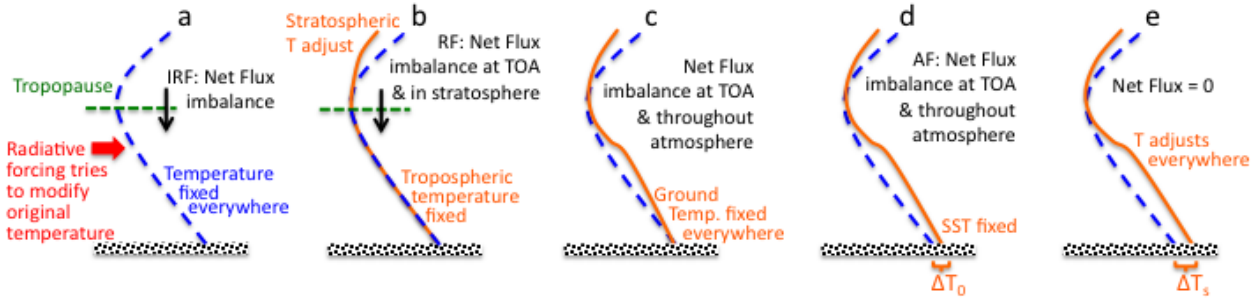

Figure 8.1: Cartoon comparing (a) instantaneous RF, (b) RF, which allows stratospheric temperature to adjust, (c) flux change when the surface temperature is fixed over the whole Earth, (d) AF, the adjusted forcing which allows atmospheric and land temperature to adjust while ocean conditions are fixed, and (e) the equilibrium response to the climate forcing agent. Updated from Hansen et al. (2005).

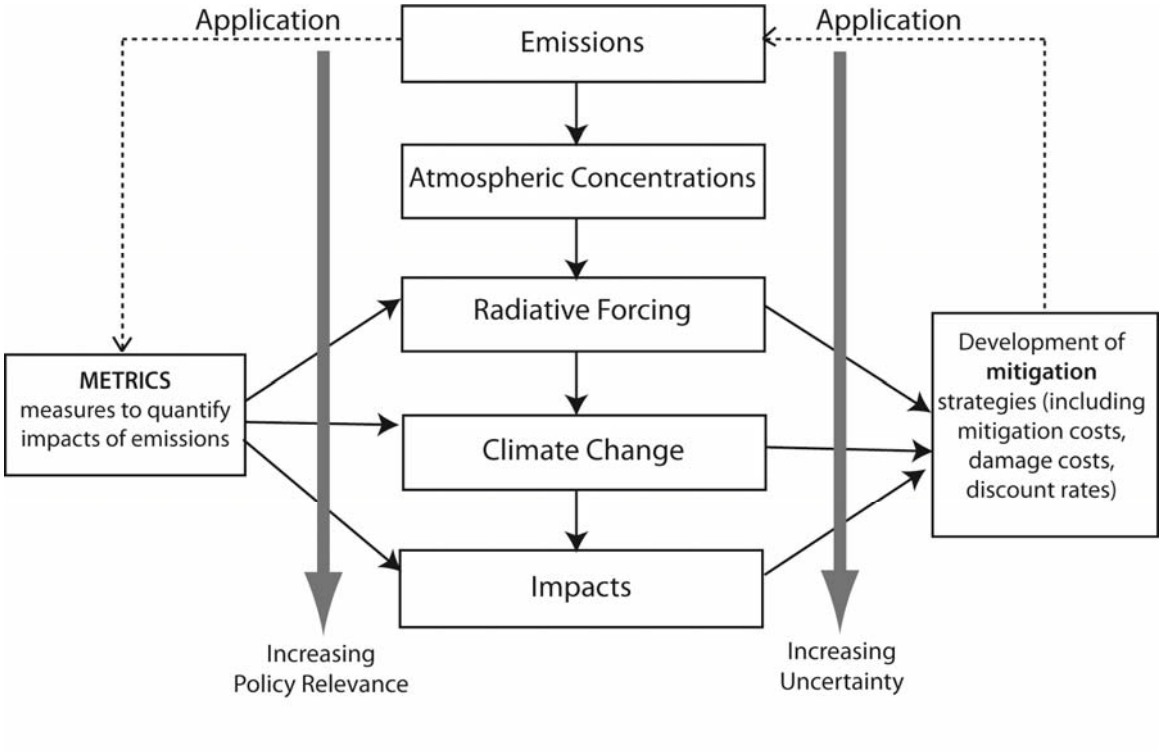

Figure 8.2: Cause-effect chain from emissions to climate change and impacts showing how metrics can be used to estimate responses to emissions (left side) and for development of multi-component mitigation (right side). (Adapted from Fuglestvedt et al. (2003) and Plattner et al. (2009)).

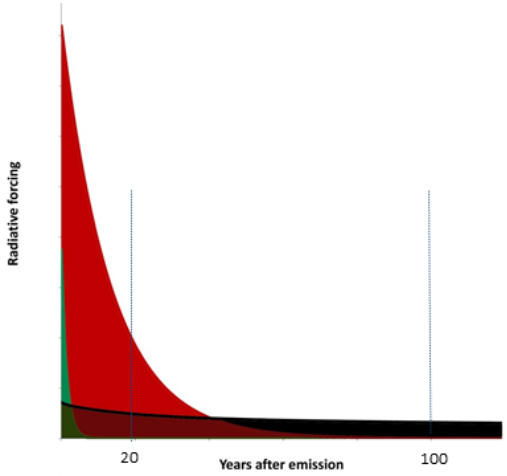

$$GWP_i(H) = \frac{\int_0^H RF_i(t)dt}{\int_0^H RF_{CO_2}(t)dt} = \frac{AGWP_i(H)}{AGWP_{CO_2}(H)}$$

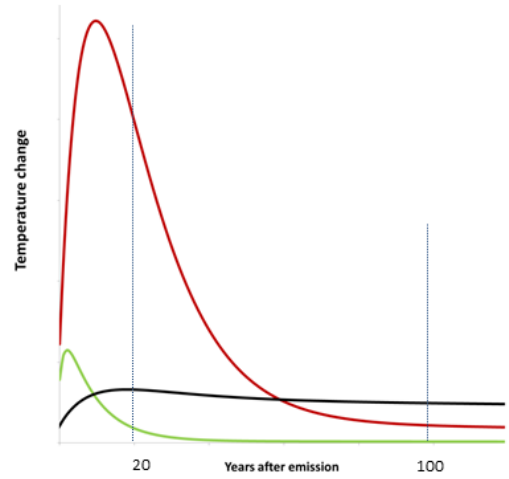

$$GTP_i(t) = \frac{AGTP(t)_i}{AGTP(t)_{CO_2}} = \frac{\Delta T(t)_i}{\Delta T(t)_{CO_2}}$$

Figure 8.3: (a) The GWP is calculated by integrating the RF due to pulses over chosen time horizons; e.g., 20 and 100 years. The black field represent the integrated RF from a pulse of CO_2, while the green and red fields represent gases with 1.5 and 13 years lifetimes, respectively. (b) The GTP is based on the temperature response for selected years after emission; e.g., 20 or 100 years.

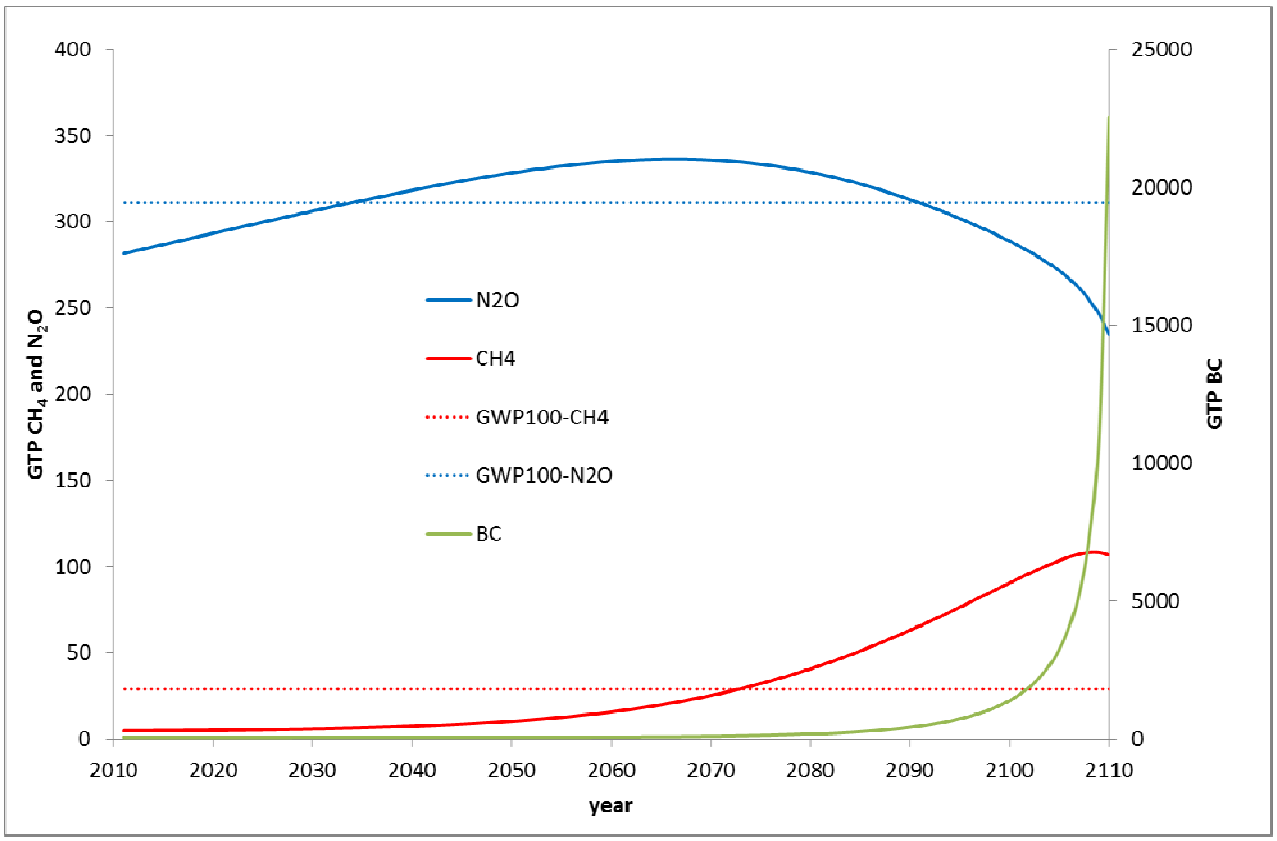

Figure 8.4: Global temperature change potential (GTP(t)) for methane, nitrous oxide and BC for each year from 2010 to the time at which the temperature change target is reached (2110). GTP(t) for CH_4 and N_2O on left axis; GTP(t) for BC on right axis. The (time-invariant) 100–year GWP is also shown for N_2O and CH_4 for comparison.

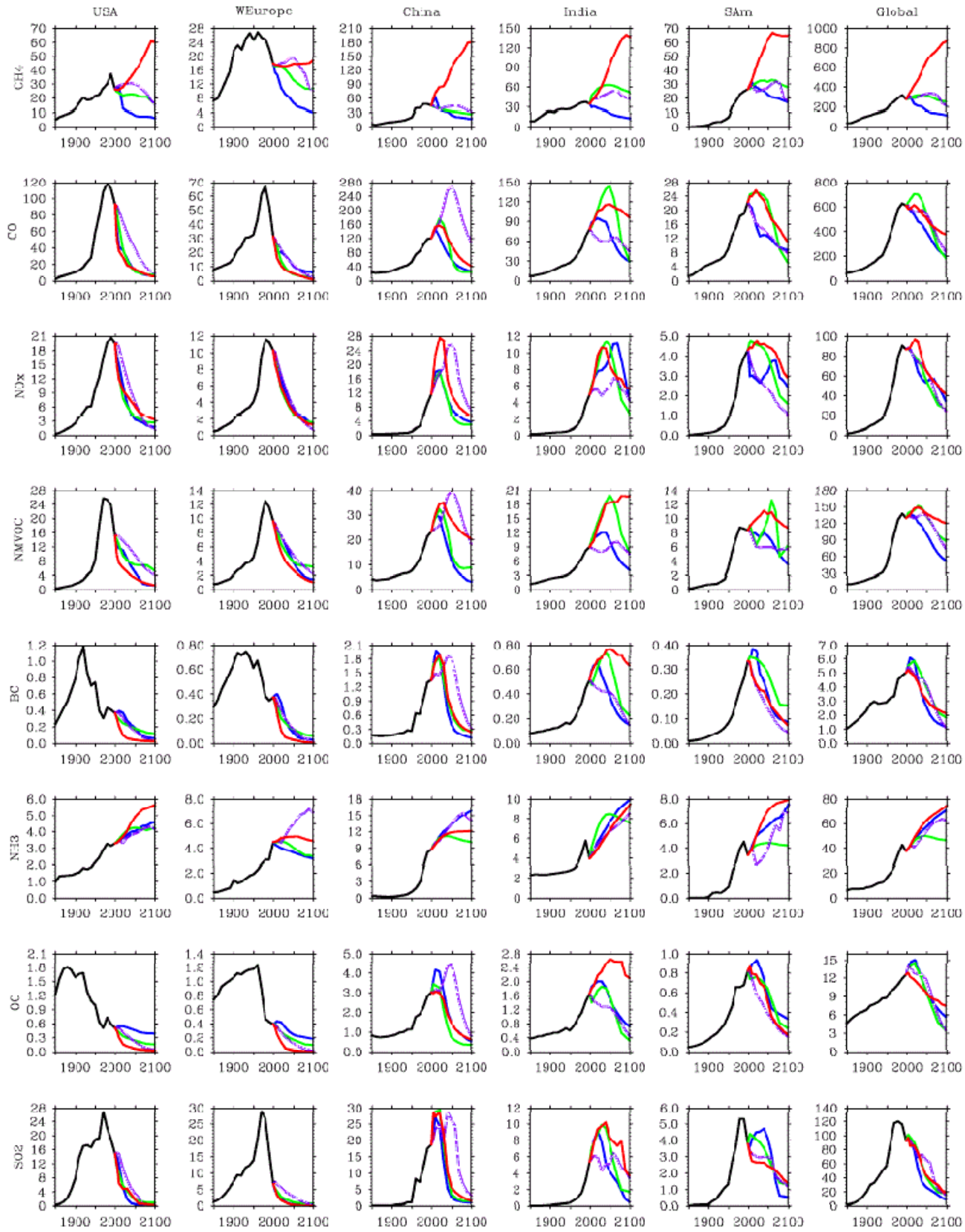

Figure 8.5: Time evolution of regional anthropogenic emissions 1850–2100 following RCP2.6 (blue), RCP4.5 (green), RCP6 (magenta) and RCP8.5 (red). Historical emissions (1850–2000) are from Lamarque et al. (2010). Regional estimates for United States of America, Western Europe, China, India and South America are shown, in addition to the global total.

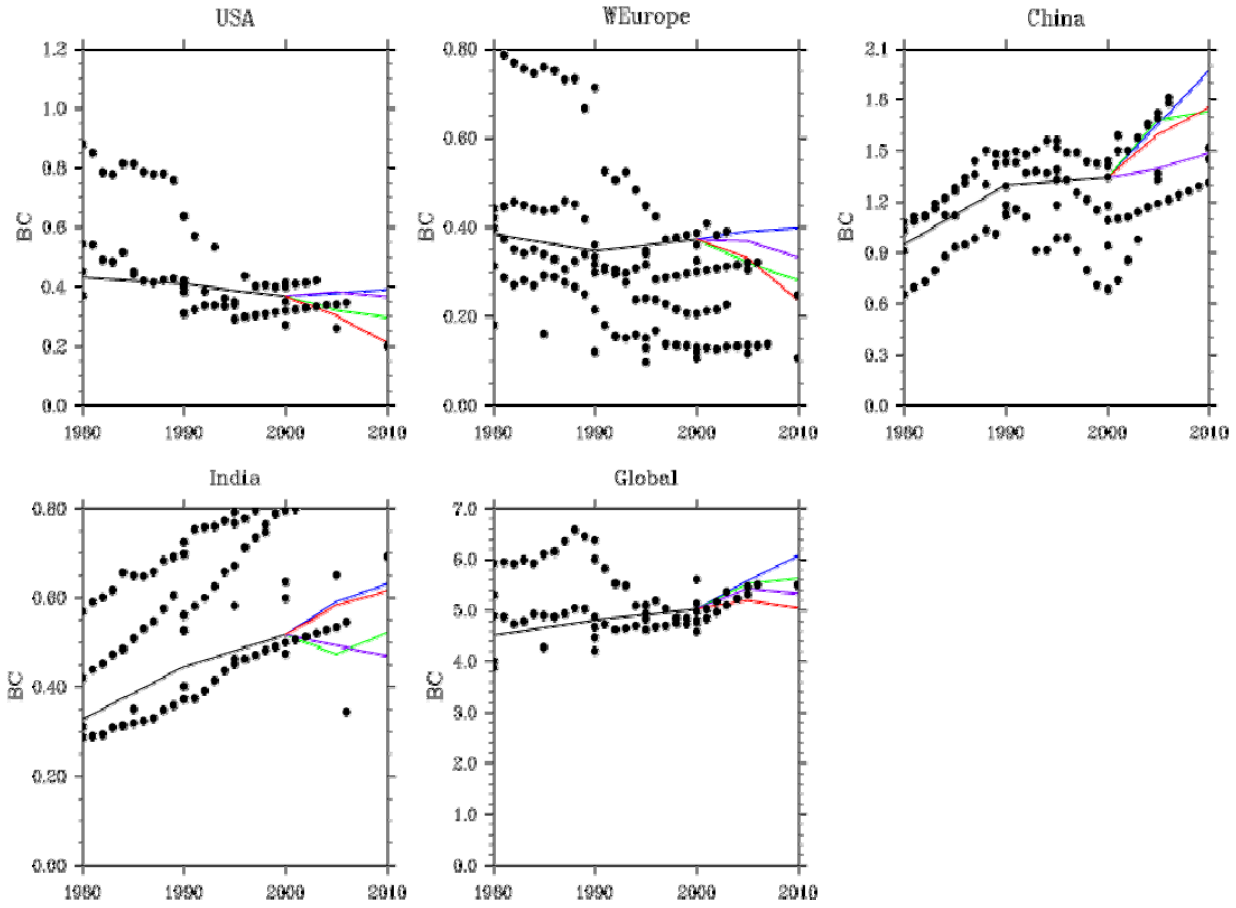

Figure 8.6: Time evolution of regional anthropogenic emissions 1980–2010 for black carbon. Black dots indicate emissions from additional inventories (adapted from Granier et al., 2011).

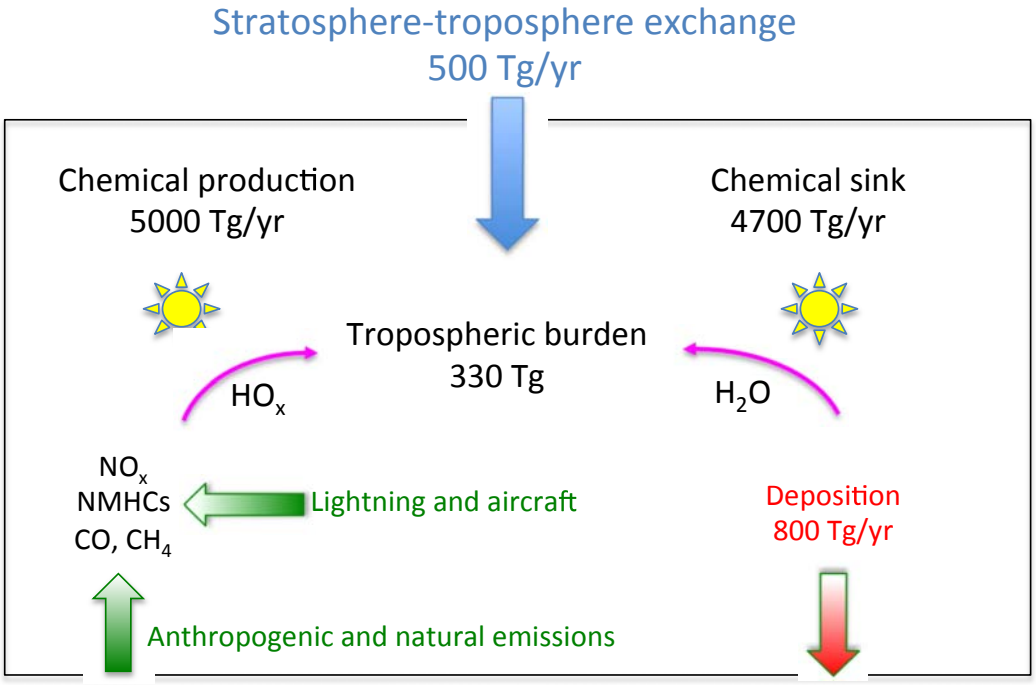

Figure 8.7: Schematic representation of the tropospheric ozone budget. Numbers are approximative and will be finalized with ACCMIP results combined with Table 8.1. Adapted from The Royal Society (2008).

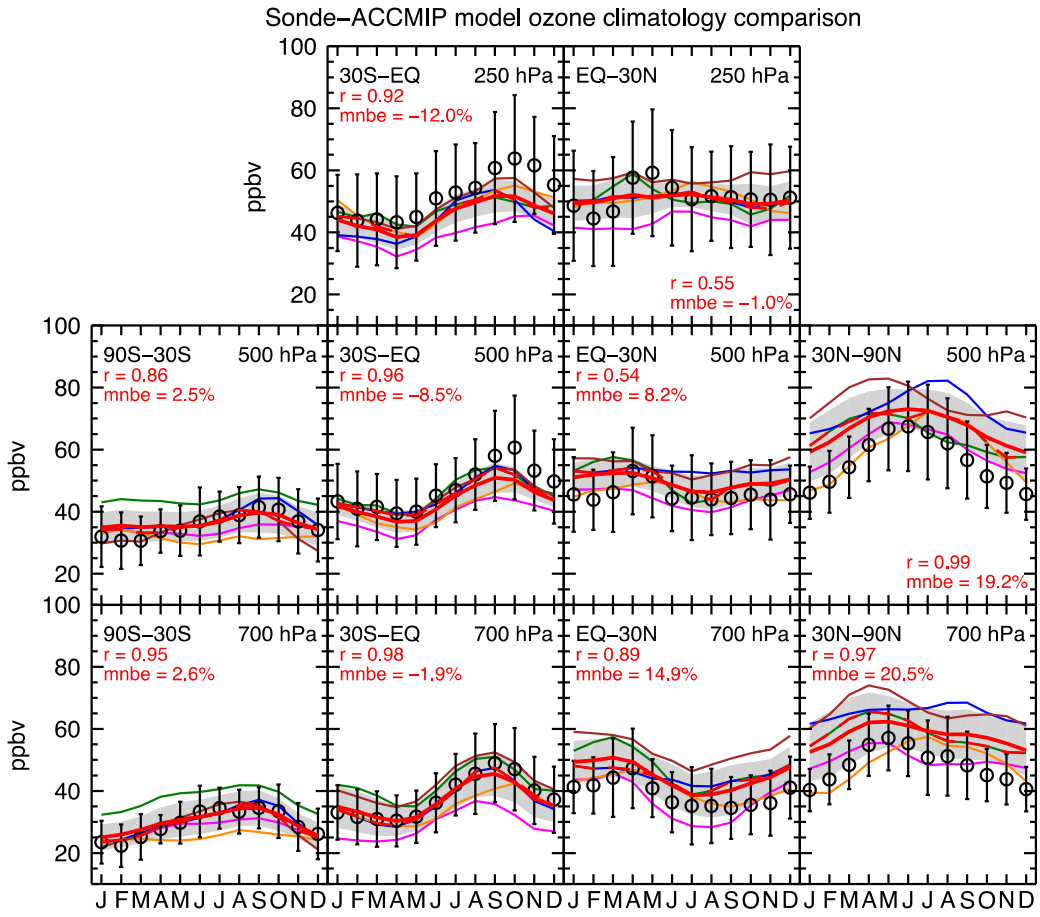

Figure 8.8: Comparisons between observations and simulations for the monthly mean ozone concentration. (Stevenson et al., 2006)-type plot for ACCMIP results.

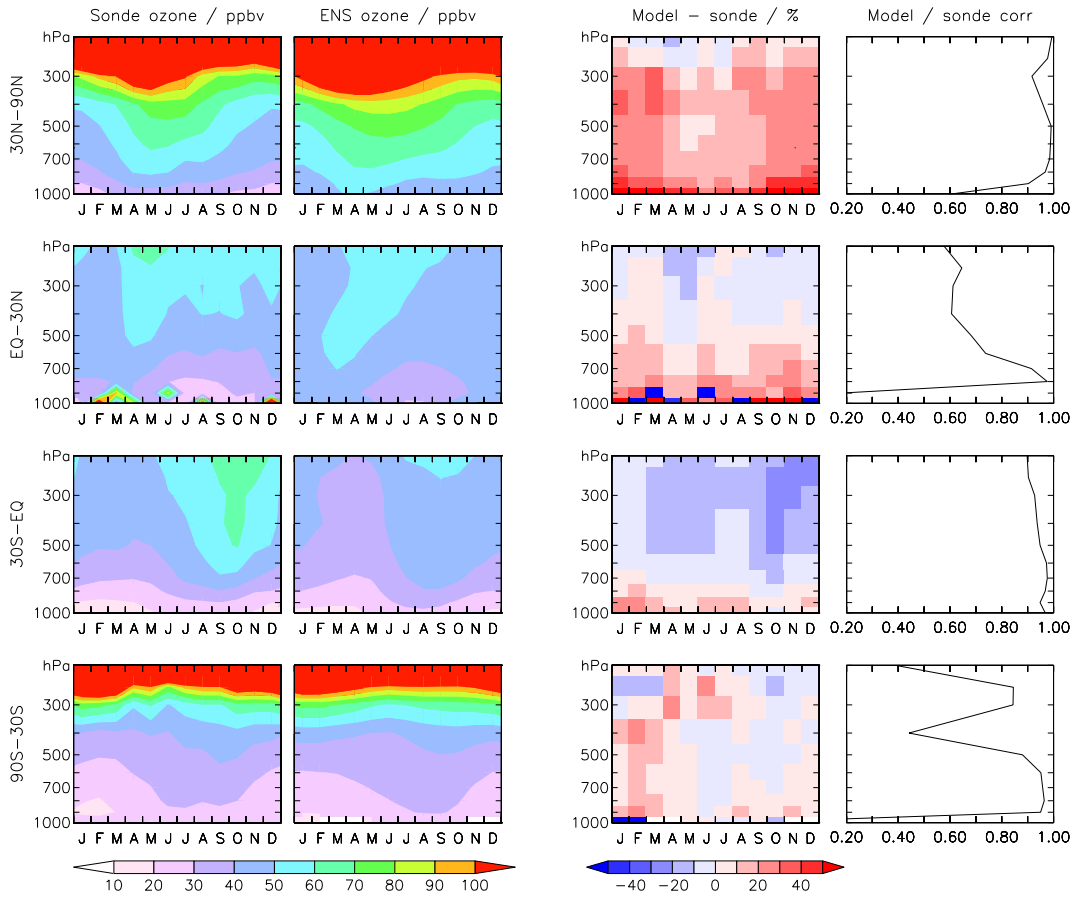

Figure 8.9: Comparison of ACCMIP ensemble mean (second column) with observations (left column). Bias (in %) and correlation are shown in columns 3 and 4.

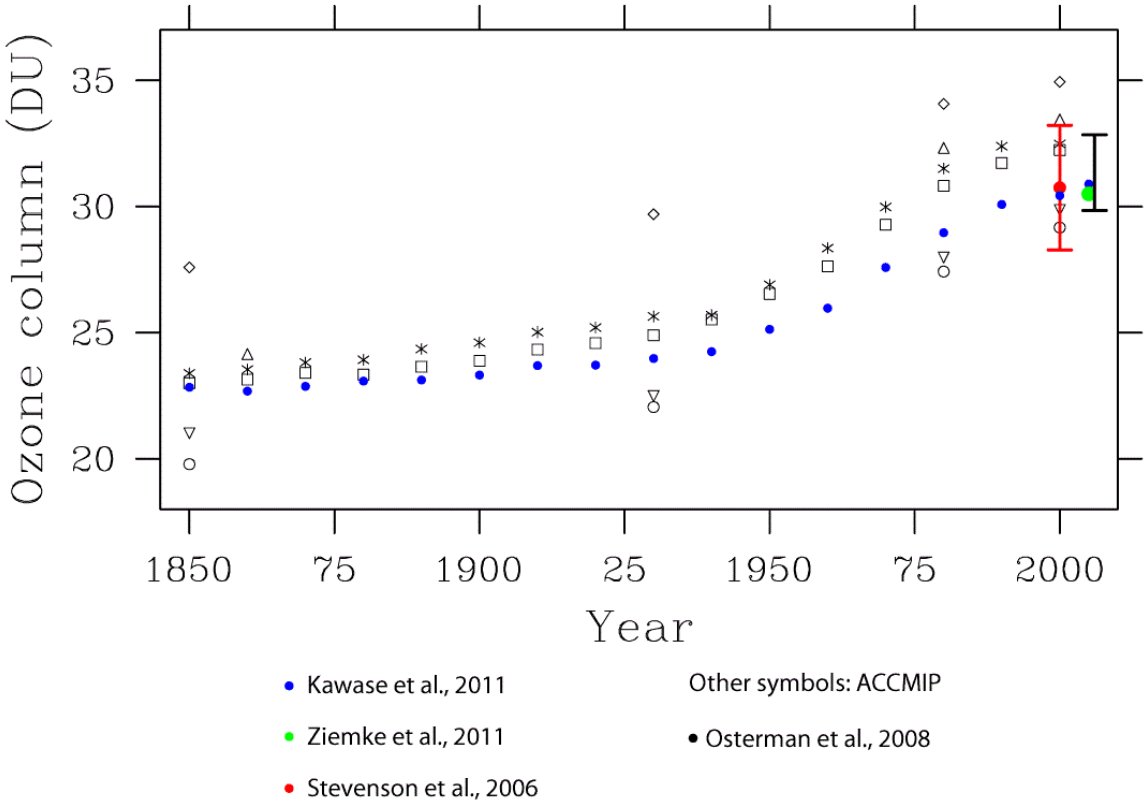

Figure 8.10: Time evolution of tropospheric ozone column (in DU) from 1850 to 2005 from ACCMIP results and Kawase et al. (2011). The OMI-MLS (Ziemke et al., 2011) and TES (Osterman et al., 2008) satellite-based climatologies are also shown, along with the ACCENT-AR4 results.

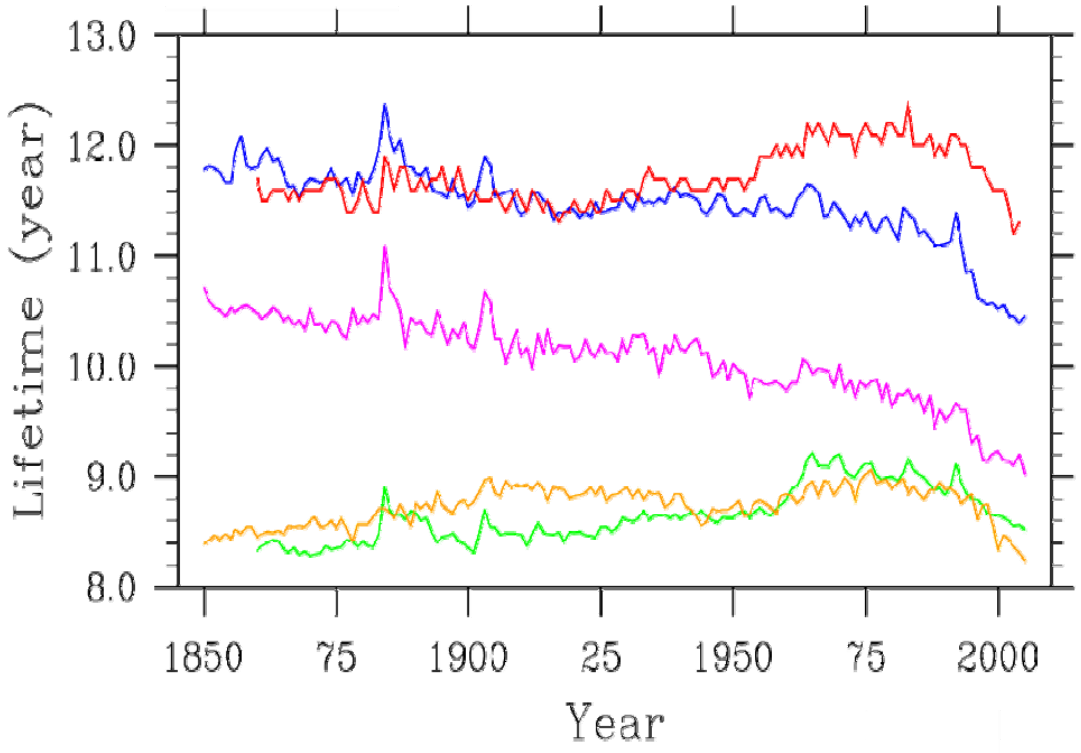

Figure 8.11: Time evolution of tropospheric methane lifetime (with respect to OH) from CMIP5 chemistry-climate models.

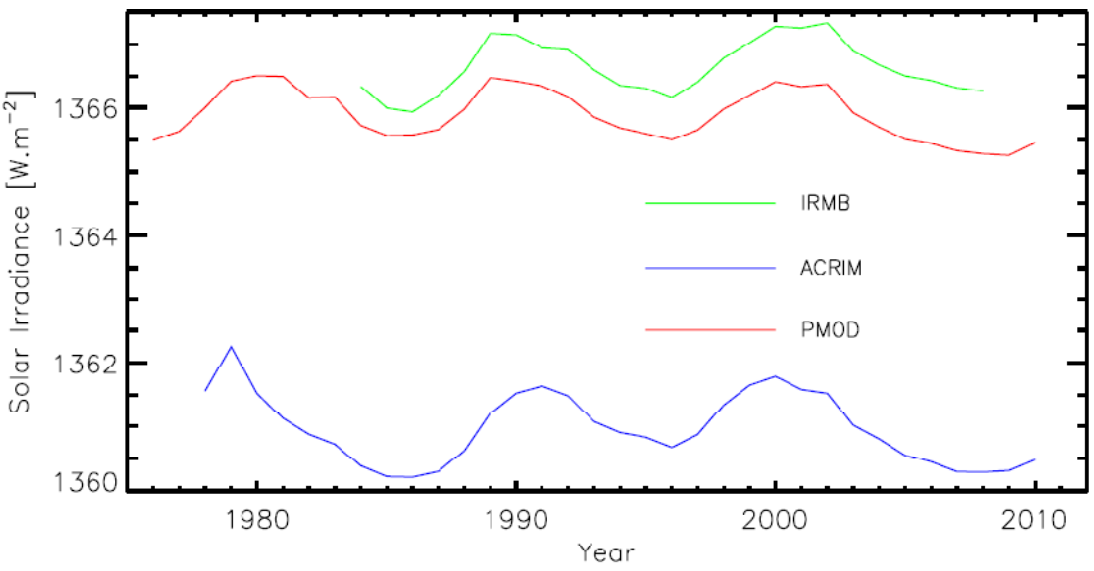

Figure 8.12: Annual average composites of measured Total Solar Irradiance: The Active Cavity Radiometer Irradiance Monitor (ACRIM) (Willson and Mordvinov, 2003) , the Institut Royal Meteorologique Belgique (IRMB) (Dewitte et al., 2004) and the Physikalisch-Meteorologisches Observatorium Davos (PMOD) (Frohlich, 2006).

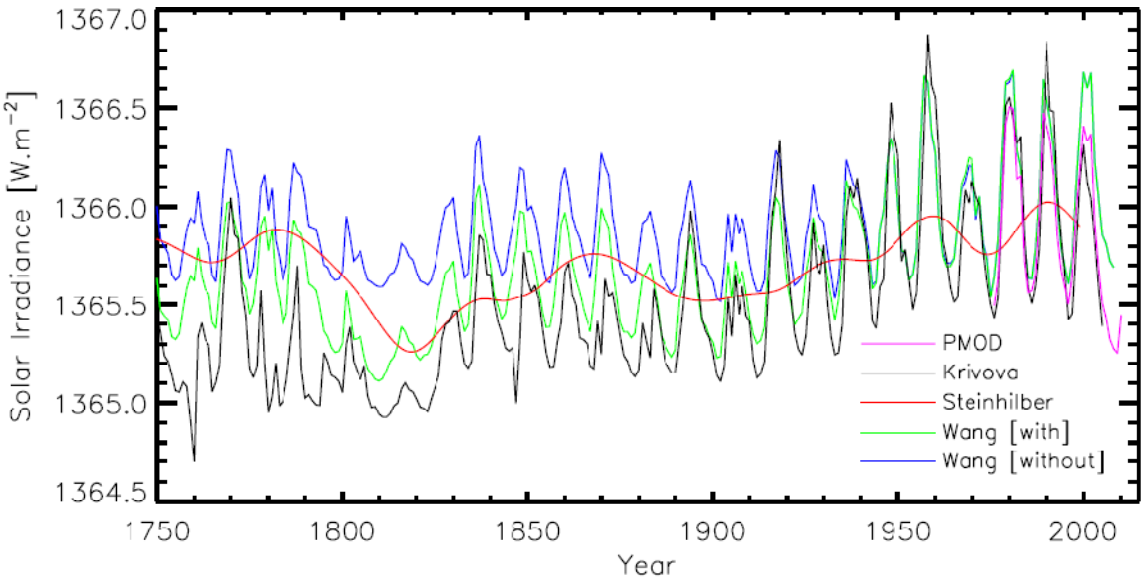

Figure 8.13: Annual mean reconstructions of Total Solar Irradiance since 1750: Wang et al. (2005), with and without an independent change in the background level of irradiance, Steinhilber et al. (2009) (here we show an interpolation of their 5-year time resolution series), The Krivova et al. (2010) time series , and the PMOD composite time series (Frohlich, 2006).

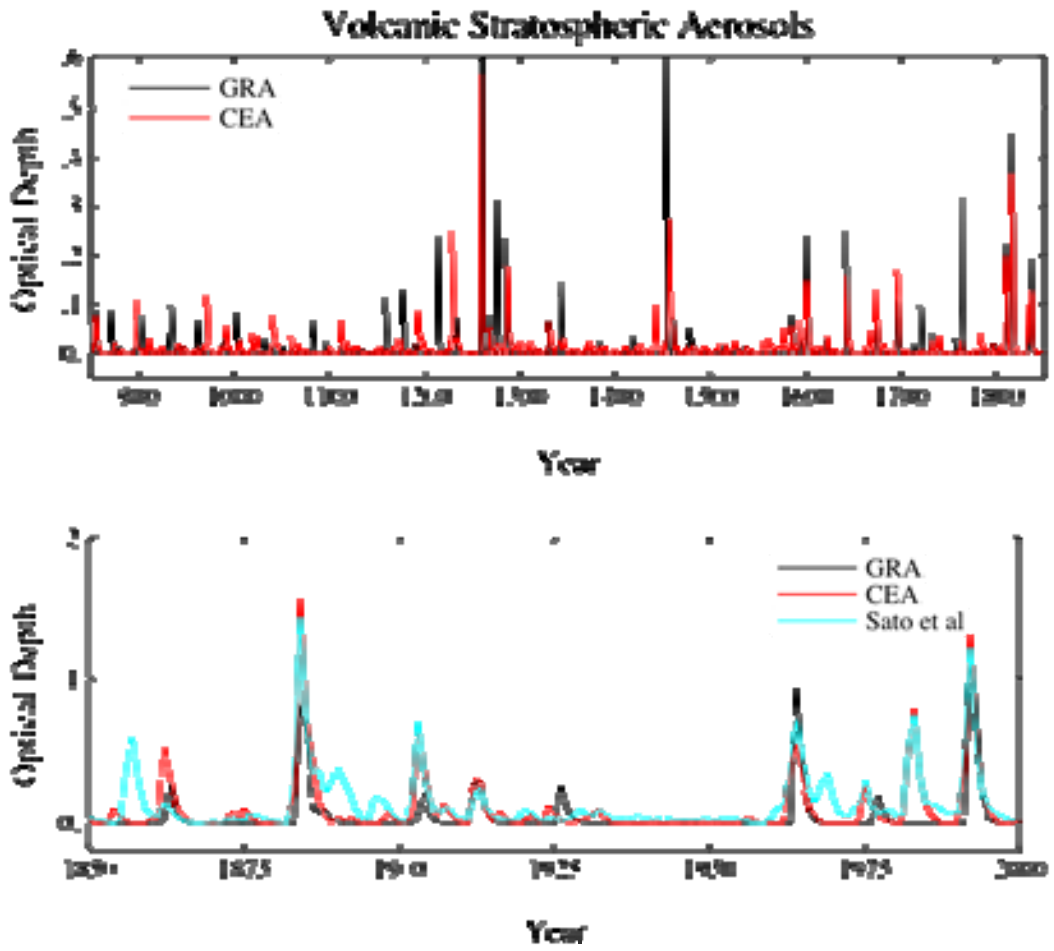

Figure 8.14: Two volcanic reconstructions of aerosol optical depth (at 550 μm) as developed for the Paleoclimate Model Intercomparison Project (top), with a comparison to the updated estimates of Sato et al. (1993) (bottom, note the different vertical scales in the two panels). Figure from Schmidt et al. (2011). [PLACEHOLDER FOR SECOND ORDER DRAFT: This will be re-drafted later for only 1750 to present; pre-1750 will be in Chapter 5.]

(a)

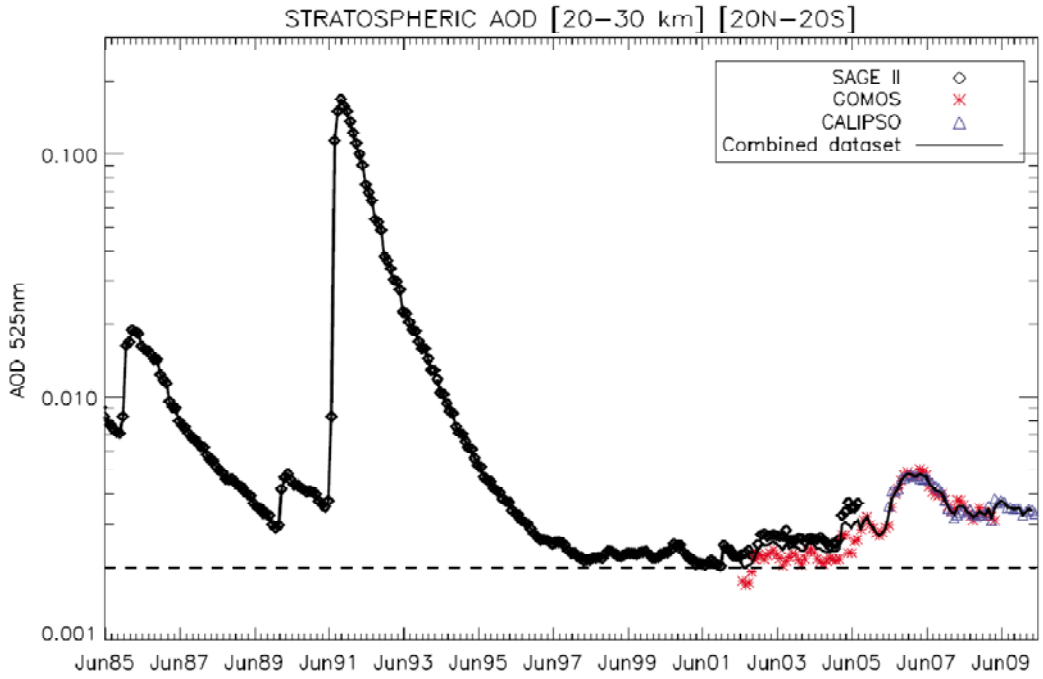

(b)

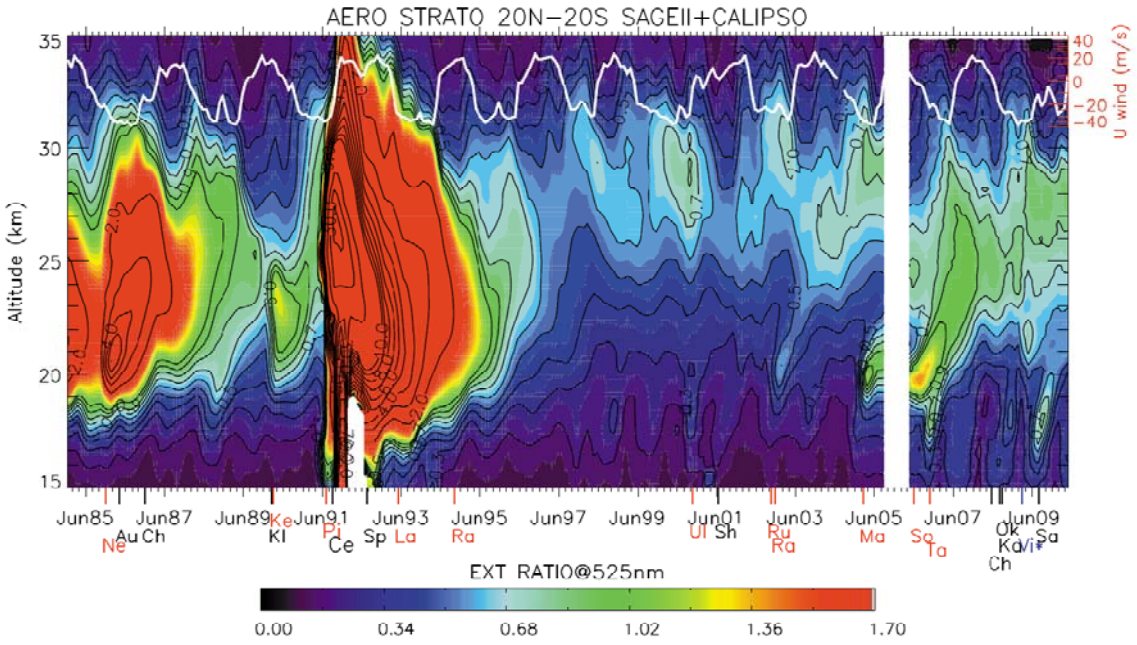

Figure 8.15: (a) Mean stratospheric Aerosol Optical Depth in the tropics [20°N–20°S] between 20–30 km since 1985 from the Stratospheric Aerosol and Gas Experiment (SAGE) II (black diamonds), the Global Ozone Monitoring by Occultation of Stars (GOMOS) (red stars), CALIOP (blue triangles) and combined satellites (black line) (Figure 5 from Vernier et al., 2011). (b) Monthly mean extinction ratio (525 nm) profile evolution in the tropics [20°N–20°S] from January 1985 to June 2010 derived from (left) SAGE II extinction in 1985–2005 and (right) CALIOP scattering ratio in 2006–2010, after removing clouds below 18 km based on their wavelength dependence (SAGE II) and depolarization properties (CALIOP) compared to aerosols. Black contours represent the extinction ratio in log•scale from 0.1 to 100. The position of each volcanic eruption occurring during the period is displayed with its first two letters on the horizontal axis, where tropical eruptions are noted in red. The eruptions were Nevado del Ruiz (Ne), Augustine (Au), Chikurachki (Ch), Kliuchevskoi (Kl), Kelut (Ke), Pinatubo (Pi), Cerro Hudson (Ce), Spur (Sp), Lascar (La), Rabaul (Ra), Ulawun (Ul), Shiveluch (Sh), Ruang (Ru), Reventador (Ra), Manam (Ma), Soufrière Hills (So), Tavurvur (Ta), Chaiten (Ch), Okmok (Ok), Kasatochi (Ka), Fire/Victoria (Vi*), Sarychev (Sa). Superimposed is the Singapore zonal wind speed component at 10 hPa (white line) (Figure 1 from Vernier et al., 2011).

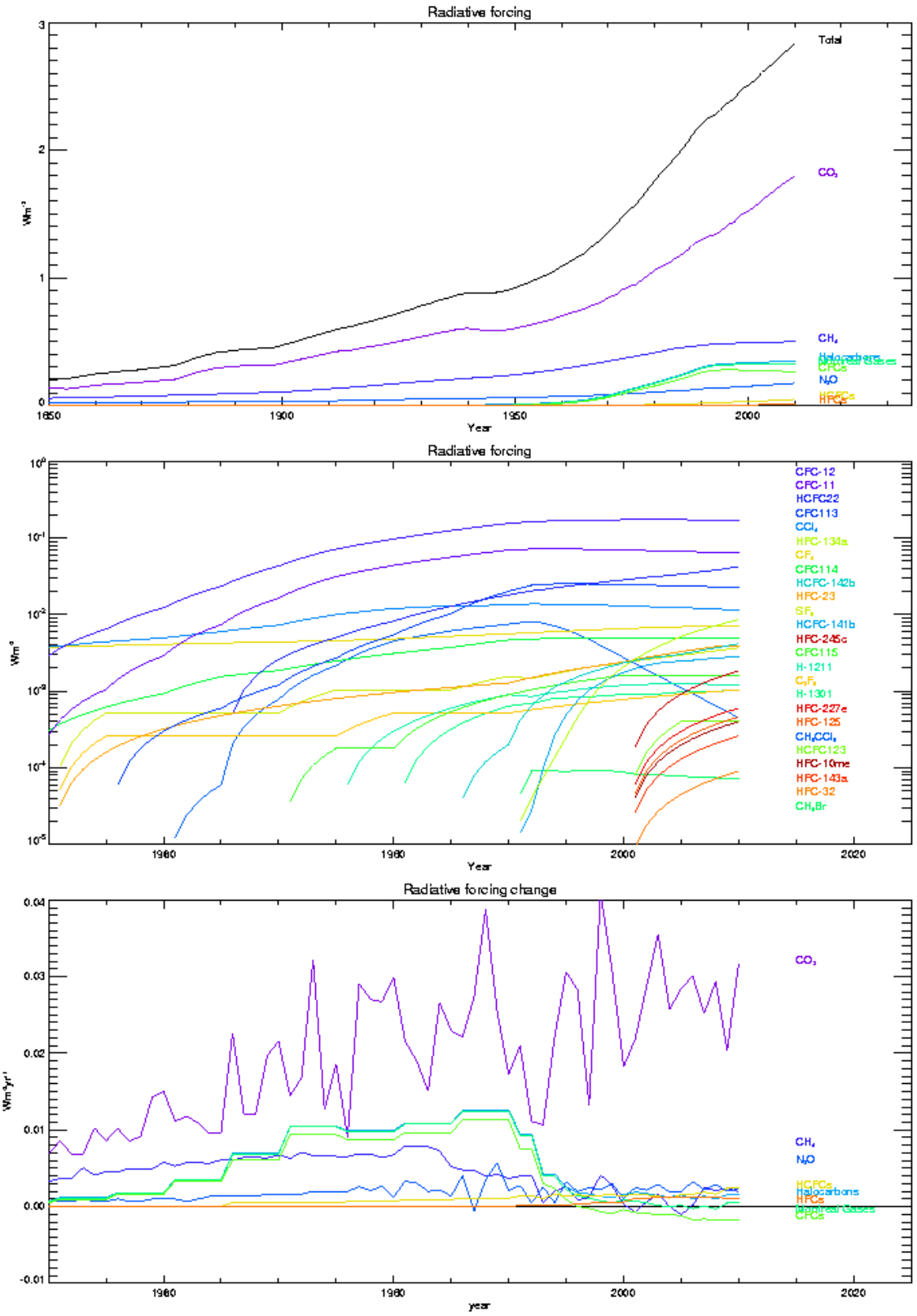

Figure 8.16: (a) Radiative forcing from the major long-lived greenhouse gases and groups of halocarbons from 1850 to 2010 (data currently from NASA GISS http://data.giss.nasa.gov/modelforce/ghgases/). (b) Radiative forcing from the minor long-lived greenhouse gases from 1950 to 2010. (c) Rate of change in forcing from the major long-lived greenhouse gases and groups of halocarbons from 1950 to 2010.

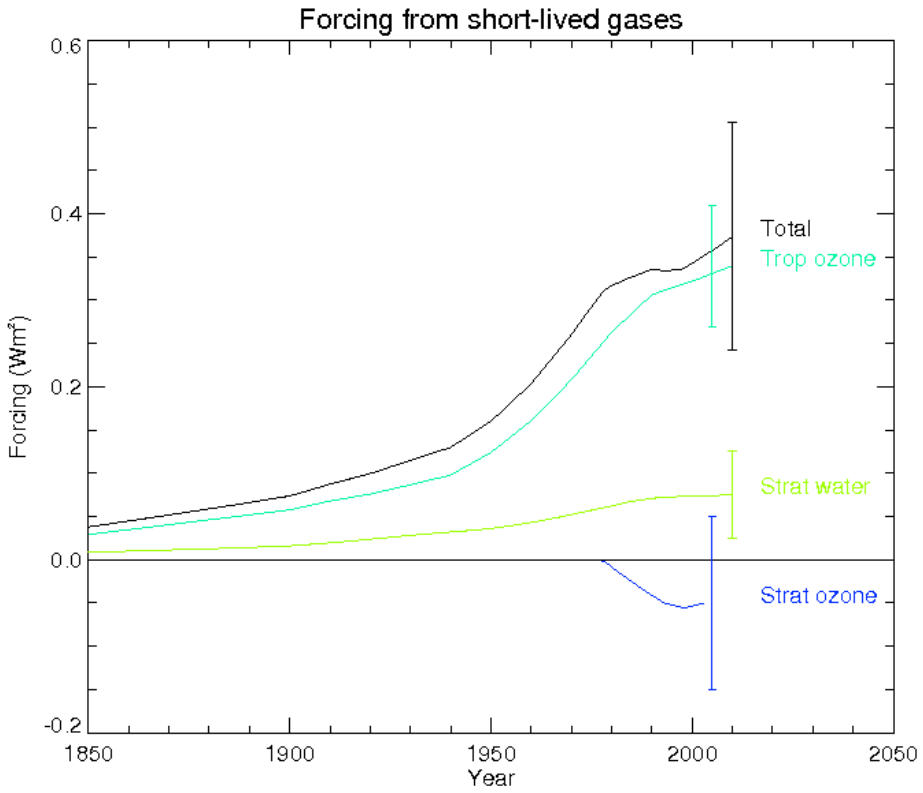

Figure 8.17: Time evolution of the forcing of short-lived components from 1850 to 2010. Tropospheric ozone data are from Skeie et al. (2011b) scaled to give 0.34 W m^{-2} at 2010, stratospheric water vapour forcing is calculated by scaling the methane forcing by 15%, stratospheric ozone forcing is from WMO (2010) scaled to give 0.05 W m^{-2} at 2010.

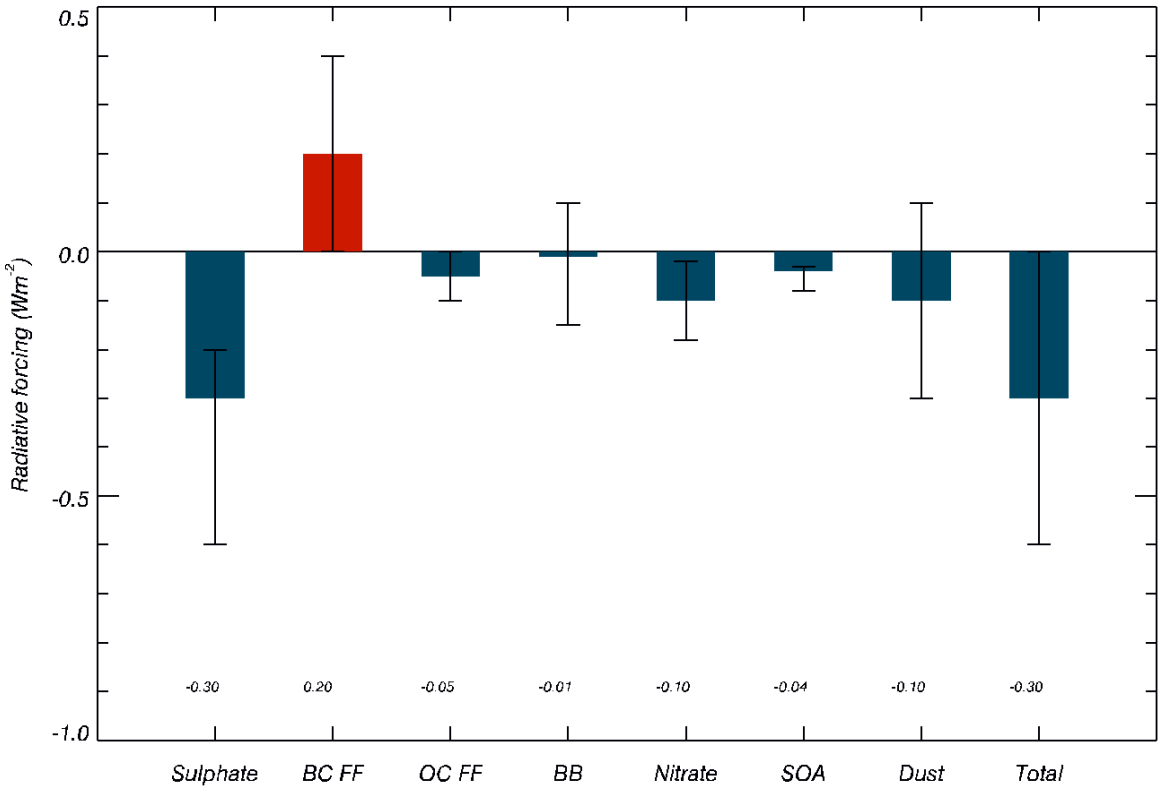

Figure 8.18: Best estimate of the RF for 7 aerosol components and the total direct aerosol effect shown as bars with lines indicating the uncertainty (90% confidence interval).

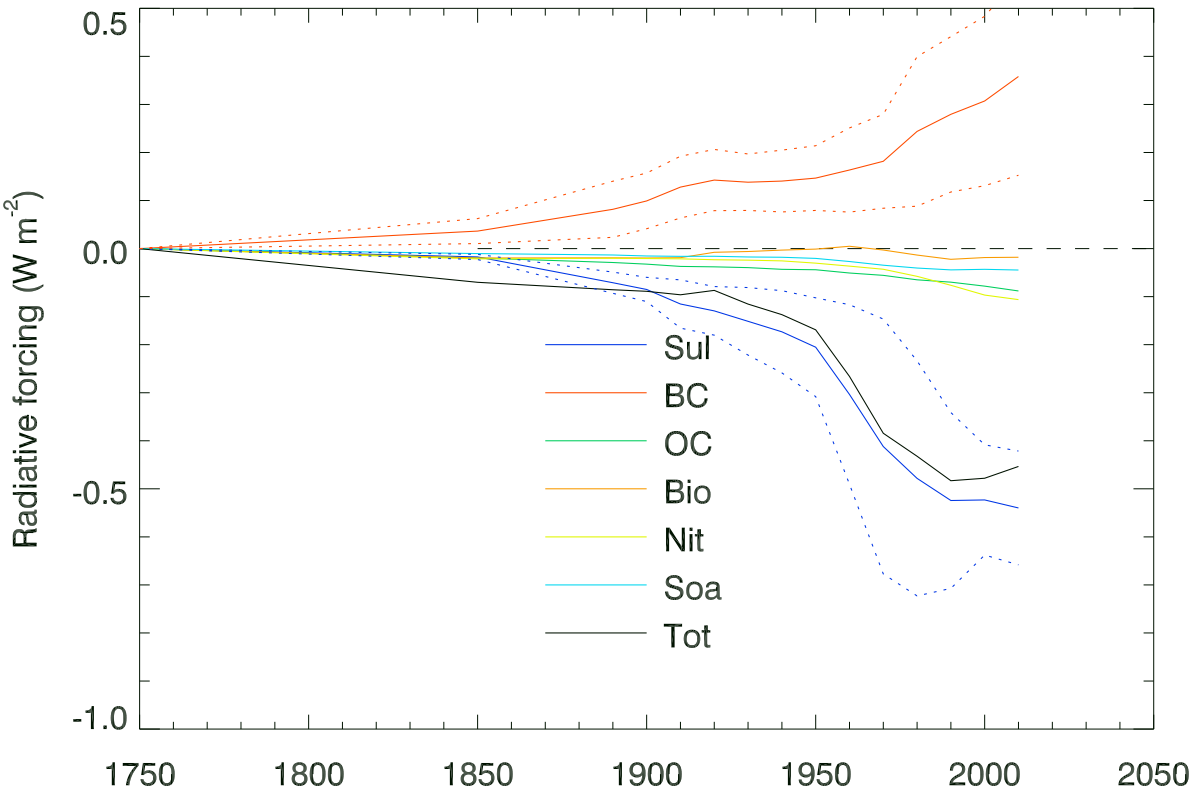

Figure 8.19: Time evolution of RF of the direct aerosol effect (total as well as by components). Solid lines show the mean of individual model results and dotted lines ± one standard deviation. [PLACEHOLDER FOR THE SECOND ORDER DRAFT: So far results from two models are used, but the figure will be updated by more models and be made consistent with the best estimates.]

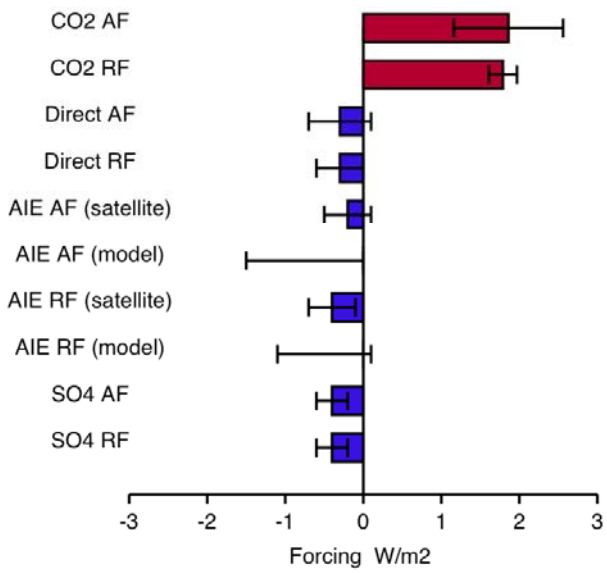

Figure 8.20: The RF and AF estimates of various forcing agents of the climate systems. The direct aerosol radiative forcing and its AF (that includes the semi-direct effects) include the effects of the components (sulphates and black carbon) also shown. The aerosol indirect effect (AIE) RF is meant to represent the Twomey effect where all cloud property remain fixed expect for changes in the drop size distribution. The aerosol indirect effect (AIE) AF includes the rapid cloud-scale adjustments, including cloud cover, and cloud water path changes. Rapid response processes differ from model to model. The observed AIE RF is taken from global satellite observations binned by fixed cloud liquid water thus representing a close analogue to the Twomey effect. [PLACEHOLDER FOR SECOND ORDER DRAFT: All the values will be made consistent with estimates from Chapter 7; BC RF and AF will be added.]

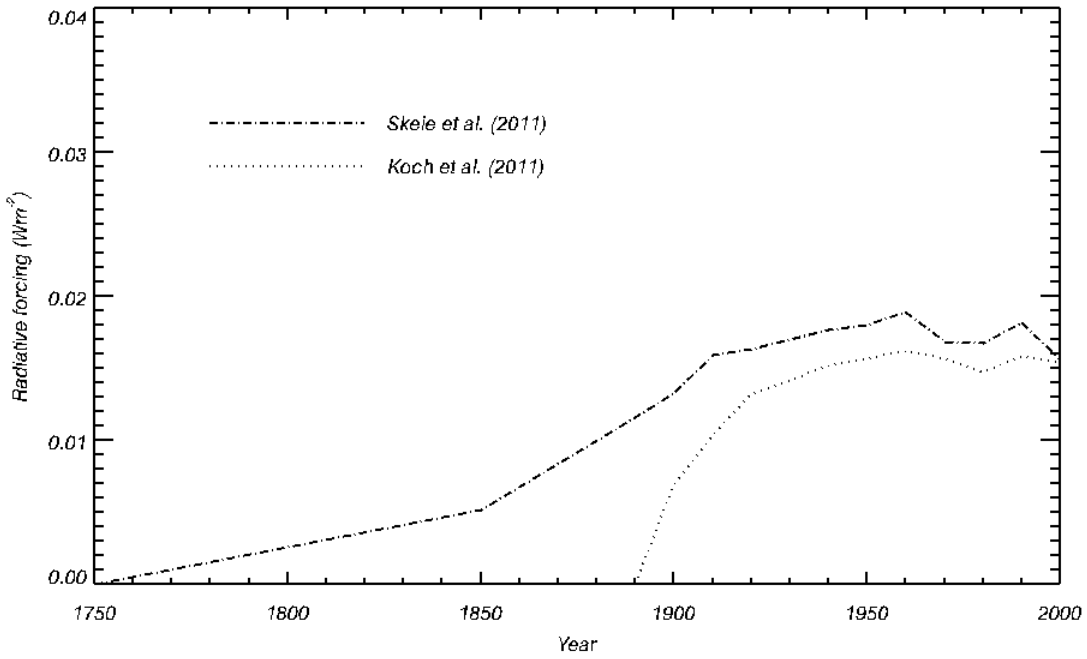

Figure 8.21: Time evolution of RF due to BC on snow and ice. The two studies included show results for somewhat different time period with Koch et al. (2011) for the period 1890–2000 and Skeie et al. (2011a) for the period 1750–2000. The figure will be updated for SOD with further studies.

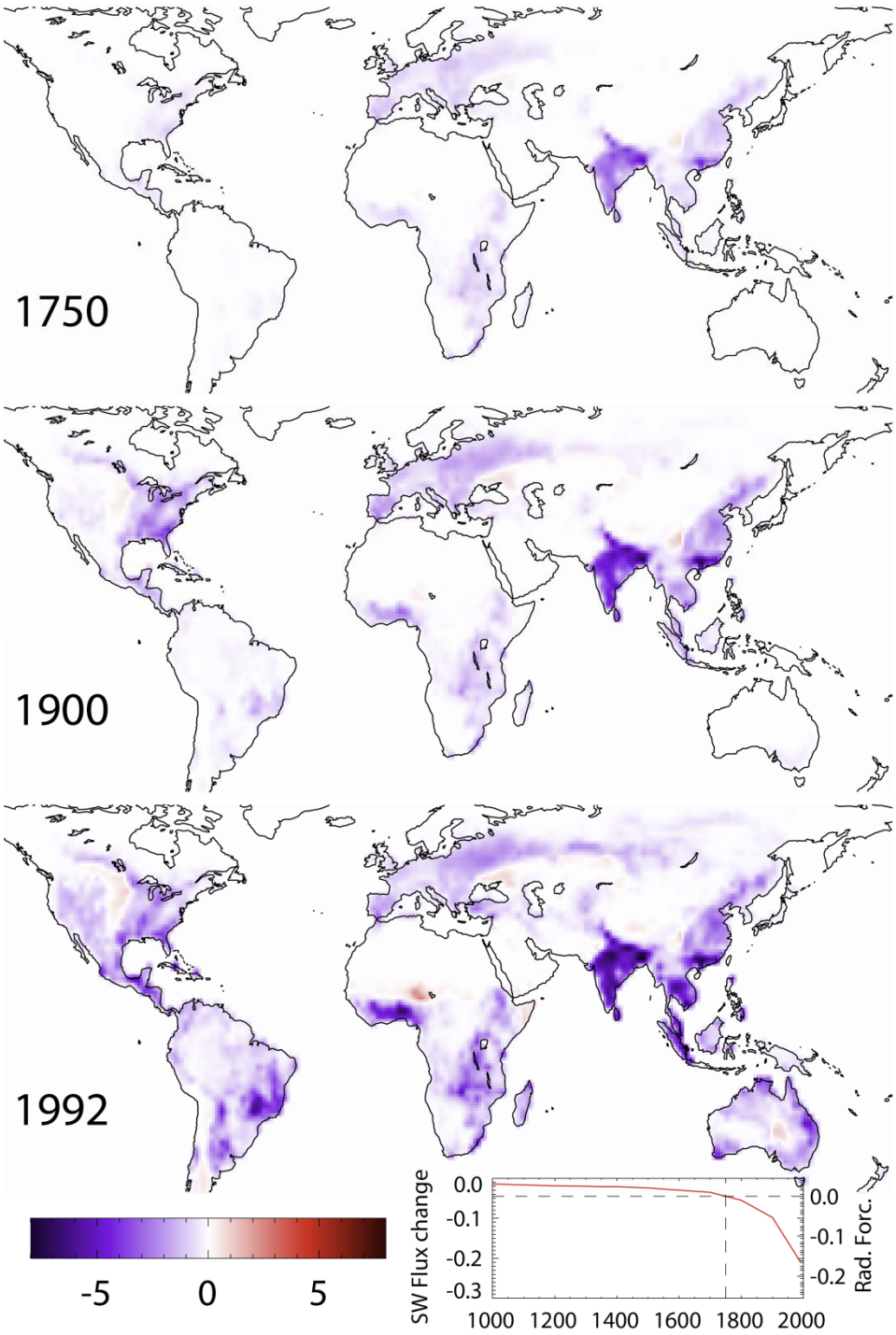

Figure 8.22: Change in TOA SW flux [W m^{-2}] following the change in albedo as a result of anthropogenic Land Use Change for three periods (1750, 1900 and 1992 from top to bottom). By definition, the RF is with respect to 1750. The lower right inset shows the globally averaged impact of the surface albedo change to the TOA SW flux (left scale) as well as the corresponding RF (right scale). Based on simulations by Pongratz et al. (2009).

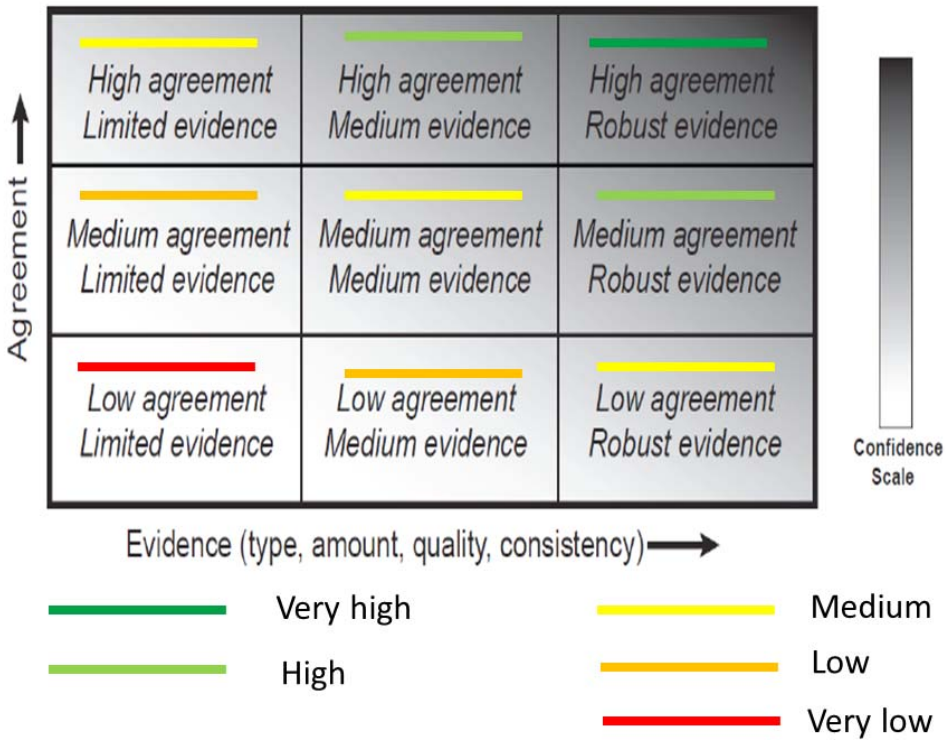

Figure 8.23: The basis for the confidence level is given as a combination of evidence (limited, medium, robust) and agreement (low, medium, and high). The confidence level is given for five levels (very high, high, medium, low, and very low) and given in colours.

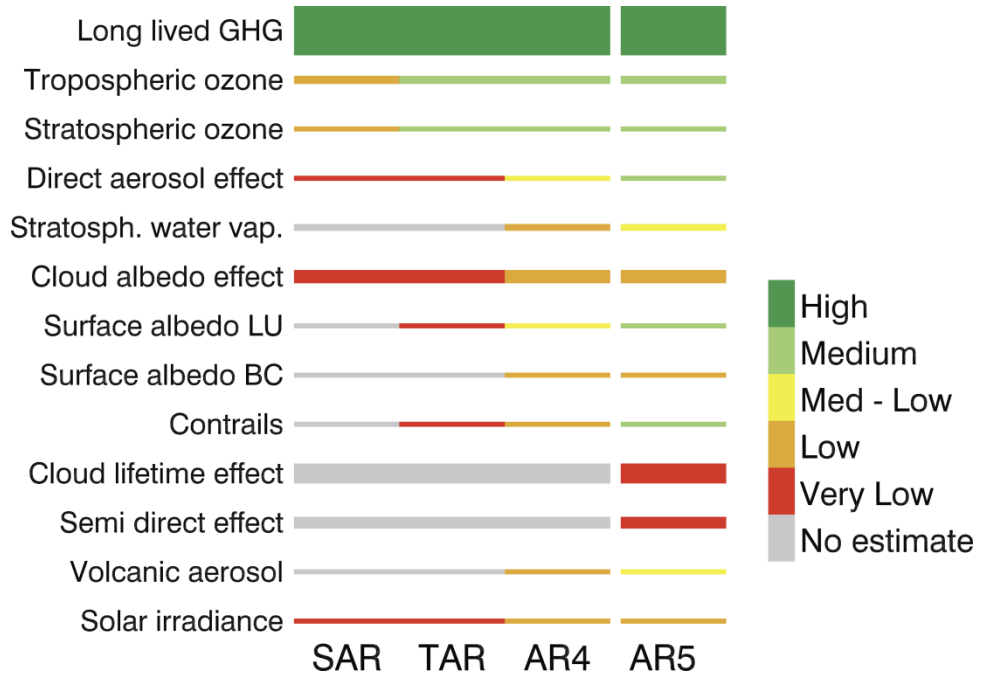

Figure 8.24: Level of scientific understanding (LOSU) of the RF mechanisms in the 4 last IPCC assessments. The LOSU terminology is not regularly used in AR5, but for comparison with previous IPCC assessments the confindence level is converted approximately to LOSU. The thickness of the bars represents the relative magnitude of the RF (with a minimum value for clarity of presentation).

(a)

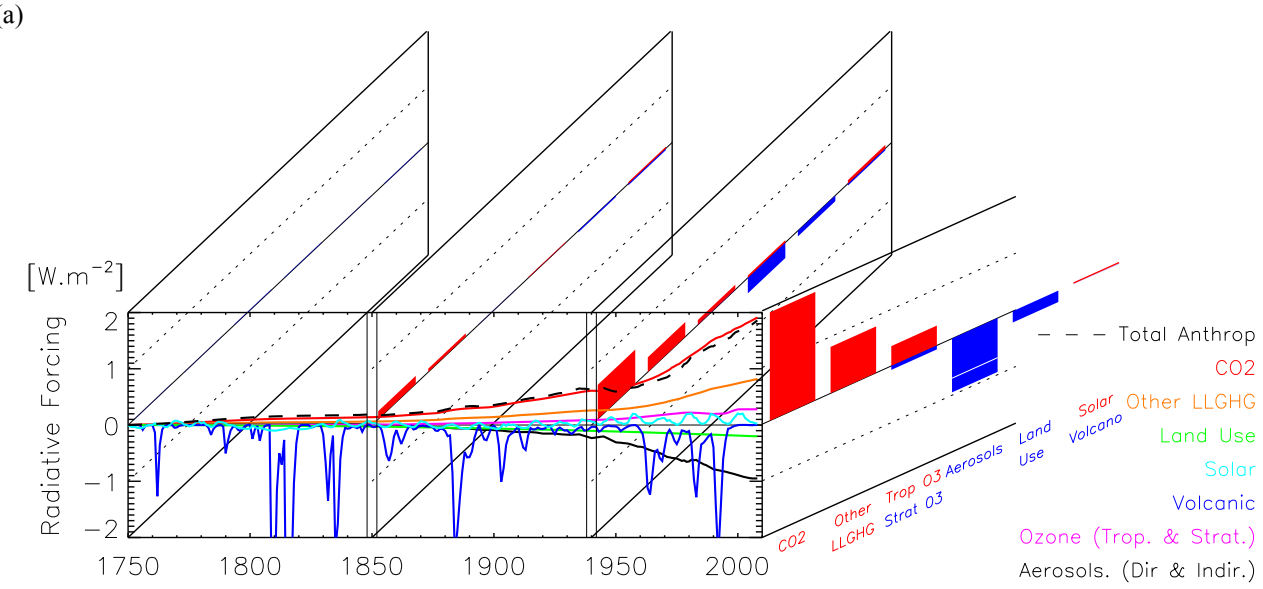
[W.m^{-2}]
Radiative Forcing
2
1
0
−1
−2
1750
1800
1850
1900
1950
2000
CO2
Other LLGHG
Trop O3
Strat O3
Aerosols
Land Use
Solar
Volcano
Total Anthrop
CO2
Other LLGHG
Land Use
Solar
Volcanic
Ozone (Trop. & Strat.)
Aerosols. (Dir & Indir.)

(b)

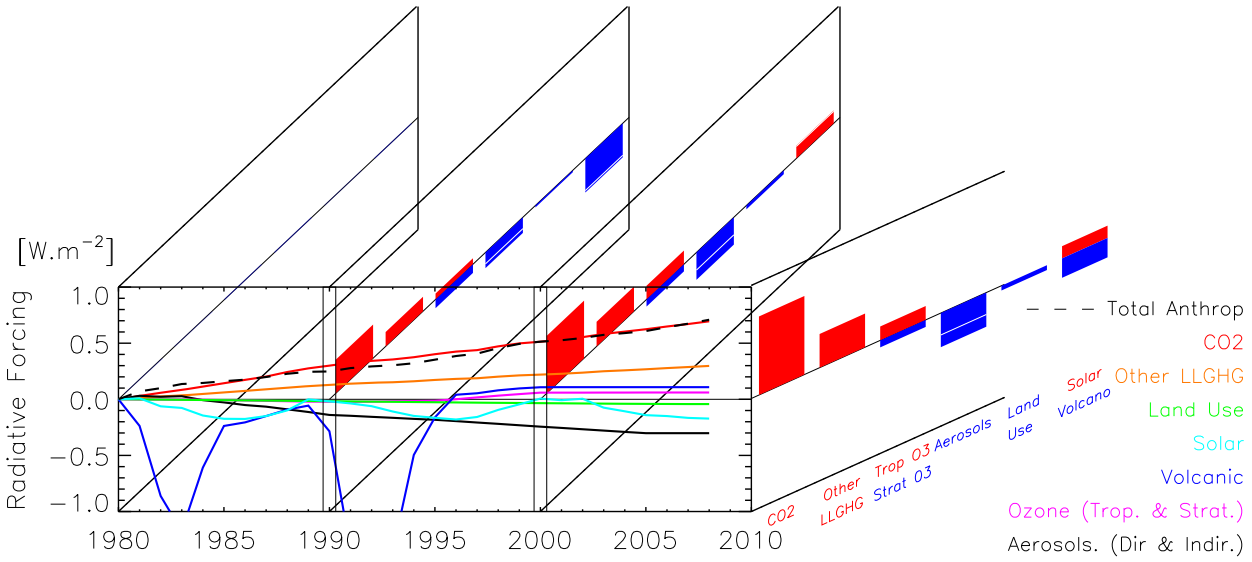
[W.m^{-2}]
Radiative Forcing
1.0
0.5
0.0
−0.5
−1.0
1980
1985
1990
1995
2000
2005
2010
CO2
Other LLGHG
Trop O3
Strat O3
Aerosols
Land Use
Solar
Volcano
Total Anthrop
CO2
Other LLGHG
Land Use
Solar
Volcanic
Ozone (Trop. & Strat.)
Aerosols. (Dir & Indir.)

(c)

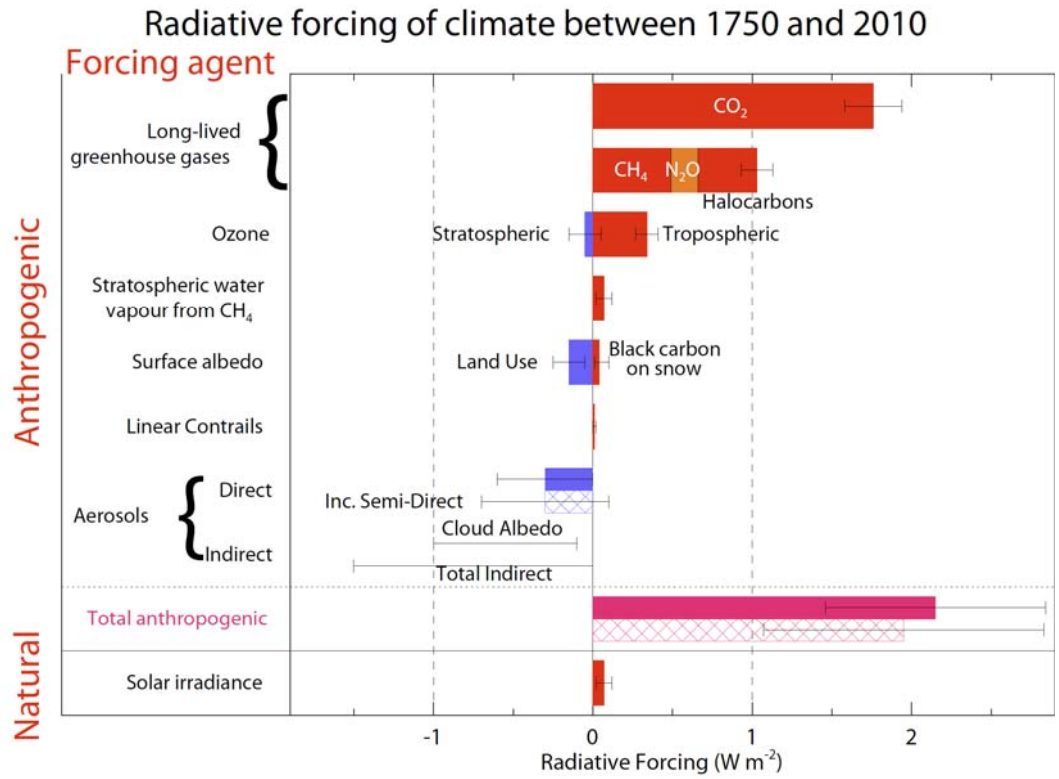

(d)

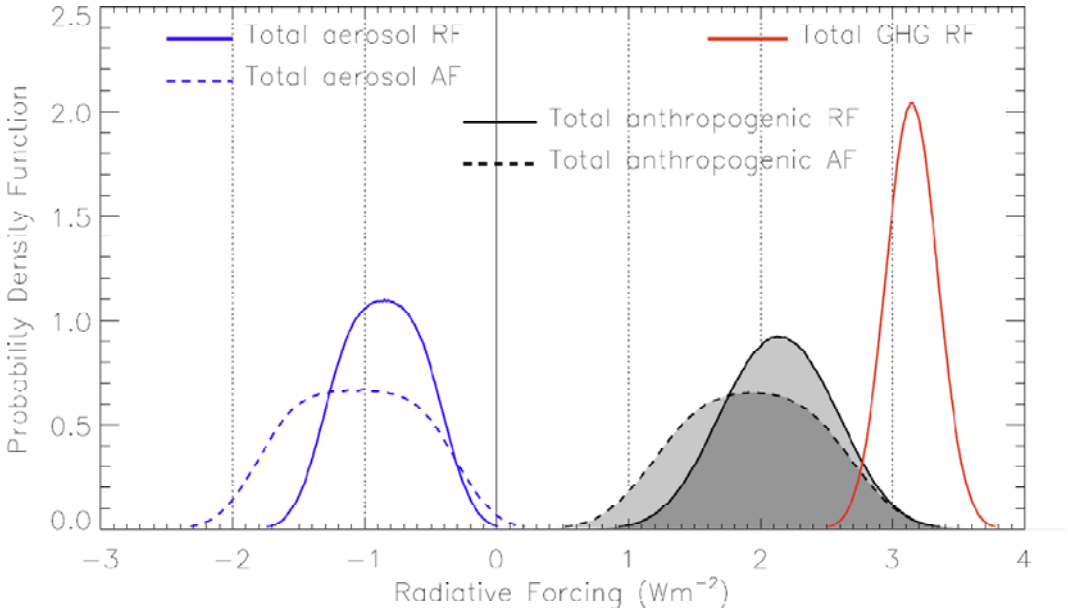

Figure 8.25: RF bar chart with time evolution of RF from major components. Panel (a) shows time evolution over the whole industrial era (1750–2010) whereas panel (b) shows the period 1980–2010 [PLACEHOLDER FOR SECOND ORDER DRAFT: The figure will be updated with ACCMIP results and current RF will be made consistent with best estimate RF.]. (c) Bar chart for RF (solid) and AF (hatched) for the period 1750–2010 (aerosol indirect forcing RF and AF are given as ranges), where the total anthropogenic RF and AF are derived from panel d. (d) Probability density function (PDF) of total GHG RF, aerosol forcing, and total anthropogenic forcing. The PDFs are generated based on uncertainties provided in Table 8.9. The combination of the individual RF agents to derive total anthropogenic forcing are done by Monte Carlo simulations and based on the method in Boucher and Haywood (2001). PDF of the RF from surface albedo changes is included in the total anthropogenic forcing, but not shown as a separate PDF. [PLACEHOLDER FOR THE SECOND ORDER DRAFT: Note that for the total anthropogenic AF, the AF for GHG and surface albedo change is assumed to be equal to RF. This assumption will be investigated before the SOD.]

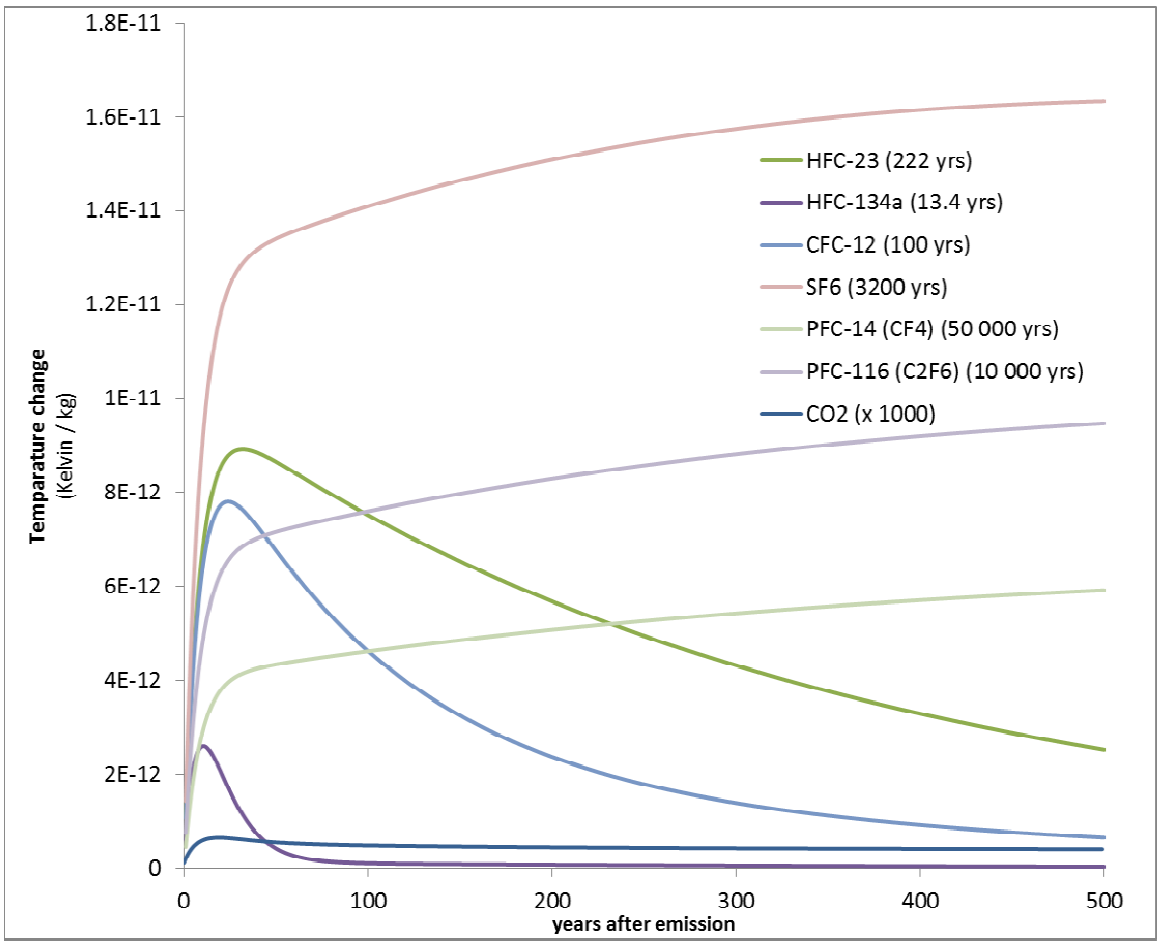

Figure 8.26: Temperature response due to 1-kg pulse emissions of greenhouse gases with a range of lifetimes (given in parentheses). Calculated with a temperature impulse response function taken from Boucher and Reddy (2007) which has a climate sensitivity of 1.06 K $(W\ m^{-2})^{-1}$, equivalent to a 3.9 K equilibrium response to 2 x CO_2.

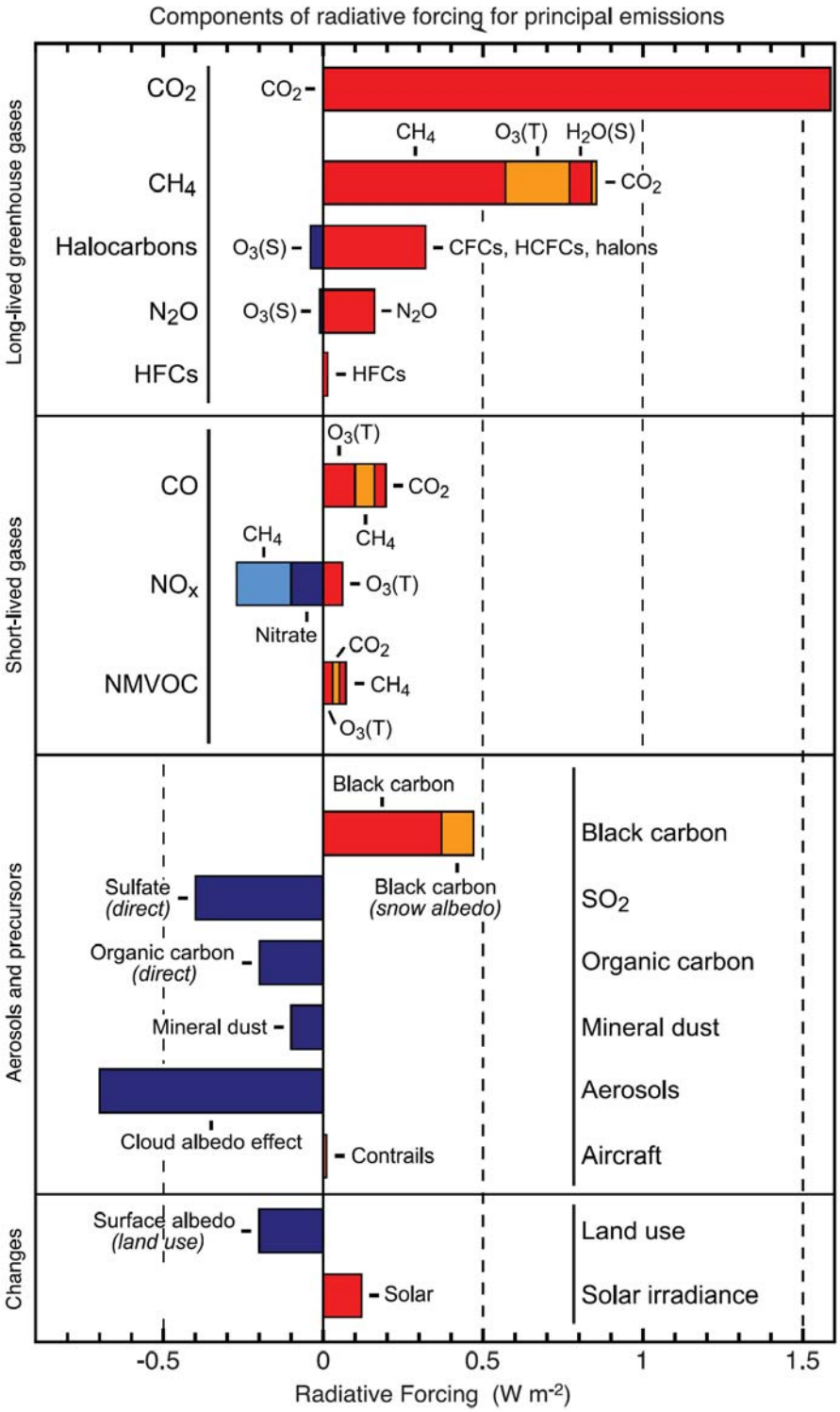

Figure 8.27: Components of RF for emissions of principal gases, aerosols and aerosol precursors and other changes. Values represent RF in 20XX due to emissions and changes since 1750. [PLACEHOLDER FOR SECOND ORDER DRAFT: Figure 2.21 from AR4 will be updated based on ACCMIP and published studies.]

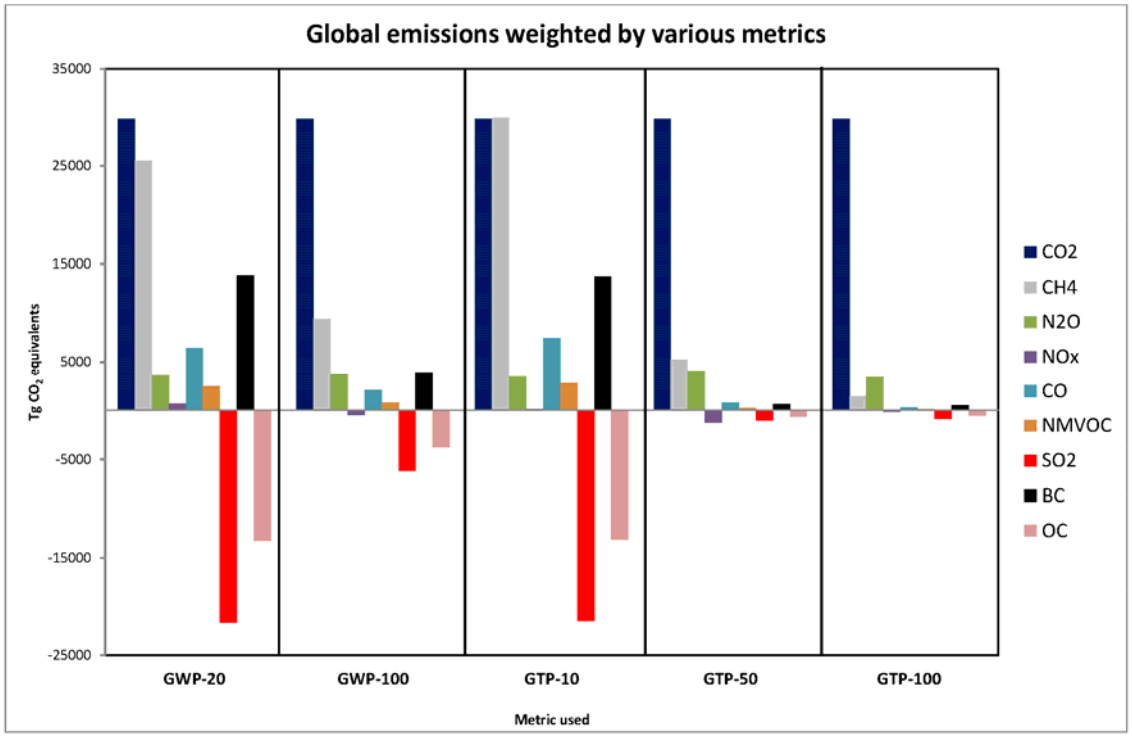

Figure 8.28: Global anthropogenic emissions weighted by GWP and GTP for chosen time horizons. [PLACEHOLDER FOR SECOND ORDER DRAFT: This figure may be merged with Figures 8.27 and 8.29 to one panel showing 4 figures together. To be updated to AR5 emissions inventory.]

(a)

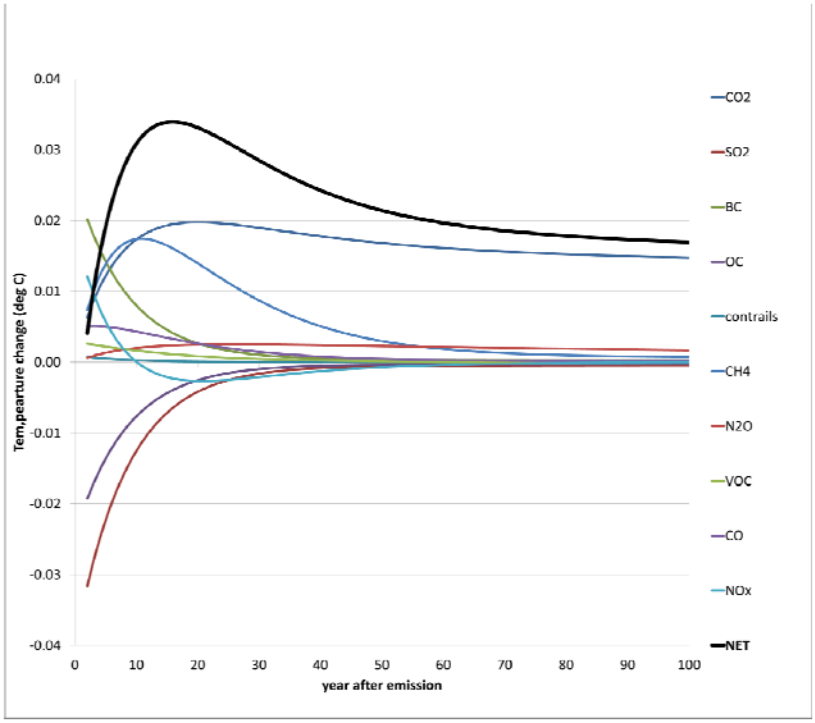

(b)

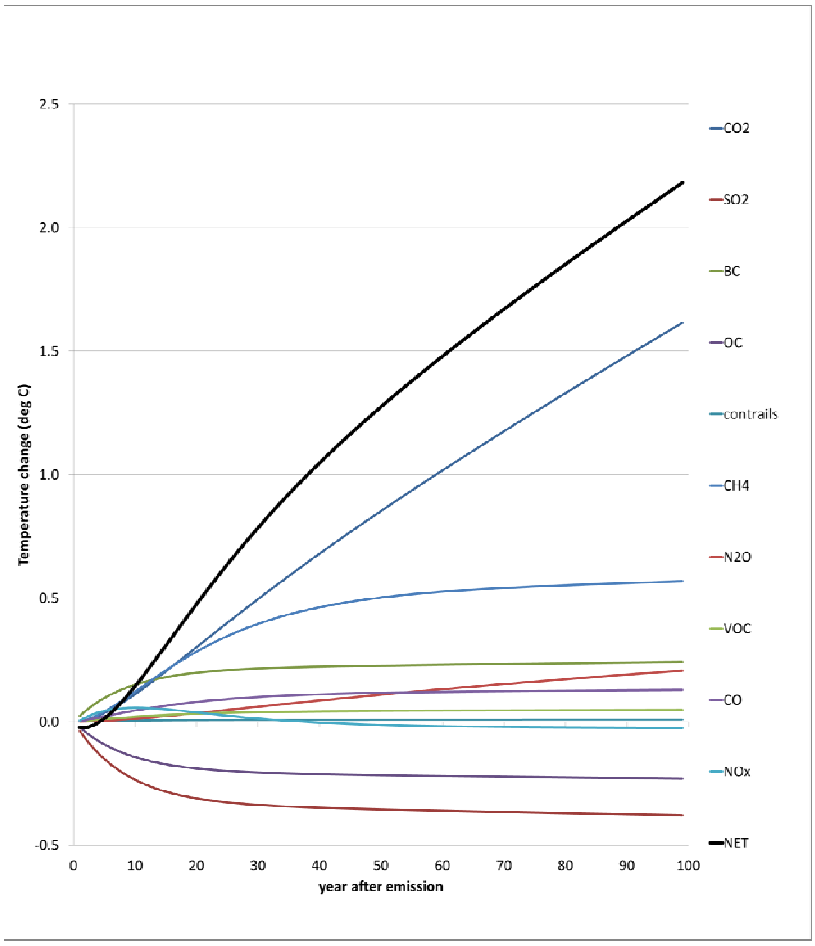

Figure 8.29: Temperature response by component for total man-made emissions for (a) a one-year pulse (year 2000) (upper) and (b) for emissions kept constant at 2000 level (lower). The effects of aerosols on clouds (and in the case of black carbon, on surface albedo) as well as aviation-induced cirrus are not included. [PLACEHOLDER FOR SECOND ORDER DRAFT: To be updated to AR5 emissions inventory.]

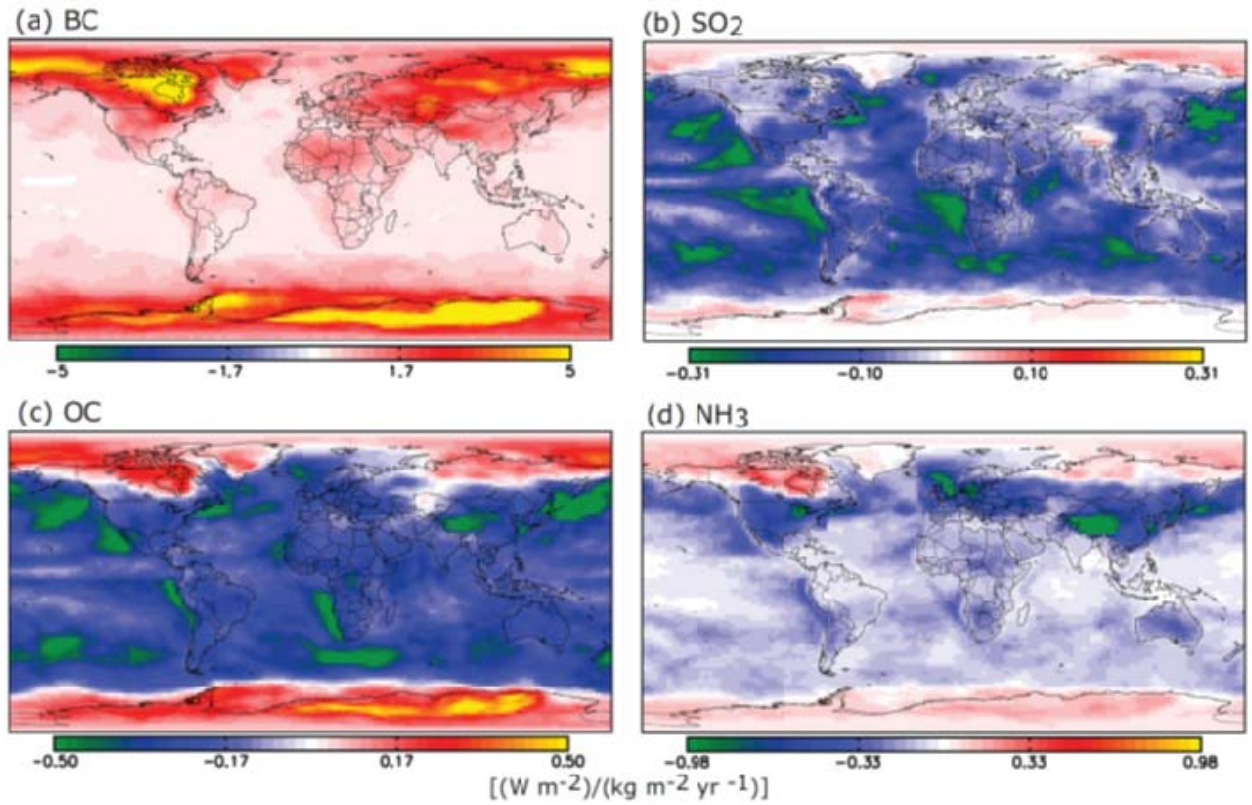

Figure 8.30: Yearly average radiative forcing efficiencies for (a) BC, (b) SO_2, (c) OC and (d) NH_3. Values in a particular grid cell show the response of global aerosol DRF to perturbations of emissions in that grid cell (Henze et al., 2011).

(a)

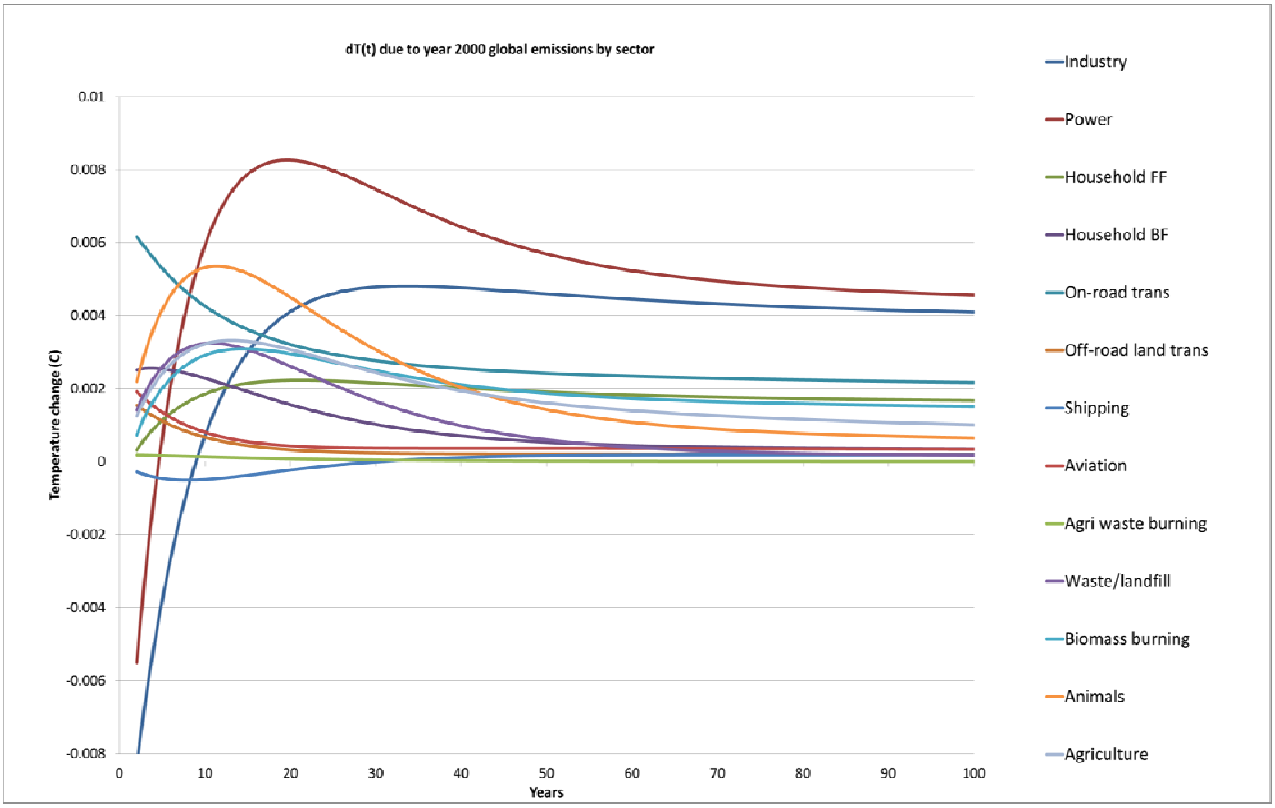

(b)

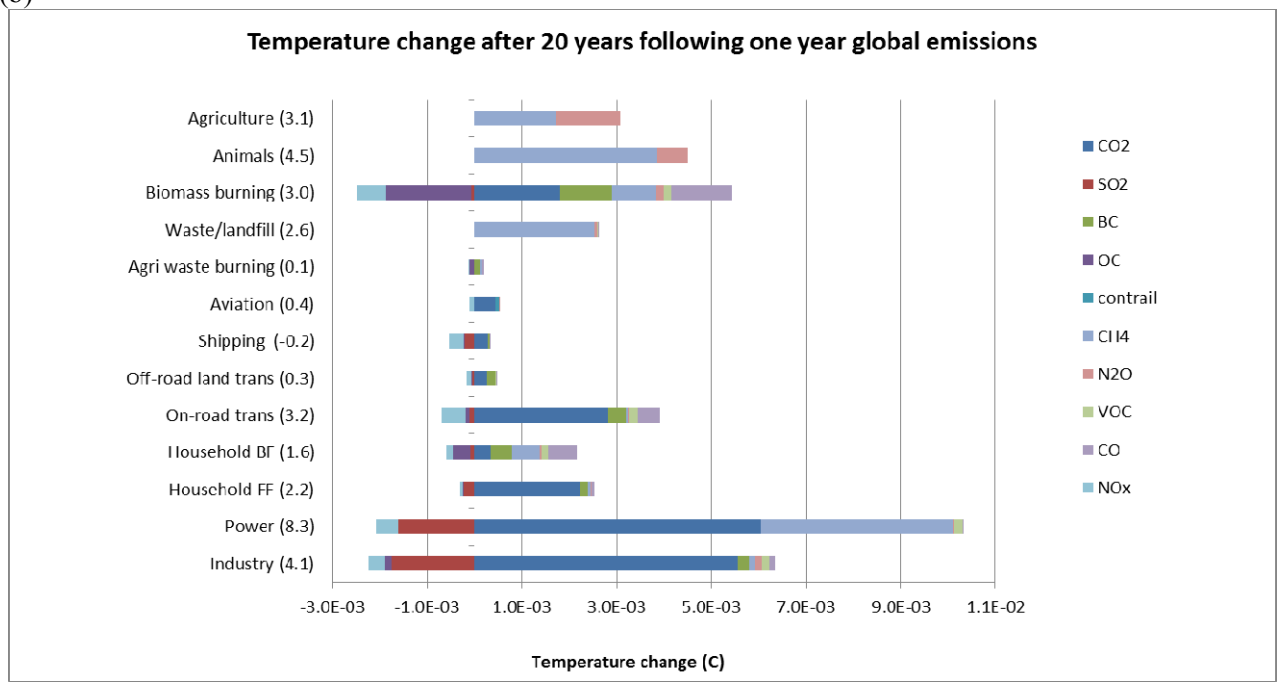

Figure 8.31: (a) Net dT(t) by sector from total man-made emissions (one year pulse); (b) Net dT(t) by sector after 20 years (for one year pulse emissions). Numbers in parentheses after the sectors give the *net* temperature effect in mK. CT: Contrails. The effects of aerosols on clouds (and in the case of black carbon, on surface albedo) and aviation-induced cirrus are not included. [PLACEHOLDER FOR SECOND ORDER DRAFT: To be updated to AR5 emissions inventory.]

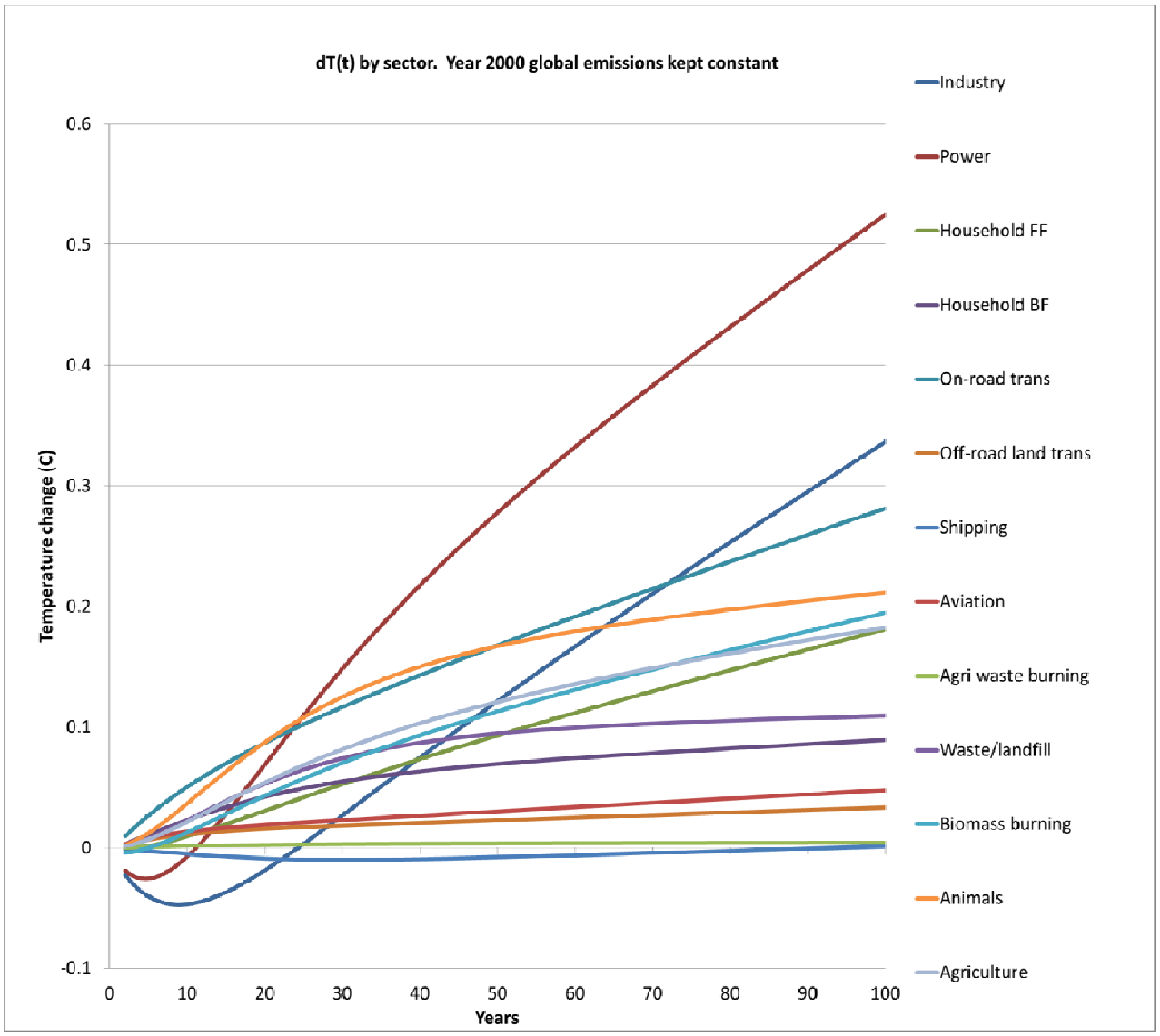

Figure 8.32: Net dT(t) by sector from total man-made emissions kept constant; CT: Contrails. The effects of aerosols on clouds (and in the case of black carbon, on surface albedo) and aviation-induced cirrus are not included. [PLACEHOLDER FOR SECOND ORDER DRAFT: To be updated to AR5 emissions inventory.]

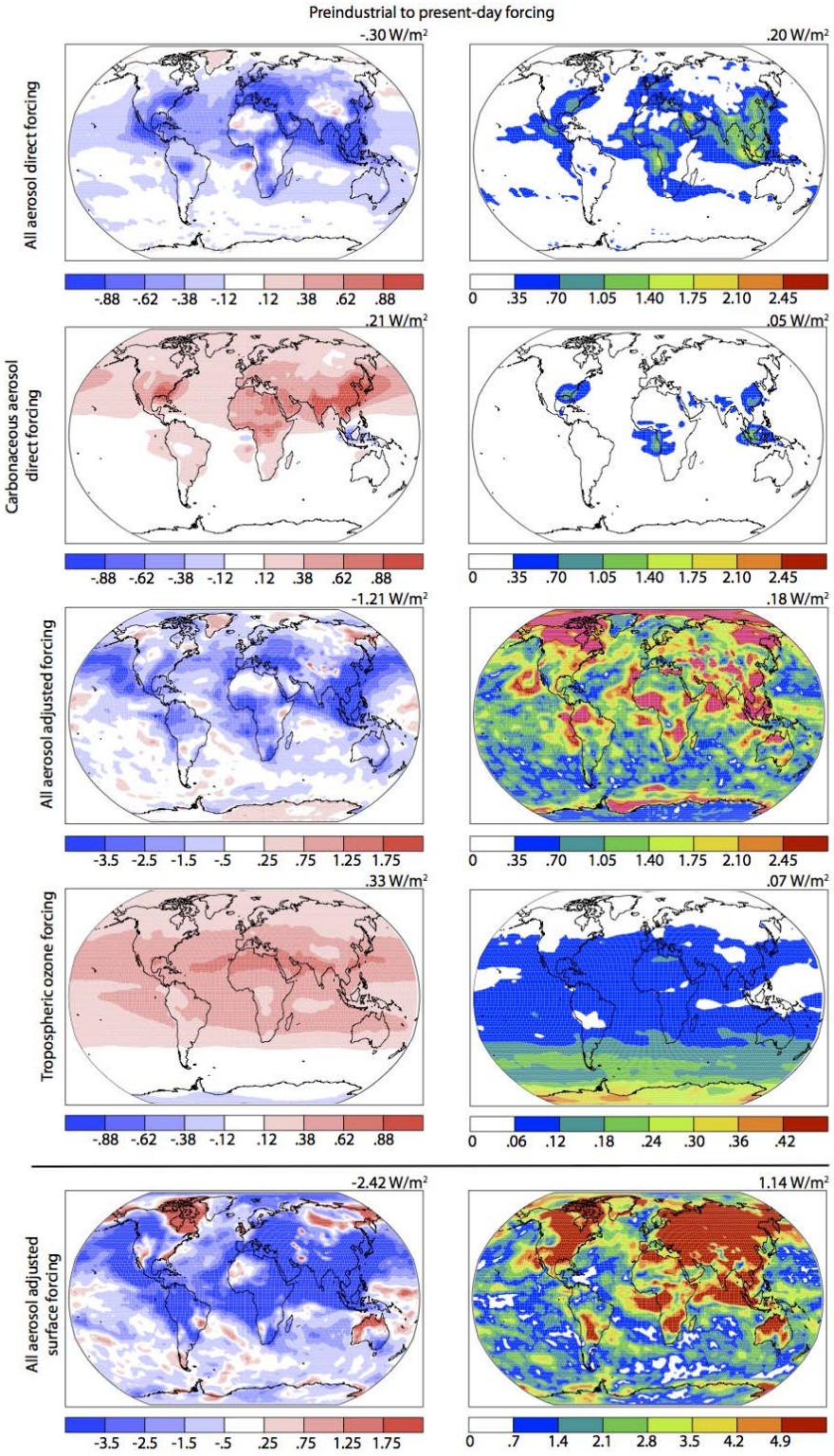

Figure 8.33: Total aerosol direct RF (first row), total carbonaceous aerosol direct RF (second row), net atmospheric aerosol AF due to aerosols (direct and indirect effects; third row), tropospheric ozone RF (fourth row), and adjusted surface forcing due to aerosols (fifth row). Average of models in left column, standard deviation in right column, with global area-weighted means given in the upper right (all in W m^{-2}). RF values from ACCMIP simulations, AF from ACCMIP and CMIP5 simulations. Note that RF and AF means are shown with different color scales, and standard deviation color scales vary between rows.

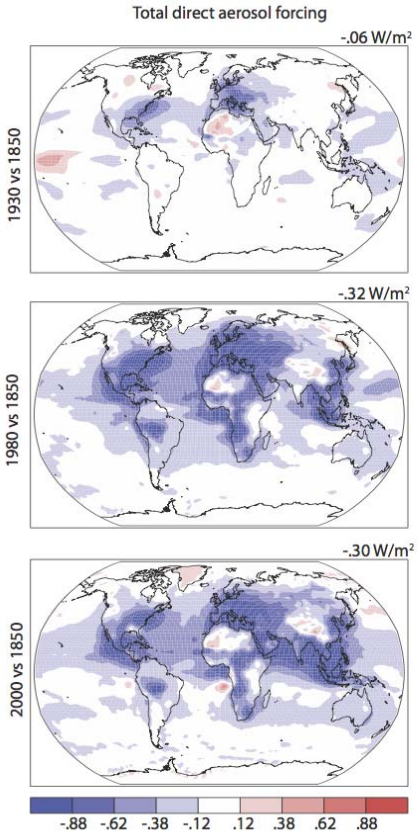

Figure 8.34: Multi-model mean direct RF (W m^{-2}) for the indicated times from all aerosols based on the ACCMIP simulations. Global area-weighted means given in the upper right. [PLACEHOLDER FOR SECOND ORDER DFAFT: Eventually to be: direct effect of all aerosols, carbonaceous aerosols, ozone, aerosol AF, and surface radiation (from aerosols) for 1930, 1980, and 2000 vs 1850.]

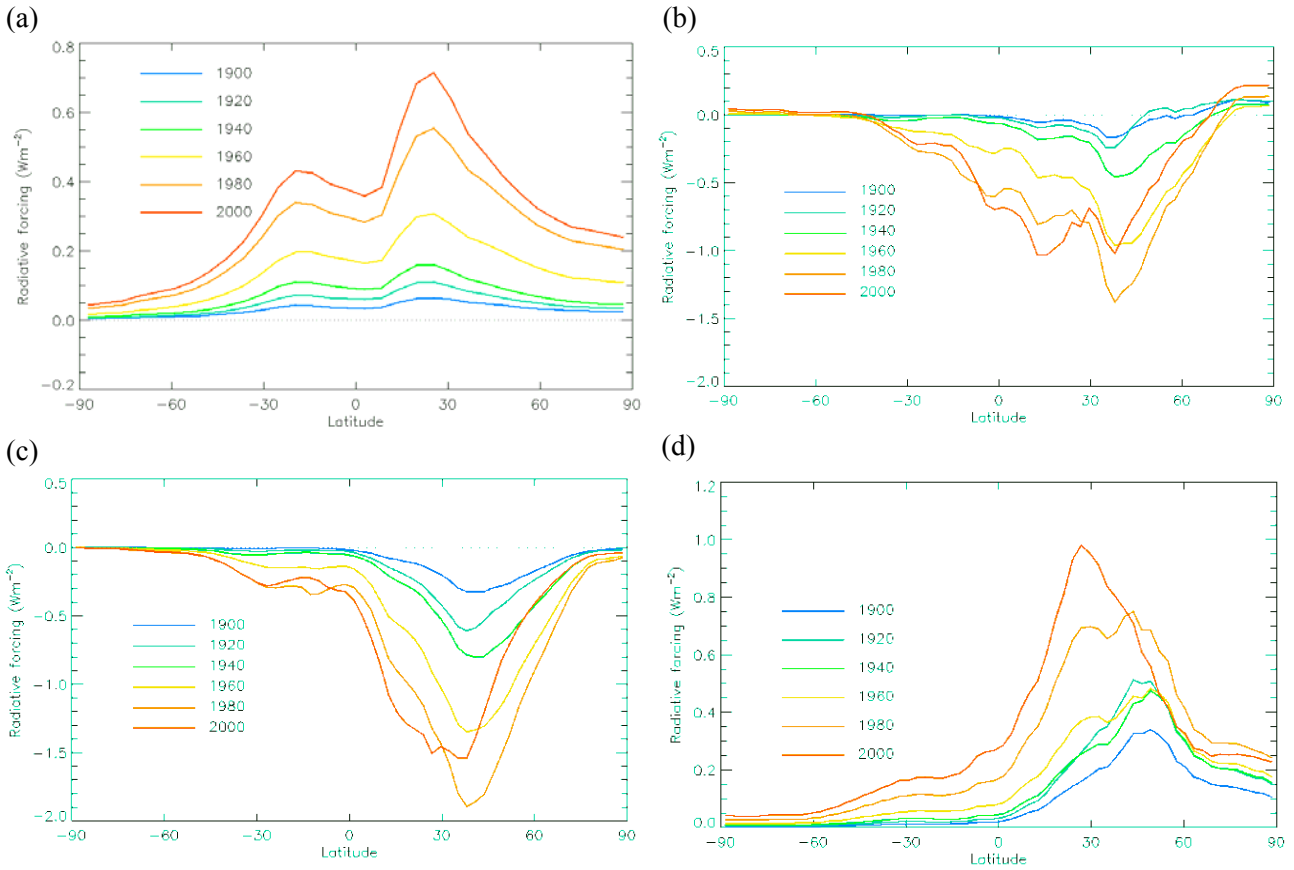

Figure 8.35: Zonal mean radiative forcing as a time evolution from 1900 to 2000 with a reference to 1850 conditions, (a) tropospheric ozone, (b) total direct aerosol effect, (c) direct aerosol effect of sulphate, (d) direct aerosol effect of BC. [PLACEHOLDER FOR SECOND ORDER DRAFT: These are preliminary results that will be updated with more modeling results.]

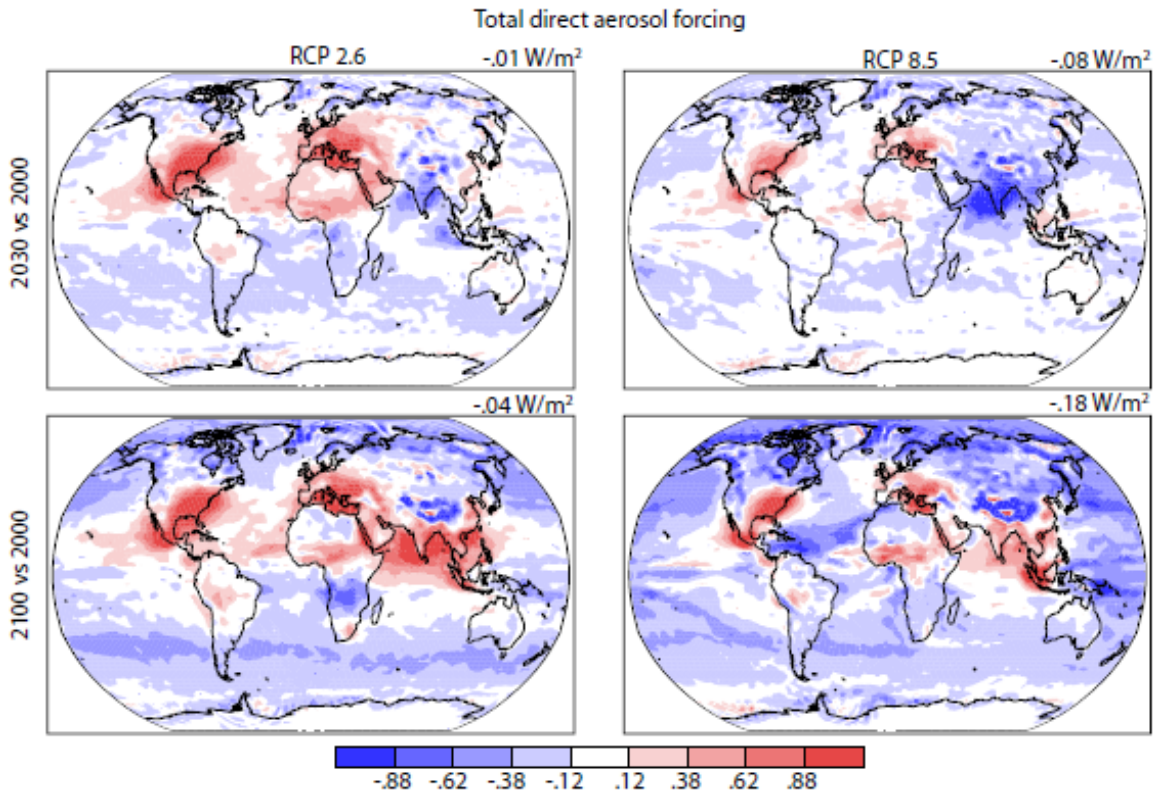

Figure 8.36: Multi-model mean direct RF (W m^{-2}) for the indicated times and RCPs from all aerosols based on the ACCMIP simulations. Global area-weighted means given in the upper right of each panel. [PLACEHOLDER FOR SECOND ORDER DRAFT: Eventually to be: direct effect of all aerosols, carbonaceous aerosols, ozone, aerosol AF, and surface radiation (from aerosols) for these times.]

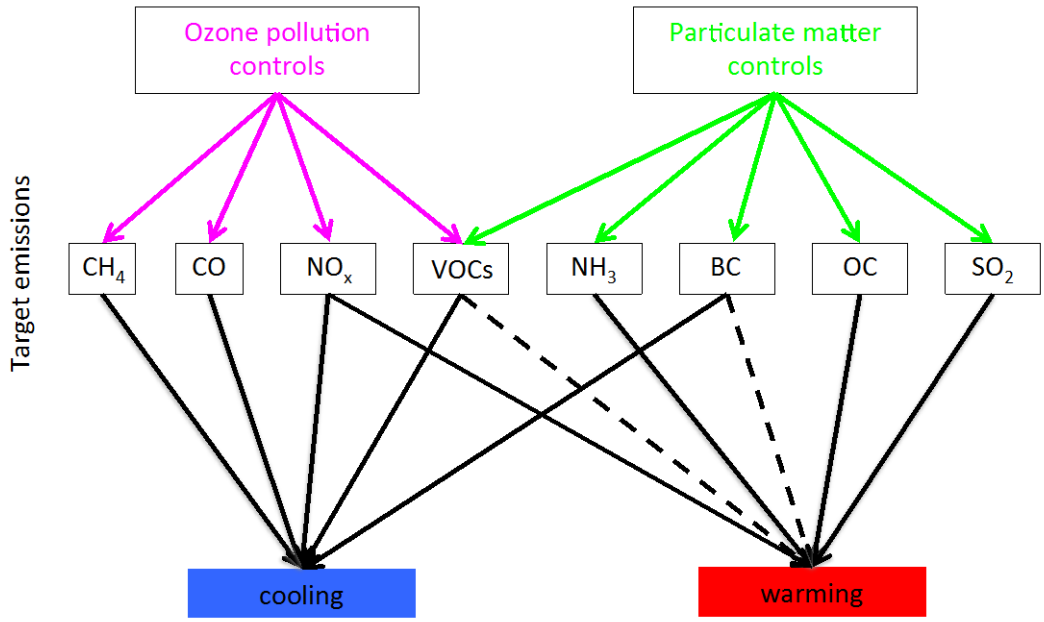

FAQ 8.2, Figure 1: Schematic diagram of the impact of pollution controls on specific emissions and climate impact. Solid black line indicates known impact, dashed line indicates uncertain impact.